

MODULOGRAPHY

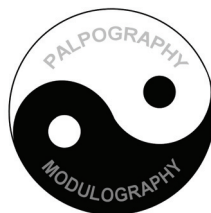
ELASTICITY IMAGING OF ATHEROSCLEROTIC PLAQUES

RADJKUMARSING ANAND BALDEWSING

COVER DESIGN:

© 2006 Radjkumarsing Anand Baldewsing.

This cover design complements, and is inspired by, the white cover of Dr. J.A. Schaar's thesis Palpography (defended in 2005, cum laude, at the Erasmus Medical Center in Rotterdam, The Netherlands, ISBN 90-8559-064-7).



PRINTED BY:

Optima Grafische Communicatie, Rotterdam, The Netherlands.

ISBN:

90-8559-172-4

MODULOGRAPHY

ELASTICITY IMAGING OF ATHEROSCLEROTIC PLAQUES

MODULOGRAFIE

VISUALISATIE VAN DE ELASTICITEIT VAN ATHEROSCLEROTISCHE PLAQUES

PROEFSCHRIFT

ter verkrijging van de graad van doctor aan de
Erasmus Universiteit Rotterdam
op gezag van de
rector magnificus

Prof.dr. S.W.J. Lamberts

en volgens besluit van het College voor Promoties.

De openbare verdediging zal plaatsvinden op

woensdag 21 juni 2006 om 15.45 uur

door

RADJKUMARSING ANAND BALDEWSING

geboren te 's-Gravenhage

PROMOTIECOMMISSIE

PROMOTOREN: Prof.dr.ir. A.F.W. van der Steen
Prof.dr. P.W.J.C. Serruys

OVERIGE LEDEN: Prof.dr.ir. A. Gisolf
Dr.ir. C.W.J. Oomens
Dr. R. Krams

The research presented in this thesis was made possible by the 2000-PIONIER grant (project number: RPG-5442) of the Dutch Technology Foundation (STW), awarded to Prof.dr.ir. A.F.W. van der Steen in 2000. The research was carried out at the Department of Biomedical Engineering, Thoraxcenter, Erasmus Medical Center in Rotterdam.

SPONSORS:

Financial support by the **Netherlands Heart Foundation** and the **Interuniversity Cardiology Institute of the Netherlands** for the publication of this thesis is gratefully acknowledged.

Financial support for the publication of this thesis was also generously provided by the following companies:

Bristol-Myers Squibb & Bristol-Myers Squibb Medical Imaging
Cardialysis
Merck Sharp & Dohme BV
Novartis Pharma AG
OrbusNeich
Pfizer
Sanofi-Aventis
Volcano Corporation

COPYRIGHT:

© 2006 Radjkumarsing Anand Baldewsing.

All rights reserved. No part of this publication may be reproduced, stored in a retrieval system, or transmitted, in any form or by any means, electronic, mechanical, photocopying, recording or otherwise, without the prior permission in writing from the proprietor(s). Some chapters are based on published manuscripts, which were reproduced with permission of the co-authors and of the publishers. Copyright of these manuscripts remains with the publishers.

Dedicated to those who are always good to me

CONTENTS

PART I: INTRODUCTION

CHAPTER 1	9
THE HEART	9
ATHEROSCLEROSIS	10
ULTRASOUND IMAGING	13
INTRAVASCULAR IMAGING OF PLAQUE COMPONENTS AND VULNERABILITY	13
INTRAVASCULAR ULTRASOUND STRAIN ELASTOGRAPHY	16
MODULUS ELASTOGRAPHY	23
OUTLINE OF THE THESIS	26
REFERENCES OF INTRODUCTION	27

PART II: FORWARD PROBLEM

CHAPTER 2	34
A Finite Element Model for Performing Intravascular Ultrasound Elastography of Human Atherosclerotic Coronary Arteries	
CHAPTER 3	48
Finite Element Modeling and Intravascular Ultrasound Elastography of Vulnerable Plaques: Parameter Variation	

PART III: INVERSE PROBLEM

CHAPTER 4	58
Assessment of Vulnerable Plaque Composition by Matching the Deformation of a Parametric Plaque Model to Measured Plaque Deformation	
CHAPTER 5	82
Robustness of Reconstructing the Young's Modulus Distribution of Vulnerable Atherosclerotic Plaques using a Parametric Plaque Model	

PART IV: GENERALIZATION

CHAPTER 6	102
Young's Modulus Reconstruction of Vulnerable Atherosclerotic Plaque Components using Deformable Curves	
CHAPTER 7	116
An Inverse Method for Imaging the Local Elasticity of Atherosclerotic Coronary Plaques	

PART V: SUMMARY

CHAPTER 8	136
Discussion and Conclusion	
CHAPTER 9	144
Discussie en Conclusie	

PART VI: APPENDICES

CHAPTER 10	152
Appendix A: Linear Elasticity Theory and Tissue Deformation Model	
CHAPTER 11	154
Appendix B: Relationship between Principal and Radial Strain	

PART VII: MISCELLANEOUS

CHAPTER 12	158
List of Symbols and Abbreviations	
CHAPTER 13	160
Modulography Filmstrips	
CHAPTER 14	168
Curriculum Vitae	
CHAPTER 15	170
List of Publications	
CHAPTER 16	174
Acknowledgement	

PART I
INTRODUCTION

THIS CHAPTER IS BASED ON THE PUBLICATION

“Intravascular Ultrasound Elastography: A Clinician’s Tool for Assessing Vulnerability and Material Composition of Plaques”,

BY BALDEWSING RA, SCHAAR JA, DE KORTE CL, MASTIK F, SERRUYS PW AND VAN DER STEEN AFW,
IN STUDIES IN HEALTH TECHNOLOGY AND INFORMATICS, 113:75-96;2005,

Copyright © 2005 IOS Press.

Parts from this publication were reprinted with their permission.

INTRODUCTION

THE HEART

HEART FUNCTION

Blood circulation caused by the pumping of the heart (Fig. 1) is vital for supplying nutrition to cells and maintenance of the human body. The heart consists of two pumps in series: one squeezes blood through the lungs for exchange of oxygen and CO₂, the other directs blood to all other tissues in the body. To fulfil its pumping function, the heart needs oxygen, which is provided by the coronary arteries.

HEART DISEASES

When the coronary arteries are narrowed, the blood flow is diminished and the heart muscle is not able to properly function anymore (Fig. 1). This type of disease is called 'angina pectoris' and reveals itself as pain in the chest. When the artery becomes totally blocked, the heart muscle is totally deprived from oxygen. This leads to myocardial infarction or even sudden cardiac death. A blockage can arise slowly due to the build up of material in the vessel wall, but also instantaneously due to a thrombosis. A thrombosis is the formation of a blood clot against the vessel wall. Thrombosis is the primary cause of acute coronary syndromes such as, angina pectoris, sudden cardiac death and myocardial infarction (Fig. 2) (Falk et al. 1995).

Thrombosis is the primary cause of acute coronary syndromes

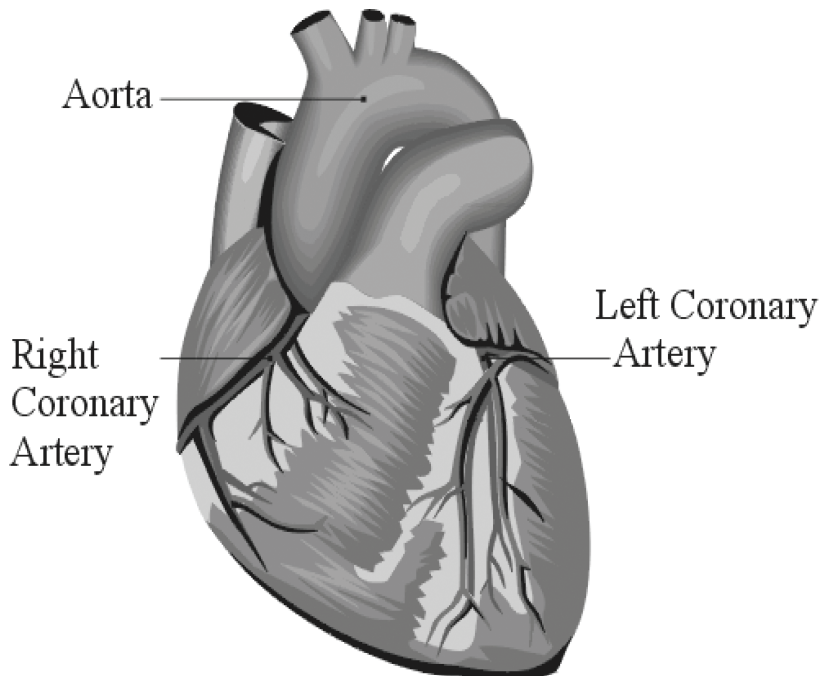


Fig. 1. The heart and its coronary arteries.

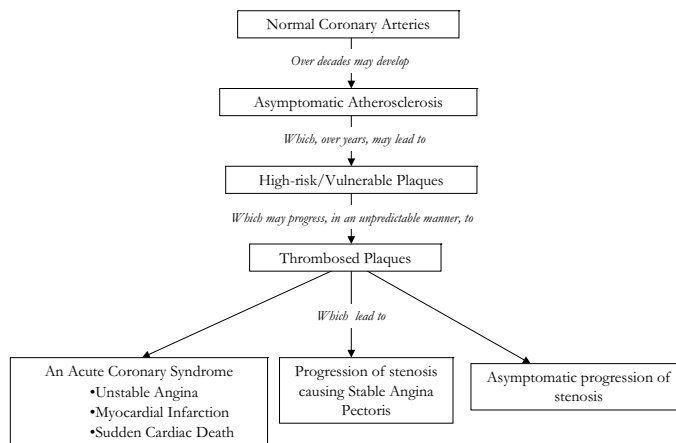


Fig. 2. Development of atherosclerosis and progression to thrombosis and clinical events.

ATHEROSCLEROSIS

Atherosclerosis, a disease of the arteries, is the primary cause of heart disease and stroke. In westernized societies, it is the underlying cause of about 50% of all deaths (Lusis 2000).

HEALTHY AND DISEASED CORONARY ARTERIES

The normal, healthy coronary wall consists of three layers: the intima, media and adventitia (Fung 1993).

-The intima is the first layer. Its endothelium (thin layer of endothium cells) is selectively permeable, which allows exchange of material between the blood and the wall.

-The media is the middle layer. It consists of smooth muscle cells, collagen and elastic fibers; together, these building blocks provide the mechanical strength of the vessel to withstand the pulsatile blood.

-The adventitia is the outer layer. It contains mainly smooth muscle cells, collagen and fibrous connective tissue; just as the media, this layer also provides mechanical strength, but mainly when the vessel is most widened.

The area inside the vessel through which the blood flows is called the lumen.

A diseased artery is characterized by build-up of various materials in its wall. This build-up material is called a plaque

A diseased artery is characterized by build up of various materials in its wall. This build up material is called a plaque. A plaque starts its formation already in early adolescence and the underlying process is called atherosclerosis (Fig. 3), which can be described, as follows (Libby 2001). (i) First, the endothelium layer dysfunctions, which leads to an increased uptake of materials from the blood into the vessel wall. (ii) The build-up material forms a small core of soft, fatty material, which mainly consists of foam cells and macrophages (inflammatory cells). (iii) The continuation of build-up material leads to a more complicated core composition, consisting of a mixture of inflammatory cells, apoptotic cells and debris. (iv) Further progression leads to a so-called 'vulnerable plaque', which is characterized by a stiff, fibrous cap that covers the soft, lipid-rich core (fig. 3, picture 4).

VULNERABLE PLAQUES

Most thrombi are caused by rupture of a so-called 'vulnerable' plaque

The primary cause of myocardial infarction is the formation of a thrombus within the coronary artery (Davies 2000). Most thrombi are caused by rupture of a so-called 'vulnerable' plaque or by erosion of its surface (endothelium) (Schaar et al. 2004a). The majority of vulnerable plaques are a thin-cap fibroatheroma (TCFA), i.e., a

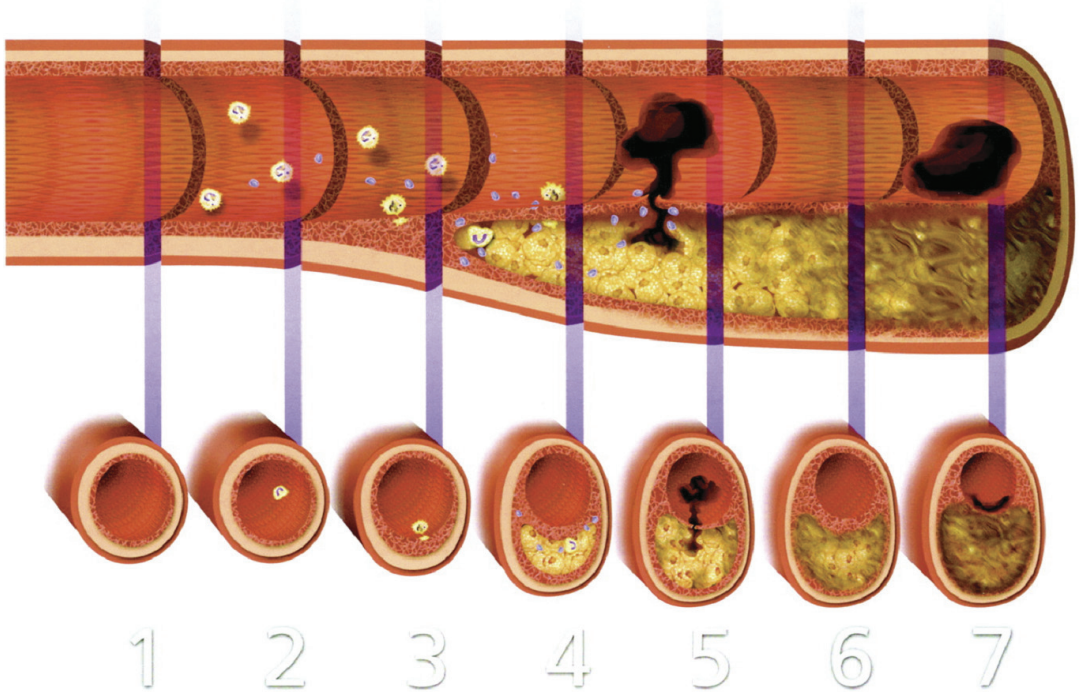


Fig. 3. Atherosclerosis: Initiation, progression and plaque formation. Figure reprinted from "Libby P, Current concepts of the pathogenesis of the acute coronary syndromes, *Circulation* 2001;104:365-72" with permission.

plaque with a stiff, fibrous cap that shields a soft, lipid-rich core from contacting the blood (Fig. 4) (Virmani et al. 2003). When this cap ruptures, the thrombogenic core contacts the blood, upon which a thrombus is formed. These TCFAs may be pictured as a pimple. When a pimple is pressed upon, its cap (the surface of the skin) ruptures and the core (material inside the pimple) will be exposed, after which the cap heals by the formation of a thrombus. Plaques with small, calcified nodules or plaques with an eroded endothelium (Fig. 4) are also vulnerable plaques that cause thrombosis, but much less frequent than TCFAs (Schaar et al. 2004a).

INTERVENTIONAL PROCEDURES

Many interventional procedures exist (Waller 1989) or are emerging (Aoki et al. 2005) to treat patients with coronary artery disease. Most of them aim at restoring the blood flow by increasing the lumen area. For example, 'Percutaneous transluminal coronary angioplasty' (in Dutch also known as 'Dotteren') is a procedure during which the coronary wall is stretched, by inflating a balloon from the inside, thus pressing the plaque further into the wall. A major drawback is that restenosis occurs. Restenosis is the wall's healing response after mechanical injury. The response primarily consists of 'neointimal growth', which is the formation of new wall-tissue; this new tissue reduces the lumen area. For example, during balloon angioplasty, injury occurs when the balloon is rubbed against the endothelium and when the wall is stretched. To overcome the problem of restenosis a drug eluting stent (DES) is placed during a 'stenting' procedure (Ong et al. 2005). A DES is a metallic wire-frame, called a stent, which is coated with a pharmaceutical drug. A DES is placed in the wall as follows. First, it is wrapped around a balloon. Then, the balloon is inflated, which causes the stent to expand. Finally, the balloon is deflated and the stent maintains its expanded shape, thus keeping the vessel wall sufficiently open. Due to the drug the restenosis process is stopped (Morice et al. 2002).

Other techniques simply remove the plaque to restore blood flow. For example, with 'Atherectomy' a small cutting device is inserted inside the vessel to cut away the plaque. With 'spark-erosion', the plaque is put under a high electric power dif-

Most interventional procedures aim at restoring the blood flow by increasing the lumen area

Other techniques simply remove the plaque to restore blood flow

ferential to ablate it (Slager et al. 1985). Similarly, laser techniques can be used for this purpose (van Leeuwen et al. 1993).

Finally, there is the 'Bypass' procedure, which leads the blood around the stenosis area through another surgically attached vessel (Sundt 2005).

All interventional procedures require feedback before, during and after the intervention. The most used feedback is provided by images of the body made with ultrasound.

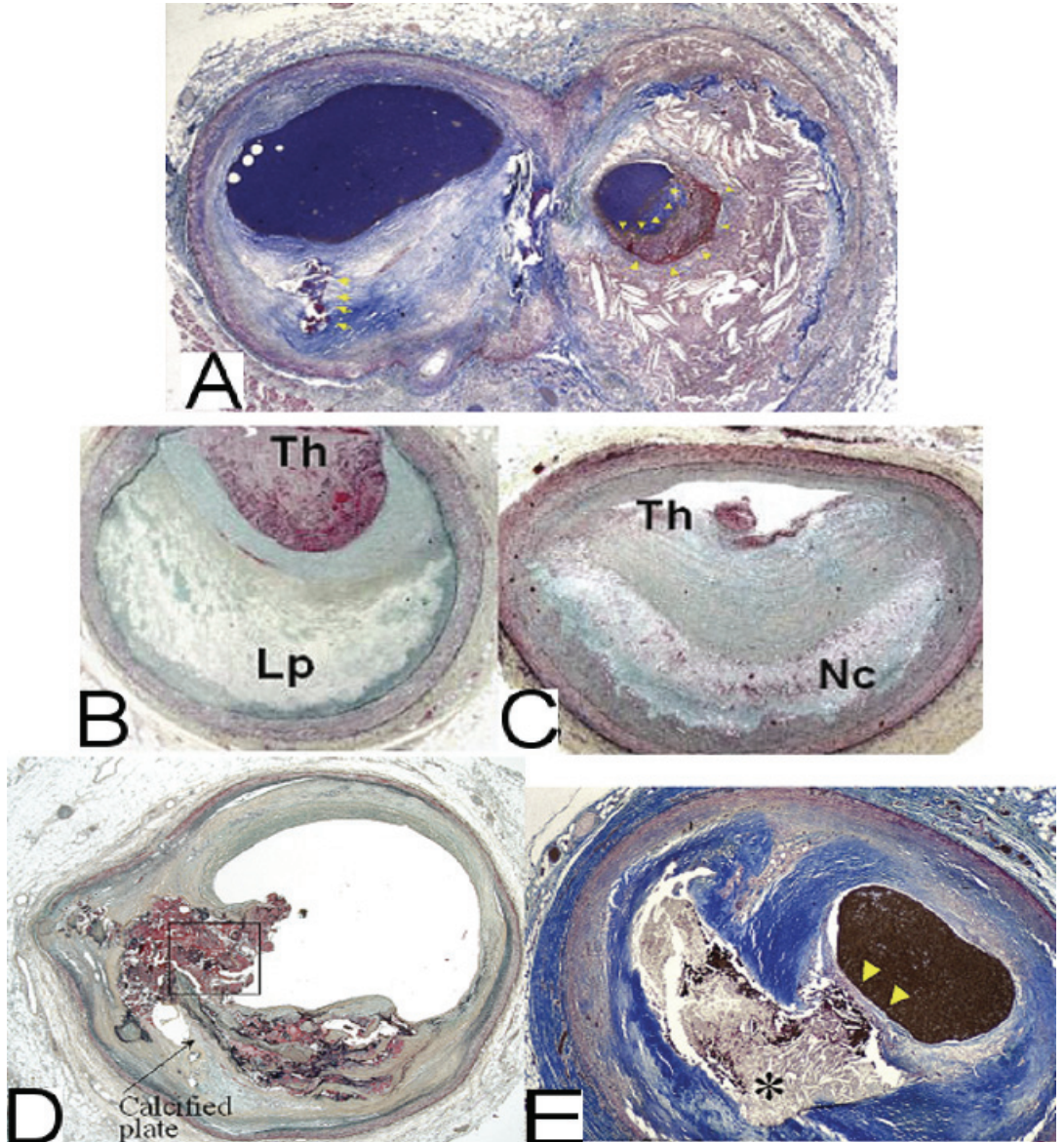


Fig. 4. Various types of plaque. (A) Ruptured plaque with thrombosis: A cross-section of a coronary artery is cut just distal to a bifurcation. The atherosclerotic plaque to the left (circumflex branch) is fibrotic and partly calcified whereas the plaque to the right (marginal branch) is lipid-rich with a nonoccluding thrombus superimposed. (B, C) Eroded plaques with thrombosis: Plaque erosion lesions from two different patients showing in (B) a lesion with lipid pool (Lp) and in (C) a necrotic core (Nc) with luminal thrombi (Th). Note a thick fibrous cap above the necrotic core in (C) and a lack of communication between it and the lumen. (D) Calcified nodule: A section of the mid right coronary artery shows an eccentric lesion with extensive calcification (calcified plate) and surface calcified nodules with loss of fibrous cap and luminal fibrin deposition. (E) Inflamed thin-cap fibroatheroma: A section of a coronary artery contains a large lipid-rich core that is covered by a thin fibrous cap. The lumen contains contrast medium injected postmortem. The fibrous cap is severely inflamed, containing many macrophage foam cells, and extravasated erythrocytes within the necrotic and avascular core just beneath the cap, indicating that the cap is ruptured nearby.

ULTRASOUND IMAGING

Ultrasound imaging is based on transmitting and receiving high frequency sound waves. A transmitted wave propagates through a medium (e.g., air, water, soft tissue) until it hits a reflecting object. The wave, then, partly passes through the object and partly will be reflected. The reflected wave is received by a transducer. The time between transmission and reception of a wave is directly related to the distance between transmitter and receiver. This principle is used by various animals, such as, dolphins or bats, to navigate or to locate pray.

Ultrasound imaging is based on transmitting and receiving high frequency sound waves

An essential discovery for the development of ultrasound imaging was the piezo-electric effect by Pierre and Jacques Curie. They discovered that an electric charge is produced by materials such as ceramics or quartz, when a force is applied to it. Similarly, these materials produce a force, when an electric voltage is applied to it. Thus, applying a voltage to a piezo-electric material results in a force, which can be used to transmit a sound wave, and vice versa, a sound wave hitting a piezo electric material produces voltage.

The piezo-electric effect

Since then, various ultrasound transducers have been developed to image (the structure of) organs (Bom et al. 1989). Transducers are devices that have a single or an arrangement of piezo-electric elements. Images are created by letting the elements of a transducer emit sound waves into the organ, upon which, the amplitude of the echos, received by the elements, are translated into an grey-level image (echogram). Since echos can be created very fast, real-time images of moving organs can be nowadays be made, even in three dimensions.

Transducers are devices with piezo-electric elements

ULTRASOUND IMAGING OF VESSELS

Vessels can be imaged from outside the body (non-invasive) or from the inside (invasive) (Saijo et al. 2003). Carotid arteries are located in the neck just below the surface of the skin. Therefore, they can be non-invasively imaged with an linear array ultrasound transducer, which consists of a series of elements lined-up, placed against the neck with sufficient resolution to discriminate the three layers of the vessel. By monitoring the diameter of these layers over time one can evaluate the effect of lipid-lowering drugs upon the overall plaque reduction.

Coronary arteries, however, cannot be imaged from outside the body with sufficient resolution. Intravascular ultrasound (IVUS) is a technique to create 2D cross-sectional echograms from within the lumen using an IVUS catheter (Bom et al. 1972, O'Donnell et al. 1997, Wells 1966). This catheter emits and receives ultrasound echos in a 360 degrees scan angle. There are two often used systems to enable a 360 degree scan. With a mechanical rotating catheter, a single transducer element is attached to a flexible axis and this axis is mechanically rotated during scanning. However, with a phased-array catheter a series of transducer elements are fixed onto the round tip of the catheter and these elements are electronically delayed to create a scan in a desired angle. The advantage of using a phased array catheter is that there are no rotational errors present. With a rotating catheter, the axis can sometimes non-uniformly rotate or get stuck, especially in a curved vessel, causing warped echograms. Furthermore, the guidewire, used to lead the rotating catheter towards the site of plaque burden, lays outside the catheter, which causes an unwanted strong bright reflection with a dark distal area in the echogram. Advantage of a rotating single element transducer is that a high frequency can be used, resulting in a better resolution. Furthermore, they have, in general, a better signal to noise ratio.

Intravascular ultrasound (IVUS) is a technique to create 2D cross-sectional echograms from within the lumen using an IVUS catheter

INTRAVASCULAR IMAGING OF PLAQUE COMPONENTS AND VULNERABILITY

Plaques that are at an increased risk of causing thrombosis are termed thrombosis-prone or vulnerable plaques (Schaar et al. 2004a). The TCFA is a vulnerable plaque since it has as vulnerability-features, an eccentric, large soft lipid pool covered by a

Vulnerable plaques are at an increased risk of causing thrombosis

thin, inflamed, fibrous cap. There exist a wide variety of so-called vulnerability-features that are suspected of making plaques vulnerable, such as, a denude or eroded endothelium, presence of surface calcified nodules, an increased angiogenesis or vasa vasorum which supplies the plaque, an increased plaque-surface temperature due to metabolic activity by macrophages, a decreased collagen or smooth muscle cells synthesis of the cap, vessel-remodeling, the cholesterol-form as indicator for lipid-pool softness, and many more.

An ideal imaging technique would give an all-embracing assessment of suspected plaque-vulnerability-features

An ideal imaging technique would give an all-embracing assessment of these suspected vulnerability-features, however, currently no such technique exists. Various intravascular techniques have been developed, or are under development, to assess one or a subset of the vulnerability-features. As such, a combination of complementary techniques will be needed to enable the identification and characterization of vulnerable plaques with a high specificity and sensitivity.

Next, a brief overview of the principles, merits and limitations of some intravascular imaging techniques is given.

INTRAVASCULAR ULTRASOUND

IVUS provides in real-time cross-sectional grey-level (echo-intensity) images of the coronary artery, which clearly show the plaque burden and remaining free luminal area. Calcified regions are identifiable as a sharp reflection with distal acoustic shadowing. However, this shadowing also prevents identification from distal plaque components. Furthermore, discrimination between fatty (hypoechoic) and fibrous (hyperechoic) material remains difficult (Komiya et al. 2000, Prati et al. 2001), partly due to the variable concentrations of cholesterol crystals in the lipid core and the dependence of the echo-intensity of fibrous components upon the incidence-angle of the ultrasound-beam (Hiro et al. 2001).

INTRAVASCULAR ULTRASOUND RADIO-FREQUENCY SIGNAL ANALYSIS

This technique calculates quantitative parameters from the radio-frequency signal that is backscattered from a small tissue volume at each depth in the tissue (Bridal et al. 1997, Spencer et al. 1997, Wickline et al. 1994). After correlating these parameters with histology of different plaque components, a cross-sectional color map is constructed in which the color indicates the type of plaque component.

For example, when only the mean signal power is calculated, plaque components (thrombus, fibrous, mixed lesion, calcification) can be differentiated (Kawasaki et al. 2002). However, its limitations, are that the mean values of lipid and media are similar. Furthermore, the catheter has to be centred in the lumen and be placed co-axial with the vessel to reduce the effect that the incidence-angle of the ultrasound-beam has upon the mean values.

Another approach is to compute parameters from the spectrum-curve of the signal received from the region of interest, such as maximum and minimum power, slope, intercept and frequencies (Nair et al. 2002). By using a classification tree, the values of these parameters are then associated to a plaque component (fibrous, fibrolipidic, calcified, calcified-necrotic). Its limitation is that the tree is created using histology from a fixed set of plaques, thus, the result for a plaque not in this set, may not be correct. Furthermore, parameter-values of fibrous and fibrolipidic tissue are overlapping.

Wavelet parameters can also be computed, which allows detection of lipid-laded plaques (Murashige et al. 2005). However, similar limitations as with the previous two approaches remain.

ANGIOSCOPY

This technique uses a catheter to directly look at the surface of the coronary artery from within with visible light. The observed color of the surface (red, yellow, white) indicates the presence of possible plaque components, respectively (thrombus, plaque, none) (Itoh et al. 1995). Furthermore, surface irregularities (a denuded endothelium, fissures or tears) are readily visible. However, only the vessel-surface is visualized, thus, no morphological depth-dependent information is obtained from possible plaque components inside the vessel. Another disadvantage is that tempo-

rarily a blood-free view has to be created. This is done by obstructing the blood flow using a vessel-occluding balloon or by displacing blood by flushing the vessel with a saline solution. Both interventions could cause ischemia (lack of oxygen supply) and vessel injury.

THERMOGRAPHY

Intracoronary thermography uses a catheter with small heat sensors, which contact the inner surface of the coronary artery, to measure its surface-temperature distribution (Diamantopoulos 2003). Inflammation by macrophages is a characteristic of atherosclerosis and a feature of plaque vulnerability. Furthermore, inflammation produces a temperature rise in the affected tissue. Consequently, it was hypothesized that vulnerable plaques might be detected by measuring local surface-temperature rises (Casscells et al. 1996). An increased temperature and temperature-heterogeneity was found in atherosclerotic parts of vessels compared to healthy parts (Stefanadis et al. 1999), as well as a correlation with macrophage density and activation (Krams et al. 2005). Limitations are a low parametric and spatial resolution (depending on the number and distribution of the heat sensors), contact induced surface-injury, the lack of depth information and a limited knowledge of the relation between measured surface-temperatures and real in vivo surface-temperatures of arteries; this is because surface-temperatures may be influenced by many other factors than the inflammation alone, such as, material properties of the catheter, geometry of the plaque, and cooling by blood flow (ten Have et al. 2004).

ELECTRICAL IMPEDANCE IMAGING

This catheter-based technique characterizes tissue by measuring their electrical impedance over a frequency range (Suselbeck et al. 2005). Electrical impedance is a complex quantity combining resistance and reactance and depends on the frequency of the alternating current employed. Biological tissues have a complex electrical impedance because they contain components that have resistive and charge-storage properties. By recording the electrical impedance over a frequency range, its frequency-dependent electric behaviour can be determined, which is used to differentiate tissues. A balloon-catheter is used with small electrodes attached to its surface, which needs to make contact with the vessel wall-surface, just as with thermography. Atherosclerotic lesions (fatty and fibrous) showed higher impedance than healthy segments (Suselbeck et al. 2005). Limitations are a possible vessel-surface damage due to balloon friction and the lack of depth information.

MAGNETIC RESONANCE IMAGING

Magnetic resonance imaging (MRI) has emerged as a leading non-invasive imaging modality for characterizing carotid plaque components (such as, thrombus, lipid pool, fibrous cap, calcium) (Leiner et al. 2005). MRI characterizes components on basis of biophysical and biochemical parameters (water content, molecular motion, chemical composition and concentration). It does this by subjecting tissue to a magnetic field, which aligns all its protons. These protons (or spins) are then excited by a radiofrequency pulse and subsequently detected by receiver coils. The detected signal intensity on the MR image is influenced by at least three basic parameters: proton density, T1 longitudinal relaxation time, T2 transverse relaxation time. The T1 and T2 relaxation times define the way that the protons return back to their resting states after the initial excitation. From the detected signal intensities and morphological appearance of the plaque on T1-weighted, proton density-weighted, and T2-weighted images, plaque components are characterized.

Imaging of deeper arteries (iliac, coronary) with non-invasive MRI is difficult, because of cardiac and respiratory motion and the poor signal-to-noise ratio caused by the distance between detector coil and artery. A solution is to place the detector coil near the plaque using an intravascular MRI catheter (IVMRI) (Larose et al. 2005). To allow proper coronary IVMRI, spatial resolution must be improved e.g., by coil-design (Farrar et al. 2005) or stronger magnets, catheters have to be made smaller and the motion of the catheter relative to the vessel and applied magnetic field has to be compensated.

SPECTROSCOPY

Raman spectroscopy is a catheter-based technique that characterizes the chemical composition of tissue by utilizing the Raman effect (van de Poll et al. 2002). This effect is created when incident light (750-850 nm) excites molecules in a tissue sample, which backscatter the light at a different wavelength. The resultant change in wavelength is the Raman effect; which is unique for a given molecule. By using this effect, chemical components in a tissue sample can be identified. Processing the spectra allows identification of various plaque components, cholesterol and calcium salt deposits (Buschman et al. 2001). Limitations are a poor tissue penetration, a strong background fluorescence, absorbance of light by blood, long acquisition time, and lack of depth information. Near infrared (NIR) spectroscopy also yields information on composition (thin cap, lipid pool and macrophages) (Moreno et al. 2002), but with the advantage of deeper penetration, by using light in the range (400-2400 nm), which reduces background fluorescence (Moreno et al. 2003). Future advances in catheter design and processing may overcome most limitations, the lack of depth information, however, remains (van de Poll et al. 2002).

OPTICAL COHERENCE TOMOGRAPHY

This technique creates cross-sectional light-intensity images of the coronary artery wall (Jang et al. 2005). To this end, laser light is transmitted from a catheter towards the tissue and will be reflected upon structures at various depths. Since, light travels extremely fast, the time between transmission and reflection cannot be directly used to represent the depth. For determining depth, interferometry is used. Based on the backscattered light-intensity, discrimination of plaque components (fibrous, fibrocalcific, lipid) (Yabushita et al. 2002) and macrophages (MacNeill et al. 2005) is feasible with very high spatial resolution ($<10\mu\text{m}$). However, its limitations are the need for balloon-inflation or saline flushing to create a blood-free view, just as with angiography, and the poor tissue penetration; both limitations may eventually be overcome (Brezinski 2005).

INTRAVASCULAR ULTRASOUND STRAIN ELASTOGRAPHY

Intravascular ultrasound (IVUS) strain elastography (de Korte 1999) and palpography (Schaar 2005) are elasticity imaging techniques that use ultrasound to compute mechanical information of tissue, such as strain, stress or modulus. This information may be crucial for identifying and characterizing plaques. This is because plaque rupture is ultimately a mechanical event: it occurs when plaques cannot withstand the internal stresses induced by the pulsating blood.

VESSEL WALL MECHANICS

Stress, strain and Young's modulus

To understand some of the structural and mechanical features that make plaques rupture-prone it is necessary to describe the basic mechanical quantities involved (Arroyo et al. 1999, MacIsaac et al. 1993). To introduce these quantities, consider an internally pressurized cylinder (as model for a healthy vessel). The stress is the force acting on a surface divided by the area of that surface. For example, the blood pressure (P) is the force that the blood exerts, per unit area, straight onto the inner layer of the vessel. When a cylinder is pressurized from within, there will be a compensatory circumferential tension, which is called the circumferential stress (S). The two opposing forces are estimated by Laplace's law for a thin-walled cylinder as

$$S = \frac{Pr}{h}$$

where S is the circumferential wall stress, P the pressure, r the radius of the vessel and h its thickness. For healthy vessels, this formula indicates geometric features that may play a role in plaque-rupture: increased stress occurs when the wall thickness decreases or, as in aortic aneurisms, the radius increases. When a stress is

applied to a material it will deform, i.e., it will change its shape. For example, when a spring with an initial length, L , is pushed upon, it will shorten with some amount, δL . The relative change in shape is called strain, ε , and is defined as

$$\varepsilon = \frac{\delta L}{L}$$

When the spring is stressed, it will strain. The amount of strain depends upon the stiffness (hardness, rigidity) of the spring, i.e., a soft spring will be more strained than a more rigid spring, when equally stressed. The mechanical property that defines the stiffness of a material is called the elastic or Young's modulus, E , and is defined as

$$E = \frac{\text{stress}}{\text{strain}}$$

A material is called isotropic, when it has the same Young's modulus in all directions. Arteries are anisotropic, i.e., the Young's modulus in their axial and circumferential direction is larger than in their radial direction (Dobrin 1978). A material has a linear elastic behaviour, when its Young's modulus remains constant over a range of applied stresses. Arteries are nonlinear since their Young's modulus increases with increasing applied stress (Dobrin 1978). Nevertheless, arteries are often assumed linear elastic, isotropic and incompressible for aiding computational analysis or understanding basic properties. Finally, there is another mechanical quantity, called the Poisson's ratio (ν), which describes the tissue's compressibility, i.e., how much a small piece of tissue will preserve its volume during deformation (Fung 1981). A value of $\nu=0.5$ indicates total incompressibility, which practically means that a small isotropic cube of tissue that is pressed in one direction, say the x -direction, with an amount of ε_x , will bulge out in the y and z direction with an amount of $\varepsilon_y=\varepsilon_z=-0.5\varepsilon_x$, respectively. When the deformation of tissue is such that there is only strain within a certain plane, say the x - y plane, then $\varepsilon_z=0$ and the tissue is said to be in a '2D plane strain' deformation-state; if additionally $\nu=0.5$ then it follows that $\varepsilon_y=-\varepsilon_x$. Since many biological tissues are nearly incompressible, a ν -value between 0.49-0.5 is often used.

*(An)isotropy,
(non)linearity and
(in)compressibility*

The above equations are appropriate for describing the mechanical behaviour for a one dimensional structure, such as the spring. However, when considering higher dimensional structures, such as vessels, they should be replaced by those shown in Appendix 1. This is because strain, stress and modulus are actually tensors (Fung 1981), which have multiple components, such a radial, circumferential and axial component. It should be realized that a key difference exists between the modulus of tissue and the strain of tissue. Tissue can be mechanically characterized by providing its modulus value, and not by providing a single strain value, since the latter depends on the level of applied stress.

Tissue can be mechanically characterized by its modulus value, but not by a single strain value

PLAQUE MECHANICS

During atherosclerosis, soft material accumulates within the vessel wall and may ultimately lead to a TCFA, which is characterized by a thin fibrous cap covering an eccentric soft lipid pool. This material composition makes them highly rupture-prone. This is due to the following mechanism. The pulsating blood pressure induces a compensatory tensile circumferential stress distribution within the vessel wall. To maintain the connection between mechanically different tissue structures (such as, a soft lipid pool or a stiff fibrous cap) during arterial deformation, relatively soft regions will carry only a fraction of the total circumferential load and the surrounding stiffer material a greater portion (Loree et al. 1992, Richardson et al. 1989). This mechanism causes circumferential stress concentrations in and around the stiff cap, which will rupture if the cap is unable to withstand this stress. This stress will increase when lipid pools soften or increase in size, or when caps stiffen and become thinner (Loree et al. 1992, Richardson et al. 1989). Furthermore, fibrous caps with inflammation by macrophages are weaker than caps without inflammation (Lendon et al. 1991, Moreno et al. 1994), i.e. they tend to rupture at a lower stress than usual; this is because macrophages are cells that reduce the interconnectedness of the stabilizing extracellular matrix.

A TCFA is highly rupture-prone due to its material composition

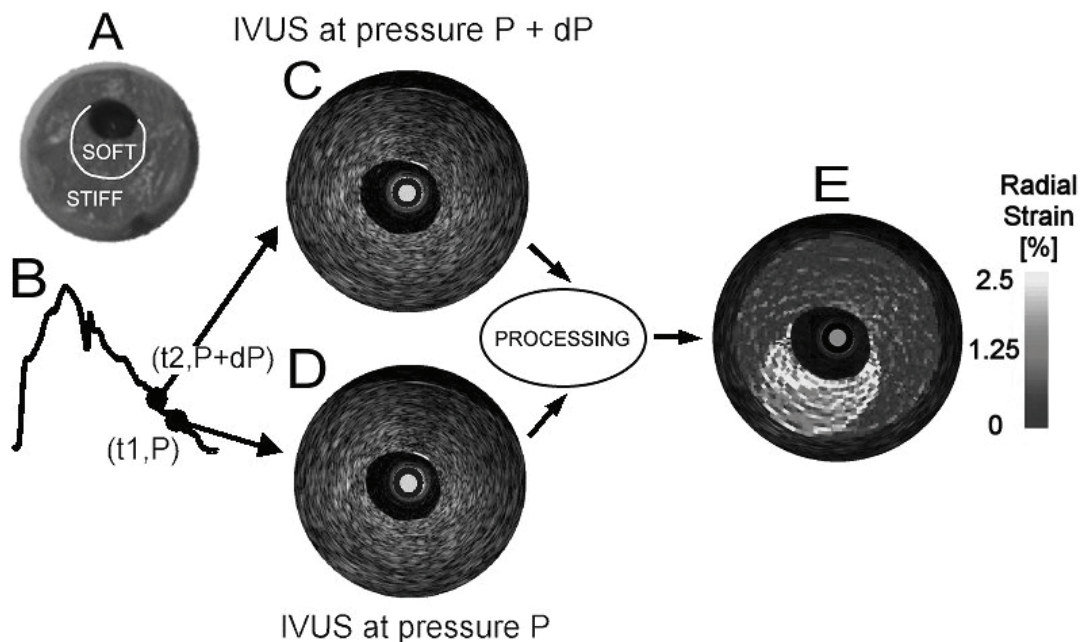


Fig. 5. Principle of intravascular ultrasound (IVUS) strain elastography measurement procedure. An intravascular ultrasound catheter is inserted into an object, in this case a vessel-mimicking phantom with a soft plaque (A). The Young's modulus of the plaque is 4.2 kPa and that of the wall 16.8 kPa. Next, at two different intraluminal pressures (B) an IVUS echogram is acquired (C and D); in this case $dP = 1$ mmHg. In each echogram, the grey circle indicates the catheter-tip of 1.1 mm diameter. Finally, the local deformation (i.e., strain) of the tissue is determined using cross-correlation processing on the acquired IVUS radio-frequency data. This information is plotted as an additional image to the IVUS echogram and called a (strain) elastogram (E). In this example, the eccentric soft plaque of a vessel-mimicking phantom is clearly visible between 4 and 8 o'clock in the elastogram, as a region of high strain, whereas this plaque cannot be identified from the IVUS echograms.

Increased circumferential stress results in increased radial strain of tissue

In general, an increased circumferential stress will result in an increased radial strain of the tissue due to the incompressibility of the tissue (Céspedes et al. 2000). Therefore, elasticity imaging methods that are capable of measuring the radial strain provide information about plaques and its components that may influence clinical decision-making.

MOTIVATION

Elastography

In 1991, Ophir and colleagues developed an elasticity imaging technique called elastography, which is based on quasi-static deformation of a linear elastic, isotropic material (Ophir et al. 1991). The tissue under inspection is deformed by applying stress (i.e., force normalized by area) on a part of its boundary. The resulting distribution of strain depends upon (i) the distribution of the tissue's material properties (Young's modulus and Poisson's ratio) and (ii) the displacement or stress conditions on the tissue boundaries. The resulting strain is determined from local tissue displacements obtained with ultrasound using two pairs of ultrasound signals, one signal obtained before and the other after deformation (Céspedes et al. 1995). The method was initially developed for detection and characterization of tumors in breast. Nowadays, this principle is also applied to many other biological objects, including prostate, kidney, liver, myocardium, skin and superficial arteries (Konofagou 2004).

The mechanical properties of fibrous and fatty plaque components are different

The mechanical properties of fibrous and fatty plaque components are different (Lee et al. 1992, 1994b, Loree et al. 1994a), thus, implementing this method for intravascular purposes has potential to identify the vulnerable plaque by (i) identification of elastically different plaque components and (ii) detection of high radial strain (as surrogate for circumferential stress). Furthermore, in intravascular applications, the arterial deformation is naturally present and is caused by the pulsating blood pressure. User-controlled deformation is also possible by inflating an intravascular balloon (Sarvazyan et al. 1993).

PRINCIPLE

The principle of IVUS strain elastography is illustrated in Fig. 5. An echogram of a vessel-phantom with a stiff wall and a soft eccentric plaque is acquired at a certain intraluminal pressure using an intravascular ultrasound catheter. Notice that there is no difference in echogenicity between the wall and the plaque, which results in a homogeneous echogram. Also a second acquisition at a higher pressure is obtained. The radial strain is processed from the two echograms, as described in the next paragraph. This strain is plotted as a complimentary image to the echogram and is called a (strain) elastogram. The elastogram reveals the presence of an eccentric region with increased strain values, thus identifying the soft eccentric plaque. The differences in strategies to perform IVUS strain elastography/palpography (i.e. assess the local deformation of the tissue) are due to (i) the way of detecting the strain and (ii) the type of source that deforms the vascular tissue (van der Steen et al. 1998).

The principle of IVUS strain palpography is similar to the principle of IVUS strain elastography. There are two minor differences that make palpography faster and more robust and, therefore, more suited for real-time in vivo applications. Firstly, palpography restricts its region of interest to the innermost layer of the arterial wall (first 450 micrometer), making it faster. Secondly, it uses a slightly larger amount of ultrasound signal making it more robust but at the expense of spatial resolution (Céspedes et al. 2000, Doyley et al. 2001). A strain image obtained with IVUS strain palpography is called a (strain) palpogram.

The principle of IVUS strain palpography is similar to the principle of IVUS strain elastography

IMPLEMENTATION

Typically for in vivo IVUS strain elastography/palpography, intraluminal pressure differences in the order of 1-5 mmHg are used. The strain, induced by this pressure differential in coronary tissue is in the order of 2%. This means that a small tissue sample with an initial length of 100 μm will be deformed to 98 μm . To differentiate between strain levels, sub-micron estimation of the tissue displacement is required.

De Korte et al. (1998) incorporated 'correlation-based' elastography (Ophir et al. 1991) for intravascular purposes and this method is called IVUS strain elastography or palpography. The processing-principle of these methods is as follows. The pulsating blood pressure strains the vascular tissue; this strain is calculated from local tissue displacements. These displacements are determined using cross-correlation analysis of the depth-gated RF-signals (Fig. 6). A cross-correlation function between two signals will have its maximum at zero if the signals are not shifted with respect to each other. If a shift between the signals is present, the maximum of the cross-correlation function is found at a position representing the displacement of the tissue. For each angle, the tissue displacement at the boundary between lumen and vessel-wall is determined. Next, the displacement of the tissue at D micrometer from the boundary is determined. The strain of the tissue is then calculated by dividing the differential tissue displacement (displacement of tissue at boundary - displacement of tissue in wall) by the distance between these two locations (=D micrometer). Strain is thus dimensionless and it is common practice to multiply it by 100 to obtain strain values around 1%. Since the strain is determined along the ultrasound beam, i.e., the radial direction, it is actually the 'radial' strain. The strain for each angle is color-coded and plotted as a ring on the IVUS echogram at the inner boundary of the vessel (Céspedes et al. 2000, Doyley et al. 2000, 2001) and this ring is called a (strain) palpogram. If the strain is determined for multiple depths per angle, the strain for the whole vessel-wall cross-section can be constructed; this additional image to the IVUS echogram is called a (strain) elastogram. For palpography, the value for D is approximately 450 micrometers and for elastography approximately 225 micrometers.

IVUS strain elastography/palpography

The used cross-correlation technique is suited for strain values smaller than 2.5%; these values are present during in vivo acquisitions when only a part of the heart cycle is used to strain the tissue (de Korte et al. 1999a). The maximum strain that will be present between the systolic and diastolic pressure is much higher. In that case, another approach that takes into account the change in shape of the signals can be applied. This 'local scaling factor estimation' technique (Alam et al. 1998, Céspedes et al. 1996) has been described for intravascular purposes (Brusseau et al. 2000) and has proven to be more robust to large deformations. The signal after com-

pression is processed as a delayed and scaled replica of the signal before deformation. An adaptive strain estimation method based on the computation of local scaling factors has been applied to compute strain elastograms of cryogel vessel phantoms and of an excised human carotid artery (Brusseau et al. 2001, 2002).

Recently, more groups have started to perform IVUS strain elastography (Choi et al. 2002, Maurice et al. 2005, Perrey et al. 2004, Saijo et al. 2004, Shi et al. 2005, Shiina et al. 2004). Frequently used IVUS catheters are the 20-MHz phased array catheter (Volcano Corporation, Inc., Rancho Cordova, CA, USA) and the 30-MHz mechanically rotating single-element catheter (ClearView, CVIS, Boston Scientific Corp., Watertown, MA, USA).

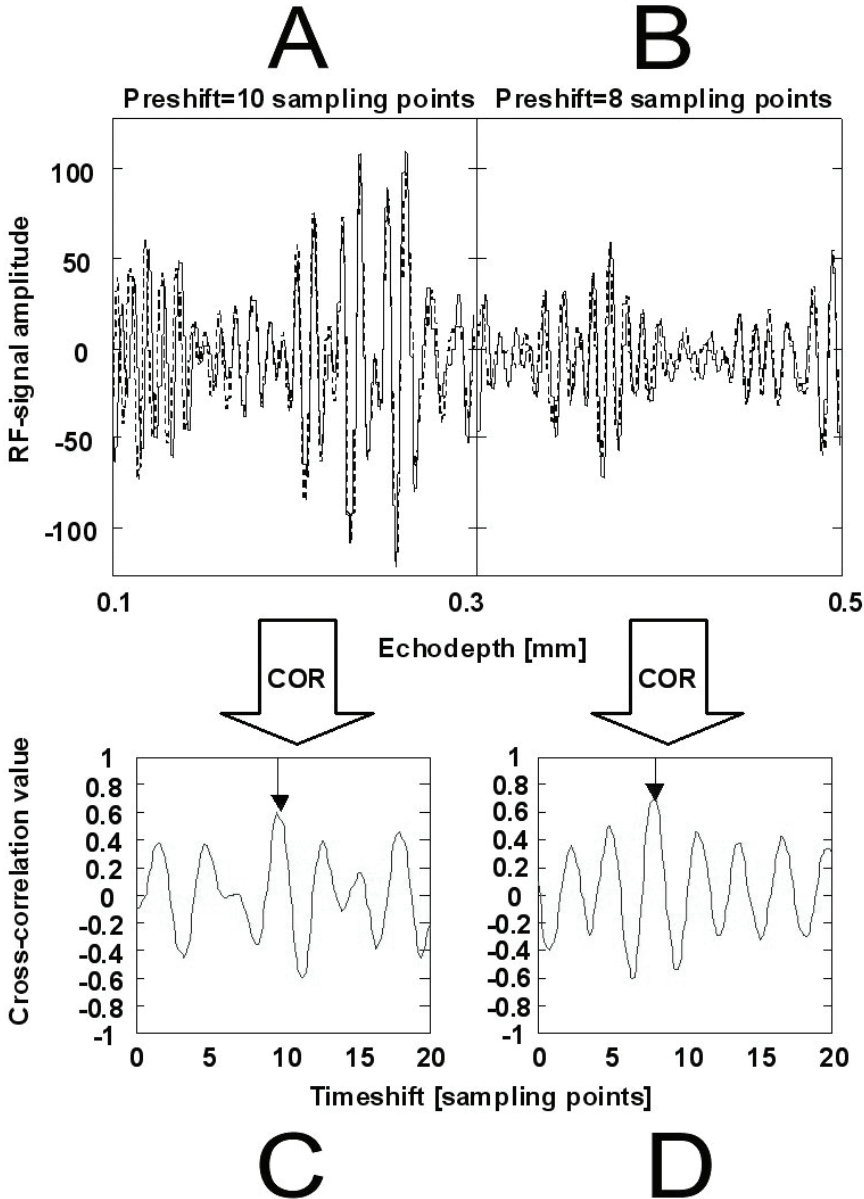


Fig. 6. Principle of displacement (or time delay) estimation using the peak of the cross-correlation coefficient function. In the upper part, two segments (A and B) of the pre-deformation (solid line) and post-deformation (dotted, and pre-shifted for better visual comparison) radio-frequency (RF) signals are shown. Both segments start at a different depths in the tissue. For each segment, the cross-correlation coefficient function between the two signals is computed (C and D). The functions show a decreasing depth (10 and 8 sampling points, respectively) of the peak with increasing echodepth. The difference in peak position represents the differential tissue displacement; normalizing this difference by the distance between the segments, i.e., 0.2 mm, gives the strain of the tissue between 0.2 and 0.4 mm.

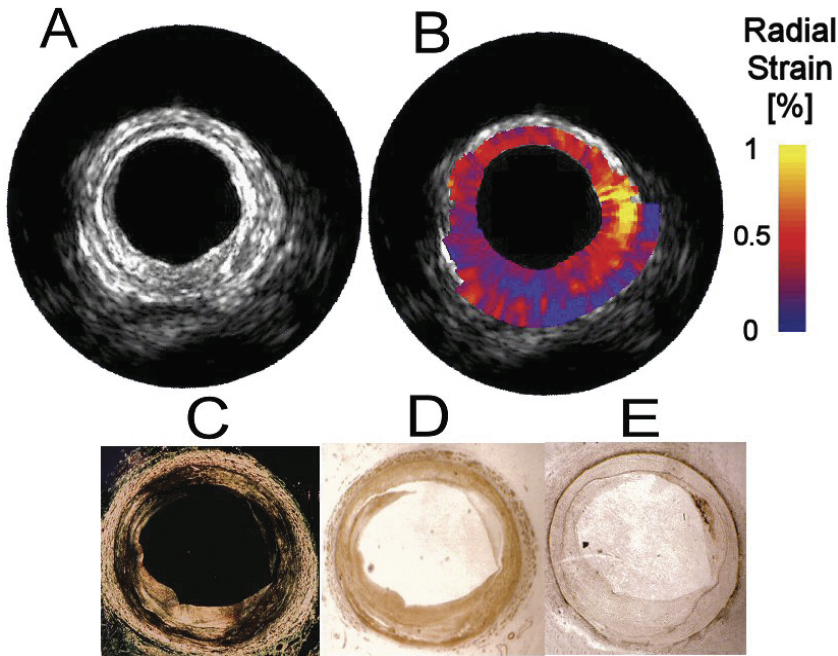


Fig. 7. IVUS strain elastography in vitro of a human femoral artery and corresponding histology. (A) IVUS echogram. (B) IVUS strain elastogram superimposed on the IVUS echogram. Histology: (C) Collagen, (D) Smooth muscle cells and (E) Macrophages. The elastogram reveals that the plaque contains a region of high strain between 1 and 4 o'clock. Histology shows that this region is heavily infiltrated by macrophages and lacks smooth muscle cells and collagen. Furthermore, the remaining plaque region between 4 and 1 o'clock shows low strain and at this region histology reveals that the plaque contains much smooth muscle cells and collagen but no macrophages.

RESULTS

In vitro validations

De Korte et al. (2000) used IVUS strain elastography to performed a validation study on excised human coronary (n=4) and femoral (n=9) arteries (Fig. 7). The results showed that the mean strain value within three plaque component types (fibrous, fibro/fatty and fatty), as determined from histology, differed significantly. This difference was independent on the type of artery (coronary or femoral) and was mainly evident between fibrous and fatty tissue. Furthermore, the plaque types did not reveal significant echo-intensity differences in the IVUS echogram. Since fibrous and fatty tissue resulted in different strain values and high strain values often co-localised with increased concentrations of macrophages, these results revealed the potential for identification of the vulnerable plaque.

Later, Schaar et al. (2003) performed a study on excised human coronary arteries in order to: (i) quantify its predictive value for detecting vulnerable plaques, and (ii) use it for characterizing vulnerable plaque features. In histology, a vulnerable plaque was defined as a plaque consisting of a thin cap (<250 micrometer) with moderate to heavy macrophage infiltration and at least 40% of atheroma. In a radial strain elastogram, a vulnerable plaque was defined as a plaque with a high strain region at the surface with adjacent low strain regions (Fig. 8). 54 cross-sections were studied. In histology, 26 vulnerable plaques and 28 non-vulnerable plaques were found. The sensitivity was 88% and the specificity 89% to detect vulnerable plaques. Linear regression showed significant correlation between the strain in caps and the amount of macrophages and a significant inverse relation between the amount of smooth muscle cells and strain. Plaques, which were declared vulnerable in IVUS strain elastography, had a significantly thinner cap than non-vulnerable plaques.

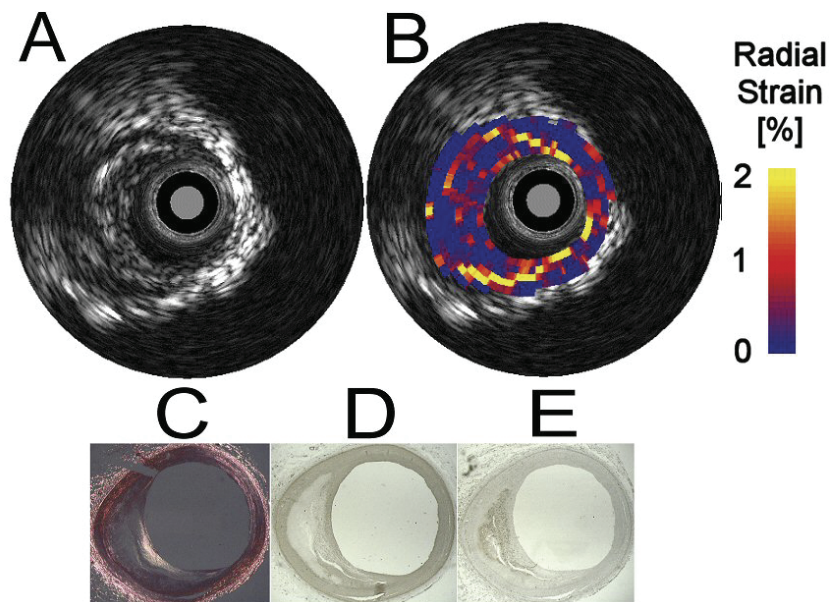


Fig. 8. IVUS strain elastography in vitro of a human coronary artery and corresponding histology. (A) IVUS echogram. (B) IVUS strain elastogram superimposed on the IVUS echogram. Histology: (C) Collagen, (D) Smooth muscle cells and (E) Macrophages. Histology shows that the plaque consists of a homogeneous soft lipid pool covered by a stiff fibrous cap with much collagen and smooth muscle cells. Increased strain is found at both shoulders of the lipid pool. In the IVUS echogram, the grey circle defines the catheter-tip of 1.1 mm diameter and the black circle removes part of the catheter ringdown diameter 2 mm.

This study showed that IVUS strain elastography has a high sensitivity and specificity to detect human vulnerable plaques in vitro and that strain in caps had a high correlation with vulnerable plaque features.

In vivo applications

In vivo animal studies with IVUS strain elastography were also performed (de Korte et al. 2002b); they verified the main findings of previous in vitro results. In vivo patient studies showed the difficulties and feasibility of IVUS strain elastography in vivo. It was applied to patients (n=12) during percutaneous transluminal coronary angioplasty (PTCA) procedures. Tissue was strained by the pulsatile blood pressure.

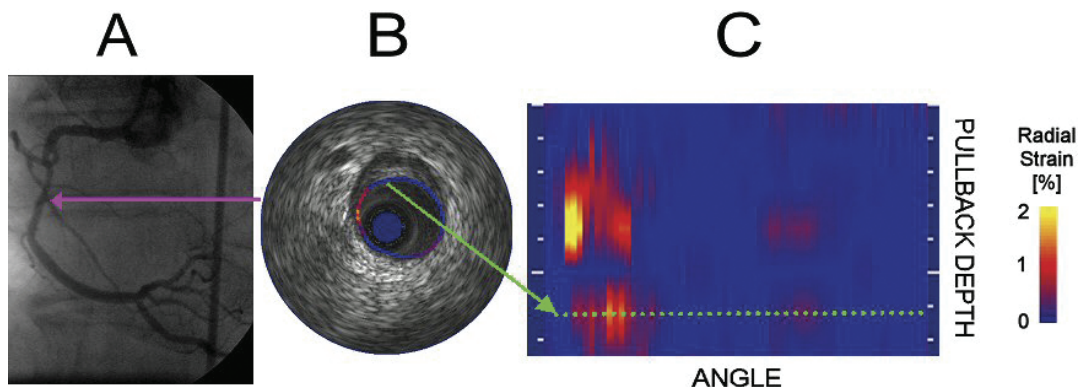


Fig. 9. 3D IVUS strain palpography of a patient in vivo. (A) Angiogram of the right coronary artery. (B) 2D IVUS strain palpogram superimposed on the IVUS echogram, which was taken at the location indicated by purple arrow in A. The echogram shows an eccentric plaque and the high strain regions with adjacent low strains at the shoulders of this plaque suggest that it is vulnerable. (C) A map of multiple 2D IVUS strain palpograms stacked after each other. The green dotted line corresponds to the palpogram shown in B. This map provides an overview of the deformability of the inner layer of the arterial wall.

This strain was determined using cross-correlation analysis of sequential radio-frequency frames. A likelihood function was computed to identify the frames corresponding to a minimal motion of the catheter in the lumen, since motion of the catheter prevents reliable strain estimation (Leung et al. 2005). Minimal motion was observed near end-diastole. Reproducible strain estimates were obtained within one cardiac cycle and over several cardiac cycles. Validation of the results was limited to the information provided by the echogram. Strain in calcified material, as identified from the echogram was significantly lower than in non-calcified tissue. The elastogram of stented plaques revealed very low strain values, except for two regions: these are between the stent struts and at the shoulders of the plaque.

Recently, Schaar et al. (2004b) used 3D IVUS strain palpography (Schaar et al. 2005) in patients undergoing percutaneous intervention to assess the incidence of a specific high-strain pattern, which has shown in vitro to have a high sensitivity and specificity for detecting the thin-cap fibroatheroma. Furthermore they explored the relation of such patterns to clinical presentation and to C-reactive protein levels. 3D strain palpograms were derived from continuous IVUS pullbacks through arteries (Fig. 9). Patients (n=55) were classified by clinical presentation as stable angina, unstable angina, or acute myocardial infarction (MI). In every patient one coronary artery was scanned (culprit vessel in stable and unstable angina, non-culprit vessel in acute MI) and the number of plaques with a vulnerable-plaque-specific strain pattern were assessed. Stable angina patients had significantly less deformable plaques per vessel (0.6 ± 0.6) than unstable angina ($p=0.0019$) patients (1.6 ± 0.7) or acute MI ($p<0.0001$) patients (2.0 ± 0.7). Levels of C-reactive protein were positively correlated with the number of mechanically deformable plaques ($R^2=0.65$, $p<0.0001$). The main conclusion was that 3D IVUS palpography detects vulnerable-plaque-specific strain patterns in human coronary arteries that correlated both with clinical presentation and levels of C-reactive protein.

MODULUS ELASTOGRAPHY

MOTIVATION

IVUS strain elastography/palpography has proven to be a valuable, clinically available tool that can be used to survey the coronary vessels and identify possible rupture-prone plaques by measuring the plaque's radial strain distribution (de Korte et al. 2000, de Korte et al. 2002b, Schaar et al. 2003, Schaar et al. 2004b, Schaar et al. 2005).

However, a strain elastogram (and also a strain palpogram) cannot be interpreted directly as a morphology and material composition image of a plaque, since there is no one-to-one relation between the local radial strain value in a strain elastogram and the local plaque component type (calcified, fibrous, fatty or tissue weakened by macrophage-inflammation). The underlying reason for this, is that the stresses that induce local strain depend upon the structural build-up of the artery, the stiffness (i.e., Young's modulus) and geometry of its plaque components; furthermore, the radial component of the strain depends upon the catheter position used during imaging (de Korte et al. 1999b, Ophir et al. 1996). Fig. 8 exemplifies this. Histology shows a TCFA that consist of a soft homogeneous lipid pool covered by a stiff fibrous cap. Because the lipid pool is soft and homogenous, one would expect high radial strain throughout the same region in the IVUS strain elastogram. However, due to the relatively stiff cap and its circumferential geometry, the stress is redirected away from the soft lipid pool, towards the cap. This results in low-strain at the center of the pool and stress concentrations (with corresponding high strain) near the shoulders of the lipid pool (Richardson et al. 1989).

To overcome this limitation, one could image the Young's modulus distribution of a plaque. In general, modulus elastography is the name for methods that compute a Young's modulus image (called a modulogram) from a strain (or displacement) image. By definition, the Young's modulus of soft tissue (e.g., lipid pool) is low and of stiff tissue (e.g., media or fibrous cap) high. There are three main reasons for performing modulus elastography: (i) tissue characterization: a modulogram can be

A strain elastogram cannot be interpreted directly as a morphology and material composition image of a plaque

The Young's modulus of soft tissue is low and that of stiff tissue is high

interpreted as a material composition image because there is large difference between the Young's moduli of various tissue components, including plaque components (Salunke et al. 1997), (ii) independence: a modulogram shows the modulus of tissue, which is a material property and, therefore, the appearance of the modulogram is independent of the geometry of tissue components and applied pressure, in contrast to strain, (iii) properties (i) and (ii) allow monitoring of atherosclerosis, which is vital for quantifying the efficiency of plaque-stabilizing pharmaceutical drugs that induce mechanical stabilization of plaques, e.g., by stiffening or reducing plaque atheroma (Aikawa et al. 1998, Lee 2000, Loree et al. 1994b).

PROBLEM STATEMENT

Ultrasound modulus elastography

Ultrasound modulus elastography solves a problem (i.e. compute a modulus from measured ultrasound) that can be classified as a parameter identification problem or inverse problem, which is present in almost every existing field of science and engineering (Dulikravich et al. 1999). In general, this problem can be formulated as follows: Given an adequate input-output description/model of a (real-life) system, compute some desired model parameters from a limited amount of data measured from the system.

For example, the real-life system might be a 3D or 2D segment of an arterial wall. The measured data can be the radial strain assessed with IVUS strain elastography. The input-output model can be a computer model that calculates as output the radial strain distribution of the segment; consequently the computer model's 'input parameters' are the geometry of the segment, the blood pressure at lumen boundary and the material properties of the wall, e.g., the Young's modulus and Poisson's ratio distribution. The desired model parameter (distribution) can be the Young's modulus distribution.

Existence, uniqueness and continuity

For practical applications the solutions to an inverse problem should satisfy the following criteria (i) existence and uniqueness; there is only one set of the desired model parameters that result in/correspond to the measurements. (ii) continuity; a slight change in the measurements (e.g. due to noise) corresponds to a slight change in the corresponding desired model parameters.

IMPLEMENTATION

General approach

The general approach to perform ultrasound modulus elastography is to firstly use ultrasound displacement/strain elastography to measure one or more components of the displacement vector and/or strain components of the deformed tissue. Next, a deformation model for computing the deformation, strain and/or stress of tissue is defined (Appendix A). This model consists of (i) a set of mathematical (partial differential) equations that describe the equilibrium of tissue, (ii) the relation between displacement and strain of tissue and, finally (iii) the constitutive equation, which defines the relation between stress and strain of tissue (Fung 1993). Many researchers approximate the behaviour of biological tissue by a linear, isotropic, nearly incompressible (Poisson's ratio > 0.49) elastic material. In those cases, the constitutive relation contains only one material parameter, namely the Young's modulus. Finally, the deformation model and the measured displacement/strain components are used to compute the modulogram by a 'direct reconstruction approach' or by an 'iterative reconstruction approach'.

Direct approach

In the direct approach the measured displacement/strain data are plugged in the deformation equations, which are mathematically manipulated so that the moduli can be considered and expressed as the unknowns. Next, the moduli are computed using a discretization (Raghavan et al. 1994) or numerical integration of the manipulated deformation equations (Skovoroda et al. 1995, Sumi et al. 1995).

Iterative approach

In the iterative approach, the deformation model is treated as a finite element (computer) model (FEM). The FEM fills the space of the tissue with a mesh that consists of small discrete (finite) elements (e.g. triangles, bricks) and each element is given a constitutive relation, i.e. Young's modulus. Next, an initial modulus value for each element defined. Finally, the modulus value of each individual mesh element or groups of mesh elements in the FEM are iteratively changed such that the computed FEM deformation output eventually resembles the measured deformation (displace-

ment or strain data). This matching is fully automatic performed by a minimization algorithm (Kallel et al. 1996).

Much research has focussed on applying these two approaches on non-vascular tissue geometries such as a breast, brain, heart or a cross-section of a homogeneous rectangular medium with a circular or rectangular inclusion. To date, only a few groups have investigated modulus elastography for vascular geometries. Most of them used an adjusted iterative reconstruction method (Beattie et al. 1998, Chandran et al. 2003, Soualmi et al. 1997, Vorp et al. 1995, Wan et al. 2001), some others an adjusted direct reconstruction method (Bank 1999, Kanai et al. 2003).

DIFFICULTIES

All these groups encountered difficulties in computing a modulus elastogram (related to uniqueness and continuity), which may be caused by noisy measurements, a limited number of measured displacement/strain components, type of boundary data (Barbone et al. 2002), using an inadequate deformation model for the tissue, converging to non-optimal local minima by the minimization algorithm. When using a single deformation (strain or displacement) field, the general, unconstrained, inverse elasticity problem in 2D is ill-posed (Barbone et al. 2002, 2004). This means, that either there doesn't exist a unique modulus elastogram that underlies a measured deformation elastogram, or (ii) there does exist a unique modulus elastogram, but this cannot be stably obtained due to aforementioned reasons.

Currently, IVUS strain elastography is the only validated, clinically available technique that provides coronary strain elastograms in vivo (de Korte et al. 2001, 2002a, 2003). Solving the inverse elasticity problem for coronary plaques using in vivo IVUS-derived local deformation (strain or displacement) is a different and difficult task, when compared with the inverse elasticity problem for other organs, such as the breast (Céspedes et al. 1993), where user-controlled, non-invasive, ultrasound-derived deformation can be used. This is because (i) plaques have a complex, heterogeneous material composition, (ii) there is an inherent decay of deformation from the lumen towards the media border, due to the inherent stress decay that is caused by the circumferential geometry of the vessel wall; along the decay direction, the signal-to-noise ratio of the measured deformation decreases, (iii) there is no control of the primary deformation source (pulsating intracoronary blood) and measurement device (catheter), which limits the applicability of available deformation-processing methods that utilize control of the source and device, (iv) with the currently used deformation processing algorithm (de Korte et al. 1998) only the radial component of the strain is measured, with a spatial resolution of merely 200 μm .

MODULOGRAPHY

None of the aforementioned modulus elastography approaches for vessels have been shown to work when using the cross-sectional radial strain distribution of an arbitrary heterogeneous atherosclerotic coronary plaque. To have a method that does works on in vivo strain data measured with IVUS elastography/palpography would mean that investigators will, finally, have an all-in-one modality that can (i) detect vulnerable plaques (Schaar et al. 2004b), (ii) assess information related to their rupture-proneness and (Schaar et al. 2003) (iii) image their elastic material composition, all in vivo.

Stimulated by this prospect and by the results of previous approaches, we developed a new approach, called Modulography (a concatenation of 'modulus' and 'graphy'), especially suited for solving the inverse elasticity problem using in vivo measured strain of coronary plaques. Compared with other approaches, our approach has two key differences (i) it uses as much as possible a priori plaque information that can be automatically derived from the echogram and strain elastogram and (ii) it, initially, focussed on the largest class of vulnerable plaques, namely the thin-cap fibroatheromas (TCFAs), which can be modelled as a geometrically simple structure. By using this a priori information, the inverse elasticity problem was geometrically constrained in such a way that a practically useful and more or less unique modulogram could be obtained in vivo in a stable manner.

The development of Modulography began by first solving the forward elasticity problem, then the inverse elasticity problem for TCFAs, and finally, making gener-

Difficulties in computing a modulus elastogram

Solving the inverse elasticity problem for coronary plaques, using in vivo IVUS-derived local deformation, is a difficult task

Modulography (a concatenation of 'modulus' and 'graphy')

alizations to our solution-approach for TCFAs, in order to allow local elasticity imaging of arbitrary plaques.

OUTLINE OF THE THESIS

- Aim of this thesis* The aim of the research described in this thesis was to develop an inverse method that automatically reconstructs the local elasticity (i.e., Young's modulus) of atherosclerotic coronary arteries from intravascular ultrasound-based radial strain measurements.
- Solve the forward elasticity problem* First, the forward elasticity problem (i.e., compute the radial strain distribution from a given Young's modulus (YM) distribution) was solved. To this end, a computer deformation model was developed that describes the measured radial strain of pressurized atherosclerotic arteries (**CHAPTER 2**). Next, this model was used to study how the measured radial strain of atherosclerotic arteries depends upon the plaque components' geometry, plaque components' material properties and the catheter position (**CHAPTER 3**).
- Solve the inverse elasticity problem for TCFAs* Having solved the forward elasticity problem, we proceed towards solving the inverse elasticity problem (i.e., find 'the' YM distribution from a given radial strain distribution) for thin-cap fibroatheroma (TCFA) plaques. To this end, a circular TCFA plaque model was developed that, in combination with the deformation model from chapter two, allowed the reconstruction of the YM distribution of TCFAs from their measured radial strain (**CHAPTER 4**). The robustness of this approach was investigated using computer-simulated TCFAs (**CHAPTER 5**).
- Solve the inverse elasticity problem for arbitrary atherosclerotic coronary arteries* Finally, we tackled the inverse elasticity problem for arbitrary atherosclerotic coronary arteries. To this end, a deformable plaque model was developed, which allowed YM reconstruction of arbitrarily shaped plaque components from their measured radial strain (**CHAPTER 6**). Next, this deformable plaque model was used in combination with (i) a procedure to approximate principal strain from measured radial strain, (ii) a strain-based YM-initialization procedure and (iii) a YM compounding procedure, to allow (local) YM-reconstruction of arbitrary atherosclerotic coronary arteries from their measured radial strain (**CHAPTER 7**).

REFERENCES OF INTRODUCTION

- Aikawa M, Rabkin E, Okada Y, Voglic SJ, Clinton SK, Brinckerhoff CE, Sukhova GK, Libby P. *Lipid lowering by diet reduces matrix metalloproteinase activity and increases collagen content of rabbit atheroma: a potential mechanism of lesion stabilization*. *Circulation* 1998;97:2433-44.
- Alam S, Ophir J, Konofagou E. *An adaptive strain estimator for elastography*. *IEEE trans UFFC* 1998;45:461-72.
- Aoki J, Rodriguez-Granillo GA, Serruys PW. *Emergent strategies in interventional cardiology*. *Rev Esp Cardiol* 2005;58:962-73.
- Arroyo LH, Lee RT. *Mechanisms of plaque rupture: mechanical and biologic interactions*. *Cardiovasc Res* 1999;41:369-75.
- Bank AJ. *Intravascular ultrasound studies of arterial elastic mechanics*. *Pathol Biol (Paris)* 1999;47:731-7.
- Barbone PE, Bamber JC. *Quantitative elasticity imaging: what can and cannot be inferred from strain images*. *Phys Med Biol* 2002;47:2147-64.
- Barbone PE, Gokhale NH. *Elastic modulus imaging: on the uniqueness and nonuniqueness of the elastography inverse problem in two dimensions*. *Inverse Problems* 2004;20:283-96.
- Beattie D, Xu C, Vito R, Glagov S, Whang MC. *Mechanical analysis of heterogeneous, atherosclerotic human aorta*. *J Biomech Eng* 1998;120:602-7.
- Bom N, Lancée CT, van Egmond FC. *An ultrasonic intracardiac scanner*. *Ultrasonics* 1972;10:72-6.
- Bom N, ten Hoff H, Lancee CT, Gussenhoven WJ, Bosch JG. *Early and recent intraluminal ultrasound devices*. *Int J Card Imaging* 1989;4:79-88.
- Brezinski ME. *Optical coherence tomography for identifying unstable coronary plaque*. *Int J Cardiol* 2005;
- Bridal SL, Fornes P, Bruneval P, Berger G. *Parametric (integrated backscatter and attenuation) images constructed using backscattered radio frequency signals (25-56 MHz) from human aortae in vitro*. *Ultrasound Med Biol* 1997;23:215-29.
- Brusseau E, Fromageau J, Finet G, Delachartre P, Vray D. *Axial strain imaging of intravascular data: results on polyvinyl alcohol cryogel phantoms and carotid artery*. *Ultrasound Med Biol* 2001;27:1631-42.
- Brusseau E, Fromageau J, Rognin NG, Delachartre P, Vray D. *Investigating elastic properties of soft biological tissues*. *IEEE Eng Med Biol Mag* 2002;21:86-94.
- Brusseau E, Perrey C, Delachartre P, Vogt M, Vray D, Ermert H. *Axial strain imaging using a local estimation of the scaling factor from RF ultrasound signals*. *Ultras Imag* 2000;22:95-107.
- Buschman HP, Motz JT, Deinum G, Romer TJ, Fitzmaurice M, Kramer JR, van der Laarse A, Brusckhe AV, Feld MS. *Diagnosis of human coronary atherosclerosis by morphology-based Raman spectroscopy*. *Cardiovasc Pathol* 2001;10:59-68.
- Casscells W, Hathorn B, David M, Krabach T, Vaughn WK, McAllister HA, Bearman G, Willerson JT. *Thermal detection of cellular infiltrates in living atherosclerotic plaques: possible implications for plaque rupture and thrombosis*. *Lancet* 1996;347:1447-51.
- Céspedes EI, de Korte CL, van der Steen AFW. *Crossambiguity and wavelet processing in ultrasound elasticity imaging*. *Proceedings of the 1996 IEEE Ultrasonics Symposium* 1996;2:1135-8.
- Céspedes EI, de Korte CL, van der Steen AFW. *Intraluminal ultrasonic palpation: assessment of local and cross-sectional tissue stiffness*. *Ultrasound in Med. & Biol.* 2000;26:385-96.
- Céspedes EI, Huang Y, Ophir J, Spratt S. *Methods for estimation of subsample time delays of digitized echo signals*. *Ultras Imag* 1995;17:142-71.
- Céspedes EI, Ophir J, Ponnekanti H, Maklad N. *Elastography: elasticity imaging using ultrasound with application to muscle and breast in vivo*. *Ultras Imag* 1993;17:73-88.
- Chandran KB, Mun JH, Choi KK, Chen JS, Hamilton A, Nagaraj A, McPherson DD. *A method for in-vivo analysis for regional arterial wall material property alterations with atherosclerosis: preliminary results*. *Med Eng Phys* 2003;25:289-98.
- Choi CD, Skovoroda AR, Emelianov SY, O'Donnell M. *An integrated compliant balloon ultrasound catheter for intravascular strain imaging*. *IEEE Trans Ultrason Ferroelectr Freq Control* 2002;49:1552-60.
- Davies MJ. *The pathophysiology of acute coronary syndromes*. *Heart* 2000;83:361-6.
- de Korte CL. *PhD thesis: Intravascular ultrasound elastography*. Erasmus University Rotterdam, ISBN:90-9012664-3, 1999;

- de Korte CL, Carlier SG, Mastik F, Doyley MM, van der Steen AFW, Céspedes EI, Serruys PW, Bom N. *Intracoronary elastography in the catheterisation laboratory: preliminary patient results*. Proceedings of the 1999 IEEE Ultrasonics Symposium 1999a;1649-52.
- de Korte CL, Carlier SG, Mastik F, Doyley MM, van der Steen AFW, Serruys PW, Bom N. *Morphological and mechanical information of coronary arteries obtained with Intravascular elastography: a feasibility study in vivo*. European Heart Journal 2002a;23:405-13.
- de Korte CL, Céspedes EI, van der Steen AFW. *Influence of catheter position on estimated strain in intravascular elastography*. IEEE Trans Ultrason Ferroelectr Freq Control 1999b;46:616-25.
- de Korte CL, Pasterkamp G, van der Steen AFW, Woutman HA, Bom N. *Characterization of plaque components using intravascular ultrasound elastography in human femoral and coronary arteries in vitro*. Circulation 2000;102:617-23.
- de Korte CL, Schaar JA, Mastik F, Serruys PW, van der Steen AFW. *Intravascular elastography: from bench to bedside*. J Interv Cardiol 2003;16:253-9.
- de Korte CL, Siervogel M, Mastik F, Strijder C, Velema E, Pasterkamp G, van der Steen AFW. *Intravascular Elastography in Yucatan pigs: validation in vivo*. European Heart Journal 2001;22:251.
- de Korte CL, Siervogel MJ, Mastik F, Strijder C, Schaar JA, Velema E, Pasterkamp G, Serruys PW, van der Steen AFW. *Identification of atherosclerotic plaque components with intravascular ultrasound elastography in vivo: a Yucatan pig study*. Circulation 2002b;105:1627-30.
- de Korte CL, van der Steen AFW, Céspedes EI, Pasterkamp G. *Intravascular ultrasound elastography of human arteries: initial experience in vitro*. Ultrasound Med Biol 1998;24:401-8.
- Diamantopoulos L. *Arterial wall thermography*. J Interv Cardiol 2003;16:261-6.
- Dobrin PB. *Mechanical properties of arteries*. Physiol Rev 1978;58:397-460.
- Doyley M, Mastik F, de Korte CL, Carlier S, Céspedes E, Serruys P, Bom N, van der Steen AFW. *Advancing intravascular ultrasonic palpation towards clinical applications*. Ultrasound Med Biol 2001;27:1471-80.
- Falk E, Shah PK, Fuster V. *Coronary plaque disruption*. Circulation 1995;92:657-71.
- Farrar CT, Wedeen VJ, Ackerman JL. *Cylindrical meanderline radiofrequency coil for intravascular magnetic resonance studies of atherosclerotic plaque*. Magn Reson Med 2005;53:226-30.
- Fung YC, *Biomechanics: Mechanical properties of living tissue*. New York, USA: Springer, 1981.
- Fung YC, *Biomechanics: Mechanical properties of living tissues*, 2nd ed. New York: Springer-Verlag, 1993.
- Hiro T, Fujii T, Yasumoto K, Murata T, Murashige A, Matsuzaki M. *Detection of fibrous cap in atherosclerotic plaque by intravascular ultrasound by use of color mapping of angle-dependent echo-intensity variation*. Circulation 2001;103:1206-11.
- Itoh A, Miyazaki S, Nonogi H, Daikoku S, Haze K. *Angioscopic prediction of successful dilatation and of restenosis in percutaneous transluminal coronary angioplasty. Significance of yellow plaque*. Circulation 1995;91:1389-96.
- Jang IK, Tearney GJ, MacNeill B et al. *In vivo characterization of coronary atherosclerotic plaque by use of optical coherence tomography*. Circulation 2005;111:1551-5.
- Kallel F, Bertrand M. *Tissue elasticity reconstruction using linear perturbation method*. IEEE Trans Med Imaging 1996;15:299-313.
- Kanai H, Hasegawa H, Ichiki M, Tezuka F, Koiwa Y. *Elasticity imaging of atheroma with transcutaneous ultrasound: preliminary study*. Circulation 2003;107:3018-21.
- Kawasaki M, Takatsu H, Noda T et al. *In vivo quantitative tissue characterization of human coronary arterial plaques by use of integrated backscatter intravascular ultrasound and comparison with angioscopic findings*. Circulation 2002;105:2487-92.
- Komiyama N, Berry G, Kolz M et al. *Tissue characterization of atherosclerotic plaques by intravascular ultrasound radiofrequency signal analysis: An in vitro study of human coronary arteries*. American Heart Journal 2000;140:565-74.
- Konofagou EE. *Quo vadis elasticity imaging?* Ultrasonics 2004;42:331-6.
- Krams R, Verheye S, van Damme LC et al. *In vivo temperature heterogeneity is associated with plaque regions of increased MMP-9 activity*. Eur Heart J 2005;26:2200-5.
- Larose E, Yeghiazarians Y, Libby P et al. *Characterization of human atherosclerotic plaques by intravascular magnetic resonance imaging*. Circulation 2005;112:2324-31.
- Lee RT. *Plaque stabilization: the role of lipid lowering*. Int J Cardiol 2000;74 Suppl 1:S11-5.

- Lee RT, Richardson G, Loree HM, Gordzinsky AJ, Gharib SA, Schoen FJ, Pandian N. *Prediction of mechanical properties of human atherosclerotic tissue by high-frequency intravascular ultrasound imaging*. *Arterioscler Thromb* 1992;12:1-5.
- Leiner T, Gerretsen S, Botnar R, Lutgens E, Cappendijk V, Kooi E, van Engelshoven J. *Magnetic resonance imaging of atherosclerosis*. *Eur Radiol* 2005;15:1087-99.
- Lendon CL, Davies MJ, Born GVR, Richardson PD. *Atherosclerotic plaque caps are locally weakened when macrophage density is increased*. *Atherosclerosis* 1991;87:87-90.
- Leung KYE, Baldewsing RA, Mastik F, Schaar JA, Gisolf A, van der Steen AFW. *Motion Compensation for Intravascular Ultrasound Palpography*. *IEEE Trans Ultrason Ferroelectr Freq Control* 2005;(in press):
- Libby P. *Current concepts of the pathogenesis of the acute coronary syndromes*. *Circulation* 2001;104:365-72.
- Loree HM, Grodzinsky AJ, Park SY, Gibson LJ, Lee RT. *Static circumferential tangential modulus of human atherosclerotic tissue*. *J Biomech* 1994a;27:195-204.
- Loree HM, Kamm RD, Stringfellow RG, Lee RT. *Effects of fibrous cap thickness on peak circumferential stress in model atherosclerotic vessels*. *Circ Res* 1992;71:850-8.
- Loree HM, Tobias BJ, Gibson LJ, Kamm RD, Small DM, Lee RT. *Mechanical properties of model atherosclerotic lesion lipid pools*. *Arterioscler Thromb* 1994b;14:230-4.
- Lusis AJ. *Atherosclerosis*. *Nature* 2000;407:233-41.
- MacIsaac AI, Thomas JD, Topol EJ. *Toward the quiescent coronary plaque*. *J Am Coll Cardiol* 1993;22:1228-41.
- MacNeill BD, Bouma BE, Yabushita H, Jang IK, Tearney GJ. *Intravascular optical coherence tomography: cellular imaging*. *J Nucl Cardiol* 2005;12:460-5.
- Maurice RL, Brusseau E, Finet G, Cloutier G. *On the potential of the Lagrangian speckle model estimator to characterize atherosclerotic plaques in endovascular elastography: in vitro experiments using an excised human carotid artery*. *Ultrasound Med Biol* 2005;31:85-91.
- Moreno PR, Falk E, Palacios IF, Newell JB, Fuster V, Fallon JT. *Macrophage infiltration in acute coronary syndromes. Implications for plaque rupture*. *Circulation* 1994;90:775-8.
- Moreno PR, Lodder RA, Purushothaman KR, Charash WE, O'Connor WN, Muller JE. *Detection of lipid pool, thin fibrous cap, and inflammatory cells in human aortic atherosclerotic plaques by near-infrared spectroscopy*. *Circulation* 2002;105:923-7.
- Moreno PR, Muller JE. *Detection of high-risk atherosclerotic coronary plaques by intravascular spectroscopy*. *J Interv Cardiol* 2003;16:243-52.
- Morice MC, Serruys PW, Sousa JE et al. *A randomized comparison of a sirolimus-eluting stent with a standard stent for coronary revascularization*. *N Engl J Med* 2002;346:1773-80.
- Murashige A, Hiro T, Fujii T, Imoto K, Murata T, Fukumoto Y, Matsuzaki M. *Detection of lipid-laden atherosclerotic plaque by wavelet analysis of radiofrequency intravascular ultrasound signals: in vitro validation and preliminary in vivo application*. *J Am Coll Cardiol* 2005;45:1954-60.
- Nair A, Kuban BD, Tuzcu EM, Schoenhagen P, Nissen SE, Vince DG. *Coronary plaque classification with intravascular ultrasound radiofrequency data analysis*. *Circulation* 2002;106:2200-6.
- O'Donnell M, Eberle MJ, Stephens DN, Litzza JL, San Vicente K, Shapo BM. *Synthetic phase arrays for intraluminal imaging of coronary arteries*. *IEEE trans UFFC* 1997;44:714-21.
- Ong AT, Serruys PW. *Technology Insight: an overview of research in drug-eluting stents*. *Nat Clin Pract Cardiovasc Med* 2005;2:647-58.
- Ophir J, Céspedes EI, Garra B, Ponnekanti H, Huang Y, Maklad N. *Elastography: ultrasonic imaging of tissue strain and elastic modulus in vivo*. *Eur J Ultrasound* 1996;3:49-70.
- Ophir J, Céspedes I, Ponnekanti H, Yazdi Y, Li X. *Elastography: a quantitative method for imaging the elasticity of biological tissues*. *Ultras Imag* 1991;13:111-34.
- Perrey C, Bojara W, Holt S, Lindstaedt M, Ermert H. *Intravascular ultrasound strain imaging with rotating single element transducer: initial in vivo experiments*. *Proceedings of the Second International Conference on the Ultrasonic Measurement and Imaging of Tissue Elasticity* 2004;49-.
- Prati F, Arbustini E, Labellarte A, Bello BD, Sommariva L, Mallus MT, Pagano A, Boccanelli A. *Correlation between high frequency intravascular ultrasound and histomorphology in human coronary arteries*. *Heart* 2001;85:567-70.
- Raghavan KR, Yagle AE. *Forward and inverse problems in elasticity imaging of soft tissues*. *Transactions on Nuclear Science* 1994;41:1639-48.

- Richardson PD, Davies MJ, Born GVR. *Influence of plaque configuration and stress distribution on fissuring of coronary atherosclerotic plaques*. The Lancet 1989;2:941-4.
- Saijo Y, Tanaka A, Owada N, Akino Y, Nitta S. *Tissue velocity imaging of coronary artery by rotating-type intravascular ultrasound*. Ultrasonics 2004;42:753-7.
- Saijo Y, van der Steen AFW. *Vascular ultrasound*. Springer, 2003, ISBN:4-431-70328-4.
- Salunke NV, Topoleski LD. *Biomechanics of atherosclerotic plaque*. Crit Rev Biomed Eng 1997;25:243-85.
- Sarvazyan AP, Emelianov SY, Skovorada AR. *Intracavity device for elasticity imaging*. US patent 5,265,612, November 30, 1993;
- Schaar JA. *PhD thesis: Palpography*. Erasmus University Rotterdam, ISBN:90-8559-064-7, 2005;
- Schaar JA, De Korte CL, Mastik F, Strijder C, Pasterkamp G, Boersma E, Serruys PW, Van Der Steen AFW. *Characterizing vulnerable plaque features with intravascular elastography*. Circulation 2003;108:2636-41.
- Schaar JA, de Korte CL, Mastik F, van Damme LC, Krams R, Serruys PW, van der Steen AFW. *Three-dimensional palpography of human coronary arteries*. Herz 2005;30:125-33.
- Schaar JA, Muller JE, Falk E et al. *Terminology for high-risk and vulnerable coronary artery plaques. Report of a meeting on the vulnerable plaque, June 17 and 18, 2003, Santorini, Greece*. Eur Heart J 2004a;25:1077-82.
- Schaar JA, Regar E, Mastik F et al. *Incidence of vulnerable plaque patterns in humans: assessment with three-dimensional intravascular palpography and correlation with clinical presentation*. Circulation 2004b;109:2716-9.
- Shi Y, Witte RS, O'Donnell M. *Identification of vulnerable atherosclerotic plaque using IVUS-based thermal strain imaging*. IEEE Trans Ultrason Ferroelectr Freq Control 2005;52:844-50.
- Shiina T, Nitta N, Yamagishi M. *Characterization of Vulnerable Coronary Plaque by Strain Power Image*. Proceedings of the Third International Conference on the Ultrasonic Measurement and Imaging of Tissue Elasticity 2004;83.
- Skovorada AR, Emelianov SY, O'Donnell M. *Tissue elasticity reconstruction based on ultrasonic displacement and strain images*. IEEE Trans Ultrason Ferroelectr Freq Control 1995;42:747-65.
- Slager CJ, Essed CE, Schuurbiens JC, Bom N, Serruys PW, Meester GT. *Vaporization of atherosclerotic plaques by spark erosion*. J Am Coll Cardiol 1985;5:1382-6.
- Spencer T, Ramo MP, Salter DM, Anderson T, Kearney PP, Sutherland GR, Fox KA, McDicken WN. *Characterisation of atherosclerotic plaque by spectral analysis of intravascular ultrasound: an in vitro methodology*. Ultrasound Med Biol 1997;23:191-203.
- Stefanadis C, Diamantopoulos L, Vlachopoulos C, Tsiamis E, Dernellis J, Toutouzas K, Stefanadi E, Toutouzas P. *Thermal heterogeneity within human atherosclerotic coronary arteries detected in vivo: A new method of detection by application of a special thermography catheter*. Circulation 1999;99:1965-71.
- Sumi C, Suzuki A, Nakayama K. *Estimation of shear modulus distribution in soft tissue from strain distribution*. IEEE Trans Biomed Eng 1995;42:193-202.
- Sundt TM. *Technology insight: randomized trials of off-pump versus on-pump coronary artery bypass surgery*. Nat Clin Pract Cardiovasc Med 2005;2:261-8.
- Suselbeck T, Thielecke H, Kochlin J, Cho S, Weinschenk I, Metz J, Borggreffe M, Haase KK. *Intravascular electric impedance spectroscopy of atherosclerotic lesions using a new impedance catheter system*. Basic Res Cardiol 2005;100:446-52.
- ten Have AG, Gijzen FJ, Wentzel JJ, Slager CJ, van der Steen AF. *Temperature distribution in atherosclerotic coronary arteries: influence of plaque geometry and flow (a numerical study)*. Phys Med Biol 2004;49:4447-62.
- van de Poll SW, Romer TJ, Puppels GJ, van der Laarse A. *Imaging of atherosclerosis. Raman spectroscopy of atherosclerosis*. J Cardiovasc Risk 2002;9:255-61.
- van der Steen AFW, de Korte CL, Céspedes EI. *Intravascular ultrasound elastography*. Ultrason Schall in Medizin 1998;19:196-201.
- van Leeuwen TG, Meertens JH, Velema E, Post MJ, Borst C. *Intraluminal vapor bubble induced by excimer laser pulse causes microsecond arterial dilation and invagination leading to extensive wall damage in the rabbit*. Circulation 1993;87:1258-63.
- Virmani R, Burke AP, Kolodgie FD, Farb A. *Pathology of the thin-cap fibroatheroma: a type of vulnerable plaque*. J Interv Cardiol 2003;16:267-72.
- Vorp DA, Rajagopal KR, Smolinski PJ, Borovetz HS. *Identification of elastic properties of homogeneous, orthotropic vascular segments in distension*. J Biomech 1995;28:501-12.

- Waller BF. *Crackers, breakers, stretchers, drillers, scrapers, shavers, burners, welders and melters. The future treatment of atherosclerotic coronary artery disease.* Journal of the American College of Cardiology 1989;13:969-87.
- Wan M, Li Y, Li J, Cui Y, Zhou X. *Strain imaging and elasticity reconstruction of arteries based on intravascular ultrasound video images.* IEEE Trans Biomed Eng 2001;48:116-20.
- Wells PNT. *Developments in medical ultrasonics.* World Med Electron 1966;66:272-7.
- Wickline SA, Miller JG, Recchia D, Sharkey AM, Bridal SL, Christy DH. *Beyond intravascular imaging: quantitative ultrasonic tissue characterization of vascular pathology.* IEEE Ultrasonics Symposium 1994;3:1588-97.
- Yabushita H, Bouma BE, Houser SL et al. *Characterization of human atherosclerosis by optical coherence tomography.* Circulation 2002;106:1640-5.

PART II
FORWARD PROBLEM

A FINITE ELEMENT MODEL FOR PERFORMING INTRAVASCULAR ULTRASOUND ELASTOGRAPHY OF HUMAN ATHEROSCLEROTIC CORONARY ARTERIES

ABSTRACT

BACKGROUND

Intravascular ultrasound elastography measures the radial strain distribution of the arterial wall and displays it in an elastogram. An elastogram adds diagnostic information that is related to the rupture-proneness of a plaque and its material composition. However, radial strain depends upon an artery's material properties, geometry and used catheter position. Therefore, not always a one-to-one correspondence between radial strain and rupture-proneness or material composition exists. Both, the dependence and the correspondence, can be quantified once a proper finite element model (FEM) for arterial deformation is available. Therefore, this paper proposes a FEM and shows that it can model the arterial strain.

METHODS

Its modelling capability was evaluated by comparing simulated with measured elastograms. Measured elastograms were processed from radio-frequency data obtained in vitro from six objects: a vessel mimicking phantom and five excised human atherosclerotic coronary arteries. A FEM was created for each object and used to simulate an elastogram; the FEM's material properties and geometry were obtained from the object's histology. Comparison was performed upon high strain regions (HSR), because these regions have proven to contain plaques that show the hallmarks of vulnerable plaques.

RESULTS

Eight HSR were automatically identified from the five arteries. Statistical tests showed that there was no significant difference between simulated and corresponding measured elastograms in location, surface area and mean strain value of a HSR.

CONCLUSION

The results demonstrate that the FEM can simulate elastograms measured from arteries. As such, the FEM may help in quantifying strain-dependencies and assist in tissue characterization by reconstructing a Young's modulus image from a measured elastogram.

THIS CHAPTER IS BASED ON THE PUBLICATION

"A Finite Element Model for performing Intravascular Ultrasound Elastography of Human Atherosclerotic Coronary Arteries",

BY BALDEWSING RA, DE KORTE CL, SCHAAR JA, MASTIK F AND VAN DER STEEN AFW,
IN ULTRASOUND IN MEDICINE AND BIOLOGY, 30(6):803-13;2004,

Copyright © 2004 World Federation of Ultrasound in Medicine and Biology.

Parts from this publication were reprinted with their permission.

INTRODUCTION

The majority of acute coronary syndromes are caused by rupture of a vulnerable plaque (Davies 2000; Falk 1999). A subclass of vulnerable plaques, called thin-cap fibroatheromas, can be described as a large, soft lipid pool covered by a thin fibrous cap (Davies 1996; Virmani et al. 2002). Besides plaque composition and geometry, inflammation caused by infiltration of macrophages is also considered to be a major determinant for plaque rupture (Libby 2002). As such, identification of these determinants allows monitoring of atherosclerosis and selecting proper interventional procedures (Schaar et al. 2004).

Acute coronary syndromes

Cheng et al. (1993) and Richardson et al. (1989) showed that there exists a high correlation between the locations of plaque rupture in histology of plaques and locations of high circumferential stress concentrations obtained with computer simulations of those plaques. Stress cannot be measured directly with any clinically available technique, it can only be estimated using computer simulations. Nevertheless, for clinical purposes, a measurable mechanical quantity is needed, related to circumferential tensile stress, to assess information on plaque composition and vulnerability, i.e., radial compressive strain.

Stress and strain

Intravascular ultrasound (IVUS) elastography is a clinically-available technique that can measure this local compressive radial strain, visualized in so-called IVUS elastograms, of human atherosclerotic coronary arteries, both in vitro and in vivo (Bruseau et al. 2001; de Korte et al. 2003; Ryan and Foster 1997). Near the lumen, this high strain highly correlates with fatty tissue or tissue regions infiltrated by macrophages (de Korte et al. 2002b). Therefore, IVUS elastography can be used to provide mechanical and morphological information about plaques (de Korte et al. 2002a). Furthermore, IVUS elastograms have the ability to indicate plaque vulnerability (Schaar et al. 2003) and may eventually identify future plaque rupture locations.

IVUS elastography

IVUS elastograms and local high-strain regions, however, cannot always be directly related to specific arterial tissue components (Céspedes et al. 1996; Mai and Insana 2002). The underlying reason is that radial strain depends upon the arterial wall's material properties, geometry, and catheter position used during imaging (de Korte et al. 1999). These factors cause strain interpretation artefacts such as target hardening due to stress decay, mechanical shadowing and elastic enhancement (Ophir et al. 1996; 2000). Therefore, an arterial finite element model (FEM) is needed to understand and correct for such artifacts.

Strain interpretation artifacts

In contrast to IVUS elastograms, Young's modulus visualizations do not suffer from such artifacts and can be directly interpreted as tissue component images or used to monitor atherosclerosis. This is possible due to the modulus contrast between soft tissues, such as lipid or inflamed tissues, and relatively stiff tissue, such as smooth muscle cells, collagen and calcifications (Cheng et al. 1993; Gow and Hadfield 1979; Lee et al. 1992; 1996; Loree et al. 1994; Mozersky et al. 1972; Salunke and Topoleski 1997; Veress et al. 2000; Weizsacker and Pinto 1988). Young's modulus imaging with iterative parameter reconstruction algorithms utilizing a FEM has been shown for simple rectangular phantoms with a circular hard/soft inclusion (Doyley et al. 2000). This is also known as solving the inverse problem. In general, this is very difficult, due to uniqueness and convergence problems. These may result

Young's modulus

from using noisy reconstruction input such as displacement/strain data (Skovoroda et al. 1995), but also from using a FEM that does not incorporate essential mechanical and structural tissue features (Moulton et al. 1995).

Computer models for arterial tissue behavior

Different research groups have proposed and used FEMs to describe arterial tissue behavior to calculate stress distributions (Salunke and Topoleski 1997). The majority modelled the large quasi-static arterial deformation behavior and a minority modelled time-dependent behavior. Some behavioral aspects that were put in these models, but never all at the same time, were hyperelasticity, linear elasticity, material nonlinearity, geometric nonlinearity, piecewise homogeneity, isotropy, transverse isotropy, orthotropy, strain-energy function existence, (nearly-) incompressibility, initial stress, initial strain, plane stress, plane strain and 3D (Hayashi and Imai 1997; Holzapfel et al. 2000; Huang et al. 2001; Lee et al. 1996; Loree et al. 1992; Ohayon et al. 2001; Veress et al. 1998; 2000).

A FEM with minimal number of parameters is needed

A major problem in applying such arterial FEMs for investigation of artifacts in IVUS elastograms and for the reconstruction of the arterial Young's modulus distribution from a measured elastogram is that the majority of those models incorporate arterial features that require many constitutive parameters to describe them (e.g., a model using transverse isotropy or orthotropy). Besides that, some models may use parameters that do not allow a direct physical modulus interpretation, e.g., models using a strain-energy function (Fung 1981). However, for use in reconstruction algorithms, the number of parameters needs to be as low as possible. This is essential for uniqueness of the reconstruction, clinical interpretation of the reconstructed parameters and acceptable reconstruction time. Secondly, the lower the number of parameters is, in a proper arterial FEM, the easier IVUS elastogram artifacts can be correlated to the parameters and explained. Consequently, a FEM with a minimal number of model parameters is needed that can simulate the arterial behaviour during elastographic measurements.

Aims of this study

In this chapter we propose a linear elastic, isotropic, plane-strain, nearly incompressible FEM, which depends only upon the Young's modulus distribution, for simulating the compressive radial strain of human atherosclerotic coronary arteries. We investigate the FEM's modelling capability by comparing measured IVUS elastograms of a phantom and arteries with corresponding FEM elastograms, i.e., simulated IVUS elastograms. The FEM's material properties and geometry were obtained from histology, since histology provides currently the only practical way to assess such information. The quantitative comparison is based upon high strain regions in elastograms. This is done, because these regions have proven to contain plaques that show the hallmarks of vulnerable plaques (Schaar et al. 2003).

MATERIALS

PHANTOM

A vessel mimicking phantom with an eccentric soft plaque embedded in a stiff wall was made from 10% polyvinyl alcohol (PVA) cryogel. Carborundum (SiC) particles (3-10 μm) were added as scattering material. The static Young's modulus of this PVA cryogel can be controlled by freezing and thawing (Chu and Rutt 1997). The higher the number of freeze-thaw cycles, the higher the resulting Young's modulus will be. A freeze-thaw cycle consisted of freezing (at $-20\text{ }^{\circ}\text{C}$) for 15 hours followed by thawing (at room temperature) for 9 hours.

Phantom preparation

The wall was created by filling cryogel into the space between the inside of a big cylinder (inner diameter $\sim 18\text{ mm}$) and the outside of a centred solid cylinder (outer diameter $\sim 9\text{ mm}$). Next, it underwent three freeze-thaw cycles. After these cycles the plaque was created: first the solid cylinder was removed and replaced by a small solid cylinder (diameter of $\sim 4\text{ mm}$) that was placed against the inside of the wall. Next, the space between the inside of the wall and the outside of the small solid cylinder was filled with cryogel and defined the plaque. Finally, both the wall and the plaque underwent one freeze-thaw cycle. During this cycle the plaque stiffened and became totally attached to the wall due to cross-linking of PVA through hydrogen bonding (Chu and Rutt 1997). In total, the wall underwent four freeze-thaw cycles

and the plaque only one. The goal was to create a phantom with an YM contrast between plaque and wall that resembles the high YM contrast of real arterial soft plaques embedded in stiff media. Chu and Rutt (1997) showed that, after approximately 4 cycles, the PVA cryogel does not stiffen much more. This resulted in a Young's modulus contrast of roughly four.

A small sample was cut (1 by 1 by 3 mm) from both the wall and the plaque to measure their static Young's modulus using a custom-designed tension set-up (applied strain: 0% up to 5%). This resulted in a modulus of 16.8 kPa for the wall and 4.2 kPa for the plaque. The length of the phantom was 150 mm.

Young's modulus measurements

ARTERIES

Atherosclerotic human coronary artery segments (n=5) were excised from patients who died of noncoronary causes. All arteries contained a substantial amount of lipid and had one of the following morphologies: a homogeneous fatty plaque covered by a thin fibrous cap, an eccentric heterogeneous plaque, or a circular heterogeneous plaque.

Various arterial plaques

METHODS

MEASUREMENT

Ultrasound experiments were performed at room temperature using a water tank equipped with two opposite insertion sheaths. One sheath was connected to a water column system, which was used for applying intraluminal pressures and to perform preconditioning. This system contained distilled water for the phantom and a degassed physiological saline solution for the arteries. The opposite sheath was connected to a device for measuring pressure. This sheath was also used to insert a 20-MHz IVUS catheter (Jomed Inc., Rancho Cordova, CA, USA) connected to an InVision echo apparatus (Jomed Inc., Rancho Cordova, CA, USA). Before inserting an artery between the sheaths, the arterial side-branches were closed with suture material to prevent leakage (Schaar et al. 2002).

In vitro set-up

Elastographic acquisition for the arteries was done after preconditioning and within 24 h postmortem (Schaar et al. 2003). Each artery was scanned with the IVUS catheter to identify a cross-section with a substantial amount of plaque. First, an IVUS echo frame was acquired at intraluminal pressure of 5 mmHg for the phantom and 80 mmHg for arteries. After 10 s, another IVUS echo frame was acquired at 6 mmHg for the phantom and 100 mmHg for the arteries. These pressures were chosen to strain the phantom and the arteries up to a maximum of 2.5%. This value is an upper limit for properly calculating strain using the cross-correlation method described in de Korte et al. (1998) with a window length of 60 radio-frequency (rf) data points and a 20-MHz center frequency of the ultrasound signal. Each echo frame consisted of 512 angles of raw rf data-lines. Each line contained 1024 data points (corresponding to 7.6 mm imaging depth) sampled at 100 MHz in 12 bits. First, the radial tissue displacement along the ultrasound beam was determined. Then, finite differences of these displacements resulted in the radial strain. The resolution of the strain measurement in the radial direction is approximately 200 μm . Strain estimates of the first three arteries were visualized between 0% (color-coded in blue) and 2% (color-coded in yellow), with only a few estimates above the 2% threshold. The last two arteries had relatively lower strains and were therefore visualized between 0 and 1.5%.

Elastographic acquisition

After having obtained the elastographic data from the arterial cross-section, its axial position in the artery was marked by inserting an echo-lucent surgical needle in the periadventitia. On this needle, a suture was mounted. Next, a reference IVUS echo frame was acquired from this cross-section. Then, the needle was removed, but the suture remained in place. This suture was used as a marker for matching histology to the reference IVUS echo frame and IVUS elastogram. After removing the artery from the water tank, it was pressure-fixed at 80 mmHg, then sectioned and finally

Matching and histology

counterstained for the presence of collagen (picro Sirius red), smooth muscle cells (actin) and macrophages (CD 68).

FINITE ELEMENT SIMULATION

Graphical user interface

The creation of complex arterial finite element geometries was done with a custom-written graphical user interface (GUI), developed using the software package MATLAB (release 11.1, the MathWorks, Inc.). The GUI allows creation and tracing of arbitrary two-dimensional regions, assigning material properties to these regions and defining displacement and pressure boundary conditions to edges of these regions. The GUI translates the collection of drawn regions to a topology format that can be used as input in a finite element package.

Finite element package

The finite element package Sepran (Septra Analysis, Technical University Delft, The Netherlands) was used to calculate the solution of the tissue deformation equations (Appendix A). The topology information of the FEM geometry given by the GUI was used as input for Sepran to create the corresponding finite element mesh. Plane-strain quadratic triangles were used as finite elements. The averaged finite element size was approximately 0.3 mm for the phantom and 0.1 mm for the arteries.

Constitutive equation

The phantom and arteries constitutive behavior was modeled as linear elastic, isotropic, nearly incompressible, plane-strain material. Therefore, the spatial distribution of only one constitutive parameter, i.e., Young's modulus, was needed to model the complete mechanical behavior (Appendix A).

Radial strain

The calculated Cartesian linear strain tensor components were scan-converted to their polar components. The radial linear strain tensor component was visualized in a FEM elastogram, using the same color-coding as used for IVUS elastograms.

Geometry and material properties

For both the phantom and arteries the FEM lumen contour and the FEM outer boundary contour (i.e., phantom wall contour and artery's media-adventitia contour, respectively) were traced from the echogram, acquired at low pressure. The finite element regions of the phantom were defined by tracing the high strain region border that was clearly visible in the IVUS elastogram. The wall region was assigned a Young's modulus of 16.8 kPa and the soft plaque region, 4.2 kPa, in accordance with the tensile measurements. Both phantom regions were assumed to be nearly incompressible and therefore assigned a Poisson's ratio of 0.4999.

The finite element regions of the artery and corresponding Young's modulus values were defined from histology: collagen (COLL), smooth muscle cells (SMC) and macrophages (MΦ) were delineated manually from their histology picture. Lipid was defined as a region in histology without COLL and SMC. Next, they were compounded to produce the final geometry picture. Each of the regions in the geometry picture was then assigned a static Young's modulus value, according to Table 1. All

TABLE 1: STATIC YOUNG'S MODULUS VALUES USED IN FEM GEOMETRIES FOR DIFFERENT TISSUE COMPONENTS AND MIXTURES OF TISSUE COMPONENTS

LIPID	SMC	COLL	LIPID+MΦ	SMC+MΦ	COLL+MΦ	SMC+LIPID	COLL+LIPID	SMC+COLL
50	1000	1500	25	500	750	500	750	1250

SMC=smooth muscle cells, COLL=collagen, MΦ=macrophages. A "+" indicates a mixture of tissue components. Young's modulus for lipid is defined as the mean of 1, 0.5, 17.4 and 202 kPa; these values are taken from (Cheng et al. 1993), (Lee et al. 1996), (Veress et al. 2000) and (de Korte 1999), respectively. Young's modulus for SMC is taken from (Lee et al. 1996). Young's modulus for COLL is defined as the mean of 630 and 2310 kPa; these values are taken from (Mozersky et al. 1972) and (Gow and Hadfield 1979), respectively. Young's moduli for the mixture components are defined by the authors of this paper.

arterial regions were assumed to be nearly incompressible and were assigned a Poisson's ratio of 0.4999.

Boundary conditions

Pressure differentials of 1 mmHg for the phantom FEM and 20 mmHg for the artery FEM were assigned, in accordance with the in vitro experiments. The outer boundaries were given a pressure differential of 0 mmHg, except for four neighbouring points on the outer boundary contour of the FEM, which were totally fixed, to prevent rigid body translation and thus to assure a unique finite element solution.

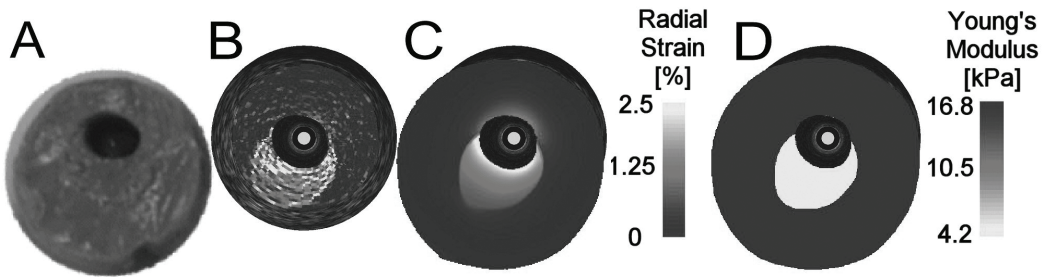


Fig. 1. In vitro IVUS elastography and FEM elastography of a vessel mimicking phantom with a soft eccentric plaque. (a) Optical image taken from the phantom, cross-section diameter 18 mm. Superimposed on IVUS echogram are (b) IVUS elastogram, (c) FEM elastogram, (d) FEM geometry and Young's modulus distribution. In the center, the grey circle defines the catheter tip diameter 1.1 mm and the black circle removes part of the catheter ringdown diameter 2 mm.

COMPARING IVUS ELASTOGRAMS WITH FEM ELASTOGRAMS

Phantom

For the phantom, the quantitative comparison procedure was as follows. First, the IVUS elastogram and FEM elastogram were divided into 36 polar segments of 10° angle-width and 6 mm radius-depth. For three specific polar segments, i.e., wall, plaque shoulder and center of plaque, the IVUS and FEM mean radial strain profiles were calculated. The difference between corresponding profiles and their standard deviations were calculated. Also a quantitative comparison based on the high strain regions features, as done for the arteries and described in the following paragraph, was performed.

Arteries

For the arteries, the quantitative comparison was based on features of high strain regions in both IVUS elastogram and FEM elastogram. This is done, because high strain regions are often related to plaque vulnerability. The high strain regions were uniquely constructed as follows: All the measured strain points higher than the strain threshold, i.e., the used maximum displayed value for strain estimates, minus 0.5, were fully automatic selected and subdivided into clusters of points. Each cluster had the property that, for each cluster point, there existed another cluster point within $500\ \mu\text{m}$ distance. This cluster procedure assured that the clusters obtained were unique. The cluster radius $R=500\ \mu\text{m}$ had to be chosen larger than the strain calculation window length of $200\ \mu\text{m}$, otherwise no clustering of strain points in the radial direction was possible.

Comparison was based on features of high-strain regions

The following high-strain cluster features were determined: geometric center (depth [mm], angle $[\circ]$), surface area [mm^2], and mean strain value [%]. The geometric center is defined as the mean of a tight boundary contour, consisting of equidistant points, placed around the cluster points. Angle (counter-clockwise, 0° at 3 o'clock) and depth are defined with respect to the center of the catheter. High strain clusters with an area less than $0.3\ \text{mm}^2$ were discarded from the comparison analysis. An IVUS high strain cluster was compared with the closest FEM strain cluster available. For each feature, a paired t-test was done to test the significance of the difference in an IVUS elastogram and a FEM elastogram.

High-strain cluster features

RESULTS

PHANTOM

Qualitative comparison of IVUS elastogram and FEM elastogram of the phantom revealed a good agreement in the strain distribution throughout the whole tissue (Fig. 1). Strain values ranged from 0 up to 2.5% in both elastograms. The IVUS elastogram shows a fluctuating strain texture through the whole elastogram, which is due to measurement noise and the gradient-based calculation of the strain. This tex-

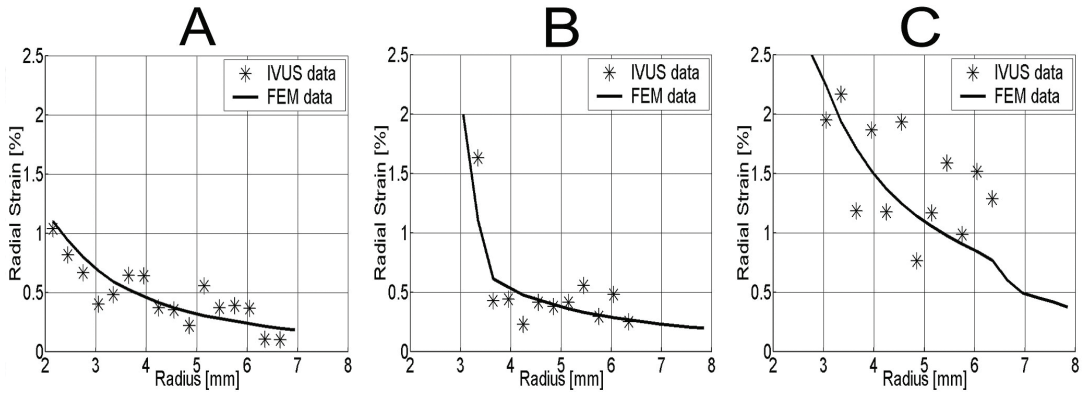


Fig. 2. IVUS and FEM radial strain profiles of the phantom. (a) Profile at 1 o'clock (wall), (b) 9 o'clock (plaque shoulder) and (c) 7 o'clock (center of plaque).

ture is not present in the FEM elastogram, since the latter visualizes the solution of a partial differential equation, which is generally continuous. Due to the imaging depth of only 7.6 mm and the eccentric position of the lumen contour with respect to the catheter, the IVUS elastogram covers only a part of the total echogram area and is smaller than the FEM elastogram area. The strain decay, i.e., the smooth transition from high strain to low strain, in both the soft plaque and hard wall is clearly visible. In both elastograms, the eccentric soft plaque shape is present and co-localizes.

TABLE 2: FEATURES OF HIGH STRAIN CLUSTERS IN IVUS ELASTOGRAMS AND CORRESPONDING FEM ELASTOGRAMS

	DEPTH (MM)		ANGLE (DEGREES)		AREA (MM ²)		STRAIN (%)	
	IVUS	FEM	IVUS	FEM	IVUS	FEM	IVUS	FEM
Phantom	2.8	2.1	253	248	8.7	6.5	2.24	2.22
absolute difference	0.7		5		2.2		0.02	
Artery 1	2.5	2.4	252	253	0.8	0.3	1.81	1.79
Artery 1	1.5	1.9	86	138	0.4	0.4	1.72	1.70
Artery 2	1.5	1.5	128	94	0.6	0.6	1.68	1.74
Artery 3	2.8	2.5	125	126	1.2	1.8	1.74	1.75
Artery 3	2.1	1.4	192	269	0.5	0.6	1.71	1.71
Artery 4	1.1	2.2	7	0	5.4	4.6	1.21	1.20
Artery 5	3.3	3.1	10	28	1.5	0.7	1.27	1.15
Artery 5	1.1	1.3	156	162	1.4	0.7	1.23	1.18
Mean	2.00	2.04	120	134	1.48	1.21	1.55	1.53
Standard deviation	0.82	0.63	84.5	95.6	1.64	1.44	0.26	0.29
Mean of abs. differences	0.4		24		0.4		0.04	
Std. dev of abs. dif.	0.3		26		0.3		0.04	
p-value	0.800		0.287		0.191		0.339	

For each high strain cluster are calculated: the location (depth, angle) of the geometrical center relative to catheter position, surface area and mean radial strain. Angles are counter clockwise, starting at 3 o'clock. Arteries 1, 2, and 3 correspond, respectively, to the arteries in Figs. 3, 4, and 5.

Quantitative comparison between IVUS elastogram and FEM elastogram revealed high agreement for strain profiles at all angles. Strain profiles at hard wall (1 o'clock), shoulder of the plaque (9 o'clock) and center of the soft plaque (7 o'clock) had a mean relative error of 19, 18 and 21 %, respectively, and standard deviations of 10 %, 14 % and 22 %, respectively (Fig. 2). Quantitative comparison of the high strain cluster features gave good agreement in most features (Table 2, Phantom part); the difference in cluster area of 2.2 mm², is likely due to the fluctuating strain texture in the IVUS elastogram on the one hand, and the smooth strain distribution in the phantom FEM elastogram on the other hand.

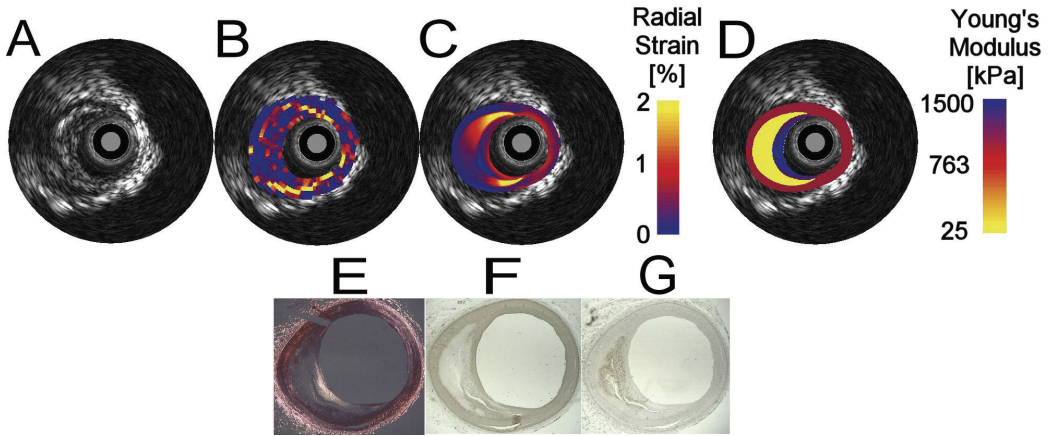


Fig. 3. In vitro IVUS elastography, FEM elastography and histology of a human atherosclerotic coronary artery with the typical morphology of a vulnerable plaque. (a) IVUS echogram. Superimposed on echogram are (b) IVUS elastogram, (c) FEM elastogram and (d) FEM geometry and Young's modulus distribution. Histology artery: (e) Collagen, (f) Smooth muscle cells and (g) Macrophages. In the center, the grey circle defines the catheter tip diameter 1.1 mm and the black circle removes part of the catheter ringdown diameter 2 mm.

ARTERIES

The echogram acquired at low pressure, superimposed IVUS elastogram, superimposed FEM elastogram and superimposed Young's modulus/geometry distribution is illustrated for three of the five arteries in Figs. 3, 4 and 5. The Young's modulus values range from 0 up to 1500 kPa. The strain values range from 0 up to 2%. A fluctuating strain texture is visible in all IVUS elastograms and is due to measurement noise and the gradient-based calculation of the strain. The size and position of the catheter tip is indicated in all Figures by a grey circle of 1.1 mm in diameter.

The artery in Fig. 3 contains a homogeneous fatty plaque covered by a stiff fibrous cap. High strain regions were found at the shoulders of the lipid pool at 11 and 6 o'clock in both the IVUS elastogram and FEM elastogram. Both elastograms show a mechanical shadowing strain artifact at the lipid pool region between 6 and 12 o'clock: straining in the center of the soft lipid is hindered by the high stiffness and circular geometry of the cap.

The artery in Fig. 4 contains a large heterogeneous plaque between 10 and 4 o'clock. In both elastograms, the high strain values are clearly visible between 9 and 12

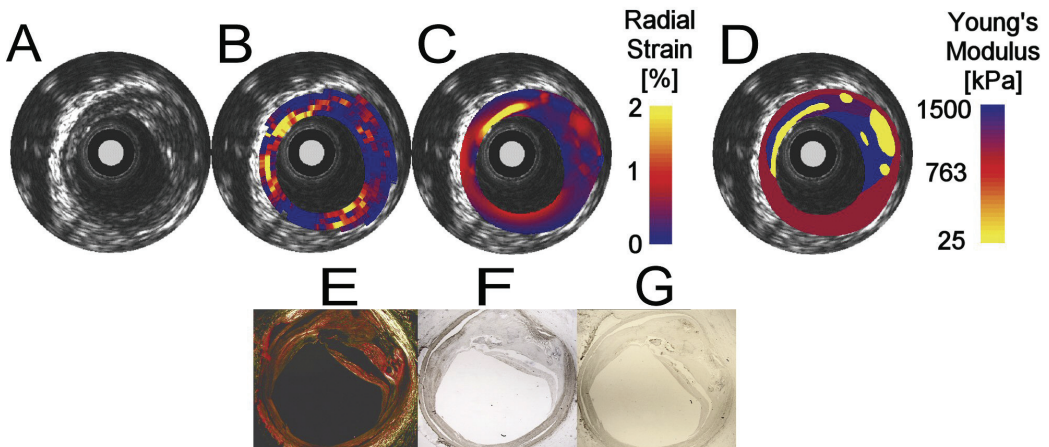


Fig. 4. In vitro IVUS elastography, FEM elastography and histology of a human atherosclerotic coronary artery with an eccentric, heterogeneous plaque at 10-4 o'clock. (a) IVUS echogram. Superimposed on echogram are (b) IVUS elastogram, (c) FEM elastogram and (d) FEM geometry and Young's modulus distribution. Histology artery: (e) Collagen, (f) Smooth muscle cells and (g) Macrophages. In the center, the grey circle defines the catheter tip diameter 1.1 mm and the black circle removes part of the catheter ringdown diameter 2 mm.

o'clock. At this location, soft tissue is present in histology and in the Young's modulus distribution image. The red-blue-red strain pattern between 12 and 3 o'clock is also present in both elastograms. At this location, a stiff collagen region is present in histology and in the Young's modulus distribution image.

The artery in Fig. 5 contains a circular heterogeneous plaque. The high strain regions in the IVUS elastograms between 6 and 9 o'clock and between 10 and 12 o'clock are also appearing in the FEM elastogram at slightly different angles, namely between 5 and 7 o'clock and between 9 and 12 o'clock. In histology, these regions are infiltrated by macrophages and have a relatively lower collagen content than surrounding regions.

Quantitative comparison of the high strain regions features (Table 2, Artery1-5 part) showed that the difference between IVUS elastograms and corresponding FEM elastograms was not significant for each of these features.

DISCUSSION

In this paper, we proposed a finite element model (FEM) for simulating measured intravascular ultrasound (IVUS) elastograms, i.e., compressive radial strain images, of a heterogeneous phantom and human atherosclerotic coronary arteries obtained in vitro. The simulating capability of this FEM was evaluated by comparing FEM elastograms with measured IVUS elastograms. The results show that simulated and measured elastograms look similar and are not statistically different.

COMPARING IVUS ELASTOGRAMS WITH FEM ELASTOGRAMS

FEM elastograms were compared with IVUS elastograms on the basis of features of high strain regions, present in both. An automatic clustering method was used to define clusters of strain points with a high strain value. The rationale for this choice of method was that it allows an unbiased, reproducible, unique and objective determination of high strain regions. The strain clusters with area less than 0.3 mm^2 were discarded, because they were likely due to noise.

CONSTITUTIVE MODEL

Linearity, isotropy, incompressibility and plane-strain

It is known that arteries in vivo and in vitro have complex biomechanical features and show a mechanically complex deformation behavior. Justification of our proposed linear elastic, isotropic, nearly incompressible, plane-strain FEM can be

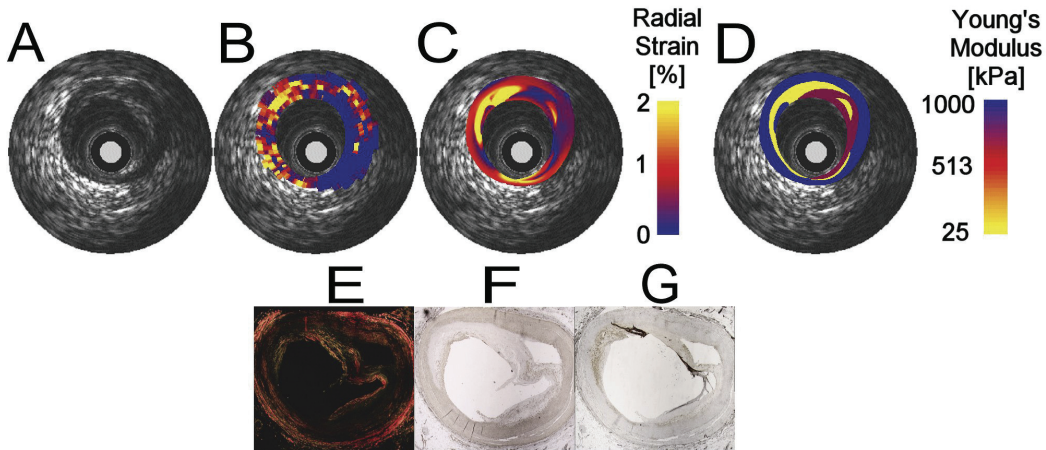


Fig. 5. In vitro IVUS elastography, FEM elastography and histology of a human atherosclerotic coronary artery with a circular, heterogeneous plaque. (a) IVUS echogram. Superimposed on echogram are (b) IVUS elastogram, (c) FEM elastogram and (d) FEM geometry and Young's modulus distribution. Histology artery: (e) Collagen, (f) Smooth muscle cells and (g) Macrophages. In the center, the grey circle defines the catheter tip diameter 1.1 mm and the black circle removes part of the catheter ringdown diameter 2 mm.

readily given, due to the semistatic character of the arterial deformation when performing IVUS elastography in vitro. For example, since the induced strain is low (< 2% for the arteries), only a small part of the artery's nonlinear stress-strain behaviour is used and it can therefore be considered to be locally linear, justifying the use of a "linear elastic" FEM model. Arterial walls may be viewed as incrementally isotropic for the range of deformations that occur in vivo (Weizsacker and Pinto 1988). According to Carew et al. (1968), arteries may be considered to be incompressible. Furthermore, Baldewising et al. (2002; 2004) showed that Poisson's ratio variations of vulnerable plaques, in the range of 0.49-0.49999, had no significant influence on the calculated FEM radial strain pattern and radial strain value. The relatively large length of the artery in vitro hinders axial deformation in the center, justifying the "plane-strain" choice.

EXPLANATION OF OBSERVATIONS

The majority of high strain regions and strain patterns in FEM elastograms colocalize with regions and patterns in IVUS elastograms in case of the phantom and, within a certain range, also in case of the arteries. Deviations may be explained as follows.

There is an overall agreement

The first reason is the difference between tissue geometry in vitro and in histology, resulting from deformation and dissection of tissue during sectioning. Consequently, soft and hard tissue regions in vitro will have a slightly different location and geometry in histology (and consequently differ slightly from the FEM geometry). Moreover, a difference in lumen contour curvature may cause locally a higher or lower strain in a FEM elastogram, either due to a change in lumen contour curvature with respect to the catheter position (de Korte et al. 1999) and/or due to stress concentration/spreading near the lumen contour. A combination of these two mechanisms may explain why, in Fig. 4 between 4 and 6 o'clock, a region with increased strain is present in the IVUS elastogram but not in the FEM elastogram. Note, that histology and FEM Young's modulus distribution were both homogenous at this region.

Differences due to sectioning

The second reason is the a priori choice of Young's modulus values assigned to regions that appear to be mechanically different in histology. These values are listed in Table 1 and represent static Young's moduli at an intraluminal pressure level of approximately 80 mmHg. The values used for the three major arterial tissue components, lipid, smooth muscle cells and collagen in Table 1, are derived from the widespread values reported by other research groups, who used arterial models mainly for stress calculation (Cheng et al. 1993; Lee et al. 1992; 1996; Veress et al. 2000; Weizsacker and Pinto 1988) and/or performed mechanical measurements on arteries (Gow and Hadfield 1979; Loree et al. 1994; Mozersky et al. 1972). Fortunately, literature shows a consistent large contrast between Young's modulus value for soft, fatty tissue and stiffer tissue such as smooth muscle cells and collagen. This important contrast is incorporated in the Young's modulus values in Table 1. The Young's moduli values for tissue components with macrophages infiltration is chosen to be relatively lower than that for tissue without such infiltration (Lendon et al. 1991). Decreasing the Young's modulus by factor 0.5 was an a priori choice that was not experimentally confirmed. Similarly, tissues mixed with lipid, have also been assigned a lower Young's modulus value than tissues without lipid.

Differences due to a priori Young's moduli assignments

CLINICAL IMPLICATIONS AND FUTURE APPLICATIONS.

The importance of having established a FEM that is able to simulate real measured IVUS elastograms of atherosclerotic human coronary arteries is twofold.

Importance of the FEM

In clinical situations, an elastogram may be measured from a patient to identify rupture-prone locations. The hypothesis is, that mechanically unstable regions near the lumen, such as regions with a large stiffness variation (e.g. a stiff plaque-cap which is locally weakened by infiltration of macrophages), are rupture-prone and might be characterized in a measured elastogram as a region near the lumen that consists of high strain with adjacent low strain. However, it is also hypothesised that mechanically stable regions may result in such strain regions, merely as a result of local stress concentrations caused by a strongly curved lumen-border. Such types of hypothesis can be investigated by using the FEM to simulate elastograms for such mechanically

Interpreting strain patterns in measured IVUS elastograms

unstable regions or curved lumen-borders. Furthermore, the FEM can be used to quantify how the appearance or disappearance of a high strain region in a measured elastogram is affected by the position of the catheter used during imaging, by simulating elastograms for different catheter positions.

Monitoring of atherosclerosis

Monitoring of atherosclerosis is vital for determining the effectiveness of pharmaceutical treatments that try to reduce the rupture-proneness of an artery, e.g., by reducing the amount of lipid or by stiffening the lipid. Lipid, smooth muscle cells and collagen are the main components of an artery and have a large stiffness contrast that is directly related to their Young's modulus stiffness-value. Therefore, the creation of an arterial Young's modulus image would be sufficient to monitor atherosclerosis. Furthermore, a Young's modulus image shows directly, by definition of a Young's modulus, the regions near the lumen that are mechanically unstable. A Young's modulus image may be produced from a measured IVUS elastogram, in the following way: first, an initial Young's modulus distribution is chosen for our FEM. Then, an automatic iterative minimization algorithm changes this Young's modulus distribution so that it produces a simulated elastogram, which resembles the measured IVUS elastogram (Baldewsing et al. 2003a; 2003b; Soualmi et al. 1997).

CONCLUSION

The experiments described in this paper demonstrate that a linear elastic, isotropic, nearly incompressible, plane-strain finite element model (FEM), which depends only upon the Young's modulus distribution, can simulate elastograms, i.e., radial strain images, which are measured from a vessel mimicking phantom and human atherosclerotic coronary arteries. As such, this FEM may assist in quantifying the relation between arterial rupture-prone locations and their appearance in a measured elastograms, and it may assist in monitoring atherosclerosis and characterizing tissue components by reconstructing a Young's modulus image from a measured elastogram.

ACKNOWLEDGEMENTS

This work is supported by the Netherlands Organization for Scientific Research (NWO) and the Dutch Technology Foundation (STW). Ton van der Steen is the 2000 NWO PIONIER Technical Sciences. We thank C. Strijder and G. Pasterkamp from Utrecht Medical Center, Department of Cardiology, Utrecht, The Netherlands for their contributions in creating the histology. We also thank R. van Loon and R. A. Boerboom from Eindhoven University of Technology, Department of Biomedical Engineering, Eindhoven, The Netherlands for their support in supplying essential finite element subroutines. Finally, we thank E. Boersma from Thoraxcenter, Erasmus Medical Center Rotterdam, The Netherlands for his feedback on statistics.

REFERENCES

- Atanackovic TM and Guran A. *Theory of elasticity, for scientists and engineers*. Boston, Birkhauser; 2000.
- Baldewsing RA, de Korte CL, Mastik F, Schaar JA and van der Steen AFW. *Comparison of finite elements model elastograms and ivus elastograms acquired from phantoms and arteries*. Proceedings of the 2002 IEEE International Ultrasonics Symposium 2002: 1873-1876.
- Baldewsing RA, Oomens CWJ and van der Steen AFW. *Intravascular Young's modulus reconstruction using a parametric finite element model*. Proceedings of the 2003 IEEE International Ultrasonics Symposium 2003a: 1879-1882.
- Baldewsing RA, Schaar JA, Mastik F, Oomens CWJ and van der Steen AFW. *IVUS modulography of vulnerable plaques using a parametric finite element model: validation on a phantom and human coronary artery*. Proceedings of the Second International Conference on the Ultrasonic Measurement and Imaging of Tissue Elasticity 2003b: 75-75.
- Baldewsing RA, de Korte CL, Schaar JA, Mastik F and van der Steen AFW. *Finite element modeling and intravascular ultrasound elastography of vulnerable plaques: parameter variation*. Ultrasonics 2004; 42(1-9): 723-729.
- Bruseau E, Fromageau J, Finet G, Delachartre P and Vray D. *Axial strain imaging of intravascular data: results on polyvinyl alcohol cryogel phantoms and carotid artery*. Ultrason Med Biol 2001; 27(12): 1631-1642.
- Carew TE, Vaishnav RN and Patel DJ. *Compressibility of the arterial wall*. Circ Res 1968; 23(1): 61-68.
- Céspedes EI, de Korte CL, van der Steen AFW, Norder B and te Nijenhuis K. *Tissue mimicking material and artifacts in intravascular elasticity imaging*. Proceedings of the 1996 IEEE Ultrasonics Symposium, IEEE Press: 1181-1184; 1996.
- Cheng GC, Loree HM, Kamm RD, Fishbein MC and Lee RT. *Distribution of circumferential stress in ruptured and stable atherosclerotic lesions. A structural analysis with histopathological correlation*. Circulation 1993; 87(4): 1179-1187.
- Chu KC and Rutt BK. *Polyvinyl alcohol cryogel: an ideal phantom material for mr studies of arterial flow and elasticity*. Magnetic Resonance in Medicine 1997; 37: 314-319.
- Davies MJ. *Stability and instability: Two faces of coronary atherosclerosis*. The Paul Dudley White lecture 1995. Circulation 1996; 94(8): 2013-2020.
- Davies MJ. *The pathophysiology of acute coronary syndromes*. Heart 2000; 83(3): 361-366.
- de Korte CL, van der Steen AFW, Céspedes EI and Pasterkamp G. *Intravascular ultrasound elastography of human arteries: initial experience in vitro*. Ultrason Med Biol 1998; 24(3): 401-408.
- de Korte CL. *Intravascular ultrasound elastography*. PhD thesis, Erasmus University Rotterdam; 1999. ISBN:90-9012664-3.
- de Korte CL, Céspedes EI and van der Steen AFW. *Influence of catheter position on estimated strain in intravascular elastography*. IEEE Trans Ultrason Ferroelectr Freq Control 1999; 46(3): 616-625.
- de Korte CL, Carlier SG, Mastik F, et al. *Morphological and mechanical information of coronary arteries obtained with intravascular elastography; feasibility study in vivo*. Eur Heart J 2002a; 23(5): 405-413.
- de Korte CL, Siervogel MJ, Mastik F, et al. *Identification of atherosclerotic plaque components with intravascular ultrasound elastography in vivo: a Yucatan pig study*. Circulation 2002b; 105(14): 1627-1630.
- de Korte CL, Schaar JA, Mastik F, Serruys PW and van der Steen AFW. *Intravascular elastography: from bench to bedside*. J Interv Cardiol 2003; 16(3): 253-259.
- Doyley MM, Meaney PM and Bamber JC. *Evaluation of an iterative reconstruction method for quantitative elastography*. Phys Med Biol 2000; 45(6): 1521-1540.
- Falk E. *Stable versus unstable atherosclerosis: clinical aspects*. Am Heart J 1999; 138(5 Pt 2): S421-5.
- Fung YC. *Biomechanics: Mechanical properties of living tissue*. New York, USA, Springer; 1981.
- Gow BS and Hadfield CD. *The elasticity of canine and human coronary arteries with reference to postmortem changes*. Circ Res 1979; 45(5): 588-594.
- Hayashi K and Imai Y. *Tensile property of atheromatous plaque and an analysis of stress in atherosclerotic wall*. J Biomech 1997; 30(6): 573-579.
- Holzappel GA, Gasser TC and Ogden RW. *A new constitutive framework for arterial wall mechanics and a comparative study of material models*. Journal of Elasticity 2000; 61: 1-48.

- Huang H, Virmani R, Younis H, et al. *The impact of calcification on the biomechanical stability of atherosclerotic plaques*. Circulation 2001; 103(8): 1051-1056.
- Lee RT, Richardson G, Loree HM, et al. *Prediction of mechanical properties of human atherosclerotic tissue by high-frequency intravascular ultrasound imaging*. Arterioscler Thromb 1992; 12: 1-5.
- Lee RT, Schoen FJ, Loree HM, Lark MW and Libby P. *Circumferential stress and matrix metalloproteinase 1 in human coronary atherosclerosis. Implications for plaque rupture*. Arterioscler Thromb Vasc Biol 1996; 16(8): 1070-1073.
- Lendon CL, Davies MJ, Born GVR and Richardson PD. *Atherosclerotic plaque caps are locally weakened when macrophage density is increased*. Atherosclerosis 1991; 87: 87-90.
- Libby P. *Inflammation in atherosclerosis*. Nature 2002; 420(6917): 868-74.
- Loree HM, Kamm RD, Stringfellow RG and Lee RT. *Effects of fibrous cap thickness on peak circumferential stress in model atherosclerotic vessels*. Circ Res 1992; 71(4): 850-858.
- Loree HM, Grodzinsky AJ, Park SY, Gibson LJ and Lee RT. *Static circumferential tangential modulus of human atherosclerotic tissue*. J Biomech 1994; 27(2): 195-204.
- Mai JJ and Insana MF. *Strain imaging of internal deformation*. Ultrasound Med Biol 2002; 28: 1475-1484.
- Moulton MJ, Creswell LL, Actis RL, et al. *An inverse approach to determining myocardial material properties*. J Biomech 1995; 28(8): 935-948.
- Mozersky DJ, Sumner DS, Hokanson DE and Strandness DE. *Transcutaneous measurement of the elastic properties of the human femoral artery*. Circulation 1972; 46: 948-955.
- Ohayon J, Teppaz P, Finet G and Rioufol G. *In-vivo prediction of human coronary plaque rupture location using intravascular ultrasound and the finite element method*. Coron Artery Dis 2001; 12(8): 655-663.
- Ophir J, Céspedes EI, Garra B, et al. *Elastography: ultrasonic imaging of tissue strain and elastic modulus in vivo*. Eur J Ultrasound 1996; 3: 49-70.
- Ophir J, Garra BS, Kallel F, et al. *Elastographic imaging*. Ultrasound Med Biol 2000; 26(Supplement 1): S23-S29.
- Richardson PD, Davies MJ and Born GVR. *Influence of plaque configuration and stress distribution on fissuring of coronary atherosclerotic plaques*. The Lancet 1989; 2: 941-944.
- Ryan LK and Foster FS. *Ultrasonic measurement of differential displacement and strain in a vascular model*. Ultrason Imaging 1997; 19(1): 19-38.
- Salunke NV and Topoleski LD. *Biomechanics of atherosclerotic plaque*. Crit Rev Biomed Eng 1997; 25(3): 243-285.
- Schaar JA, de Korte CL, Mastik F and van der Steen AFW. *Effect of temperature increase and freezing on intravascular elastography*. Ultrasonics 2002; 40(1-8): 879-81.
- Schaar JA, de Korte CL, Mastik F, et al. *Characterizing vulnerable plaque features by intravascular elastography*. Circulation 2003; 108: 2636-2641.
- Schaar JA, Muller JE, Falk E, et al. *Terminology for High-risk and Vulnerable Coronary Artery Plaques*. Eur Heart J 2004;25(12): 1077-1082.
- Skovoroda AR, Emelianov SY and O'Donnell M. *Tissue elasticity reconstruction based on ultrasonic displacement and strain images*. IEEE trans UFFC 1995; 42(4): 747-765.
- Soualmi L, Bertrand M, Mongrain R and Tardif JC. *Forward and inverse problems in endovascular elastography*. Acoustical Imaging. S. Lees and L. A. Ferrari. New York, USA, Plenum. 23: 203-209; 1997.
- Veress AI, Cornhill JF, Herderick EE and Thomas JD. *Age-related development of atherosclerotic plaque stress: a population-based finite-element analysis*. Coron Artery Dis 1998; 9(1): 13-19.
- Veress AI, Vince DG, Anderson PM, et al. *Vascular mechanics of the coronary artery*. Z Kardiol 2000; 89(Suppl 2): 92-100.
- Virmani R, Burke AP, Farb A and Kolodgie FD. *Pathology of the unstable plaque*. Prog Cardiovasc Dis 2002; 44(5): 349-56.
- Weisacker HW and Pinto JG. *Isotropy and anisotropy of the arterial wall*. J Biomech 1988; 21(6): 477-487.

FINITE ELEMENT MODELING AND INTRAVASCULAR ULTRASOUND ELASTOGRAPHY OF VULNERABLE PLAQUES: PARAMETER VARIATION

ABSTRACT

BACKGROUND

More than 60 % of all myocardial infarction is caused by rupture of a vulnerable plaque. A vulnerable plaque can be described as a large, soft lipid pool covered by a thin fibrous cap. Plaque material composition, geometry, and inflammation caused by infiltration of macrophages are considered as major determinants for plaque rupture. For diagnostic purposes, these determinants may be obtained from elastograms (i.e. radial strain images), which are derived from IntraVascular UltraSound (IVUS) measurements. IVUS elastograms, however, cannot be interpreted directly as tissue component images, because radial strain depends upon plaque geometry, plaque material properties, and used catheter position. To understand and quantify the influence of these parameters upon measured IVUS elastograms, they were varied in a finite element model (FEM) that simulates IVUS elastograms of vulnerable plaques.

METHODS

IVUS elastography measurements were performed on a vessel mimicking phantom, with a soft plaque embedded in a hard wall, and an atherosclerotic human coronary artery containing a vulnerable plaque. Next, FEMs were created to simulate IVUS elastograms of the same objects. In these FEMs the following parameters were varied: Young's modulus (E), Poisson's ratio (ν) in range 0.49-0.4999, catheter position (translation of 0.8 mm), and cap-thickness (t) in range 50-350 micrometers. For each variation, the resulting Peak Radial Strain (PRS) was determined and visualized.

RESULTS

Measured static E for phantom was 4.2 kPa for plaque and 16.8 kPa for wall. Variation of E -wall in range 8.4-33.2 kPa and/or E -plaque in range 2.1-8.4 kPa using the phantom FEM, gave a PRS variation of 1.6 %, i.e. from 1.7 % up to almost 3.3 %; for variation in ν this was only 0.07 %, i.e. from 2.37 % up to 2.44 %. Variation of E -lipid in range 6.25-400 kPa and E -cap in range 700-2300 kPa using the artery FEM, gave a PRS variation of 3.1 %, i.e. from 0.6 % up to 3.7 %. The PRS was higher for lower E -lipid and E -cap; it was located at a shoulder of the lipid pool. Variation of ν gave merely a variation of 0.17 %. Variation of t and E -cap resulted in a PRS variation of 1.4 %, i.e. from 0.3 % up to 1.7 %; thinner and weaker caps gave higher PRS. Catheter position variation changed radial strain value.

CONCLUSION

Measured IVUS elastograms of vulnerable plaques depend highly upon the Young's modulus of lipid and cap, but hardly upon the Poisson's ratio (> 0.49). Different catheter positions result in different IVUS elastograms, but the diagnostically important high strain regions near the lipid shoulders are often still detectable. Peak radial strain increases when the cap weakens or the cap-thickness decreases.

THIS CHAPTER IS BASED ON THE PUBLICATION

"Finite Element Modeling and Intravascular Ultrasound Elastography of Vulnerable Plaques: Parameter Variation",

BY BALDEWSING RA, DE KORTE CL, SCHAAR JA, MASTIK F AND VAN DER STEEN AFW,
IN ULTRASONICS, 42(1-9):723-29;2004,

Copyright © 2004 Elsevier.

Parts from this publication were reprinted with their permission.

INTRODUCTION

More than 60 % of all myocardial infarction is caused by rupture of a vulnerable plaque (Casscells et al. 2003). A vulnerable plaque can be described as a large, soft lipid pool covered by a thin fibrous cap (Davies 1996). Plaque material composition, geometry, and inflammation caused by infiltration of macrophages are considered as major determinants for plaque rupture (Pasterkamp et al. 2002). As such, identification of these determinants may assist in estimating plaque vulnerability, monitoring plaque progression and selecting interventional procedures.

Acute coronary syndromes

IntraVascular Ultrasound (IVUS) elastography is a clinically available technique that assess information related to these determinants, by measuring the local incremental radial strain, visualized in so called IVUS elastograms, of human atherosclerotic arteries, both in vitro and in vivo (de Korte et al. 2002b, de Korte et al. 2002a).

IVUS elastography

IVUS elastograms, however, cannot be directly interpreted as tissue component images (de Korte et al. 1996). The underlying reason is that radial strain, depicted in IVUS elastograms, depends upon plaque composition, plaque geometry, and catheter position used during imaging (de Korte et al. 1999). These factors cause strain interpretation artefacts like strain hardening due to stress decay, mechanical shadowing, and elastic enhancement (Ophir et al. 1996). Nevertheless, assessment of diagnostic information, like plaque composition and geometry of plaque components, from IVUS elastograms is still needed. Therefore it is necessary to quantify how plaque composition and geometry appear in IVUS elastograms and to investigate how their appearance depends upon the catheter position. Besides that, Young's modulus reconstruction methods may use an IVUS elastogram as input. To allow a good reconstruction, it is necessary to know if IVUS elastograms have a high dependency upon plaque composition and geometry.

Strain interpretation artifacts

In this chapter we use a linear elastic, isotropic, plane strain, (nearly) incompressible Finite Element Model (FEM) for simulating IVUS elastograms, i.e. incremental radial strain images, of a vessel mimicking phantom containing a soft eccentric plaque and a human coronary artery containing a vulnerable plaque. The FEM is then used to visualize and quantify the changes in IVUS elastograms for variations in Young's moduli, Poisson's ratio, cap thickness, and catheter position.

Aims of this study

MATERIALS

PHANTOM AND ARTERY

A vessel mimicking phantom with an eccentric soft plaque embedded in a stiff wall was made from 10% polyvinyl alcohol (PVA) cryogel. Carborundum (SiC) particles (3-10 μm) were added as ultrasound scattering material. The static Young's modulus of this PVA cryogel can be controlled by freezing and thawing (Chu and Rutt 1997). The higher the number of freeze-thaw cycles, the higher the resulting Young's modulus will be. A freeze-thaw cycle consisted of freezing (at -20 degrees Celsius) for 15 hours followed by thawing (at room temperature) for 9 hours.

Phantom preparation

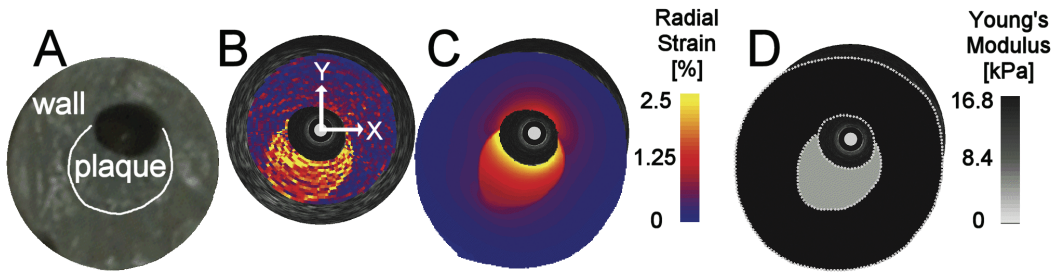


Fig. 1. In vitro IVUS elastography and FEM elastography of a vessel mimicking phantom with a soft eccentric plaque: (A) Cross-section phantom \varnothing 18 mm. Superimposed on IVUS echogram are (B) IVUS elastogram, (C) FEM elastogram, (D) FEM geometry and Young's modulus distribution. At the soft plaque between 4 and 9 o'clock a strain hardening artefact is visible. In the centre, the grey circle defines the catheter tip \varnothing 1.1 mm and the black circle removes part of the catheter ringdown \varnothing 2 mm.

INTRAVASCULAR ULTRASOUND MEASUREMENTS

In a water tank set-up, ultrasound data was acquired using a 20-MHz IVUS catheter connected to an InVision echo apparatus (Jomed Inc., Rancho Cordova, CA). First, an IVUS Radio Frequency (RF) data frame was acquired at intraluminal pressure of 80 mmHg for the artery and 5 mmHg for the phantom. After 10 seconds, another IVUS RF data frame was acquired at 100 mmHg for the artery and 6 mmHg for the phantom. These RF data frames were acquired after preconditioning of the artery. Next, cross-correlation techniques were applied to the RF data frames to calculate the local compressive incremental radial strain as described in (de Korte et al. 1998). Heretofore, the radial tissue displacement along the ultrasound beam was determined. Next, finite differences of these displacements resulted in the local radial strain, with a resolution of approximately 200 μ m. For visualisation purposes, the strain values below 0 % were clipped to 0 % (i.e. given a value of 0 %) and strain values higher than 2 % were clipped to 2 % in case of the artery, and 2.5 % in case of the phantom. The amount of clipped values was always less than 5 %.

FINITE ELEMENT SIMULATION

Finite element package and tissue deformation model

The finite element package Sepran (Septra Analysis, TU-Delft, Delft, The Netherlands) was used to calculate the strain of tissue. Plane strain quadratic triangles were used as finite elements. The averaged finite element size was approximately 0.3 mm

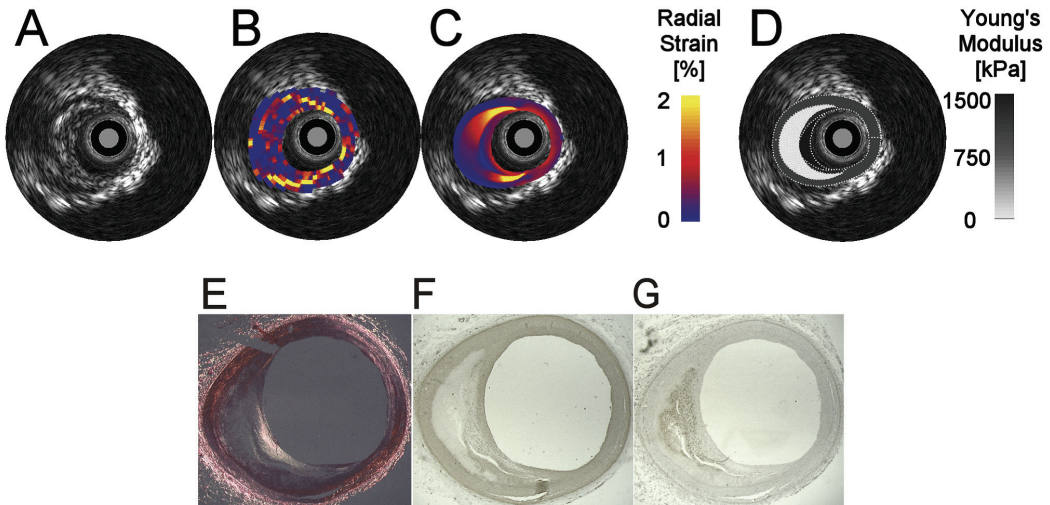


Fig. 2. In vitro IVUS elastography, FEM elastography, and histology of a post mortem human coronary artery with the typical morphology of a vulnerable plaque: (A) IVUS echogram. Superimposed on echogram are (B) IVUS elastogram, (C) FEM elastogram, (D) FEM geometry and Young's modulus distribution. Histology artery: (E) Collagen, (F) Smooth muscle cells, and (G) macrophages. Note the typical high strain regions at the shoulders of the moon shaped, soft lipid pool in (B) and (C). At this lipid pool a mechanical shadowing strain artefact is visible. In the centre, the grey circle defines the catheter tip \varnothing 1.1 mm and the black circle removes part of the catheter ringdown \varnothing 2 mm.

for the phantom and 0.1 mm for the artery. The phantom and arterial tissue was modeled as linearly elastic, isotropic, plane strain, (nearly) incompressible material. Therefore only the Young's modulus and Poisson's ratio are needed to describe their complete mechanical behavior. Radial strain was calculated by using the catheter position in the echogram as the origin of the polar coordinate system. They were clipped in the same way as the measured strain.

The finite element geometry of the phantom (fig. 1D) was generated by tracing its IVUS echogram and IVUS elastogram. The wall and plaque regions were assigned a Young's modulus of 16.8 kPa and 4.2 kPa respectively, in accordance with the mechanical measurements. Both regions were given a Poisson's ratio of 0.4999.

Geometry and material values

The finite element geometry of the artery (fig. 2D) was created, by tracing both the echogram and histology. This resulted in three main regions: media, lipid, and cap. Since the collagen amount was relatively higher in the center of the cap, it was subdivided into a center with two adjacent regions. The assigned Young's moduli were taken from (Baldewsing et al. 2004) and were 25, 1000, 1250 and 1500 kPa, respectively for lipid, media, left/right cap regions, and center of cap. All regions were given a Poisson's ratio of 0.4999. The details of creating the finite element geometry for phantom and artery, and the rationale for the choice of the material values is described in (Baldewsing et al. 2002, 2004).

Pressure differentials of 1 mmHg for the phantom FEM and 20 mmHg for the artery FEM were assigned, in accordance with the in vitro experiments. The outer boundaries were given a pressure differential of 0 mmHg, except for 4 consecutive outer boundary contour points, which were totally fixed, to prevent rigid body translation and thus assure an unique finite element solution.

Boundary conditions

PARAMETER VARIATIONS

The following parameter variations (Table 1) of the Young's modulus (E), Poisson's

TABLE 1: PARAMETER VARIATIONS IN VARIOUS FINITE ELEMENT MODELS

	PHANTOM FEM	ARTERY FEM	PARAMETRIC FEM
E* plaque [kPa]	2.1-8.4 ^a		
E wall [kPa]	8.4-33.2 ^a		
E lipid[kPa]		6.25-400 ^b	
E cap [kPa]		700-2300 ^b	500-2500 ^c
ν * cross-section[-]	0.49-0.49999	0.4-0.49999	
Cap thickness [μ m]			50-350 ^c
Catheter position [mm]		0.8 ^T	

^{a, b, c}: Denote that parameters are varied simultaneously.

*: E denotes Young's modulus, ν denotes Poisson's ratio.

T: Translation (right, up, left, and down) away from reference position.

ratio (ν), cap thickness (t) and catheter position were performed using a Finite Element Model (FEM):

E of phantom wall (8.4-33.2 kPa), E of phantom plaque (2.1-8.4 kPa), and ν of phantom (0.49-0.49999); using the phantom FEM. E of artery lipid (6.25-400 kPa) at different E of cap (700-2300 kPa), and ν of artery (0.4-0.4999); using the artery FEM. Cap thickness (50-350 μ m) using different E of cap (500-2500 kPa); using a Parametric FEM (PFEM) version for the artery. The PFEM consist of 4 circles defining a lipid, media, and cap region. The circles have dimensions that resemble the dimensions of the artery. The same pressure differential and initial material values were used as for the artery FEM. Catheter position translations (0.8 mm) with respect to the position used during imaging in figure 2; using the artery FEM. Peak radial strain was calculated as the mean of the 10 % highest strain values in an elastogram.

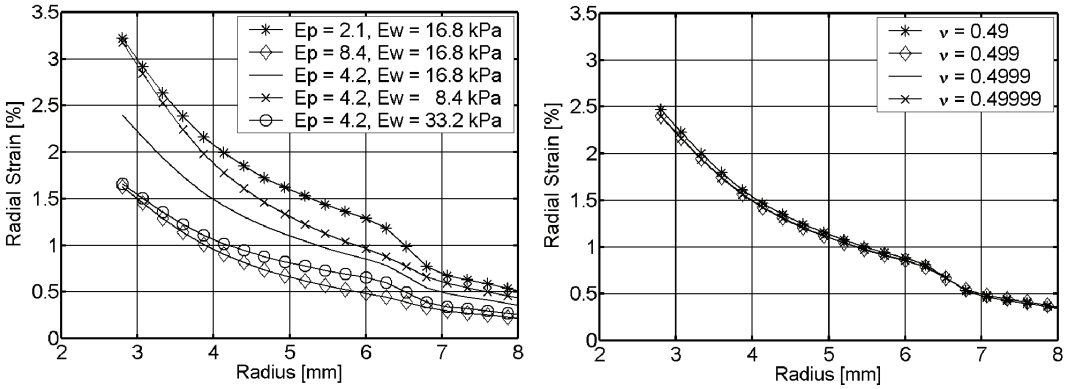


Fig. 3. Phantom material variation around measured values (4.2 kPa for plaque and 16.8 kPa for wall): (Left) FEM radial strain profiles of phantom at 7 o'clock for different Young's moduli of plaque E_p and wall E_w . (Right) The same profiles for different Poisson's ratios of whole phantom ν . Note the high dependency of radial strain upon the Young's moduli, in contrast to the low dependency upon Poisson's ratio.

RESULTS

PHANTOM RESULTS

Strain artefact

Figures 1B and 1C show good agreement between measurement and simulation. They also show a strain hardening artefact (Ophir et al. 1996) at the plaque region between 4 and 9 o'clock: The Young's modulus of the plaque is constant (fig. 1A and fig. 1D), but the radial strain is not constant; instead it is decaying.

Phantom material variation

Figure 3 shows that Young's modulus variation of phantom wall and/or plaque, around experimentally measured values, gave a Peak Radial Strain (PRS) variation of almost 1.6 %, i.e. from 1.7 % up to 3.3 %. For variation in Poisson's ratio of the whole phantom this was only 0.07 %, i.e. from 2.37 % up to 2.44 %.

ARTERY RESULTS

There is an overall agreement

Figure 2B and 2C show good agreement between measurement and simulation. They also show a mechanical shadowing strain artefact (Ophir et al. 1996) at the lipid pool region between 6 and 12 o'clock: The Young's modulus of the lipid pool is constant (fig. 2E, 2F, 2G and 2D), but the radial strain in the lipid pool is not; instead it is decaying from the shoulders of the lipid pool towards the center of the lipid pool.

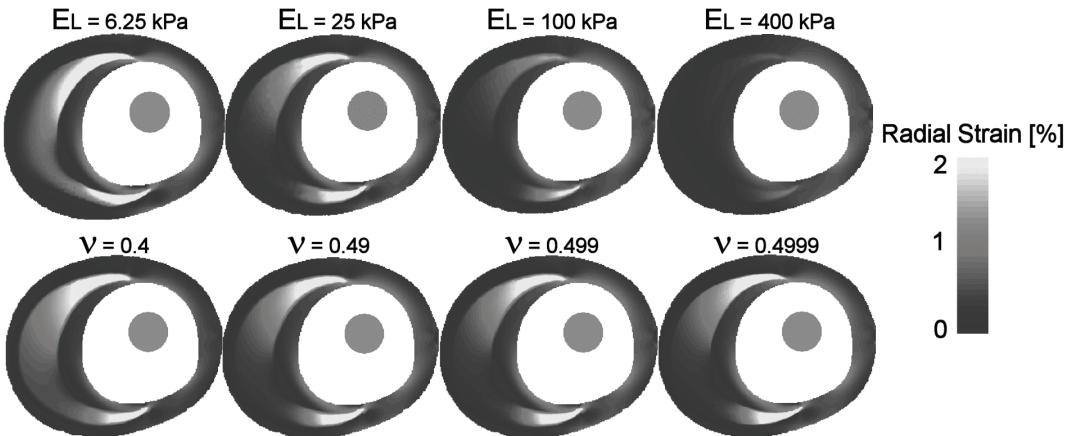


Fig. 4. Artery material variation for fixed cap stiffness: (Top row) Radial strain distribution for different Young's moduli of lipid E_L and (bottom row) for different Poisson's ratio of whole artery ν . Note the big decrease in radial strain, at the shoulders of the lipid pool, when E_L is varied, while there is no visible change when ν is varied. The grey circle indicates the catheter tip \varnothing 1.1 mm.

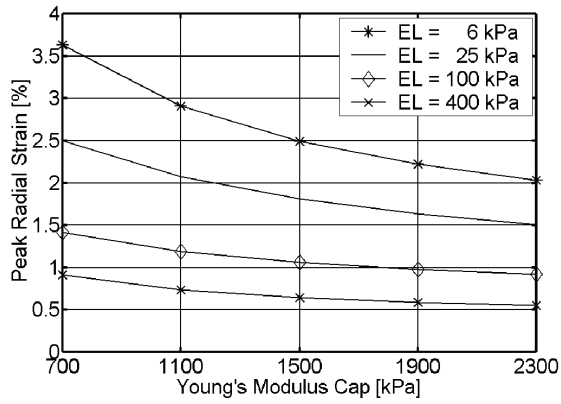


Fig. 5. Artery material variation for different stiffnesses of lipid and cap: Peak radial strain as function of Young's modulus of lipid (EL) and cap. For softer caps and lipid pools, the peak strains are higher; they are located mainly at a lipid shoulder.

Figure 4 shows a big decrease in radial strain at the shoulders of the lipid pool when the Young's modulus of the lipid pool EL is varied, while there is no visible change when ν of the whole artery is varied. *Lipid pool material variation*

Figure 5 shows the same results for different Young's moduli of the total cap. The PRS increases when the cap weakens, and is mainly located at a shoulder of the lipid pool. The PRS is higher for softer lipid pools. The total PRS variation was 3.1 %, i.e. from 0.6 % up to 3.7 %. In contrast, ν -variation of the whole artery gave a PRS variation only 0.17 %. *Cap material variation*

Figure 6, shows a monotonic increase of PRS with decreasing cap thickness; the weaker the cap, the higher the PRS. The curves seem to converge to each other, when cap thickness approaches zero. The total PRS variation was 1.4 %, i.e. from 0.3 % up to 1.7 %. *Cap thinning and cap weakening*

Figure 7 shows that catheter position variation in the artery FEM, changes the radial strain values. In all the four cases changes in radial strain value are mainly apparent at the lipid pool shoulders, nevertheless a high strain spot is still detectable at these shoulders. *Catheter position variation*

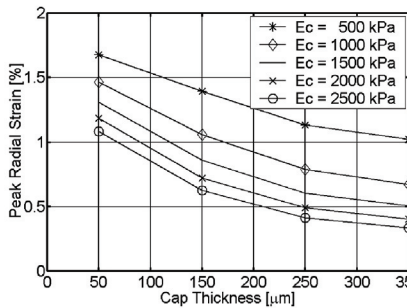
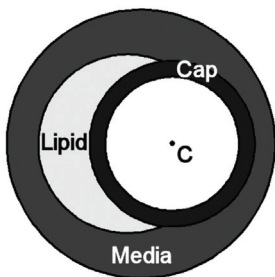


Fig. 6. Peak radial strain as function of cap thinning and cap weakening:

(Left) Parametric finite element model geometry for typical vulnerable plaques. Diameter of lumen circle is 3 mm. Young's moduli of lipid and media are 25 and 1000 kPa, respectively.

(Right) Peak radial strain as function of cap thickness for different cap stiffness E_c . For weaker or thinner cap, the peak strains are higher; they are located mainly at a lipid shoulder.

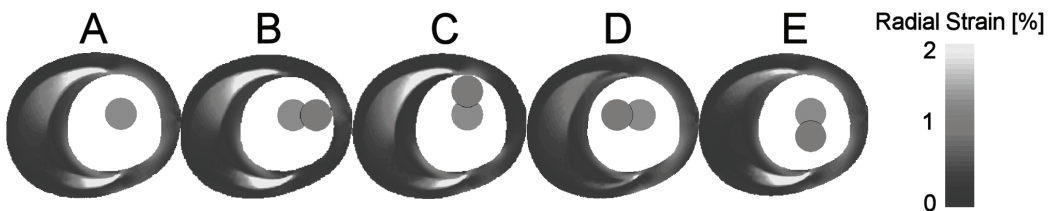


Fig. 7. Catheter position variation in artery: The radial strain distribution is visualized for different catheter positions, which are 0.8 mm translated towards the lumen boundary. The high strain value and area near the lipid shoulders change when the catheter position is varied.

DISCUSSION

We visualized and quantified the influence of plaque material composition, plaque geometry, and used catheter position upon (peak) radial strain depicted in IVUS elastograms using finite element models. The parameter variations were performed on finite element models mimicking a real phantom, real artery and a typical vulnerable plaque. It was shown that the parameter variations have substantial influence on the radial strain, except for the Poisson's ratio.

Realistic ranges for parameter variations

The ranges in which the material parameters were varied are realistic: The Young's modulus variations for the phantom model were done around the experimentally measured values; for the artery they covered values measured and/or used by other research groups. The used phantom material, and arteries in general, are known to be (nearly) incompressible and thus have a Poisson's ratio value larger than 0.49.

The tissue deformation model can be justified

Although the models used in this study do not incorporate all the complex biomechanical features that arteries possess, the use of the linear elastic, isotropic, plane strain, (nearly) incompressible finite element models in this study can be justified. This justification is due to the small semi-static incremental character of the tissue deformation when performing IVUS elastography and is given in (Baldewsing et al. 2004).

INTERPRETATION OF RESULTS

The strain hardening artefact in the plaque of the phantom (fig. 1) is caused by stress decay. The stress decay results from the circular geometry of the whole phantom. The mechanical shadowing artefact in the lipid pool of the artery (fig. 2) is caused by a combination of a relatively high stiff cap and its circumferentially distributed geometry, hindering compression behind it. The peak radial strain curves in figure 6 seem to converge to one peak radial strain value when the cap thickness approaches zero. This is expected, since a cap thickness of zero implies that there is no cap, but only the lipid pool that causes the peak radial strain. Catheter position variation changed the radial strain values (fig. 7). This is caused by the fact that, at each tissue point, the radial strain is a projection of the maximum strain value onto the ultrasound beam direction (i.e. line between tissue point and catheter); misalignment between these two directions causes underestimation of the maximum strain. The simulation experiments and results are also expected to be valid in an in vivo situation, although a correction for the possible external pressure sources (e.g. heart and veins) should be applied on the boundaries of the FEM models.

CLINICAL IMPLICATIONS AND FUTURE APPLICATIONS

The parameter variation results may be used to relate (peak) radial strain, as measured with IVUS elastography, to underlying plaque morphology and material state (vulnerability). The results also show that precise Poisson's ratio value, in the incompressibility range, is not needed for simulating incremental radial strain of arteries. Besides that, the results indicate that IVUS elastograms of typical vulnerable plaques are highly sensitive for Young's modulus variations of lipid and cap, which is a necessary property for iterative Young's modulus reconstruction methods, that try to convert an elastogram into a Young's modulus image. Such an image may be interpreted as a plaque component image due to the large Young's modulus contrast between plaque components. The results demonstrate that IVUS palpography (i.e. IVUS elastography restricted to the first 0.5 mm of lumen tissue) is less affected by the strain artefacts than IVUS elastography and is still able to obtain the diagnostically important high strain regions at the lipid shoulders for various, non-centered catheter positions. Finally, the results explain the cause of strain artefacts in IVUS elastograms of typical vulnerable plaques, such as strain hardening and mechanical shadowing; these artifacts may even be compensated for using a finite element model.

CONCLUSION

We have measured IVUS elastograms in vitro from a heterogeneous phantom, containing a soft eccentric plaque, and a human coronary artery containing a vulnerable plaque. For both phantom and artery, finite element models were created. These models were used to vary the material properties, geometry, and catheter position to investigate their influence upon the incremental radial strain depicted in measured IVUS elastograms. The results suggest that:

- Measured IVUS elastograms depend highly upon the Young's modulus of lipid and cap, but hardly upon the Poisson's ratio (>0.49) of a plaque.
- Different catheter positions result in different IVUS elastograms; nevertheless, the diagnostically important high strain regions at the lipid shoulders are still detectable.
- Peak radial strain increases when cap thickness decreases; the weaker the cap, the higher the peak radial strain.

ACKNOWLEDGEMENT

This work is supported by the Netherlands Organization for Scientific Research (NWO) and the Dutch Technology Foundation (STW).

REFERENCES

- Baldewsing RA, de Korte CL, Mastik F, Schaar JA, van der Steen AFW. *Comparison of finite elements model elastograms and ivus elastograms acquired from phantoms and arteries*. Proceedings of the 2002 IEEE International Ultrasonics Symposium 2002;1873-6.
- Baldewsing RA, de Korte CL, Schaar JA, Mastik F, van der Steen AFW. *A finite element model for performing intravascular ultrasound elastography of human atherosclerotic coronary arteries*. Ultrasound in Medicine and Biology 2004;30(6):803-13.
- Casscells W, Naghavi M, Willerson JT. *Vulnerable atherosclerotic plaque: A multifocal disease*. Circulation 2003;107:2072-5.
- Chu KC and Rutt BK. *Polyvinyl alcohol cryogel: an ideal phantom material for mr studies of arterial flow and elasticity*. Magnetic Resonance in Medicine 1997; 37: 314-19.
- Davies MJ. *Stability and instability: Two faces of coronary atherosclerosis. The Paul Dudley White lecture 1995*. Circulation 1996;94:2013-20.
- de Korte CL, Carlier SG, Mastik F, Doyley MM, van der Steen AFW, Serruys PW, Bom N. *Morphological and mechanical information of coronary arteries obtained with Intravascular elastography: a feasibility study in vivo*. European Heart Journal 2002a;23:405-13.
- de Korte CL, Céspedes EI, van der Steen AFW. *Influence of catheter position on estimated strain in intravascular elastography*. IEEE transactions on Ultrasound, Ferroelectrics and Frequency Control 1999;46:616-25.
- de Korte CL, van der Steen AFW. *Intravascular ultrasound elastography: an overview*. Ultrasonics 2002b;40:859-65.
- de Korte CL, van der Steen AFW, Céspedes EI, Pasterkamp G. *Intravascular ultrasound elastography of human arteries: initial experience in vitro*. Ultrasound in Medicine and Biology 1998;24:401-8.
- Ophir J, Céspedes EI, Garra B, Ponnekanti H, Huang Y, Maklad N. *Elastography: ultrasonic imaging of tissue strain and elastic modulus in vivo*. European Journal Ultrasound 1996;3:49-70.
- Pasterkamp G, Virmani R. *The erythrocyte: a new player in atheromatous core formation*. Heart 2002;88:115-6.

PART III
INVERSE PROBLEM

ASSESSMENT OF VULNERABLE PLAQUE COMPOSITION BY MATCHING THE DEFORMATION OF A PARAMETRIC PLAQUE MODEL TO MEASURED PLAQUE DEFORMATION

ABSTRACT

BACKGROUND

IntraVascular UltraSound (IVUS) elastography visualizes local radial strain of arteries in so-called elastograms to detect rupture-prone plaques. However, due to the unknown arterial stress distribution, these elastograms cannot be directly interpreted as a morphology and material composition image. To overcome this limitation we have developed a method that reconstructs a Young's modulus image from an elastogram. This method is especially suited for thin-cap fibroatheromas (TCFAs), i.e., plaques with a media region containing a lipid pool covered by a cap.

METHODS

Reconstruction is done by a minimization algorithm that matches the strain image output, calculated with a Parametric Finite Element Model (PFEM) representation of a TCFA, to an elastogram by iteratively updating the PFEM geometry and material parameters. These geometry parameters delineate the TCFA media, lipid pool and cap regions by circles. The material parameter for each region is a Young's modulus, E_{MEDIA} , E_{LIPID} and E_{CAP} , respectively. The method was successfully tested on computer-simulated TCFAs ($n=2$), one defined by circles, the other by tracing TCFA histology, and additionally on a physical phantom ($n=1$) having a stiff wall (measured $E_{\text{MEDIA}}=16.8$) with an eccentric soft region (measured $E_{\text{LIPID}}=4.2$). Finally, it was applied on human coronary plaques in vitro ($n=1$) and in vivo ($n=1$).

RESULTS

The corresponding simulated and measured elastograms of these plaques showed radial strain values from 0% up to 2% at a pressure differential of 20, 20, 1, 20 and 1 mmHg respectively. The used/reconstructed Young's moduli [kPa] were for the circular plaque $E_{\text{LIPID}}=50/66$, $E_{\text{MEDIA}}=1500/1484$, $E_{\text{CAP}}=2000/2047$, for the traced plaque $E_{\text{LIPID}}=25/1$, $E_{\text{MEDIA}}=1000/1148$, $E_{\text{CAP}}=1500/1491$, for the phantom $E_{\text{LIPID}}=4.2/4$ kPa, $E_{\text{MEDIA}}=16.8/16$, for the in vitro plaque $E_{\text{LIPID}}=n.a./29$, $E_{\text{MEDIA}}=n.a./647$, $E_{\text{CAP}}=n.a./1784$ kPa and for the in vivo plaque $E_{\text{LIPID}}=n.a./2$, $E_{\text{MEDIA}}=n.a./188$, $E_{\text{CAP}}=n.a./188$ kPa.

CONCLUSION

The method can successfully reconstruct the Young's modulus distribution of a TCFA from its elastogram.

THIS CHAPTER IS BASED ON THE PUBLICATION

*“Assessment of Vulnerable Plaque Composition by
Matching the Deformation of a Parametric Plaque Model to Measured Plaque Deformation”*,

BY BALDEWSING RA, SCHAAR JA, MASTIK F, OOMENS CWJ AND VAN DER STEEN AFW,
IN IEEE TRANSACTIONS ON MEDICAL IMAGING (SPECIAL ISSUE ON VASCULAR IMAGING), 24(4):514-28;2005,

Copyright © 2005 IEEE.

This material is posted here with permission of the IEEE. Such permission of the IEEE does not in any way imply IEEE endorsement of any of Erasmus University's products or services. Internal or personal use of this material is permitted. However, permission to reprint/republish this material for advertising or promotional purposes or for creating new collective works for resale or redistribution must be obtained from the IEEE by writing to pubs-permissions@ieee.org. By choosing to view this document, you agree to all provisions of the copyright laws protecting it.

INTRODUCTION

The majority of acute coronary syndromes, such as unstable angina, myocardial infarction or sudden cardiac death, are caused by coronary thrombosis (Davies 2000, Falk et al. 1995). More than 60% of these thrombi are caused by rupture of vulnerable, thin-cap fibroatheroma (TCFA) plaques (Virmani et al. 2000). Their morphological features are a large lipid core, covered by a thin fibrous cap. Considered as major determinants for their rupture are their material composition, geometry, and cap inflammation caused by infiltration of macrophages (Davies 2001). As such, identification of these rupture-determinants is of vital diagnostic importance (Schaar et al. 2004).

Acute coronary syndromes and plaque rupture determinants

IntraVascular Ultrasound (IVUS) elastography is a technique that determines arterial radial strain by cross-correlation processing on a pair of IVUS radio-frequency signals; each signal is measured with an IVUS catheter at a different intraluminal pressure (Brusseau et al. 2002, Choi et al. 2002, de Korte et al. 2003, Perrey et al. 2003, Ryan et al. 1997, Saijo et al. 2004, Shapo et al. 1996, Talhami et al. 1994). This arterial radial strain is visualized in a so-called (strain) elastogram. IVUS elastography is clinically available and has proven to be capable of detecting the presence of human TCFAs in vitro with a sensitivity of 88% and specificity of 89%, merely by inspecting the elastogram for a specific strain pattern that consists of high strain with adjacent low strain on the surface of a plaque (Schaar et al. 2003). In vivo animal experiments and in vitro human experiments demonstrated that discrimination between fibrous and fatty plaques is possible, merely by determining the average radial strain value of the plaque (de Korte et al. 2000b, de Korte et al. 2002b). The in vivo animal experiments also showed that the presence of a high strain spot at the plaque surface had a sensitivity of 92% and a specificity of 92% for identifying macrophages. Although these studies have shown that a specific radial strain pattern and the average radial strain of a plaque can provide valuable information, there doesn't exist a one-to-one relation between the local radial strain value in an IVUS elastogram and the local tissue component type (calcified, fibrous, fatty or tissue infiltrated by macrophages). The underlying reason is that the local stresses that induce local radial strain depend upon the structural configuration of the artery and the material properties and geometry of its plaque components. Furthermore, radial strain depends on the catheter position used during imaging (Baldewsing et al. 2004b, de Korte et al. 1996, de Korte et al. 1999, Ophir et al. 1996). Thus, IVUS elastograms cannot be interpreted directly as plaque component images.

IVUS elastograms cannot be directly interpreted as plaque component images

This limitation can be overcome by calculating an image of the Young's modulus distribution. Such an image can be interpreted as a morphology and material composition image of a plaque, due to the large differences between Young's moduli of plaque components, like calcifications, healthy arterial tissue, lipids or tissues weakened by infiltration of macrophages (Bergel 1961, de Korte et al. 2000b, Dobrin 1978, Fung 1981, Gow et al. 1979, Lee et al. 1991, Lee et al. 1992, Lendon et al. 1991, Loree et al. 1994a, Lu et al. 2003, Matsumoto et al. 2002, Mozersky et al. 1972, Salunke et al. 1997, Yamada et al. 1970). Many researchers have used displacement and/or strain components that were derived from simulated or measured ultrasound data or other imaging modalities in combination with tissue deformation equations, to compute a Young's modulus image. Usually a 'direct' or 'iterative' reconstruction method is employed. With a direct reconstruction method the deformation equa-

Reconstructing an image of the Young's modulus distribution

tions are rewritten to express the moduli as unknowns. Subsequently, they are solved by means of an analytical formula or by a discretization or numerical integration approach. With iterative reconstruction, the moduli values of each individual mesh element or groups of mesh elements in a finite element model representation of the tissue are iteratively updated such that the computed model output eventually resembles the experimentally measured data (e.g., displacement or strain components). Many groups have applied these methods on a two dimensional cross-section of a homogeneous rectangular medium with a circular or rectangular inclusion using a direct method (Cohn et al. 2000, Raghavan et al. 1994, Skovoroda et al. 1995, Sumi et al. 2000, Wellman et al. 1999, Zhu et al. 2003) or an iterative method (Bishop et al. 2000, Doyley et al. 2000, Fu et al. 2000, Kallel et al. 1996). Some applied an iterative method to breast (Miga 2003, Plewes et al. 2000, Samani et al. 2001), prostate (Sarvazyan 1998), brain (Van Houten et al. 1999) or heart (Moulton et al. 1995). However, only a few groups considered arteries. Some of them used an iterative method (Beattie et al. 1998, Chandran et al. 2003, Soualmi et al. 1997, Vorp et al. 1995), others a direct method (Bank 1999, Kanai et al. 2003, Wan et al. 2001).

Reconstruction problems

Both inversion techniques suffer to different degree from stability problems like non-uniqueness and non-convergence. Various groups (Barbone et al. 2002, Barbone et al. 2004, Beattie et al. 1998, Kallel et al. 1996, Moulton et al. 1995, Skovoroda et al. 1995, Sumi et al. 1995) have mentioned possible causes, such as measurement noise, a limited number of measured displacement or strain components, boundary data that is erroneous or of an incorrect type, a Finite Element Model (FEM) with too many (physically not interpretable) parameters, or an inappropriate FEM.

A new reconstruction method specially suited for TCFAs

The ultimate clinical goal is to obtain a diagnostically useful and easily interpretable modulus image of an arbitrary complex atherosclerotic plaque using a modulus imaging method, which suffers as little as possible from stability problems. To proceed towards this goal and to be able to investigate and quantify reconstruction problems in a systematic way, we developed a new reconstruction method specially suited for TCFAs (Davies 2001, Schaar et al. 2004, Virmani et al. 2003). Our method uses an iterative reconstruction approach to produce a Young's modulus image. To this end, the deformation output, calculated with a Parametric Finite Element Model (PFEM) representation of a TCFA plaque, is matched to plaque deformation measured with IVUS elastography. The PFEM uses a minimum number of morphology and material composition parameters, but is still able to model a variety of these TCFAs. The resulting Young's modulus image of the plaque shows both the morphology and Young's modulus value of three main plaque components, namely lipid, cap and media and is therefore fast and easy to interpret in clinical settings.

Aims of this study

The aims of this study are twofold: Firstly, to describe the new reconstruction method. Secondly, to demonstrate its ability to successfully reconstruct Young's modulus images from elastograms obtained from five TCFA plaques. These elastograms are simulated using finite element models, measured from vessel-mimicking material, and measured from human coronary arteries in vitro and in vivo.

MATERIALS

A. SIMULATED ARTERIES WITH PLAQUE

Two different finite element models were constructed for a realistic TCFA; one TCFA was defined using circles, the other by tracing TCFA histology.

B. PHANTOM WITH PLAQUE

One vessel-mimicking phantom with an eccentric, soft region embedded in a stiff wall was made from 10% PolyVinyl Alcohol (PVA) Cryogel (Chu et al. 1997) as described in (Baldewising et al. 2004a). Carborundum (SiC) particles (3-10 μm) were added as ultrasound scattering material. The static Young's moduli were measured in a custom designed tension set up. The static Young's modulus was 4.2 kPa for the

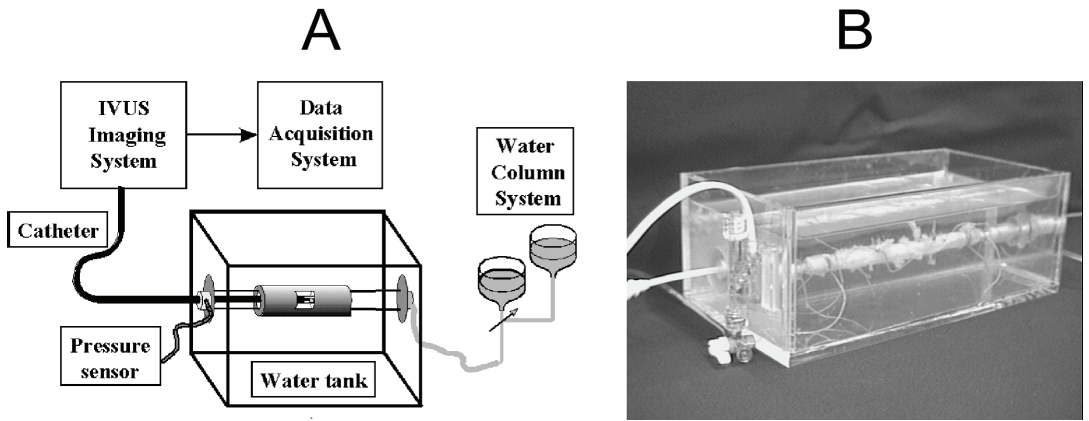


Fig. 1. (A) Experimental set-up consisting of a water column system, water tank, pressure sensor, catheter, IVUS imaging system and data acquisition system. (B) Photograph of the water tank containing an atherosclerotic human artery; all arterial side branches are closed with suture.

plaque and 16.8 kPa for the wall. The pressure-free phantom had a length of 150 mm, an outer diameter of 18 mm, and an inner diameter of approximately 4 mm.

C. HUMAN CORONARY ARTERIES WITH PLAQUE

A coronary artery segment with a TCFA was excised from one patient who died of a non-coronary cause. Furthermore, *in vivo* measured IVUS radio-frequency data were obtained from a non-culprit coronary artery of one patient referred for percutaneous transluminal coronary angioplasty. The IVUS data revealed the presence of a large eccentric plaque.

METHODS

A. ELASTOGRAPHY SIMULATIONS AND MEASUREMENTS

Elastograms were simulated for two TCFA using the finite element package SEP-RAN (Septra Analysis, Technical University Delft, The Netherlands). Linear elastic, isotropic, nearly incompressible (Poisson's ratio $\nu = 0.4999$), plane strain finite element models were used for this purpose, because it has been demonstrated (Baldewsing et al. 2004a) that such models are appropriate to simulate radial strain elastograms that are measured *in vitro* from human atherosclerotic coronary arteries using IVUS elastography. The geometry of the first TCFA was defined by using circles. The geometry of the second TCFA was defined by tracing the histology of an excised human coronary artery with a TCFA. The material properties of the TCFA components (Table 1) and pressure differential of 20 mmHg were taken from values

Elastography simulations

TABLE 1: YOUNG'S MODULUS (E) AND POISSON'S RATIO (ν) USED IN FINITE ELEMENT MODELS FOR ARTERIAL PLAQUE CROSS-SECTIONS.

MATERIAL PARAMETER	PLAQUE 1	PLAQUE 2
E lipid [kPa]	50	25
E cap [kPa]	2000	1500/1250
E media [kPa]	1500	1000
ν cross-section[-]	0.4999	0.4999

reported in (Baldewsing et al. 2004a, 2004b). Histology revealed a layer of collagen and a layer of smooth muscle cells resulting in the two Young's moduli values for different regions in the cap. The finite element mesh consisted of plane-strain triangular finite elements with extended quadratic interpolation functions. The averaged

finite element size was approximately 0.1 mm. The radial strain was calculated with respect to the geometric center of the lumen border.

Experimental setup for elastography measurements

The experimental setup for performing elastography measurements with the phantom and in vitro artery consisted of a water tank equipped with two insertion sheaths (fig. 1). The water tank was connected via the distal sheath to a water column system, which contained distilled water for the phantom and a degassed physiological saline solution for the in vitro artery. The phantom and in vitro artery were subsequently mounted between the two sheaths. Also the arterial side-branches were closed with suture material to prevent leakage (Schaar et al. 2002). The column system was used to apply intraluminal pressures and to perform preconditioning. Preconditioning of the artery was done by loading the artery with 100 mmHg pressure and subsequently unloading it to ambient pressure, for at least five cycles (Lally et al. 2004). A 20-MHz 64-element phased array IVUS catheter (Volcano Inc., Rancho Cordova, CA) connected to an InVision echo apparatus (Volcano Inc., Rancho Cordova, CA) was inserted in the proximal sheath. The pressure was monitored using a pressure sensor that was also connected to the proximal sheath.

Elastography measurements with phantom and in vitro artery

Elastography measurements for the in vitro artery were done within 24 hours post mortem and directly after preconditioning (Schaar et al. 2003). First, an IVUS echo frame was acquired at an intraluminal pressure of 5 mmHg for the phantom and 80 mmHg for the artery. After 10 seconds, another IVUS echo frame was acquired at 6 mmHg for the phantom and 100 mmHg for the in vitro artery. Each echo frame consisted of 512 angles of raw radio-frequency (RF) data-lines sampled at 100 MHz in 12 bits. Each line contained 1024 data points (corresponding to 7.6 mm imaging depth). The intraluminal pressures were chosen to strain the phantom and the artery up to a maximum of 2.5%. This strain value is an upper limit for properly calculating the local radial strain using the cross-correlation method described by de Korte et al. (1998) with a window length of 60 RF data points, 50% window overlap and a 20-MHz center frequency of the ultrasound signal. This cross-correlation technique was applied to the ultrasound data to calculate the local radial strain. First, the radial tissue displacement along the ultrasound beam was determined. Then, finite differences of these displacements resulted in the local radial strain. Since a window length of 60 RF data points was used with 50% window overlap, the spatial resolution of the strain determination was 30 RF data points in the radial direction (approximately 200 μm). Strain estimates of the phantom, in vitro artery and in vivo artery were clipped respectively between 0% (color coded in black) and an upper strain value (color coded in white).

Histology

The histology of the in vitro artery was created from the tubular segment that was elastographically imaged. This segment was pressure-fixed at 80 mmHg, sectioned, and counterstained for the presence of collagen (picro Sirius red), smooth muscle cells (alpha-actin) and macrophages (CD-68).

Elastography measurements in vivo

A multiframe averaging method similar to the one described in Doyley et al. (2001) was used to compute a compounded elastogram. First, IVUS echo frames were acquired at 30 fps. Next, at the diastolic phase of a cardiac cycle, when catheter motion is minimal, a consecutive sequence of 7 echo frames was selected. Each consecutive frame pair was highly correlated, i.e., the sum-of-absolute-differences between the RF-envelopes of a consecutive frame pair divided by the sum of RF-envelopes of the first frame was less than 0.1. Furthermore, the total incremental rotation of the catheter was less than 1 degree. The measured intraluminal pressure was 53 mmHg for the first frame and 60 mmHg for the seventh frame; intraluminal pressure difference between consecutive frames was 1 mmHg. From each consecutive frame pair an elastogram was computed using the method describe above for the phantom and in vitro artery. Finally, a compounded elastogram was computed by averaging the 6 elastograms (Baldewising et al. 2004c); throughout this chapter this elastogram is denoted as 'in vivo measured elastogram'.

B. PARAMETRIC MODEL-BASED RECONSTRUCTION METHOD

The main components of the reconstruction method were the Parametric Finite Element Model (PFEM) for a plaque, the forward problem calculation, and minimization algorithm used:

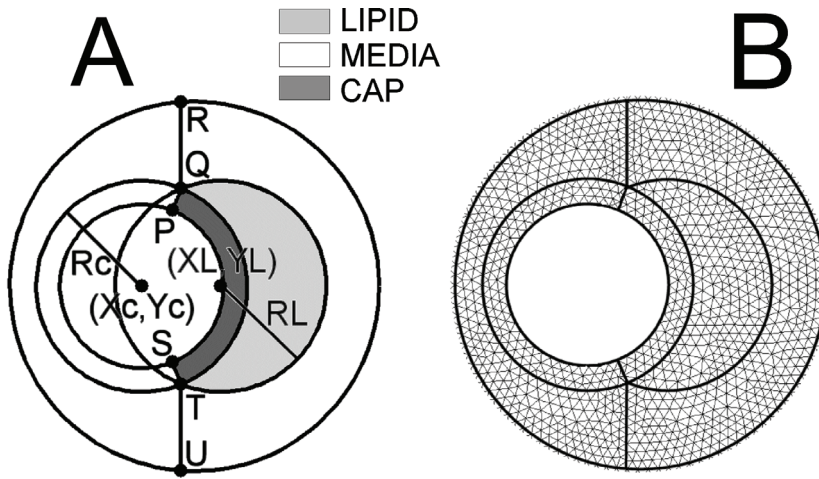


Fig. 2. Parametric Finite Element Model for a Vulnerable Plaque. (A) Each circle is parameterized by its center (X, Y) and a radius R . The dynamic control points $P, Q, R, S, T,$ and U are used to define the three plaque components. (B) Finite element mesh regions corresponding to geometry in A. Letters L and c denote lipid and cap, respectively.

An idealized TCFA (Virmani et al. 2003) was used as model for a plaque. Our model is a variation of the PFEM used by Loree et al. (1992). Our PFEM geometry consisted of a media area containing a lipid pool, which was covered by a cap. The borders of the lipid, cap, and media areas were defined using circles (fig. 2A). Lipid was defined as region QTQ , cap as region $PQTSP$ and media as the remaining area. Each circle was parameterized by its center with Cartesian coordinates (X, Y) and radius R . Arterial tissue was modeled in the PFEM as linear elastic, isotropic, nearly incompressible (Poisson's ratio $\nu=0.4999$), plane strain material (Baldewsing et al. 2004a, Baldewsing et al. 2004b). The lipid, cap, and media regions were assumed homogenous. The Young's modulus values of these regions were denoted as E_{LIPID} , E_{CAP} , and E_{MEDIA} , respectively.

First, parameters were specified that define the geometry and Young's modulus values of the PFEM, and pressure boundary conditions. Then, a mesh topology file was created from these parameters using MATLAB (release 12.1, the MathWorks, Inc.). Next, the finite element package SEPRAN used this file to calculate a finite element mesh consisting of plane-strain triangular elements (e.g., fig. 2B) with extended quadratic interpolation functions. Then, it calculated the Cartesian strain tensor components in these mesh points. Finally, MATLAB converted these Cartesian components to their polar equivalents using the catheter center as origin. The radial strain component field was subsequently interpolated onto a reference grid, i.e., square equidistant grid of 100 by 100 points. This radial strain field was called a PFEM elastogram. For each reconstruction, the size of the square reference grid was chosen such that it tightly surrounded the arterial wall region. The whole process from defining the PFEM parameters up to the calculation of the PFEM elastogram was fully automatic. The simulated and measured elastograms were also interpolated onto the corresponding reference grid.

A Constrained Sequential Quadratic Programming minimization algorithm (Optimization Toolbox, MATLAB) was used, that automatically searches a local minimum of a non-linear objective function, i.e., quantification of the difference between PFEM elastogram and a simulated or measured input-elastogram, by iteratively updating the PFEM parameters. At every iteration the six PFEM geometry and three PFEM material parameters were all simultaneously updated. The objective function was defined as the Root-Mean-Squared (RMS) error between PFEM elastogram and input-elastogram. The RMS error was calculated from the strain values that belong to those reference grid points that are shared by the input-elastogram (i.e., simulated or measured elastogram) and the PFEM elastogram. At every iteration the RMS error decreases. The average time between two iterations was 45 seconds on a computer with a 3 GHz Xeon processor.

PFEM for a plaque

Forward problem (i.e., radial strain image calculation)

Minimization algorithm

Description of the algorithm

A detailed mathematical description of the algorithm can be found in the Optimization Toolbox of MATLAB. The basic steps were as follows. At each major iteration a simultaneous update for all parameters was computed by solving a quadratic subproblem. This subproblem was generated by approximating the Hessian matrix of the Lagrangian function, using a quasi-Newton updating method. The solution of this subproblem was then used to form a search direction for a line search method, which resulted in the update.

Positioning of PFEM lumen and media circle

For all reconstructions, the PFEM lumen circle was defined (i.e., its center coordinates and radius was determined) as the largest circle within the lumen border. Similarly, the PFEM media circle was defined as the smallest circle enclosing the media contour. For both the in vitro and in vivo artery, the media contour was defined as the media-adventitia border, which was visible in the echogram as an echolucent contour with distal brightening. In case of the phantom, whose diameter was 18 mm and thus exceeded the 15.2 mm diameter of the echogram, the part of the wall boundary that was visible in the echogram was extrapolated. For the two simulated arteries, the media contour was already defined during their creation.

Nonlinear constraints

In order to maintain the morphology of an idealized TCFA (fig. 2A) and to automatically calculate a proper finite element mesh (e.g., fig. 2B) during the minimization process, the following nonlinear geometry constraints were enforced upon the PFEM geometry parameters: (i) The lipid circle must have exactly two intersection points with the cap circle (Q and T). (ii) The cap circle must always contain the lumen circle. (iii) The lipid circle must always be inside the media circle. The other dynamic mesh-control points (P, R, S, and U in fig. 2A) were automatically calculated and used to define the three plaque regions. Point P (and analogously S) was defined as the projection of point Q onto the lumen circle. Point R and U were located on the media circle such that line QR and TU bisected the angle between two direction-vectors that were defined as the outward normal of respectively the lipid and cap circle at point Q and T. The separation of the media region by the two line pieces RQ and TU was done to make the finite element meshing of the media region more robust.

Linear constraints

Furthermore, to speed-up the minimization process, the range of each PFEM parameter was restricted to stay within a user-defined lower bound and upper bound value. These bounds were, by definition, linear constraints and chosen as follows. The centers of the cap and lipid pool circles were restricted to stay within the smallest square that fitted around the PFEM media circle. The radii of the cap and lipid pool were nonnegative and bounded by the radius of the PFEM media circle. The Young's moduli were all chosen to be positive. For the two simulated arteries, the upper bound was set arbitrarily at 500 kPa higher than the Young's modulus of the stiffest plaque components, namely that of the cap. Similarly, the upper bound of the phantom was set at 25 kPa, which is arbitrarily higher than the measured Young's moduli of its components, namely 4.2 and 16.8 kPa. For the in vitro artery, the same upper bound was used as for the simulated artery that was traced from histology, because they showed resemblance in their geometry and their elastograms showed similar maximal strain at the same pressure differential of 20 mmHg. Finally, the in vivo artery showed approximately the same maximum strain as the in vitro and the two simulated arteries, however at a 20 times lower pressure differential, namely 1 mmHg, therefore the upper bound was set proportionally lower, at 300 kPa.

The minimization algorithm was terminated after 25 iterations or if the decrease in RMS error was less than 10^{-8} .

Initialization of reconstruction method

At the start of each reconstruction an initial state is required for the PFEM geometry and material parameters that are varied by the minimization algorithm, namely the lipid and cap circle parameters and the Young's modulus of the lipid, cap and media region. Each initial state was chosen so that it differed from the actual underlying plaque composition. For all the reconstructions, the cap and lipid pool circles were

put arbitrarily in the direction of the plaque. For all reconstructions, except the first, an initial modulus contrast was used between the plaque components, by setting the modulus of the cap and media close to the upper-bound value and the modulus of the lipid close to the lower-bound value. Finally, the phantom only consisted of two regions: a soft homogenous region within a stiff homogenous wall. To model this situation appropriately, the following additional constraints were enforced upon the PFEM during the minimization: (i) the cap circle was kept fixed during the minimization and (ii) the Young's modulus of this cap region was kept equal to the Young's modulus of the lipid region.

C. UNIQUENESS ESTIMATION

For the *in vivo* case, the actual underlying plaque composition was unknown. Therefore, multiple reconstructions were performed using a set of different initial states. This was done (i) to enhance the chance of finding a successful reconstruction, i.e., finding a reconstruction with a PFEM elastogram that highly resembles the measured elastogram and (ii) to estimate the uniqueness of a successful reconstruction. The initial states were defined, as follows: The cap circle had the same center as the lumen circle and was given a cap thickness of 100, 200 or 300 μm . The lipid circle was the same for all initial states, was slightly positioned in the direction of the plaque and occupied only a small area of the plaque. The initial Young's modulus values for the lipid pool (E_{LIPID}), cap (E_{CAP}) and media (E_{MEDIA}), were set at the following values: 0.1 or 10 kPa for E_{LIPID} and 100, 150, 200, 250 or 299 kPa for E_{CAP} ; the initial E_{MEDIA} value was set equal to the initial E_{CAP} value. These initial parameter values for cap thickness, E_{LIPID} and $E_{\text{CAP}} (= E_{\text{MEDIA}})$ resulted in $3^2 \cdot 5 = 30$ different initial states.

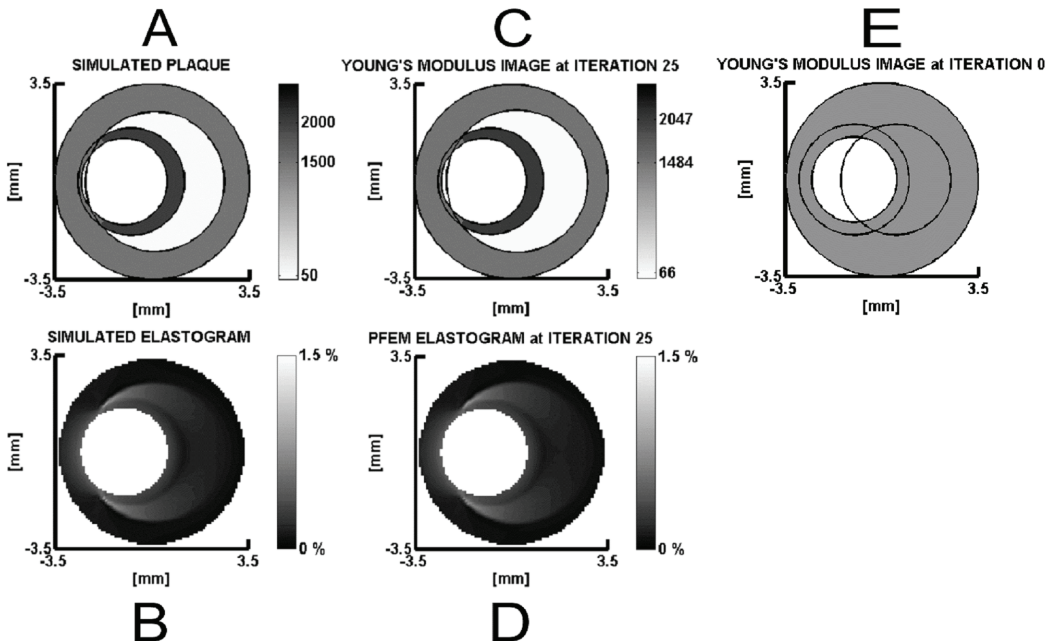


Fig. 3. Reconstruction from a simulated elastogram of a thin-cap fibroatheroma that consists of circles. (A) Young's modulus image in kPa used for simulating the plaque. (B) Simulated elastogram computed using A. (C) Reconstructed Young's modulus image in kPa. (D) PFEM elastogram computed using C; the RMS error is 0.016%. (E) Initial state at start of the reconstruction process: The Young's modulus of the lipid, cap and media plaque component is 1185 kPa.

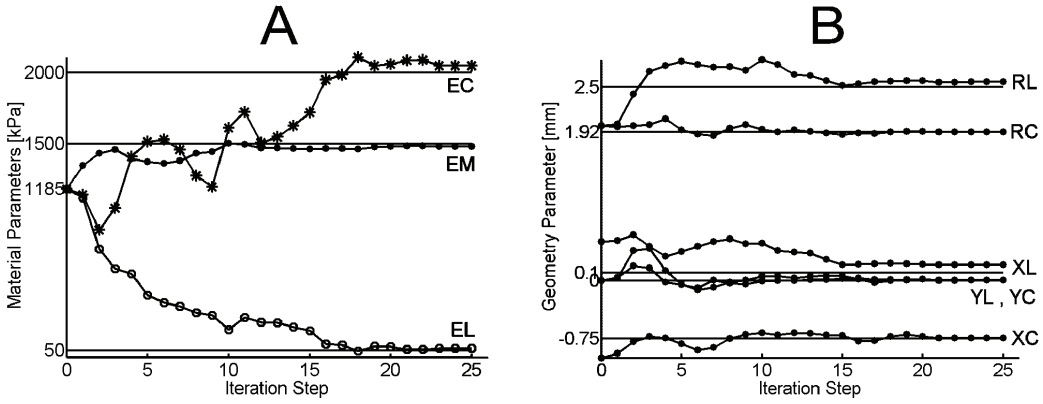


Fig. 4. PFEM-parameters versus iteration-step curves for the simulated TCFA that consists of circles. (A) Material parameters: Young's moduli for lipid pool (EL), cap (EC) and media (EM). Geometry parameters: Center coordinates and radius of the lipid pool circle (XL,YL) and RL, and cap (XC,YC) and RC. The solid lines are the parameter values used to create the simulated TCFA.

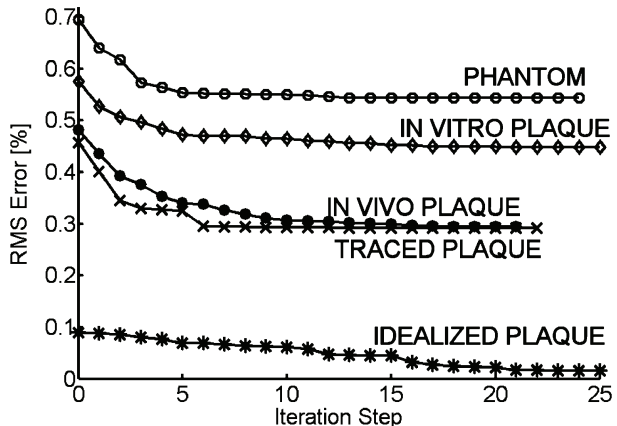
RESULTS

A. SIMULATED PLAQUES

Plaque 1: TCFA defined by circles

Figure 3A shows a simulated arterial TCFA that is defined by circles. The circumferential geometry and relatively high stiffness of the cap causes the arterial stress to concentrate on the cap, especially at its edges and around the corners of the lipid pool (Richardson et al. 1989); this redistribution mechanism causes the typical regions of high radial strain at the corners of the lipid pool in figure 3B and the relatively low strain at the center of the lipid pool (Loree et al. 1992). This elastogram shows a perfect example of the specific strain pattern, which consists of high strain with adjacent low strain on the surface of the plaque, that has proven to detect the presence of human TCFA's in vitro with a sensitivity of 88% and specificity of 89% (Schaar et al. 2003). The reconstructed Young's modulus image (fig. 3C) highly resembles the morphology and material composition of the simulated arterial TCFA in figure 3A (respectively, $E_{LIPID}=66$, $E_{CAP}=2047$, and $E_{MEDIA}=1484$ kPa versus $E_{LIPID}=50$, $E_{CAP}=2000$, and $E_{MEDIA}=1500$ kPa). Also the input-elastogram (fig. 3B) and the PFEM elastogram (fig. 3D) show a high resemblance. The initial state (fig. 3E) has no Young's modulus contrast between the three plaque components. Figure 4 shows the evolution of the PFEM material and geometry parameters during the reconstruction process; figure 4B shows quantitatively that the geometry of each plaque component is closely approximated. Figure 5B shows for each reconstruction presented in this paper the RMS error, which always decreases during the reconstruction process.

Fig. 5. RMS-error versus iteration-step curves for each of the five reconstructions presented in this paper. The idealized plaque denotes the simulated thin-cap fibroatheroma that consists of circles and the traced plaque denotes the simulated thin-cap fibroatheroma that is traced from arterial histology.



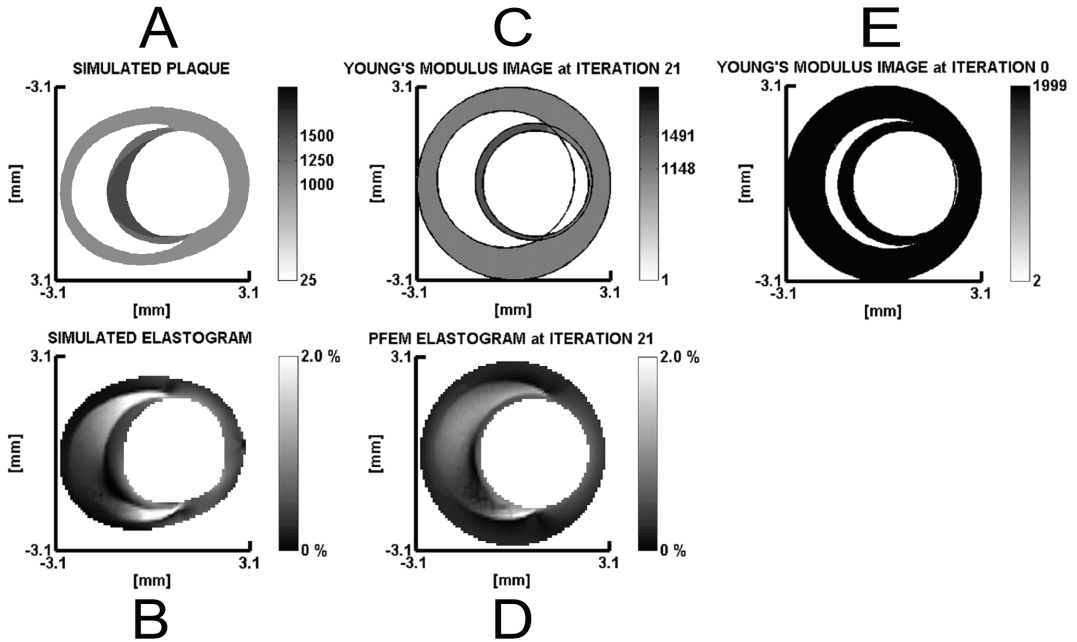


Fig. 6. Reconstruction using a simulated elastogram of a thin-cap fibroatheroma that is traced from arterial histology. (A) Young's modulus image in kPa traced from histology and used for simulating the plaque. (B) Simulated elastogram computed using A. (C) Reconstructed Young's modulus image in kPa. (D) PFEM elastogram computed using C; the RMS error is 0.29%. (E) Initial state at start of the reconstruction process.

Figure 6A shows a simulated TCFA that was traced from arterial histology. Just as plaque 1 it results in a simulated elastogram (fig. 6B) with similar typical regions of high and low strain. The Young's modulus image (fig. 6C) shows that both the morphology (which is not delineated by circles) and material composition of the simulated TCFA (fig. 6A) are successfully approximated (respectively, $E_{LIPID}=1$, $E_{CAP}=1491$, and $E_{MEDIA}=1148$ kPa versus $E_{LIPID}=25$, $E_{CAP}=1500$ (and cap side-regions 1250), and $E_{MEDIA}=1000$ kPa). Also a high resemblance between input-elastogram (fig. 6B) and PFEM elastogram (fig. 6D) is visible. The initial state (fig. 6E) has a large Young's modulus contrast between lipid and the other two plaque components and both the cap and lipid circle are positioned slightly in the direction of the plaque.

Plaque 2: TCFA defined by tracing histology

B. PHANTOM

Figure 7A shows the composition of the vessel-mimicking phantom that has a soft region embedded in a stiff wall. The echogram (fig. 7B) cannot be used to identify the two mechanically different regions. However, the measured elastogram (fig. 7C) reveals the presence of the soft region by means of the high strain region. This region shows a typical radial strain decay that results from a decreasing stress; this natural stress decrease is due to the circumferential vessel geometry. Only a limited range of phantom material is contained in the elastogram due to the limited imaging depth of the catheter (approximately 7.6 mm). The heterogeneous strain texture throughout the elastogram is caused by measurement noise and the gradient based calculation of strain. The Young's modulus image in figure 7D shows that both the circular morphology and material composition of the phantom are successfully approximated (respectively, $E_{LIPID}=4$ and $E_{MEDIA}=16$ kPa versus $E_{LIPID}=4.8$ and $E_{MEDIA}=16.8$ kPa). A high resemblance is obtained between input-elastogram (fig. 7C) and PFEM elastogram (fig. 7E). The initial state (fig. 7F) has a large Young's modulus contrast between the soft region (i.e., lipid) and stiff wall (i.e., media) and

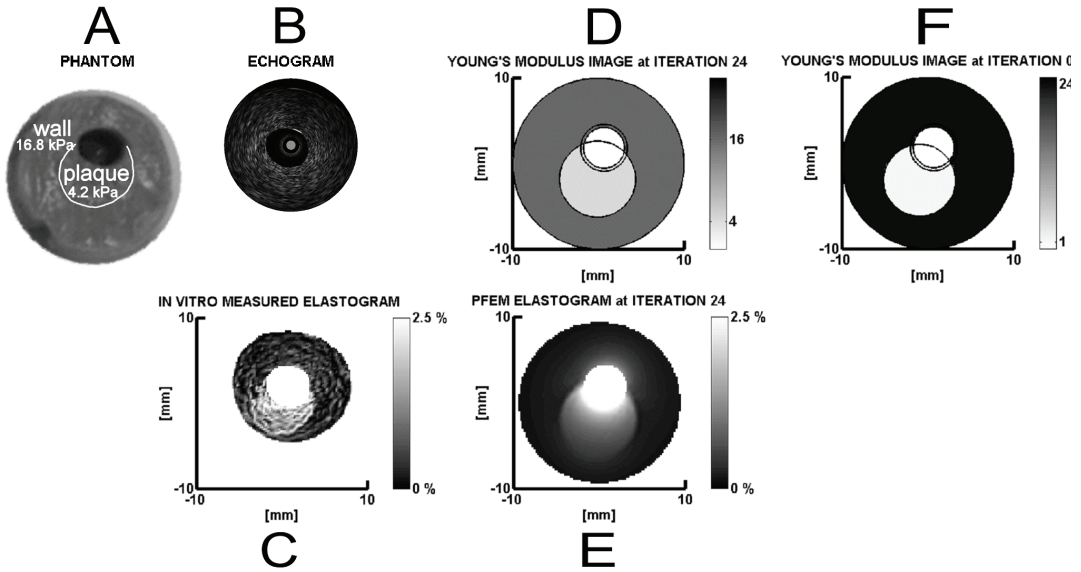


Fig. 7. Reconstruction using a measured elastogram from a vessel-mimicking phantom; it has a soft region embedded in a stiff wall. (A) Young's modulus image. (B) Echogram. (C) Measured elastogram. (D) Reconstructed Young's modulus image in kPa. (E) PFEM elastogram computed using D; the RMS error is 0.54%. (F) Initial state at start of the reconstruction process.

the lipid circle is positioned near the location indicated by the high strain region in the measured elastogram (fig. 7C).

C. HUMAN CORONARY ARTERIES WITH PLAQUE

In vitro plaque

Figs. 8A-C show that the *in vitro* plaque is a TCFA with a stiff media containing an even stiffer cap which overlays a soft lipid pool. The echogram (fig. 8D) reveals the plaque location but cannot be used to discriminate between its components, e.g., cap and lipid pool. Similarly as with plaque 1 and 2, the measured elastogram (fig. 8E)

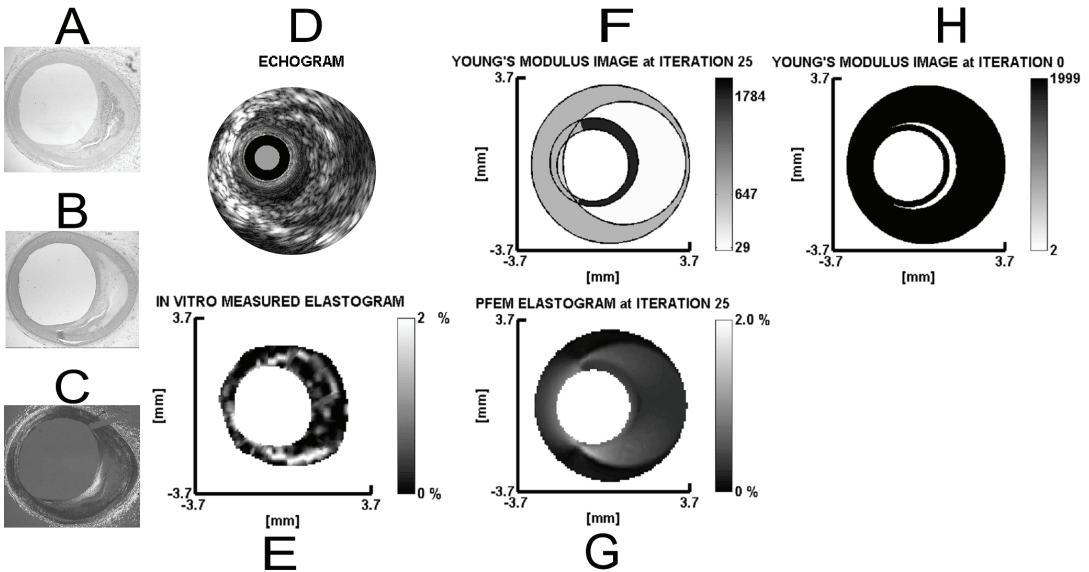


Fig. 8. Reconstruction using an *in vitro* measured elastogram from a human coronary artery with a thin-cap fibroatheroma. (A) Macrophages. (B) Smooth Muscle Cells. (C) Collagen. (D) Echogram. (E) In vitro measured elastogram. (F) Reconstructed Young's modulus image in kPa. (G) PFEM elastogram computed using F; the RMS error is 0.45%. (H) Initial state at start of the reconstruction process.

suggests the presence of the TCFA by means of the specific strain pattern. The heterogeneous strain texture throughout the elastogram is due to measurement noise and the gradient-based calculation of the strain. The Young's modulus image (fig. 8F) shows that both the morphology and stiffness contrast of the arterial plaque components are in qualitative agreement with, respectively, the morphology and stiffness contrast information provided by the histology of the plaque. Both the measured elastogram (fig. 8E) and PFEM elastogram (fig. 8G) show a low strain region at the center of the plaque and a high strain region at both corners of the plaque. However, both high strain regions in the PFEM elastogram are not as thin and elongated as in the measured elastogram. The initial state (fig. 8H) has a large Young's modulus contrast between lipid and other two plaque components and both the cap and lipid circle are positioned slightly in the direction of the plaque.

The echogram (fig. 9A) reveals the presence of a large eccentric plaque between 10 and 5 o'clock, but it cannot be used to identify the possible cap and lipid component of the plaque. Similarly as with plaque 1, plaque 2 and the in vitro plaque, the in vivo measured elastogram (fig. 9B) shows the specific strain pattern that suggests the presence of a TCFA. The reconstructed Young's modulus image (fig. 9C) is a likely candidate for the real underlying plaque composition, since the measured elastogram (fig. 9B) and PFEM elastogram (fig. 9D) show two co-localizing regions of high strain at the corners of the plaque and a region of low strain at the center of the plaque. The initial state has a large Young's modulus contrast between lipid and other plaque components and the lipid circle is positioned slightly towards the plaque.

In vivo plaque

D. UNIQUENESS OF IN VIVO PLAQUE RECONSTRUCTION

From the 30 reconstructions, only 5 were successful, i.e., five showed a PFEM elastogram that highly resembled the measured elastogram. These five PFEM elastograms had the following features clearly in common with the measured elastogram (i) a region of high strain at each corner of the plaque and (ii) a region of low strain at the center of the plaque (e.g., figs. 9D, 10B, 10C). Their RMS errors lay between 0.29% and 0.30%, which was lower than the RMS errors of the 22 unsuccessful

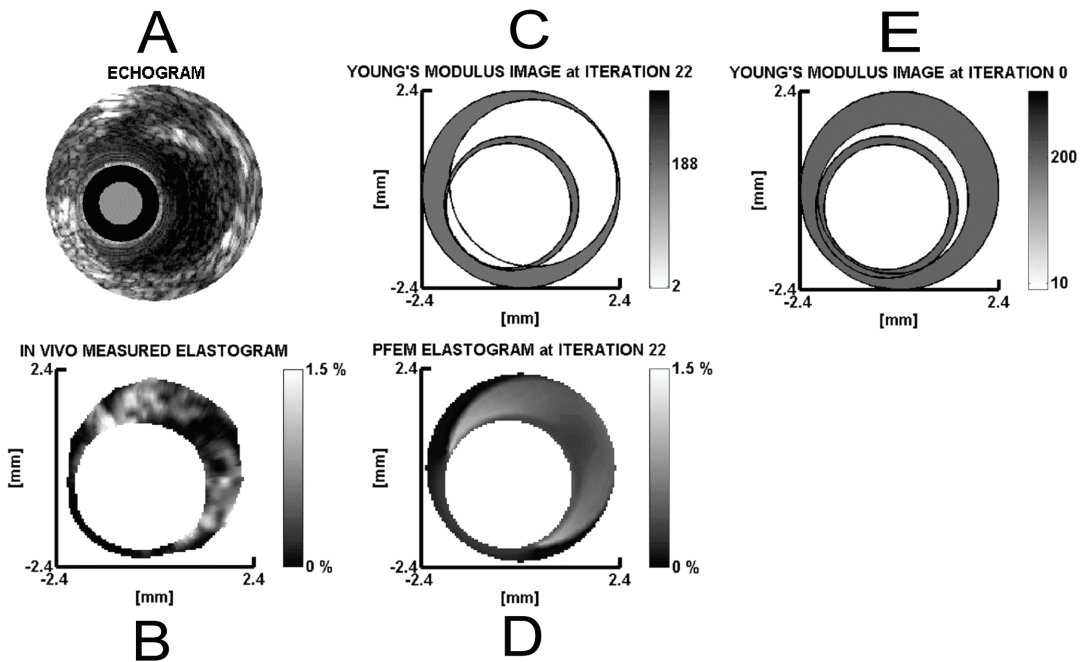


Fig. 9. Reconstruction using an in vivo measured elastogram of a human coronary artery with a vulnerable plaque. (A) Echogram. (B) In vivo measured elastogram. (C) Reconstructed Young's modulus image in kPa. (D) PFEM elastogram computed using C; the RMS error is 0.29%. (E) Initial state at start of the reconstruction process.

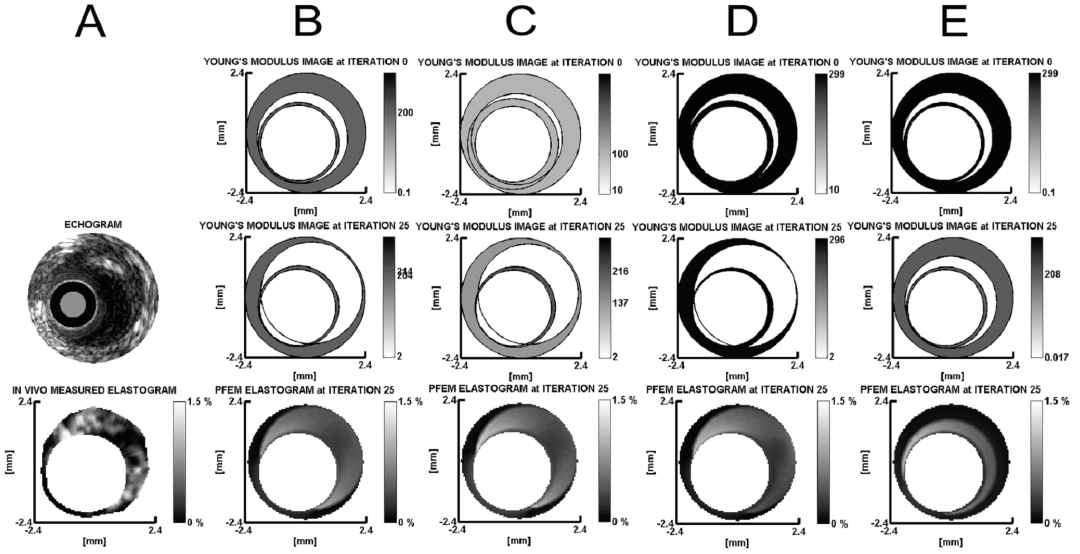


Fig. 10. Typical successful and unsuccessful reconstruction results obtained from the in vivo measured elastogram of the human coronary artery with a vulnerable plaque. (A) Echogram and in vivo measured elastogram. Columns (B) and (C) each shows a successful reconstruction; the RMS error for both is 0.29%. (C) An unsuccessful reconstruction whose PFEM elastogram has only one region with high strain in common with the measured elastogram; the RMS error is 0.32% (D) Another unsuccessful reconstruction whose PFEM elastogram does not have a region of low strain at the centre of the plaque in common with the measured elastogram; the RMS error is 0.38%. All Young's moduli are in kPa.

reconstructions ranging from 0.31% up to 0.37%. The majority of unsuccessful reconstructions resulted in a PFEM elastogram with only one region of high strain at the corner of the plaque (e.g., fig 10D) or lacked a region of low strain at the center of the plaque (e.g., fig 10E). Within each of the 5 successful reconstructions, the morphology (size, shape and position) of a plaque component (i.e., lipid pool or cap) was visually almost identical (e.g., figs. 9C, 10B, 10C). Furthermore, there was a consistent large modulus contrast between the lipid pool and the other two stiffer components (i.e., cap and media). E_{LIPID} varied only between 1.8 and 2.4 kPa with a mean \pm -std of 2.1 \pm 0.2 kPa. There was less consistency in both E_{CAP} and E_{MEDIA} , since E_{CAP} varied between 145 and 280 kPa with a mean \pm -std of 209 \pm 44 kPa and E_{MEDIA} between 137 and 209 kPa with a mean \pm -std of 179 \pm 27 kPa.

DISCUSSION

A new reconstruction method to image the morphology and material composition of vulnerable plaques

We have described a new reconstruction method to image the morphology and material composition of vulnerable plaques. This method needs a plaque's elastogram, i.e., radial strain image, in order to reconstruct the plaque's Young's modulus distribution. It accomplishes this by iteratively matching the radial strain image output of a parametric plaque finite element model to the elastogram. Reconstructions using elastograms obtained from simulated plaques, a vessel-mimicking phantom with a plaque and an in vitro human coronary plaque demonstrated that this method could closely approximate the morphology and material composition of the three main plaque components, namely lipid pool, cap, and media. Furthermore, the reconstruction of a plaque, using an in vivo measured elastogram from a patient, was described. Finally, this elastogram was used as a realistic example to investigate the uniqueness of the reconstruction method.

YOUNG'S MODULI OF PLAQUE COMPONENTS

In this study, the sets of Young's moduli values that were used for the two simulated plaques (Table 1), for the phantom ($E_{LIPID}=4.2$ kPa, $E_{MEDIA}=16.8$ kPa), and those that were reconstructed from the in vitro plaque ($E_{LIPID}=29$, $E_{MEDIA}=647$, $E_{CAP}=1784$ kPa) and in vivo plaque ($E_{LIPID}=2$, $E_{MEDIA}=188$, $E_{CAP}=188$ kPa), all had a Young's modulus value for the non-fibrous plaque component (e.g., lipid pool) that was much lower than the fibrous (e.g., media and cap) plaque components: Such a stiffness difference has been consistently observed by researchers that performed measurements or used a modulus reconstruction approach to determine static moduli values for human atherosclerotic plaque components (Table 2).

Consistently observed Young's modulus difference between plaque components

TABLE 2: MEASURED AND RECONSTRUCTED STATIC YOUNG'S MODULI (E) OF HUMAN ATHEROSCLEROTIC PLAQUE COMPONENTS

	NON-FIBROUS	FIBROUS	CALCIFIED
Loree et al. (1994) Circumferential tensile E ^{A, D}	927+/-468 (n=12)	2312+/-2180 (n=9)	1466+/-1284 (n=5)
Lee et al. (1992) Radial compressive E ^{A, D, E}	41.2+/-18.8 (n=14)	81.7+/-33.2 (n=18)	354+/-245.4 (n=11)
De Korte et al. (2000) Incremental pressure-strain E ^{A, D}	222 (n=13)	493 (n=62)	
Kanai et al. (2003) Incremental circumferential E ^{B, D}	81+/-40 (n=9)	1000+/-630 (n=9)	
Beattie et al. (1998) Bi-linear isotropic E ^{B, D}	3.81, strain<18.2% 38.8, strain>18.2% (n=4)	483, strain<8.2% 1820, strain>8.2% (n=7)	3990, strain<5.3% 10700, strain>5.3% (n=1)

Young's moduli (E) are in kPa and given as mean+/-standard deviation ('n' = number of samples).

^A = Measured, ^B = Reconstructed, ^C = In vivo, ^D = In vitro, ^E = Only plaque-cap.

The following methods were applied to obtain the Young's moduli values listed in Table 2: Loree et al. (1994a) used uniaxial mechanical tensile testing on specimens at a physiological applied circumferential tensile stress of 187.5 mmHg. Lee et al. (1992) used uniaxial mechanical compressive testing on specimens that were classified by their IVUS appearance; the modulus was defined as the ratio between the increase in equilibrium-stress, namely from 30 to 90 mmHg, to the resulting strain after creep. De Korte et al. (2000a) used IVUS elastography to measure the radial strain that resulted by increasing the pressure from 80 to 100 mmHg. Kanai et al. (2003) used a direct reconstruction method to measure local thickness changes of vessel wall layers with an 'ultrasonic phased tracking' method during physiological pressurization. Moduli were subsequently computed with an analytical formula, derived using the assumption that the artery was incompressible, isotropic and that the arterial pressure decreased linearly with the distance from lumen to adventitia. Beattie et al. (1998) used an iterative FEM-based reconstruction method in combination with measured radial displacement fields (one at 40 mmHg and one at 80 mmHg intraluminal pressure). Plaque regions were assumed homogeneous and were identified a priori from histology, after having measured displacement fields by particle tracking on cross-sectional digital images. The following FEM material deformation features were used: isotropic, incompressible and plane stress.

Methods for measurement and reconstruction of Young's moduli

This large variation in moduli values for a specific plaque component, and also for normal arterial wall (Gow et al. 1979, Mozersky et al. 1972), can be attributed to factors that differ between research groups, such as (Dobrin 1978, Fung 1981, Yamada et al. 1970):

Large variation in moduli values for a specific plaque component

- (i) Type of elastic modulus: dynamic, static, visco-elastic, anisotropic, incremental, pressure-strain, compressive, tensile, shear.
- (ii) Type and host of artery: coronary, femoral, etc. from animal or human.
- (iii) Environment: in vitro, in vivo, mechanical constraints, temperature.
- (iv) History: preconditioning, (duration of) cold storage and age.
- (v) Amount of pre-deformation/pressurization or longitudinal pre-stretch: arterial constituents stiffen with increasing tension.

(vi) Classification protocol: macroscopic classification into categories like fatty, fibro-fatty, fibrous, calcified etc. or microscopic classification into individual arterial constituents like smooth muscle cells, elastin, collagen, etc. In contrast to microscopic arterial constituents, global plaque constituents do not allow a clear and unique classification, because they are usually not small enough to be considered homogeneous.

(vii) Assumptions regarding the geometry of the arterial plaque components and the used constitutive material deformation models.

Discrimination

Despite these variations, discrimination between non-fibrous, fibrous and calcified plaque components is possible thanks to several-fold stiffness differences between these components. These differences are necessary for a successful application of reconstruction methods.

Excising an artery may induce mechanical stiffening

A pressure difference of 20 mmHg for the in vitro artery and only 1 mmHg for the in vivo artery resulted in both cases in elastograms with radial strains up to 2%. This result is in agreement with previous studies (de Korte et al. 2000a, de Korte et al. 2002a). The difference suggests that excising an artery may induce mechanical stiffening (Gow et al. 1979, Schaar et al. 2002). This is possibly caused by differences in factors between situations in vitro and in vivo (e.g., cell inactivity or too much longitudinal pre-stretch). As expected from linear elasticity this pressure difference of a factor of 20 with similar strain is reflected in the reconstructed arterial Young's moduli values.

PFEM MATERIAL DEFORMATION FEATURES

In this study, we have used a linear elastic, isotropic, nearly incompressible, plain strain constitutive material model for (i) simulating the small-strain arterial deformation behavior (strain < 2.5%) at a level in the physiological intraluminal pressure range (50-150 mmHg) and (ii) for reconstructing the morphologies and Young's moduli of plaque components. Many other research groups have also used all, or only a subset, of these constitutive features for describing arterial deformation at a level in this pressure range, for example:

Linear elasticity (Chandran et al. 2003, Cheng et al. 1993, Finet et al. 2004, Kanai et al. 2003, Lee et al. 1994, Loree et al. 1992, Loree et al. 1994b, Ohayon et al. 2001, Soualmi et al. 1997, Veress et al. 2000, Wan et al. 2001),

Isotropy (Beattie et al. 1998, Chandran et al. 2003, Cheng et al. 1993, Hayashi et al. 1997, Huang et al. 2001, Kanai et al. 2003, Kim et al. 2004, Lee et al. 1994, Lee et al. 1996, Loree et al. 1994b, Lupotti et al. 2003, Soualmi et al. 1997, Veress et al. 2000, Veress et al. 2002, Wan et al. 2001),

(Near) incompressibility (Beattie et al. 1998, Chandran et al. 2003, Holzapfel et al. 1998, Huang et al. 2001, Kanai et al. 2003, Kim et al. 2004, Lee et al. 1994, Lee et al. 1996, Lupotti et al. 2003, Soualmi et al. 1997, Veress et al. 2000, Wan et al. 2001, Weizsacker et al. 1988) and

Plane strain (Cheng et al. 1993, Finet et al. 2004, Hayashi et al. 1997, Huang et al. 2001, Kim et al. 2004, Lee et al. 1994, Lee et al. 1996, Loree et al. 1992, Ohayon et al. 2001, Soualmi et al. 1997, Veress et al. 2000, Veress et al. 2002, Wan et al. 2001).

The use of most of these modeling features can be justified, as follows:

Linear elasticity

When performing IVUS elastography, the measured arterial strains are low, i.e., the strain between two consecutive IVUS RF frames is less than 2.5%. Consequently, only a small part of the artery's nonlinear stress-strain behavior is used and the arterial deformation can, therefore, be considered locally linear.

Incompressibility

According to Carew et al. (Carew et al. 1968) arteries may be considered incompressible. Furthermore, our group has demonstrated (Baldeusing et al. 2004b) that Poisson's ratio variations of vulnerable plaques, in the range 0.49-0.49999, had no significant influence on the strain pattern and strain values in simulated elastograms of those plaques.

Isotropy

Although arteries are anisotropic (i.e., their radial, circumferential and/or longitudinal Young's modulus values are different) when their deformation is considered over an intraluminal pressure range of 0 mmHg up to 200 mmHg (Yamada et al.

1970), anisotropy can be considerably less prevalent when focusing on in vivo physiological intraluminal pressures. For example, Weisacker and Pinto (1988) showed that the overall response of vascular tissue is highly non-linear and anisotropic. However, they also concluded that for the range of deformations that occur in vivo, the arterial wall can be considered as incrementally isotropic. Furthermore, our group (Baldewsing et al. 2004a) has demonstrated that a linear elastic, isotropic, nearly incompressible, plane strain constitutive material model can appropriately simulate the arterial small-strain behavior within the physiological intraluminal pressure range during IVUS elastography measurements of atherosclerotic arteries in vitro. Furthermore, when isotropy may not be a good approximation for a certain artery, it is still likely that the erroneous reconstructed isotropic Young's moduli show a diagnostically useful stiffness contrast between the lipid pool and the media/cap components, merely because this contrast is large for real plaque components.

A deforming 3D arterial tubular segment is in a condition of '2D plain strain' when those cross-sections that are perpendicular to its longitudinal axis exhibit only strains in the cross-sectional plane (e.g., circumferential and radial strain) and no strain in the direction perpendicular to it (e.g., longitudinal strain). Most large healthy vessels that do not suffer from external forces, maintain a constant longitudinal length in vivo due to the constraint provided by arterial side branches and perivascular connective tissue (Dobrin 1978). Consequently, the condition of '2D plane strain' is defensible for such vessels. However, for atherosclerotic coronary arteries wrapped around the heart, this condition may not always be applicable because the following sources may introduce an unknown distribution of tensile and compressive longitudinal strain throughout some cross-sections: (i) deformation of the heart (ii) curvature of the coronary longitudinal axis (iii) longitudinal coronary plaque dimensions that are smaller than the diameter of the coronary. These longitudinal strains may result in an erroneous reconstruction when assuming a '2D plain strain' condition. Future comparative 3D-versus-'2D plane strain' simulation studies are needed to estimate the influence of those longitudinal strain sources.

2D plane strain

The lipid, cap and media plaque component regions were each assumed to be homogenous, i.e., within a region they had the same Young's modulus value. Many other groups have applied this homogeneity assumption for simulating stress within atherosclerotic plaques or for reconstructing their material properties, e.g., (Beattie et al. 1998, Chandran et al. 2003, Cheng et al. 1993, Finet et al. 2004, Hayashi et al. 1997, Huang et al. 2001, Lee et al. 1993, Lee et al. 1994, Lee et al. 1996, Loree et al. 1992, Ohayon et al. 2001, Veress et al. 1998, Veress et al. 2000). We have deliberately required the homogeneity of each plaque component for the following reasons: (i) The assumption of homogeneity makes it possible to characterize each of the three plaque components by just one material parameter (i.e., Young's modulus). If this assumption would be dropped, then many moduli would be required for approximating the arterial Young's modulus distribution, namely one modulus for each small finite element in the arterial cross-section. A low number of reconstruction parameters is needed to increase the chance for obtaining a stable (i.e., highly unique and not overly sensitive to local minima) reconstruction (ii) For clinical applications, a clinician is aided by an arterial stiffness image that is fast and easy to interpret. The assumption of homogeneity contributes to that purpose. Of course, the drawback of the homogeneity assumption is that it narrows the class of plaques that can be correctly reconstructed.

Homogeneity

PFEM GEOMETRIC FEATURES

In this study we have used an idealized thin-cap fibroatheroma as PFEM for a plaque; the borders of its plaque components are delineated with circles. This PFEM is a variation of the PFEM model used by Loree et al. (1992). It has only 15 parameters (i.e., three for each of the four PFEM circles and a Young's modulus for the each of the three plaque components), but can still model the diagnostically important class of vulnerable plaques, having as morphological features a media area containing a lipid pool which is covered by a cap (Virmani et al. 2002, 2003). Although there exist other types of vulnerable plaques, such as eroded plaques or plaques containing calcified nodules, the idealized thin-cap fibroatheroma (TCFA) has been used as geometric model for the PFEM for the following reasons.

The borders of plaque components are delineated with circles

(i) TCFAs are considered to be the precursor lesion of plaque-rupture and they account for the majority of plaque-ruptures (Virmani et al. 2002).

(ii) The use of an idealized thin-cap fibroatheroma PFEM, should be considered as a trade-off between (a) an important class of stable reconstructable plaques, namely the TCFAs and (b) a large class of non-stable reconstructable plaques.

Non-obstructing vulnerable plaques have an almost perfect circular lumen

(iii) The use of a circle for the PFEM lumen is an approximation for the lumen geometries of vulnerable plaques. This approximation is not only practical for computational purposes (i.e., closed-form, analytical formulas are available for computing the dynamic control points of the PFEM in fig. 2A), but it is also often a good approximation for the shape of the lumen: IVUS studies have shown that normal arteries have an almost perfect circular lumen border (Nissen et al. 1991). Furthermore, IVUS and pathological studies (Glagov et al. 1987, Losordo et al. 1994) have shown that during the accumulation of plaque within the normal vessel wall, arteries exhibit 'compensatory enlargement' or 'outward/positive remodeling', i.e., the lumen cross-sectional area is maintained while plaque accumulates; this compensation is maintained up to the point where the plaque area occupies approximately 40% of the (vessel wall + lumen) area. These observations, may partly explain why, during clinical trials, our group often observes that the majority of non-obstructing vulnerable plaques have an almost perfect circular lumen. Indeed, there does exist a small class of vulnerable plaques whose lumen shape is far from perfectly circular. For such plaques the application of a different, advanced PFEM model, whose lumen and/or media borders are manually traced or automatically contour-detected from the IVUS echogram, might be an appropriate solution. This is, however, at the expense of more processing, since no closed-form solutions are then available for computing the dynamic control points P, R, S and U of the PFEM in fig. 2A.

(iv) Delineation of PFEM plaque component borders by curve-parameterizations other than circles (e.g., ellipses) potentially allows a closer approximation of arbitrarily shaped plaque components. However, the use of such parameterizations requires more defining parameters (e.g., an ellipse is described by 5 defining parameters, a circle by only 3). This may decrease the chance for obtaining a successful reconstruction, i.e., finding a reconstruction with a PFEM elastogram that highly resembles the measured elastogram, since a PFEM with more parameters, will introduce more local minima and will increase the non-uniqueness of a reconstruction.

Lumen and media border

The more non-circular the real lumen is, the more unreliable the reconstructed moduli are when using a circle for the PFEM lumen. This is due to local eccentricities that may cause local circumferential stress concentrations/spreading and, consequently, result in local increases/decreases of radial strain values, an effect that cannot be accounted for by the current PFEM. Nevertheless, the reconstruction results from the phantom and the simulated plaque that was traced from histology, demonstrated that a good approximation of both the geometry and Young's moduli for each plaque component was still possible, despite the fact that these components, including the lumen and media border, were not delineated by circles. A discrepancy in circularity between media borders is not expected to be of much impact, since the stress and strain are there much lower than near the lumen (due to natural stress decay caused by the circumferential geometry of the vessel wall).

INITIALIZATION STRATEGY

Use practically available a priori information

To maximize the chance for obtaining a successful reconstruction, all practically available a priori information in echograms and elastograms should be used to define an initial state for the PFEM: the lipid circle should be positioned towards the direction of plaque thickening. This strategy was applied for all reconstructions. Radial strain patterns in elastograms also indicate possible configurations for the PFEM components that will likely produce a PFEM elastogram that resembles the measured elastogram. This strategy was applied to improve the reconstruction in fig. 7. Finally, a Young's modulus contrast between the lipid and media/cap plaque components was used in all reconstructions (in fig. 3, the reconstruction was also successful without using initial Young's modulus contrast).

Initial Young's moduli values

The closer the initial Young's modulus values are chosen to the actual values of the plaque components, the higher the chance for obtaining a successful and correct

reconstruction. However, a reasonable initial choice is not practically retrievable from literature, since those values are too widespread (e.g., table 2). Thus, to determine reasonable initial values for a specific in vitro or in vivo situation, first multiple reconstructions should be performed for one plaque, using a wide range of different initial values for each plaque component, similar as was done for the in vivo human coronary plaque reconstruction. Then, the moduli of the most successful reconstruction can be used as a practical initial choice for reconstructions with other plaques.

JUDGMENT OF RECONSTRUCTION

The reconstruction method uses a minimization algorithm to find a local minimum of the RMS error between the simulated or measured elastogram and the PFEM elastogram. Without knowing the actual plaque composition one does not know how good a successful reconstruction approximates it or if a global minimum has been found. To get an indication if a global minimum has been found one may perform multiple reconstructions with different initial states and check if the majority of successful reconstructions approximate one Young's modulus image. The only way to judge how good a reconstruction approximates the actual unknown plaque composition is by comparing the similarity of structural patterns (e.g., regions of high and low radial strain) in both elastograms. This strategy was applied for the reconstruction using the in vivo measured elastogram.

Compare the similarity of regions with high (or low) strain in both elastograms.

UNIQUENESS

The reconstruction results for the first three plaques (i.e., two simulated arteries and the phantom) have demonstrated that the reconstruction method can successfully approximate the geometry and stiffness of plaque components. However, it was not demonstrated or proven that these reconstructions were unique. Theoretically it is possible that different PFEM geometries and/or moduli of the plaque components give a similar PFEM strain elastogram or a very different PFEM strain elastogram that has the same RMS error (Barbone et al. 2004). Practically, this seems highly unlikely because of the strong geometrical constraints that are imposed upon the PFEM model. The results from the in vivo case support this hypothesis because they demonstrated that the level of uniqueness for a successful reconstruction was high with respect to (i) the morphology of the reconstructed plaque components and (ii) the reconstructed stiffness contrast between the lipid pool and other two stiffer components. However, with respect to the absolute values of the reconstructed moduli of the stiff plaque components, the uniqueness level was only moderately high. Furthermore, from the 30 reconstructions that were performed, only those reconstructions with the lowest RMS errors were successful; this suggests that a low RMS error might be a good criterion for automatically selecting the most successful reconstruction(s) from a set of reconstructions.

The level of uniqueness for a successful reconstruction was high

CLINICAL IMPLICATIONS AND APPLICATIONS

The current results suggest that our reconstruction method is a new way of intravascular tissue characterization that may be suitable for clinical applications, such as (i) tissue characterization: to allow the selection of proper interventional procedures and (ii) monitoring of atherosclerosis: to quantify the effect of pharmaceutical treatments aimed at stabilizing plaques, e.g., by stiffening (Aikawa et al. 1998, Loree et al. 1994b) or reducing the lipids (Schartl et al. 2001). Furthermore, this method allows investigation and explanation of strain artifacts in elastograms and it may be applied to quantify the amount of stiffening of arterial plaque components within the physiological intraluminal pressure range. Finally, this method only needs an elastogram as input. Therefore, any imaging modality capable of measuring elastograms may be used. Our reconstruction method may potentially also be applied in other clinically relevant situations where circular objects are present in an almost homogeneous medium that is strained, e.g., superficial atherosclerotic arteries, such as the carotid or femoral.

A new way of intravascular tissue characterization

LIMITATIONS

Although the presented reconstruction results are promising, there are still some issues related to the robustness of the reconstruction method that have to be quantified in future studies, such as:

Influence of measurement noise

(i) Measurement noise. The results from the phantom and in vitro plaque showed that in the presence of measurement noise it was still possible to obtain a successful reconstruction. However, the contribution of measurement noise upon the degradation of a reconstruction has not been quantified.

Dependence upon catheter position

(ii) Catheter position. The radial strain distribution in a simulated or measured elastogram depends upon the position of the catheter within the lumen (de Korte et al. 1999). Consequently, different catheter positions within the same plaque result in different radial strain elastograms. Because these elastograms are different, it seems reasonable to expect that the corresponding reconstructions are different. However, this is unlikely, since the position of the catheter that is used for a simulation or measurement of an elastogram is also used in the PFEM.

CONCLUSION

A new reconstruction method is described for obtaining morphology and material composition images of arterial vulnerable plaques. This method reconstructs a Young's modulus image from a measured elastogram, i.e. radial strain image of a plaque, by iteratively matching an elastogram calculated with a parametric plaque finite element model to the measured elastogram. This method has successfully reconstructed Young's modulus images from elastograms that were

- (i) simulated with finite element models of plaques,
- (ii) measured from a synthetic plaque and
- (iii) measured from an in vitro human coronary plaque. It has also been applied on an elastogram of a plaque measured in vivo in a patient.

ACKNOWLEDGEMENTS

This work was supported by the Netherlands Organization for Scientific Research (NWO) and the Dutch Technology Foundation (STW). We thank C. Strijder and G. Pasterkamp from Utrecht Medical Center, Department of Cardiology, Utrecht, The Netherlands for their contributions in creating the histology. Finally, we thank D. Goertz from Erasmus Medical Center, Department of Biomedical Engineering, Thoraxcenter, Rotterdam, The Netherlands for proofreading this manuscript.

REFERENCES

- Aikawa M, Rabkin E, Okada Y, Voglic SJ, Clinton SK, Brinckerhoff CE, Sukhova GK, Libby P. *Lipid lowering by diet reduces matrix metalloproteinase activity and increases collagen content of rabbit atheroma: a potential mechanism of lesion stabilization*. *Circulation* 1998;97:2433-44.
- Baldewsing RA, de Korte CL, Schaar JA, Mastik F, van der Steen AFW. *A finite element model for performing intravascular ultrasound elastography of human atherosclerotic coronary arteries*. *Ultrasound Med Biol* 2004a;30:803-13.
- Baldewsing RA, De Korte CL, Schaar JA, Mastik F, van der Steen AFW. *Finite element modeling and intravascular ultrasound elastography of vulnerable plaques: parameter variation*. *Ultrasonics* 2004b;42:723-9.
- Baldewsing RA, Schaar JA, Mastik F, Oomens CWJ, van der Steen AFW. *Young's modulus reconstruction for assessing vulnerable atherosclerotic plaque composition in vivo*. *Proceedings of the 2004 IEEE International Ultrasonics Ferroelectrics and Frequency Control 50th Anniversary Conference, 2004c, Montreal, Canada*, pages 368-371.
- Bank AJ. *Intravascular ultrasound studies of arterial elastic mechanics*. *Pathol Biol (Paris)* 1999;47:731-7.
- Barbone PE, Bamber JC. *Quantitative elasticity imaging: what can and cannot be inferred from strain images*. *Phys Med Biol* 2002;47:2147-64.
- Barbone PE, Gokhale NH. *Elastic modulus imaging: on the uniqueness and nonuniqueness of the elastography inverse problem in two dimensions*. *Inverse Problems* 2004;20:283-96.
- Beattie D, Xu C, Vito R, Glagov S, Whang MC. *Mechanical analysis of heterogeneous, atherosclerotic human aorta*. *J Biomech Eng* 1998;120:602-7.
- Bergel DH. *The static elastic properties of the arterial wall*. *Journal of Physiology* 1961;156:445-57.
- Bishop J, Samani A, Sciarretta J, Plewes DB. *Two-dimensional MR elastography with linear inversion reconstruction: methodology and noise analysis*. *Phys Med Biol* 2000;45:2081-91.
- Brusseau E, Fromageau J, Rognin NG, Delachartre P, Vray D. *Investigating elastic properties of soft biological tissues*. *IEEE Eng Med Biol Mag* 2002;21:86-94.
- Carew TE, Vaishnav RN, Patel DJ. *Compressibility of the arterial wall*. *Circ Res* 1968;23:61-8.
- Chandran KB, Mun JH, Choi KK, Chen JS, Hamilton A, Nagaraj A, McPherson DD. *A method for in-vivo analysis for regional arterial wall material property alterations with atherosclerosis: preliminary results*. *Med Eng Phys* 2003;25:289-98.
- Cheng GC, Loree HM, Kamm RD, Fishbein MC, Lee RT. *Distribution of circumferential stress in ruptured and stable atherosclerotic lesions. A structural analysis with histopathological correlation*. *Circulation* 1993;87:1179-87.
- Choi CD, Skovoroda AR, Emelianov SY, O'Donnell M. *An integrated compliant balloon ultrasound catheter for intravascular strain imaging*. *IEEE Trans Ultrason Ferroelectr Freq Control* 2002;49:1552-60.
- Chu KC, Rutt BK. *Polyvinyl alcohol cryogel: an ideal phantom material for mr studies of arterial flow and elasticity*. *Magnetic Resonance in Medicine* 1997;37:314-9.
- Cohn NA, Kim BS, Erkamp RQ, Mooney DJ, Emelianov SY, Skovoroda AR, O'Donnell M. *High-resolution elasticity imaging for tissue engineering*. *IEEE Trans Ultrason Ferroelectr Freq Control* 2000;47:956-66.
- Davies MJ. *The pathophysiology of acute coronary syndromes*. *Heart* 2000;83:361-6.
- Davies MJ. *Going from immutable to mutable atherosclerotic plaques*. *Am J Cardiol* 2001;88:2F-9F.
- de Korte CL, Carlier SG, Mastik F, Doyley MM, van der Steen AF, Serruys PW, Bom N. *Morphological and mechanical information of coronary arteries obtained with intravascular elastography; feasibility study in vivo*. *Eur Heart J* 2002a;23:405-13.
- de Korte CL, Céspedes EI, van der Steen AFW. *Influence of catheter position on estimated strain in intravascular elastography*. *IEEE Trans Ultrason Ferroelectr Freq Control* 1999;46:616-25.
- de Korte CL, Pasterkamp G, van der Steen AF, Woutman HA, Bom N. *Characterization of plaque components with intravascular ultrasound elastography in human femoral and coronary arteries in vitro*. *Circulation* 2000a;102:617-23.
- de Korte CL, Pasterkamp G, van der Steen AFW, Woutman HA, Bom N. *Characterization of plaque components using intravascular ultrasound elastography in human femoral and coronary arteries in vitro*. *Circulation* 2000b;102:617-23.
- de Korte CL, Schaar JA, Mastik F, Serruys PW, van der Steen AFW. *Intravascular elastography: from bench to bedside*. *J Interv Cardiol* 2003;16:253-9.

- de Korte CL, Siervogel MJ, Mastik F, Strijder C, Schaar JA, Velema E, Pasterkamp G, Serruys PW, van der Steen AFW. *Identification of atherosclerotic plaque components with intravascular ultrasound elastography in vivo: a Yucatan pig study*. Circulation 2002b;105:1627-30.
- de Korte CL, van der Steen AFW, Céspedes EI, Pasterkamp G. *Intravascular ultrasound elastography of human arteries: initial experience in vitro*. Ultrasound Med Biol 1998;24:401-8.
- Dobrin PB. *Mechanical properties of arteries*. Physiol Rev 1978;58:397-460.
- Doyley M, Mastik F, de Korte CL, Carlier S, Céspedes E, Serruys P, Bom N, van der Steen AFW. *Advancing intravascular ultrasonic palpation towards clinical applications*. Ultrasound Med Biol 2001;27:1471-80.
- Doyley MM, Meaney PM, Bamber JC. *Evaluation of an iterative reconstruction method for quantitative elastography*. Phys Med Biol 2000;45:1521-40.
- Falk E, Shah PK, Fuster V. Coronary plaque disruption. Circulation 1995;92:657-71.
- Finet G, Ohayon J, Rioufol G. *Biomechanical interaction between cap thickness, lipid core composition and blood pressure in vulnerable coronary plaque: impact on stability or instability*. Coron Artery Dis 2004;15:13-20.
- Fu D, Levinson SF, Gracewski SM, Parker KJ. *Non-invasive quantitative reconstruction of tissue elasticity using an iterative forward approach*. Phys Med Biol 2000;45:1495-509.
- Fung YC. *Biomechanics: Mechanical properties of living tissue*. New York, USA: Springer, 1981.
- Glagov S, Weisenberg E, Zarins CK, Stankunavicius R, Kolettis GJ. *Compensatory enlargement of human atherosclerotic coronary arteries*. N Engl J Med 1987;316:1371-5.
- Gow BS, Hadfield CD. *The elasticity of canine and human coronary arteries with reference to postmortem changes*. Circ Res 1979;45:588-94.
- Hayashi K, Imai Y. *Tensile property of atheromatous plaque and an analysis of stress in atherosclerotic wall*. J Biomech 1997;30:573-9.
- Holzapfel GA, Weizsacker HW. *Biomechanical behavior of the arterial wall and its numerical characterization*. Comput Biol Med 1998;28:377-92.
- Huang H, Virmani R, Younis H, Burke AP, Kamm RD, Lee RT. *The impact of calcification on the biomechanical stability of atherosclerotic plaques*. Circulation 2001;103:1051-6.
- Kallel F, Bertrand M. *Tissue elasticity reconstruction using linear perturbation method*. IEEE Trans Med Imaging 1996;15:299-313.
- Kanai H, Hasegawa H, Ichiki M, Tezuka F, Koiwa Y. *Elasticity imaging of atheroma with transcutaneous ultrasound: preliminary study*. Circulation 2003;107:3018-21.
- Kim K, Weitzel WF, Rubin JM, Xie H, Chen X, O'Donnell M. *Vascular intramural strain imaging using arterial pressure equalization*. Ultrasound Med Biol 2004;30:761-71.
- Lally C, Reid AJ, Prendergast PJ. *Elastic behavior of porcine coronary artery tissue under uniaxial and equibiaxial tension*. Ann Biomed Eng 2004;32:1355-64.
- Lee RT, Gordzinsky AJ, Frank EH, Kamm RD, Schoen FJ. *Structure-dependent dynamic mechanical behavior of fibrous caps from human atherosclerotic plaques*. Circulation 1991;83:1764-70.
- Lee RT, Loree HM, Cheng GC, Lieberman EH, Jaramillo N, Schoen FJ. *Computational structural analysis based on intravascular ultrasound imaging before in vitro angioplasty: prediction of plaque fracture locations*. Journal of American College of Cardiology 1993;21:777-82.
- Lee RT, Loree HM, Fishbein MC. *High stress regions in saphenous vein bypass graft atherosclerotic lesions*. J Am Coll Cardiol 1994;24:1639-44.
- Lee RT, Richardson G, Loree HM, Gordzinsky AJ, Gharib SA, Schoen FJ, Pandian N. *Prediction of mechanical properties of human atherosclerotic tissue by high-frequency intravascular ultrasound imaging*. Arterioscler Thromb 1992;12:1-5.
- Lee RT, Schoen FJ, Loree HM, Lark MW, Libby P. *Circumferential stress and matrix metalloproteinase 1 in human coronary atherosclerosis. Implications for plaque rupture*. Arterioscler Thromb Vasc Biol 1996;16:1070-3.
- Lendon CL, Davies MJ, Born GVR, Richardson PD. *Atherosclerotic plaque caps are locally weakened when macrophage density is increased*. Atherosclerosis 1991;87:87-90.
- Loree HM, Grodzinsky AJ, Park SY, Gibson LJ, Lee RT. *Static circumferential tangential modulus of human atherosclerotic tissue*. J Biomech 1994a;27:195-204.
- Loree HM, Kamm RD, Stringfellow RG, Lee RT. *Effects of fibrous cap thickness on peak circumferential stress in model atherosclerotic vessels*. Circ Res 1992;71:850-8.

- Loree HM, Tobias BJ, Gibson LJ, Kamm RD, Small DM, Lee RT. *Mechanical properties of model atherosclerotic lesion lipid pools*. *Arterioscler Thromb* 1994b;14:230-4.
- Losordo DW, Rosenfield K, Kaufman J, Pieczek A, Isner JM. *Focal compensatory enlargement of human arteries in response to progressive atherosclerosis. In vivo documentation using intravascular ultrasound*. *Circulation* 1994;89:2570-7.
- Lu X, Yang J, Zhao JB, Gregersen H, Kassab GS. *Shear modulus of porcine coronary artery: contributions of media and adventitia*. *Am J Physiol Heart Circ Physiol* 2003;285:H1966-75.
- Lupotti FA, Mai JJ, Pellot-Barakat C, Insana MF. *Vascular elasticity from regional displacement estimates*. *Proceedings of the 2003 IEEE International Ultrasonics Symposium* 2003;1895-8.
- Matsumoto T, Abe H, Ohashi T, Kato Y, Sato M. *Local elastic modulus of atherosclerotic lesions of rabbit thoracic aortas measured by pipette aspiration method*. *Physiol Meas* 2002;23:635-48.
- Miga MI. *A new approach to elastography using mutual information and finite elements*. *Phys Med Biol* 2003;48:467-80.
- Moulton MJ, Creswell LL, Actis RL, Myers KW, Vannier MW, Szabo BA, Pasque MK. *An inverse approach to determining myocardial material properties*. *J Biomech* 1995;28:935-48.
- Mozersky DJ, Sumner DS, Hokanson DE, Strandness DE. *Transcutaneous measurement of the elastic properties of the human femoral artery*. *Circulation* 1972;46:948-55.
- Nissen SE, Gurley JC, Grines CL, Booth DC, McClure R, Berk M, Fischer C, DeMaria AN. *Intravascular ultrasound assessment of lumen size and wall morphology in normal subjects and patients with coronary artery disease*. *Circulation* 1991;84:1087-99.
- Ohayon J, Teppaz P, Finet G, Rioufol G. *In-vivo prediction of human coronary plaque rupture location using intravascular ultrasound and the finite element method*. *Coron Artery Dis* 2001;12:655-63.
- Ophir J, Céspedes EI, Garra B, Ponnekanti H, Huang Y, Maklad N. *Elastography: ultrasonic imaging of tissue strain and elastic modulus in vivo*. *Eur J Ultrasound* 1996;3:49-70.
- Perrey C, Braeeker G, Bojara W, Lindstaedt M, Holt S, Ermert H. *Strain imaging with intravascular ultrasound array scanners: validation with phantom experiments*. *Biomed Tech (Berl)* 2003;48:135-40.
- Plewes DB, Bishop J, Samani A, Sciarretta J. *Visualization and quantification of breast cancer biomechanical properties with magnetic resonance elastography*. *Phys Med Biol* 2000;45:1591-610.
- Raghavan KR, Yagle AE. *Forward and inverse problems in elasticity imaging of soft tissues*. *Transactions on Nuclear Science* 1994;41:1639-48.
- Richardson PD, Davies MJ, Born GVR. *Influence of plaque configuration and stress distribution on fissuring of coronary atherosclerotic plaques*. *The Lancet* 1989;2:941-4.
- Ryan LK, Foster FS. *Ultrasonic measurement of differential displacement and strain in a vascular model*. *Ultrason Imaging* 1997;19:19-38.
- Saijo Y, Tanaka A, Owada N, Akino Y, Nitta S. *Tissue velocity imaging of coronary artery by rotating-type intravascular ultrasound*. *Ultrasonics* 2004;42:753-7.
- Salunke NV, Topoleski LD. *Biomechanics of atherosclerotic plaque*. *Crit Rev Biomed Eng* 1997;25:243-85.
- Samani A, Bishop J, Plewes DB. *A constrained modulus reconstruction technique for breast cancer assessment*. *IEEE Trans Med Imaging* 2001;20:877-85.
- Sarvazyan A. *Mechanical imaging: a new technology for medical diagnostics*. *Int J Med Inf* 1998;49:195-216.
- Schaar JA, De Korte CL, Mastik F, Strijder C, Pasterkamp G, Boersma E, Serruys PW, Van Der Steen AFW. *Characterizing vulnerable plaque features with intravascular elastography*. *Circulation* 2003;108:2636-41.
- Schaar JA, de Korte CL, Mastik F, van der Steen AFW. *Effect of temperature increase and freezing on intravascular elastography*. *Ultrasonics* 2002;40:879-81.
- Schaar JA, Muller JE, Falk E et al. *Terminology for high-risk and vulnerable coronary artery plaques. Report of a meeting on the vulnerable plaque, June 17 and 18, 2003, Santorini, Greece*. *Eur Heart J* 2004;25:1077-82.
- Schartl M, Bocksch W, Koschyk DH, Voelker W, Karsch KR, Kreuzer J, Hausmann D, Beckmann S, Gross M. *Use of intravascular ultrasound to compare effects of different strategies of lipid-lowering therapy on plaque volume and composition in patients with coronary artery disease*. *Circulation* 2001;104:387-92.
- Shapo BM, Crowe JR, Skovoroda AR, Eberle M, Cohn NA, O'Donnell M. *Displacement and strain imaging of coronary arteries with intraluminal ultrasound*. *IEEE Trans Ultrason Ferroelectr Freq Control* 1996;43:234-46.
- Skovoroda AR, Emelianov SY, O'Donnell M. *Tissue elasticity reconstruction based on ultrasonic displacement and strain images*. *IEEE Trans Ultrason Ferroelectr Freq Control* 1995;42:747-65.

- Sumi C, Nakayama K, Kubota M. *An effective ultrasonic strain measurement-based shear modulus reconstruction technique for superficial tissues--demonstration on in vitro pork ribs and in vivo human breast tissues*. Phys Med Biol 2000;45:1511-20.
- Sumi C, Suzuki A, Nakayama K. *Estimation of shear modulus distribution in soft tissue from strain distribution*. IEEE Trans Biomed Eng 1995;42:193-202.
- Talhami HE, Wilson LS, Neale ML. *Spectral tissue strain: a new technique for imaging tissue strain using intravascular ultrasound*. Ultrasound Med Biol 1994;20:759-72.
- Van Houten EE, Paulsen KD, Miga MI, Kennedy FE, Weaver JB. *An overlapping subzone technique for MR-based elastic property reconstruction*. Magn Reson Med 1999;42:779-86.
- Veress AI, Cornhill JF, Herderick EE, Thomas JD. *Age-related development of atherosclerotic plaque stress: a population-based finite-element analysis*. Coron Artery Dis 1998;9:13-9.
- Veress AI, Vince DG, Anderson PM, Cornhill JF, Herderick EE, Klingensmith JD, Kuban BD, Greenberg NL, Thomas JD. *Vascular mechanics of the coronary artery*. Z Kardiol 2000;89:92-100.
- Veress AI, Weiss JA, Gullberg GT, Vince DG, Rabbitt RD. *Strain measurement in coronary arteries using intravascular ultrasound and deformable images*. J Biomech Eng 2002;124:734-41.
- Virmani R, Burke AP, Farb A, Kolodgie FD. *Pathology of the unstable plaque*. Prog Cardiovasc Dis 2002;44:349-56.
- Virmani R, Burke AP, Kolodgie FD, Farb A. *Pathology of the thin-cap fibroatheroma: a type of vulnerable plaque*. J Interv Cardiol 2003;16:267-72.
- Virmani R, Kolodgie FD, Burke AP, Farb A, Schwartz SM. *Lessons from sudden coronary death: a comprehensive morphological classification scheme for atherosclerotic lesions*. Arterioscler Thromb Vasc Biol 2000;20:1262-75.
- Vorp DA, Rajagopal KR, Smolinski PJ, Borovetz HS. *Identification of elastic properties of homogeneous, orthotropic vascular segments in distension*. J Biomech 1995;28:501-12.
- Wan M, Li Y, Li J, Cui Y, Zhou X. *Strain imaging and elasticity reconstruction of arteries based on intravascular ultrasound video images*. IEEE Trans Biomed Eng 2001;48:116-20.
- Weizsacker HW, Pinto JG. *Isotropy and anisotropy of the arterial wall*. J Biomech 1988;21:477-87.
- Wellman PS, Howe RD. *Extracting features from tactile maps*. MICCAI 1999;1133-42.
- Yamada H, Evans F. *Strength of biological materials*. Baltimore, USA: The Williams & Wilkins Company, 1970.
- Zhu Y, Hall TJ, Jiang J. *A finite-element approach for Young's modulus reconstruction*. IEEE Trans Med Imaging 2003;22:890-901.

ROBUSTNESS OF RECONSTRUCTING THE YOUNG'S MODULUS DISTRIBUTION OF VULNERABLE ATHEROSCLEROTIC PLAQUES USING A PARAMETRIC PLAQUE MODEL

ABSTRACT

BACKGROUND

Assessment of atherosclerotic plaque composition is crucial for quantitative monitoring of atherosclerosis and for quantifying the effect of pharmaceutical plaque-stabilizing treatments during clinical trials. We assess this composition by applying a geometrically constrained, iterative, inverse solution method to reconstruct a modulus elastogram (i.e., Young's modulus image) from a plaque's strain elastogram (i.e., radial strain image), which is measured using intravascular ultrasound strain elastography. This reconstruction method is especially suited for thin-cap fibroatheromas (TCFAs), i.e., plaques with a thin fibrous cap overlying a lipid pool. Because a plaque's strain elastogram depends upon the plaque's material composition, catheter position within the vessel and measurement noise, this paper investigates how robust the reconstruction is when these parameters are varied.

METHODS

To this end, a standard plaque was defined as the modulus elastogram that was reconstructed from an in vivo measured strain elastogram of a human coronary plaque. This standard plaque was used to computer-simulate different strain elastograms, by varying the (i) geometry and material properties of its plaque components, (ii) catheter position and (iii) level of added strain noise. Robustness was evaluated by quantifying the correctly reconstructed size, shape and Young's modulus of each plaque component region and minimal cap-thickness.

RESULTS

The simulations showed that TCFAs can be adequately reconstructed; the thinner and stiffer the cap or the softer and larger the lipid pool, the better is the reconstruction of these components and minimal cap-thickness. Furthermore, reconstructions were (i) independent of catheter position and (ii) independent of strain noise.

CONCLUSION

The method can robustly reconstruct the Young's modulus distribution of TCFAs from their measured elastogram. As such, it has potential to monitor robustly and quantitatively atherosclerosis in vivo.

THIS CHAPTER IS BASED ON THE PUBLICATION

"Robustness of Reconstructing the Young's Modulus Distribution of Vulnerable Atherosclerotic Plaques using a Parametric Plaque Model"

BY BALDEWSING RA, MASTIK F, SCHAAR JA, OOMENS CWJ AND VAN DER STEEN AFW,
IN ULTRASOUND IN MEDICINE AND BIOLOGY, 31(12):1631-45;2005,

Copyright © 2005 World Federation of Ultrasound in Medicine and Biology.
Parts from this publication were reprinted with their permission.

INTRODUCTION

The majority of acute coronary syndromes, such as unstable angina, myocardial infarction or sudden cardiac death, are caused by coronary thrombosis (Davies 2000; Falk et al. 1995). More than 60% of thrombi are caused by rupture of a thin-cap fibroatheroma (TCFA) plaque (Virmani et al. 2000; 2003). Rupture of the cap will bring the lipid in touch with the blood, which can start the formation of a thrombus and thus obstruct the coronary artery. The morphological features of a TCFA are a thin cap overlaying a large lipid pool. Considered as major determinants for their rupture are the material properties and geometry of its plaque components and cap weakening caused by macrophage-inflammation (Davies 2001; Schaar et al. 2004). As such, assessment of these rupture-determinants (MacNeill et al. 2003) is essential for properly diagnosing patients and for monitoring the effect of pharmaceutical treatments aimed at stabilizing plaques, e.g., by stiffening (Aikawa et al. 1998; Loree et al. 1994b) or reducing the lipids (Schartl et al. 2001).

Intravascular ultrasound (IVUS) strain elastography is a clinically available technique that measures local arterial radial strain and visualizes it in a so-called IVUS strain elastogram to assess information about these rupture determinants (de Korte et al. 2003). Specific global radial strain patterns and global regions with a high averaged radial strain have proven to provide information about these rupture determinants and histological features of vulnerable plaques (Schaar et al. 2003). However, there is no one-to-one relation between the local radial strain value in a strain elastogram and the local plaque component type (calcified, fibrous, fatty or tissue weakened by macrophage-inflammation). The underlying reason is that the stresses that induce local radial strain depend upon the structural build-up of the artery, the material properties and geometry of its plaque components and the catheter position used during imaging (de Korte et al. 1999; Ophir et al. 1996). Thus, a strain elastogram cannot be interpreted directly as a morphology and material composition image of a plaque.

This limitation can be overcome by calculating a modulus elastogram (i.e., an image of the Young's modulus distribution). In particular, the large difference between Young's moduli of plaque components allows their direct discrimination (Bergel 1961; de Korte et al. 2000; Dobrin 1978; Fung 1981; Gow and Hadfield 1979; Lee et al. 1991; Lendon et al. 1991; Loree et al. 1994a).

Currently, it is still not known what the necessary and sufficient conditions are to reconstruct practically a clinically useful arterial Young's modulus image using deformation data (displacement and/or strain) measured from an arbitrary atherosclerotic plaque. To address this problem and to be able to investigate and quantify arterial reconstruction problems, we have recently developed a Young's modulus reconstruction method (Baldewsing et al. 2005) which uses a geometrically-constrained iterative solution approach. This method reconstructs from a plaque's strain elastogram, which is measured using IVUS strain elastography, an approximation of both the geometry and Young's modulus value of the lipid pool, cap and media region. It does this by automatically and iteratively matching the radial strain image output, calculated with a parametric finite element model (PFEM) of a plaque, to the measured strain elastogram of the plaque.

Acute coronary syndromes and plaque rupture determinants

IVUS elastograms cannot be directly interpreted as plaque component images

Image of the Young's modulus distribution

Young's modulus reconstruction method

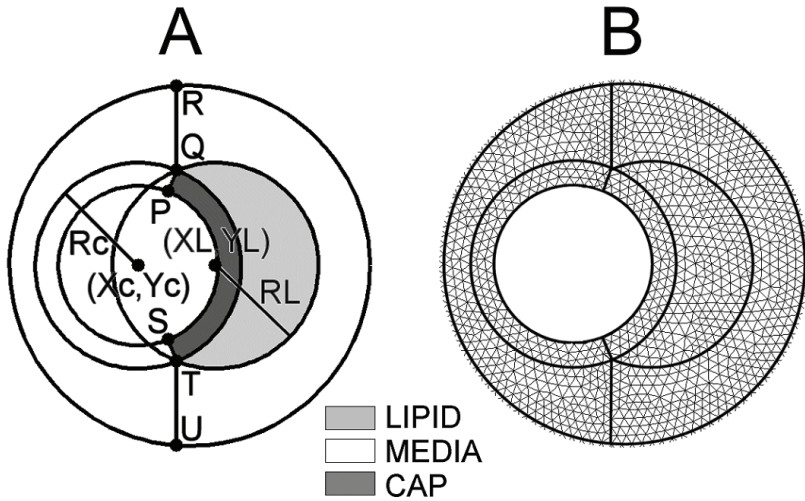


Fig. 1. Parametric finite element model for a vulnerable plaque. (a) Each circle is parameterised by its centre (X,Y) and a radius R . The dynamic control points P, Q, R, S, T and U define the three plaque component regions. (b) Finite element mesh regions corresponding to geometry in (a). Letters L and c denote lipid and cap, respectively.

Robustness and aims of this study

Robustness of this reconstruction method is crucial to monitor properly the effect of pharmaceutical treatments aimed at stabilizing plaques. As such, we evaluate, in this study, the method's robustness by investigating (i) which plaques can be correctly reconstructed and (ii) whether reconstructions depend upon the catheter position within the lumen (de Korte et al. 1999) and the level of strain noise. To this end, a plaque is reconstructed from an in vivo measured strain elastogram of a human atherosclerotic coronary artery. Next, this plaque is used to define a representative standard plaque. Then, this standard plaque is used to simulate different strain elastograms by varying both separately and simultaneously (i) the catheter position, (ii) strain-measurement noise and (iii) the morphology and stiffness of its plaque components. Afterwards, a Young's modulus is reconstructed from each of these simulated strain elastograms. Finally, to answer the questions related to the robustness, each reconstructed Young's modulus image is qualitatively and quantitatively compared with the plaque that was used to create the simulated strain elastogram.

MATERIALS AND METHODS

IVUS MODULUS ELASTOGRAPHY

The geometrically-constrained iterative reconstruction method described by Baldewsing et al. (2005) is used to obtain a modulus elastogram from a plaque's IVUS strain elastogram. This method is especially suited for producing modulus elastograms of thin-cap fibroatheromas (TCFAs). A description of its main components follows.

Plaque geometry and material deformation model

An idealized "thin-cap fibroatheroma" (Virmani et al. 2003) is used as a PFEM for a plaque (Fig. 1a). The PFEM is modelled as a linear elastic, isotropic, incompressible (Poisson's ratio 0.4999), plane strain material (Baldewsing et al. 2004a; 2004b). The lipid, cap and media region are each assumed to be homogeneous and their Young's modulus values are denoted as E_{LIPID} , E_{CAP} and E_{MEDIA} , respectively.

Forward problem calculation

The forward problem consists of calculating the radial strain of the PFEM when it is pressurized. First, the parameters are specified that define the geometry and Young's moduli values of the PFEM and pressure boundary conditions. Next, the finite element package SEPRAN (Septra Analysis, Technical University Delft, The Netherlands) calculates the Cartesian linear strain tensor components using plane strain triangular mesh elements (e.g., Fig. 1b). Then, MATLAB (release 12.1, the MathWorks, Inc.) converts them to polar components using a user-defined catheter posi-

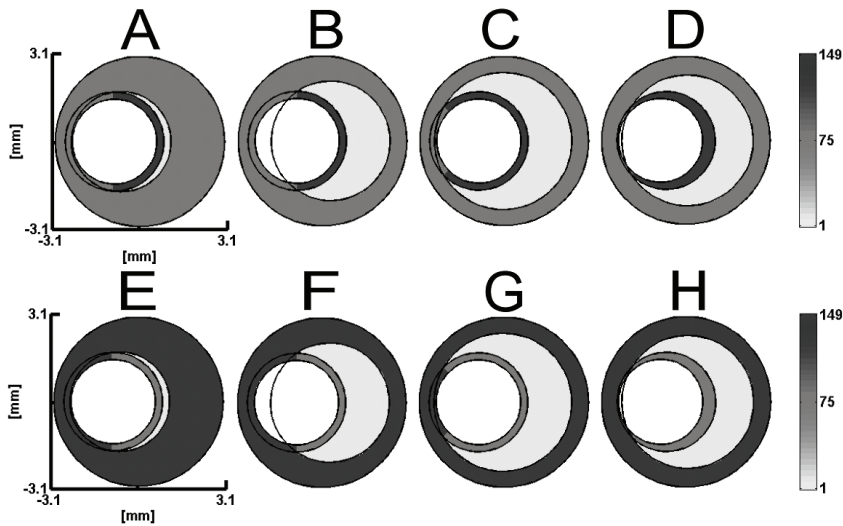


Fig. 2. Initial states used for a reconstruction. Young's moduli are in kPa. All initial states have a stiff cap overlaying a soft lipid pool.

tion as origin. Finally, the radial strain field is interpolated onto a fixed square equidistant grid of 100 by 100 points. This radial strain field is called a PFEM strain elastogram. The whole process from defining the PFEM parameters up to the calculation of the PFEM strain elastogram is fully automatic.

The modulus elastogram of a plaque is determined by a constrained sequential-quadratic-programming minimization algorithm (Optimization Toolbox, MATLAB). This algorithm finds values for the geometry and stiffness parameters of the PFEM such that the corresponding PFEM strain elastogram displays high similarity with the measured IVUS strain elastogram of the plaque. The similarity of the strain elastograms is quantified as the root-mean-squared (RMS) error between their strain values. The minimization algorithm fully automatically searches a local minimum of the RMS error by iteratively updating the three stiffness and six geometry parameters (i.e., those defining the centre and radius of the cap and lipid pool circle) of the PFEM. The geometry parameters of the lumen and media circle are fixed during minimization, since they are approximately known from the IVUS echogram. The minimization algorithm causes every update to result in a lower RMS error. The algorithm was stopped after 35 iterations or when the decrease in RMS error was less than $0.5 \cdot 10^{-4}$ for three consecutive iteration steps. The resulting set of PFEM geometry and stiffness parameters defines the modulus elastogram.

Minimization Algorithm

At the start of the minimisation process, the algorithm requires an initial state, i.e., initial set of values for of the PFEM geometry and stiffness parameters. For each measured strain elastogram, the minimisation algorithm uses a fixed set of eight different initial states (Fig. 2) to compute eight candidate modulus elastograms. The candidate modulus elastogram that gives the smallest RMS error is taken as the final modulus elastogram. The main reasons for choosing this set of initial states was to incorporate practically available a priori plaque information: (i) the IVUS echogram shows the location of the plaque, which is characterized by intimal thickening and (ii) the IVUS strain elastogram indicates the presence of a soft region by means of a typical strain pattern at the shoulder of the plaque, consisting of high strain with adjacent low strain (Schaar et al. 2003). Therefore, all initial states were given a soft lipid pool region that is positioned towards the location of the plaque.

Initialisation

To maintain the configuration of a TCFA and to calculate automatically a proper finite element mesh (e.g., Fig. 1b) during the minimisation process, the following nonlinear constraints have been enforced upon the PFEM geometry parameters. a) The lipid circle must have exactly two intersection points with the cap circle (Q and T). b) The cap circle must always contain the lumen circle. c) The lipid circle must always be inside the media circle. The other dynamic mesh-control points (P, R, S,

Constraints

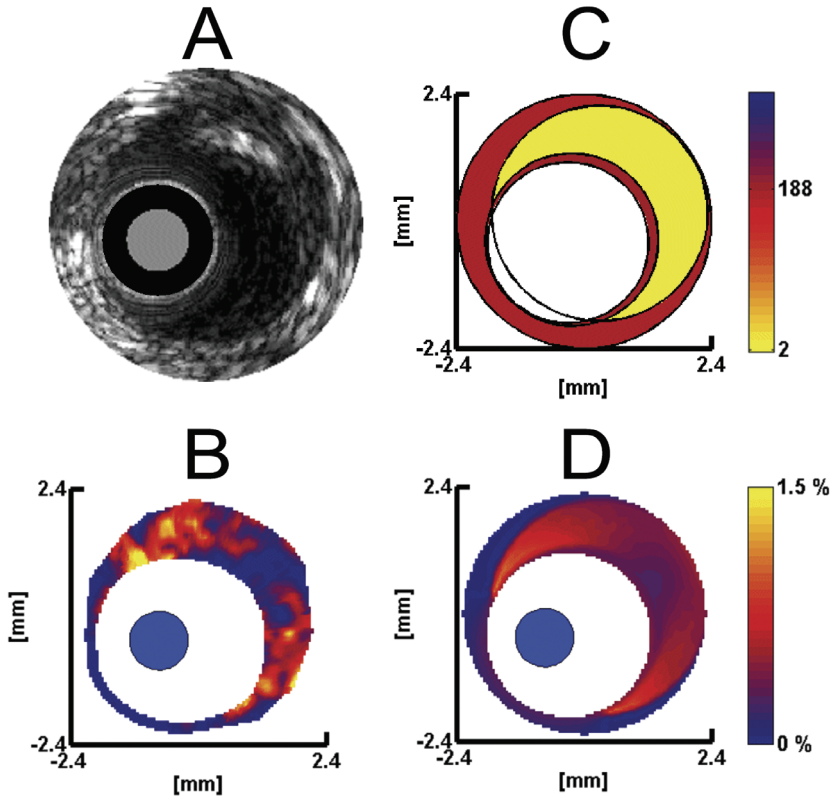


Fig. 3. Young's modulus reconstruction of a human coronary artery with a possible vulnerable plaque. (a) Echogram of the artery. The grey dot, \varnothing 1.1 mm, indicates the catheter and the black ring removes part of the catheter ringdown. (b) In vivo measured radial strain elastogram of the artery. (c) Modulus elastogram reconstructed from (b) after 16 iterations. (d) PFEM strain elastogram computed using (b). RMS error between (b) and (d) is 0.29%. Young's moduli are in kPa and intraluminal pressure difference is 1 mmHg.

and U in Fig. 1a) are automatically calculated and used to define the three plaque regions.

IVUS STRAIN ELASTOGRAPHY IN VIVO

IVUS strain elastograms were processed from IVUS data acquired from a patient with a nonobstructing eccentric plaque (Fig. 3a), as follows. First, a 20-MHz 64-element phased array IVUS catheter of 1.1 mm diameter connected to an InVision echo apparatus (both from Volcano Corporation, Inc., Rancho Cordova, CA, USA) was used to scan a segment of the patient's artery at 30 radio-frequency (RF) data frames per second. Each frame consisted of 512 equidistant angles of raw RF data lines sampled at 100 MHz in 12 bits. Each line contained 1024 equidistant data points (corresponding to 7.6 mm imaging depth). To increase the elastographic signal-to-noise ratio (SNR), a compounded strain elastogram (Doyley et al. 2001) was processed, as follows. At the diastolic phase of a cardiac cycle, when catheter motion is minimal, a consecutive sequence of seven data frames could be selected, such that each consecutive frame pair was highly correlated. For each consecutive frame pair, cross-correlation techniques were applied to the ultrasound data to calculate the local radial strain, as described by de Korte et al. (1998). To this end, first, the radial tissue displacement along the ultrasound beam was determined using a cross-correlation window length of 60 rf data points with 50% window overlap. Then, finite differences of these radial displacements resulted in the local radial strain. The spatial resolution of the radial strain measurement in the radial direction is 30 rf data points (i.e., 200 μ m). The seven consecutive data frames had an interframe pressure difference of 1 mmHg. The compounded strain elastogram (Fig. 3b) was computed by spatially averaging the six individual strain elastograms (Baldeuswing et al. 2004c).

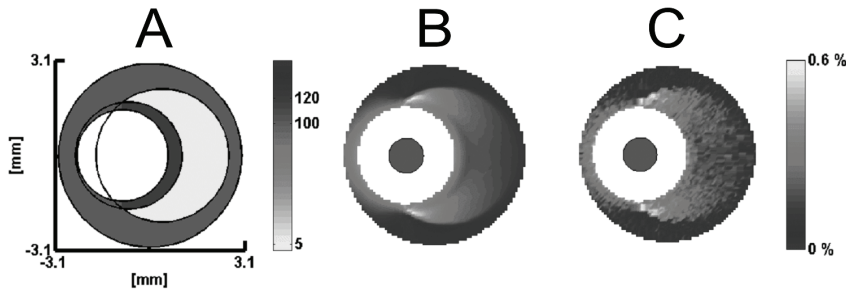


Fig. 4. Definition of standard plaque. (a) Standard plaque. (b) PFEM strain elastogram computed using (a). (c) Noisy strain elastogram computed by adding default strain-noise to (b). Young's moduli are in kPa and intraluminal pressure difference is 1 mmHg. Blue dot, diameter 1.1 mm, indicates catheter.

DEFINITION OF STANDARD PLAQUE

Next, IVUS modulus elastography was used to compute a modulus elastogram from the in vivo measured compounded strain elastogram of the patient (Fig. 3b). This strain elastogram showed a strain pattern consisting of high strain with adjacent low strain at the shoulders of the plaque, which is a typical characteristic of vulnerable plaques (Schaar et al. 2003); the strain was less than 2% at a pressure differential of 1.0 mmHg. The reconstructed modulus elastogram (Fig. 3c) is a likely candidate for the real underlying plaque composition, since the measured strain elastogram (Fig. 3b) and PFEM strain elastogram (Fig. 3d) show two colocalising regions of high radial strain at the shoulders of the plaque and a region of low radial strain at the centre of the plaque. The PFEM parameters that defined this modulus elastogram (Fig. 3c) were modified and used to define a standard plaque (Fig. 4a). This modification was done (i) to allow the plaque parameter variations described later in this section and (ii) to use dimensions for the lumen and media circle that are representative for atherosclerotic human coronary arteries (Glagov et al. 1987).

SIMULATING IVUS STRAIN ELASTOGRAMS

To each simulated strain elastogram (e.g., Fig. 4b) of a simulated plaque (e.g., Fig. 4a), strain-noise was added (e.g., Fig. 4c). This addition was done at the same spatial grid positions where local radial strain values are normally processed with IVUS strain elastography (i.e., 512 lines emanating from the catheter at equidistant angles; each line has a grid position at every 200 μm). At each grid position, a strain noise value was drawn from a normal distribution with mean = 0 and standard deviation = $a \cdot \epsilon_{rr} + b$, with $a=0.2\%$, $b=0.04\%$ and ϵ_{rr} = radial strain value in the simulated strain elastogram. This model and its coefficients are derived from data published by de Korte et al. (2002) and Doyley et al. (2001). By averaging multiple in vivo strain elastograms of patients and by determining strain filters for a vessel phantom, they showed that the elastographic SNR as function of the mean radial strain (μ) was constant at the strain range [0.25%, 1.5%]. Because the SNR was defined as the ratio between μ and the standard deviation of the radial strain (σ), it immediately follows that σ is a linearly increasing function of μ . A simulated strain elastogram with strain noise added is denoted as "noisy strain elastogram" throughout the paper.

PARAMETER VARIATIONS

The standard plaque was used to compute noisy strain elastograms, by varying the geometry and stiffness of its plaque components, the position of the catheter and the level of strain noise.

Geometry Variation

The geometry of the lipid pool and the cap region in the standard plaque were changed by varying the user-defined control points A, B, C, D and E in Fig. 5a. Points A and D are located on the cap circle at the x-axis, B and C are each at an intersection of the cap with the lipid pool circle and E is on the lipid pool circle at

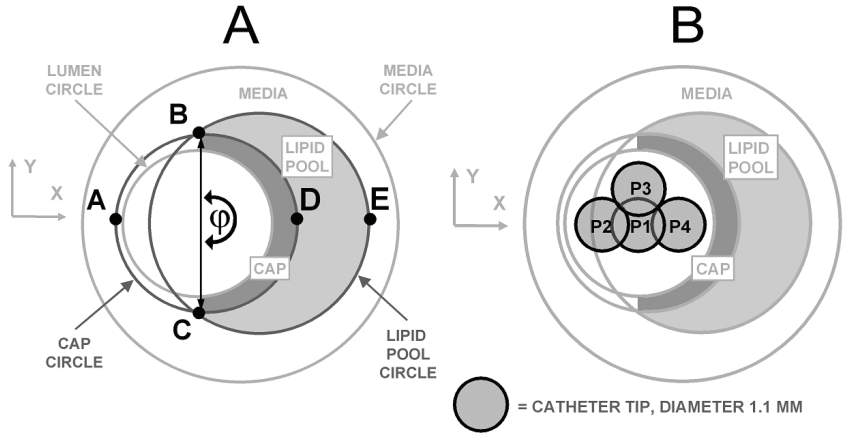


Fig. 5. Parameter variations using the standard plaque. (a) Standard plaque. Points A-E and angle ϕ are used to define various plaque configurations. (b) Standard plaque. Positions P1-4 indicate specific catheter positions.

the x-axis. ϕ is the angle between points B and C. The thickness of the lipid pool is defined as the distance between D and E.

The lipid pool size and shape were altered by varying points B, C and E, while forcing the lipid pool circle to go (uniquely) through these three points, in the following two ways:

Lipid pool thickness

- "Lipid pool thickness variation": points B and C were fixed and point E was varied in the x direction such that the lipid pool thickness became respectively 488, 975 and 1900 μm .

Lipid pool angle

- "Lipid pool shoulders angle variation": the lipid pool thickness was fixed and points B and C were varied symmetrically with respect to the x axis by setting $j\phi$ respectively at 3° , 90° , 180° and 270° .

The cap size and shape were altered using points A, B, C and D in the following three ways:

Global cap change

- "Global cap change": point A was fixed and the radius of the cap circle was varied such that the distance between point D and the lumen circle became respectively 225, 675 and 900 μm .

Local cap change

- "Local cap change": points B and C were fixed and point D was positioned at a distance of respectively 50, 100, 225 and 450 μm from the lumen.

Eccentric cap change

- "Eccentric cap change": similar as "Global cap change"; however, here the cap change was in the direction of the y-axis and, as such, this change is eccentric with respect to the lipid pool and plaque. This eccentric cap change was accomplished as follows: first, the cap circle was centred around the lumen circle, then the cap circle was given a radius that is 50 μm longer than the lumen circle radius. Finally, point C was fixed and the radius of the cap circle was varied such that the distance between the highest point of the cap circle and the highest top of the lumen circle became, respectively, 225, 450, 675 and 900 μm .

Stiffness Variation

The following variations of the Young's modulus of the lipid pool (E_{LIPID}) and the cap (E_{CAP}) were used: $E_{\text{LIPID}} = 1.5, 10, 15, 30, 49$ kPa and $E_{\text{CAP}} = 135, 120, 90, 60$ kPa.

Catheter Position Variation

Figure 5b shows the four catheter positions P1, P2, P3 and P4 that were used. P1 is at the lumen centre, P2 is opposite the plaque, P3 is near a shoulder of the plaque and P4 is towards the plaque. The eccentricity of these catheter positions was, respectively, 0%, 50%, 50% and 50%. Eccentricity was defined as the ratio between the off-centred distance of the catheter-centre and the lumen radius of 1.5 mm. The catheter position variation was done with the standard plaque and with the plaques and noise levels that are described below at "combined variations".

Noise Level Variation

The default strain noise model coefficients $a=0.2\%$ and $b=0.04\%$ were both increased by factors of two and four. This was done with the standard plaque and with the plaques and catheter positions listed in Table 4.

Combined Variations

Some of the abovementioned geometrical variations of the cap and lipid pool were combined with a catheter position variation and an increase in strain noise level. These selected configurations are listed in Table 4.

ROBUSTNESS EVALUATION

Robustness of IVUS modulus elastography was evaluated by quantitatively comparing the modulus elastogram of a simulated plaque with its corresponding reconstructed modulus elastogram. The comparison was performed upon specific features of a simulated plaque component region and corresponding reconstructed plaque component region. These features were the region overlap (RO), surface area (SA) and Young's modulus (YM) of the lipid and cap components and the minimal cap-thickness. The RO error between two regions, A and B, was defined as $100\% \cdot (1 - 2 \cdot [\text{area of their intersection}] / [\text{area of A} + \text{area of B}])$. The error in their YM, SA and minimal cap-thickness was quantified with the relative error (RE) measure. The RE of a quantity Q with reference value QA and reconstructed value QB was defined as $RE = 100\% \cdot [QB - QA] / [QA]$. The minimal cap-thickness was defined as the shortest distance between cap border QT and lumen border PS (Fig. 1a). Finally, a qualitative judgment was performed by visually comparing both modulus elastograms as well as the similarity of structural strain patterns in corresponding strain elastograms.

PRINCIPAL STRAIN ELASTOGRAM

The effect that a change in catheter position has upon a radial strain distribution in an IVUS strain elastogram of a plaque can be completely explained by the "principal strain elastogram" (Fung 1969) of that plaque. For tissue material in a 2D plane strain state, a principal strain elastogram visualises at each tissue-point a 2D line segment. This line segment has the orientation at which the tissue is maximally strained; its length is equal to the amount of strain. For an isotropic, incompressible, plane strain material, the relation between the radial strain (ϵ_{rr}) and the maximum compressive strain (ϵ_{mc}), at each tissue point, equals $\epsilon_{rr} = \epsilon_{mc} \cdot \cos(2 \cdot \alpha)$, where α is the angle between the ϵ_{mc} line-segment and the line between catheter centre and tissue point (i.e., the line that defines the radial direction) (Appendix B). Principal strain elastograms, visualizing ϵ_{mc} , were calculated for the standard plaque (Fig. 9b1), a plaque with a soft cap (Fig. 9b2) and a plaque with a stiff lipid pool (Fig. 9b3).

TABLE 1: RECONSTRUCTION ERRORS AND RMS ERRORS FOR VARIOUS GEOMETRICALLY DIFFERENT PLAQUES THAT WERE IMAGED AT VARIOUS CATHETER POSITIONS AND AT THREE DIFFERENT STRAIN NOISE LEVELS

PARAMETER VALUES	NOISE LEVEL	REGION OVERLAP ERROR(%)		SURFACE AREA ERROR(%)		YOUNG'S MODULUS ERROR REL.(%), ABS.(KPA)			CAP THICKNESS ERROR REL.(%), ABS.(μM)		R.M.S. ERROR (%)
		Cap	Lipid	Cap	Lipid	Cap	Lipid	Media			
Lipid pool shoulders angle at 90° catheter at P3	1a, 1b	6	3	8	-3	-16, -19	44, 2	-1, -1	6, 24	0.043	
	2a, 2b	11	5	10	-5	-29, -34	99, 5	-3, -3	5, 18	0.075	
	4a, 4b	13	6	31	-5	-28, -33	-30, -2	-3, -3	23, 89	0.128	
Global cap change 675 μm catheter at P4	1a, 1b	3	14	1	-23	-11, -13	-18, -1	2, 2	16, 56	0.042	
	2a, 2b	10	5	-15	10	19, 22	25, 1	-5, -5	0.1, 0.3	0.075	
	4a, 4b	17	22	8	-3	-38, -46	-24, -1	41, 41	-39, -139	0.131	
Local cap change 50 μm catheter at P3	1a, 1b	4	1	4	1	21, 25	-25, -1	-2, -2	-8, -4	0.051	
	2a, 2b	17	2	-24	2	21, 25	44, 2	2, 2	-40, -20	0.083	
	4a, 4b	11	2	-20	0	21, 26	21, 1	-15, -15	-23, -11	0.152	
Eccentric cap change 450 μm catheter at P4	1a, 1b	10	3	-18	1	23, 28	-4, 0	-4, -4	-5, -3	0.048	
	2a, 2b	5	1	-9	2	22, 26	-12, -1	1, 1	3, 1	0.081	
	4a, 4b	14	4	-25	4	23, 28	12, 1	0, 0	-8, -4	0.144	

The default strain noise level has $a=0.2\%$, $b=0.04\%$. Each plaque had the same Young's moduli as the standard plaque, namely, a lipid pool, cap and media Young's modulus of 5, 120 and 100 kPa, respectively. The geometry was also the same, unless stated otherwise in the Table.

TABLE 2: RECONSTRUCTION ERRORS AND R.M.S. ERRORS FOR GEOMETRICALLY DIFFERENT PLAQUES

PARAMETER VALUE	REGION OVERLAP ERROR(%)		SURFACE AREA ERROR(%)		YOUNG'S MODULUS ERROR REL.(%),ABS.(kPA)			CAP THICKNESS ERROR REL.(%),ABS.(μM)	R.M.S. ERROR (%)	
	Cap	Lipid	Cap	Lipid	Cap	Lipid	Media			
	Lipid pool thickness (μm)	488 975 1900	10 13 8	32 10 2	-9 -20 -15	71 22 3	24, 28 22, 27 20, 24	62, 3 30, 1 -15, -1	-2, -2 -4, -4 -3, -3	54, 127 -22, -52 -5, -12
Lipid pool shoulders angle (°)	3 90 180 270	92 19 11 12	61 9 5 9	2227 48 -19 -22	43 -13 11 19	24, 29 -25, -30 23, 27 24, 24	36, 2 -33, -2 -3, 0 56, 3	6, 6 5, 5 4, 4 -16, -16	-8, -35 40, 153 -1, -3 -15, -16	0.058 0.043 0.048 0.060
Global cap change (μm)	225 450 675 900	11 11 9 31	3 5 8 27	-20 -19 -15 -29	7 11 17 58	21, 25 23, 27 23, 28 25, 30	21, 1 -3, 0 9, 0 122, 6	-2, -2 4, 4 5, 5 4, 4	-3, -4 -1, -3 -1, -4 -16, -112	0.051 0.048 0.046 0.043
Local cap change (μm)	50 100 225 450	19 13 17 11	3 5 2 5	46 -23 -25 -19	-1 8 4 11	-38, -45 21, 25 22, 26 23, 27	-56, -3 55, 3 37, 2 -3, 0	48, 48 0, 0 -2, -2 4, 4	78, 39 -27, -26 -29, -64 -1, -3	0.060 0.051 0.047 0.048
Eccentric cap change (μm)	225 450 675 900	20 11 22 7	3 4 4 4	46 -4 -25 -5	-3 7 8 -3	-40, -48 23, 28 23, 28 -36, -43	0, 0 4, 0 -27, 1 -19, 1	37, 37 1, 1 7, 7 49, 49	14, 7 -0.8, -0.4 23, 12 -0.6, -0.3	0.058 0.058 0.057 0.064

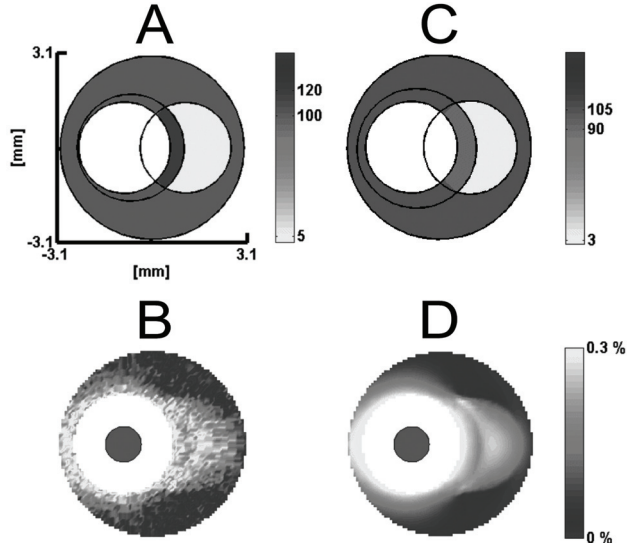
The catheter was positioned at the lumen centre (position P1). The strain noise level was default, i.e., $a=0.2\%$, $b=0.04\%$. Each plaque had the same Young's moduli as the standard plaque, namely, a lipid pool, cap and media Young's modulus of 5, 120 and 100 kPa, respectively. The geometry was also the same, unless stated otherwise in the Table.

RESULTS

PLAQUE GEOMETRY VARIATION

Figure 6a shows a plaque that has a small lipid pool ($\varphi = 90^\circ$), which is covered by a cap. Figure 6b shows the corresponding noisy strain elastogram. There is a region of high radial strain at the lipid pool and a radial-strain gradient within this region, near the interface between cap and lipid pool. The geometry and stiffness of the cap and lipid pool are qualitatively correctly reconstructed (Figs. 6a, c). Furthermore,

Fig. 6. Young's modulus reconstruction of a plaque that has a small lipid pool. (a) Modulus elastogram of the plaque. (b) Noisy radial strain elastogram computed using (a) and added with default strain noise. (c) Modulus elastogram reconstructed from (b) after 29 iterations. (d) PFEM strain elastogram computed using (c). RMS error between (b) and (d) is 0.043%. Young's moduli are in kPa and intraluminal pressure difference is 1 mmHg. Blue dot, diameter 1.1 mm, indicates catheter.



there is a high resemblance between the PFEM strain elastogram that corresponds to this reconstruction (Fig. 6d) and the noisy strain elastogram (Fig. 6b).

Quantitative inspection of the various reconstruction errors according to geometrical variation type (Table 1) resulted in the following general tendencies:

- Lipid pool shoulders angle: each angle resulted in small reconstruction errors, except for very small angles (e.g., $\varphi = 3^\circ$).
- Lipid pool thickness change: thicker lipid pools resulted in smaller reconstruction errors.
- Global cap change: globally thinner caps resulted in smaller reconstruction errors.
- Local cap change: larger local-cap-thicknesses resulted in smaller reconstruction errors.
- Eccentric cap change: each cap eccentricity resulted in small reconstruction errors.

PLAQUE STIFFNESS VARIATION

Figure 7a shows a reference plaque that has a large lipid pool which is covered by a relatively soft cap ($E_{\text{CAP}}=60$ kPa). The corresponding noisy strain elastogram (Fig. 7b) has a region of high radial strain throughout the plaque (i.e., cap + lipid pool region). Furthermore, there is no radial-strain gradient within this plaque, particularly not at the interface between cap and lipid pool. There is, however, a clear strain gradient at the interface between lipid pool and media. Figure 7c and Fig. 7e each show a reconstruction of the reference plaque. Both reconstructions have a PFEM strain elastogram that highly resembles the noisy strain elastogram. Within the plaque, they all have high radial strain that is high at the lumen border and gradually decays. For both reconstructions, the distal border of the lipid pool was correctly reconstructed. However, both reconstructions had cap geometries that differ from each other and also from the reference plaque (Fig. 7a); Fig. 7c shows a cap that is very thin and stiff and Fig. 7e shows a cap that is almost as stiff as the reference cap but thinner. Although the lipid pool was well reconstructed, in contrast to the cap, this example illustrates that slightly nonunique reconstructions can be obtained when there is low stiffness-contrast between the plaque components.

Slightly nonunique reconstructions can be obtained when there is low stiffness-contrast between the plaque components

Nevertheless, quantitative inspection of the reconstruction errors according to stiffness variation type (Table 2) showed that better reconstructions with smaller reconstruction errors were obtained when there was higher stiffness-contrast between the plaque components; in particular:

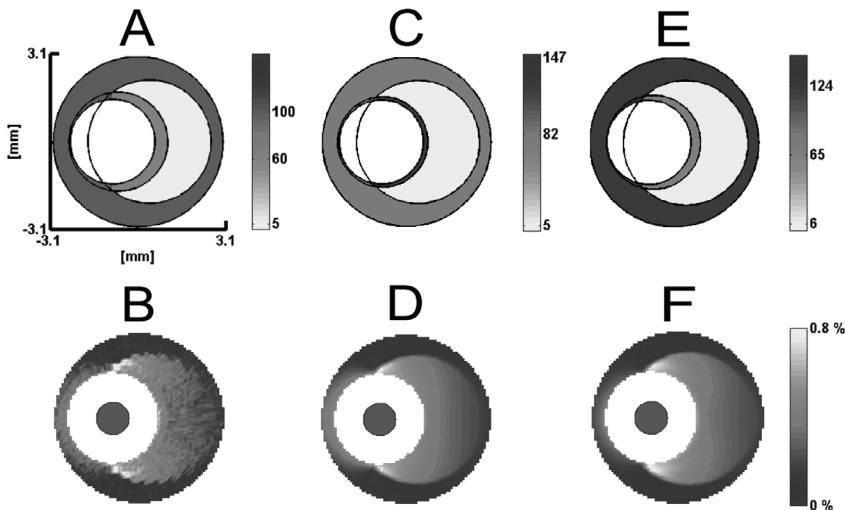


Fig. 7. Young's modulus reconstruction of a plaque that has a soft cap. (a) Modulus elastogram of the plaque. (b) Noisy radial strain elastogram computed using (a) and added with default strain noise. (c) Modulus elastogram reconstructed from (b) after 18 iterations. (d) PFEM strain elastogram computed using (c). RMS error between (b) and (d) is 0.058%. (e) Modulus elastogram reconstructed from (b) after 24 iterations. (f) PFEM strain elastogram computed using (e). RMS error between (b) and (f) is 0.067%. Young's moduli are in kPa and intraluminal pressure difference is 1 mmHg. Blue dot, diameter 1.1 mm, indicates catheter.

- Lipid pool stiffness: softer lipid pools resulted in smaller reconstruction errors.
- Cap stiffness: stiffer caps result in smaller reconstruction errors.

TABLE 3: RECONSTRUCTION ERRORS AND RMS ERRORS FOR PLAQUES WITH DIFFERENT LIPID POOL OR CAP YOUNG'S MODULUS

PARAMETER VALUE		REGION OVERLAP ERROR(%)		SURFACE AREA ERROR(%)		YOUNG'S MODULUS ERROR REL.(%), ABS.(KPA)			CAP THICKNESS ERROR REL.(%), ABS.(μM)		R.M.S. ERROR (%)
		Cap	Lipid	Cap	Lipid	Cap	Lipid	Media	Cap	Lipid	
Lipid pool stiffness (kPa)	1	3	5	-6	10	21, 25	16, 0	4, 4	-4, -9	0.054	
	5	11	5	-19	11	23, 27	-3, 0	4, 4	-1, -3	0.048	
	10	13	6	-22	0	23, 28	-16, -2	4, 4	-9, -22	0.045	
	15	10	7	-15	-5	23, 28	-45, -7	5, 5	19, 46	0.045	
	30	10	11	1	-14	24, 29	-70, -21	1, 1	58, 137	0.045	
	49	13	22	9	-36	23, 27	-82, -40	6, 6	77, 183	0.044	
Cap stiffness (kPa)	135	6	4	-11	-1	10, 13	13, 1	7, 7	-16, -37	0.047	
	120	11	5	-19	11	23, 27	-3, 0	4, 4	-1, -3	0.048	
	90	32	8	-46	17	64, 58	36, 2	-9, -9	-39, -93	0.051	
	60	49	9	-63	20	145, 87	9, 0	-18, -18	-57, -135	0.058	

The catheter was positioned at the lumen centre (position P1). The strain noise level was default, i.e., a=0.2%, b=0.04%. Each plaque had the same geometry as the standard plaque. The Young's moduli were also the same, namely, a lipid pool, cap and media Young's modulus of 5, 120 and 100 kPa, respectively, unless stated otherwise in the Table.

CATHETER POSITION VARIATION

Figure 8a, shows the plaque that was used to simulate noisy elastograms for different catheter positions. Fig. 8b1-4 shows that the corresponding radial strain distributions differ. The radial strain values at a lipid pool shoulder are higher (Fig. 8b2) or

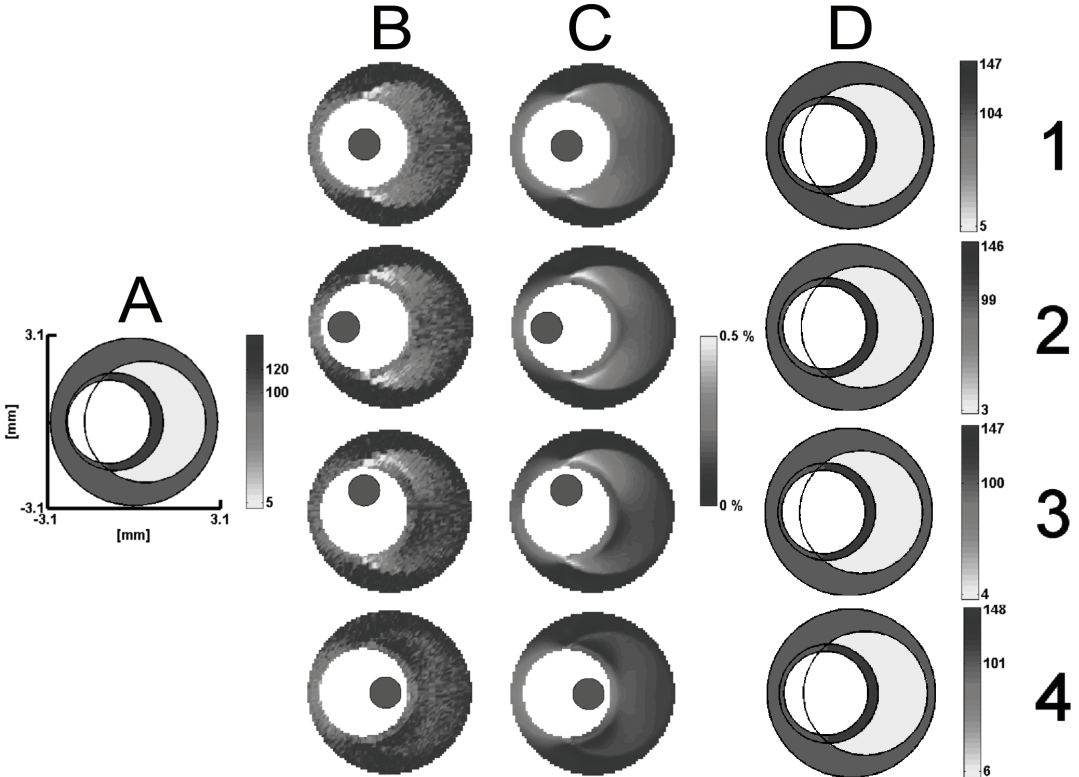


Fig. 8. Young's modulus reconstruction of a plaque for different catheter positions. (a) Modulus elastogram of the plaque. (b) Noisy radial strain elastograms computed using (a) and added with default strain noise, for different catheter positions, i.e., positions defined in Fig. 5B. (c) PFEM strain elastograms. c1, c2, c3 and c4 are computed using d1, d2, d3 and d4, respectively. RMS errors between b1 and c1, b2 and c2, b3 and c3 and b4 and c4 are 0.048%, 0.054%, 0.051% and 0.044%, respectively. (d) Modulus elastograms. d1, d2, d3 and d4 are reconstructed from b1, b2, b3 and b4, respectively, after 20, 23, 24 and 17 iterations, respectively. Young's moduli are in kPa and intraluminal pressure difference is 1 mmHg. Blue dot, diameter 1.1 mm, indicates catheter.

lower (Fig. 8b4) than in Fig. 8b1. In Fig 8b3, they are higher in the shoulder closest to the catheter and lower in the other shoulder than in Fig. 8b1. Each strain elastogram shows radial strain-gradients, either at the borders or within the lipid pool. The geometry and stiffness of the cap and lipid pool are qualitatively correctly reconstructed (Figs. 8d1-4). Furthermore, each PFEM strain elastogram (Figs. 8c1-4) resembles the corresponding noisy elastogram (Figs. 8b1-4).

Quantitative inspection of the various reconstruction errors (Table 3) shows that, for each catheter position, a reconstruction was obtained with small reconstruction errors.

PRINCIPAL STRAIN ELASTOGRAM

Figure 9a1 shows the plaque that was used for the catheter position variations and Fig. 9b1 shows the corresponding principal strain elastogram. Regions with a relatively high principal strain are located (i) close to the lumen and (ii) within the shoulders of the lipid pool. Notice that the principal strain line-segments near the lumen are oriented towards the centre of the lumen, but those within the lipid pool shoulders are oriented mainly to the left of the lumen centre. Furthermore, at the interface between media and lipid pool (solid arrow) and cap and lipid pool (dashed arrow), there are clear differences in principal strain value and orientation; this is due to the high stiffness-contrast between lipid pool and cap. However, the other two plaques (Fig. 9a2-3) have low stiffness-contrast between lipid pool and cap and, consequently, lack these clear principal strain differences at one or both interfaces. Such plaques are likely to be nonuniquely reconstructed, e.g., Fig. 7 and table 2.

Any radial strain elastogram of the standard plaque (Fig. 9a1) will show a radial strain value ($=\epsilon_{rr}$) that differs in magnitude from the principal strain value ϵ_{mc} , according to the formula $\epsilon_{rr} = \epsilon_{mc} \cdot \cos(2 \cdot \alpha)$, where α is the angle between the principal strain line segment and the line between catheter centre and tissue point. Indeed, when the catheter is positioned opposite (Fig. 8b2) or towards (Fig. 8b4) the

Plaques with low principal strain differences between lipid pool and cap are likely to be non-uniquely reconstructed

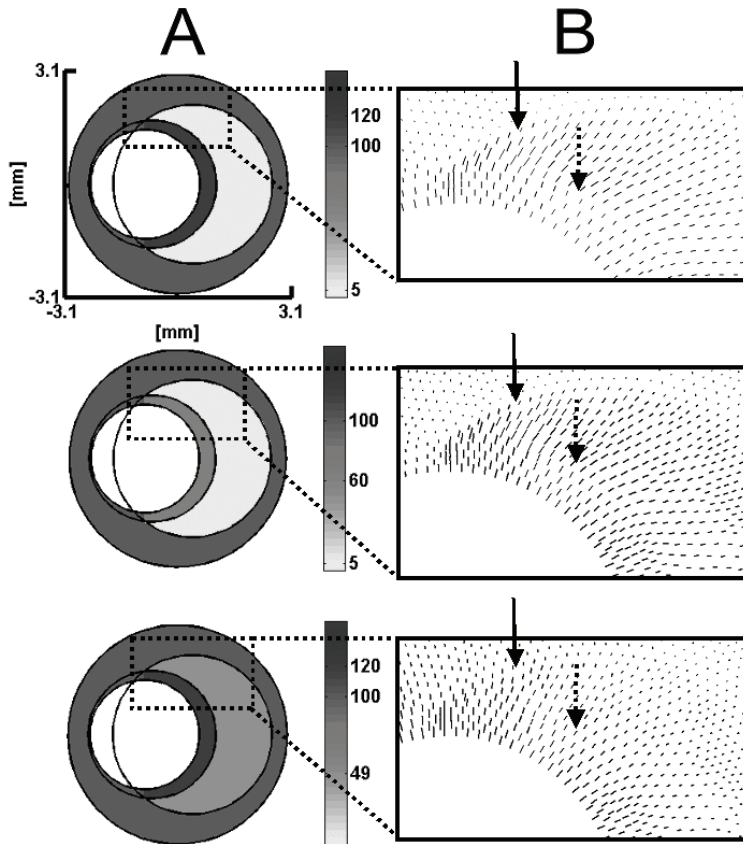


Fig. 9. Principal strain elastograms. (a1) Standard plaque. (a2) Plaque with a soft cap. (a3) Plaque with a stiff lipid pool.

1 (b1-3) Principal strain elastogram near a lipid pool shoulder: each line-segment has the orientation at which the tissue is maximally strained; its length is equal to the amount of compressive strain.

2 In b1, notice the clear difference in orientation and value of the principal strain line-segments at the lipid pool to media interface (solid arrow) and at the cap to lipid pool interface (dashed arrow).

Similarly, in b2, notice the lack of this clear difference at the cap to lipid pool interface (dashed arrow).

3 In b3, these differences do not occur at either interface (solid and dashed arrow). Young's moduli are in kPa and intraluminal pressure difference is 1 mmHg.

plaque, there is an increase or decrease, respectively, in ϵ_{rr} within the lipid pool shoulder. This is because α is close to 0° or 45° , respectively, for tissue points within the lipid pool shoulders.

TABLE 4: RECONSTRUCTION ERRORS AND RMS ERRORS FOR THE STANDARD PLAQUE THAT WAS IMAGED AT VARIOUS CATHETER POSITIONS OR AT DIFFERENT STRAIN NOISE LEVELS

PARAMETER VALUE		REGION OVERLAP ERROR(%)		SURFACE AREA ERROR(%)		YOUNG'S MODULUS ERROR REL.(%), ABS.(KPA)			CAP THICKNESS ERROR REL.(%), ABS.(μ M)		R.M.S. ERROR (%)
		Cap	Lipid	Cap	Lipid	Cap	Lipid	Media	Cap	Lipid	
Catheter position	P1 (lumen centre)	11	5	-19	11	23, 27	-3, 0	4, 4	-1, -3	0.048	
	P2 (opposite plaque)	5	3	-7	5	22, 26	-38, -2	-1, -1	17, 40	0.054	
	P3 (plaque shoulder)	9	5	-16	10	22, 27	-16, -1	0, 0	-3, -6	0.051	
	P4 (towards plaque)	9	7	-16	13	23, 28	22, 1	1, 1	6, 14	0.044	
Strain noise level	1a, 1b	11	5	-19	11	23, 27	-3, 0	4, 4	-1, -3	0.048	
	2a, 2b	4	6	-8	12	22, 27	3, 0	-1, -1	-10, -24	0.079	
	4a, 4b	10	8	-18	17	22, 27	13, 1	0, 0	-2, -5	0.141	

The default strain noise level has $a=0.2\%$, $b=0.04\%$. The standard plaque had a lipid pool, cap and media Young's modulus of 5, 120 and 100 kPa, respectively.

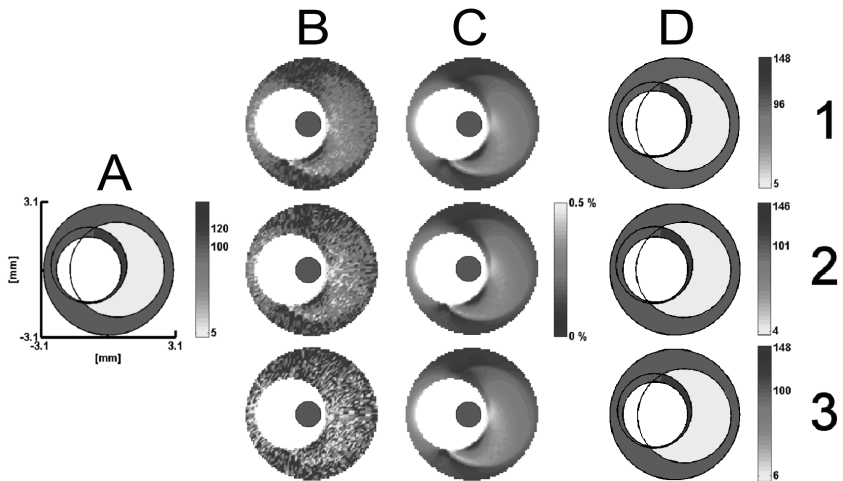
COMBINED VARIATION OF STRAIN NOISE LEVEL, CATHETER POSITION AND GEOMETRY

Figure 10a shows a standard plaque that has a lipid pool which is covered by an eccentric cap. This cap is thin on one side and thick on the opposite side. Figures 10b1-3 show the corresponding noisy strain elastograms for increasing strain noise level. The catheter was positioned towards the plaque. There is low or high radial strain at the location where the cap is thin or thick, respectively. Furthermore, within the plaque (i.e., lipid pool + cap), there are clear radial-strain gradients visible. For increasing strain noise levels, these gradients stay visible, although less clearly. The geometry and stiffness of the cap and lipid pool are qualitatively correctly reconstructed, despite the increases in strain noise level (Figs. 10d1-3). Furthermore, each PFEM strain elastogram (Figs. 10c1-3) resembles the corresponding noisy strain elastogram (Figs. 10b1-3), although this is less clear for the last elastogram pair (Fig. 10b3 and 10c3).

Quantitative inspection of the various reconstruction errors (Table 4) and (Table 3, "noise level") shows that, for the various combinations of catheter position, cap geometry, lipid pool geometry and noise level, small reconstruction errors resulted, although they increased with the strain noise level.

Fig. 10. Young's modulus reconstruction of a plaque that has an eccentric cap, for different strain-noise levels and an off-centred catheter position.

(a) Modulus elastogram of the plaque.



(b) Noisy radial strain elastograms computed using (a). b1, b2 and b3 were respectively added with default, two times default and four times default strain noise.

(c) PFEM strain elastograms. c1, c2 and c3 are computed using d1, d2 and d3, respectively. RMS errors between b1 and c1, b2 and c2 and b3 and c3 are 0.048%, 0.081% and 0.144%, respectively.

(d) Modulus elastograms. d1, d2 and d3 are reconstructed from b1, b2 and b3, respectively, after 20, 25 and 24 iterations, respectively. Young's moduli are in kPa and intraluminal pressure difference is 1 mmHg. Blue dot, diameter 1.1 mm, indicates catheter.

DISCUSSION

For the purpose of monitoring atherosclerosis and quantifying the effect of pharmaceutical plaque-stabilising drugs, a geometrically-constrained iterative Young's modulus reconstruction method has been developed for arterial plaques. The current study investigated, by means of computer simulations, how robust that method is in reconstructing a plaque's modulus elastogram from its radial strain elastogram.

DIFFERENCE BETWEEN NONVASCULAR AND VASCULAR STRAIN ELASTOGRAMS

Modulus reconstruction seems to be unnecessary for many organs (e.g., prostate, kidneys and breast), since it has been shown that their axial strain elastograms are good surrogates for their modulus elastograms (Srinivasan et al. 2004). For the configuration of a circular lesion inside a homogenous background, this is especially the case when a low modulus contrast exists between lesion and background, because, then, the contrast transfer efficiency (CTE), i.e., axial strain ratio between lesion and background divided by their true modulus ratio, is close to one (Ponnekanti et al. 1995). However, relatively soft lesions, in contrast to stiff lesions, have suboptimal CTE: due to the confinement by the stiff background, the soft lesion behaves as if it were stiffer (Varghese et al. 2001).

Modulus reconstruction seems unnecessary

These results are not applicable for the configuration of a TCFA, although (i) the axial and radial strain components are in the same direction as the applied load and (ii) the lipid pool may be interpreted as the lesion and the media and cap areas as the background. The main reason seems to be the different overall geometry, namely the rectangular background versus the tubular TCFA. This causes (i) a natural decay from lumen towards adventitia of the stress and strain components (Fung 1981; Richardson 2002), (ii) tensile circumferential stress-concentrations (Loree et al. 1992; Richardson et al. 1989) and associated compressive radial strain-concentrations near the lipid pool shoulders, (iii) a circumferential stress component that is much greater than the radial stress component (Fung 1981) and (iv) a heterogeneous distribution of principal and radial strain inside the mechanically homogeneous lipid pool (this paper). In fact, the presented results show, in contrast to nonvascular geometries, that better reconstructions are expected and obtained for softer lipid pools and worse reconstructions, for stiffer lipid pools.

For TCFA's, reconstructions are necessary

GENERAL OBSERVATIONS

The cap and lipid pool component of TCFA's can be reconstructed with greater precision (i) when caps are thinner and lipid pools are larger (Table 1) and/or (ii) when caps are stiffer and lipid pools are softer (Table 2). The reason for this is that plaque components with such geometries or large stiffness-contrasts will result in larger principal strain differences (either in its value or orientation) between these two components. Consequently, their radial strain elastograms will more uniquely characterise the underlying plaque composition and thus lead to a better reconstruction.

Reconstructions are better when (i) caps are thinner/stiffer or (ii) lipid pools are larger/softer

Figure 8 and Table 3 exemplify the independence of catheter position. Although the radial strain distributions differed considerably as function of catheter position, still each corresponding reconstruction resulted in the same correct modulus elastogram. This is because (i) the plaque had a large stiffness-contrast between lipid pool and cap and (ii) during the reconstruction, the catheter was at the position that was used for the creation of the noisy strain elastogram.

Catheter position

Figure 10 and Table 4 show that the presence of strain noise still allows the reconstruction of correct modulus elastograms for various plaque configurations and catheter positions. This is even the case for very high levels of strain noise, although less often (Table 4). For most cases, the independence of strain noise upon a correct reconstruction may be explained by the fact that the noisy strain elastograms preserve the radial strain patterns at the various noise levels. However, increasing the strain noise level causes larger fluctuations in the RMS-error as function of the nine PFEM parameters and thus, the higher the chance for a reconstruction to converge to a nonoptimal local minimum instead of the global minimum.

Measurement noise

Theoretically, it is possible that different PFEM geometries and/or moduli of the plaque components give a similar PFEM strain elastogram or, on the other hand, a

Uniqueness

very different PFEM strain elastogram that has the same RMS error (Barbone and Gokhale 2004). Practically, this is rare (Baldewsing et al. 2005) because of the strong geometrical constraints that are imposed upon the PFEM model. The results of this study show that the cap is the only component that may sometimes be nonuniquely reconstructed: slightly thinner and stiffer or slightly thicker and softer caps resulted in visually identical PFEM strain elastograms. With respect to the vulnerability of the plaque, this slight nonuniqueness is not of importance.

Miscellaneous observations

The Tables show that the YM of the lipid pool and media are reconstructed with less absolute error than is the YM of the cap. This may be caused by the fact that they occupy a larger cross-sectional area than the cap does and, thus, have more influence upon the RMS error during reconstruction. The large reconstruction errors for a plaque with an angle of only 3° between the shoulders of its lipid pool (Table 1) might be caused by the large "difference" between the composition of this plaque and each of the initial states used (Fig. 2). The minimal cap-thickness was often well reconstructed; only for a low stiffness-contrast between plaque components or for a very small thickness of the lipid pool, an error larger than 30% resulted.

PFEM GEOMETRIC AND MATERIAL-DEFORMATION FEATURES

The reconstruction method uses as geometric model for a plaque, an idealised TCFA that consists of circles and uses a linear elastic, isotropic, incompressible (Poisson's ratio=0.4999), plane strain material deformation model for simulating arterial strain. Baldewsing et al. (2005) (i) discussed that these simplistic geometric and material deformation features are essential for increasing the stability of the reconstruction method and the uniqueness of the reconstructions and (ii) discussed the appropriateness of the material deformation model and the possible reconstruction errors introduced by the geometric features of the PFEM when considering in vivo situations.

JUDGEMENT OF A RECONSTRUCTION IN VIVO

Compare similarity of structural strain patterns between strain elastograms

Since the actual plaque composition is unknown during in vivo applications, one does not know how well a reconstruction approximates to it. Thus, the only practical way to judge the approximation is by comparing the similarity of structural strain patterns (e.g., regions of high and low radial strain) between the PFEM strain elastograms and the measured strain elastogram.

STUDY LIMITATIONS

In this study, we used an idealized thin-cap fibroatheroma (TCFA) as PFEM for a plaque. Although other types of vulnerable plaques exist, such as eroded plaques or plaques containing calcified nodules, the idealised TCFA has been used as geometric model for the following reasons. (i) TCFAs are considered to be the precursor lesion of rupture and they account for the majority of plaque rupture (Virmani et al. 2002). (ii) The idealisation is essential to allow the parametric analyses and quantifications of the reconstructions that were performed in this paper. (iii) Its use allows a stable and unique reconstruction of TCFAs, as opposed to the situation where a geometrically less- or nonconstrained FEM is used to allow the reconstruction of a larger class of plaques (TCFAs, heterogeneous plaques and plaques containing calcified nodules) then, uniqueness and stability are compromised.

CLINICAL APPLICATIONS

A new way of intravascular tissue characterisation

This reconstruction method is a new way of intravascular tissue characterisation that may be suitable for clinical applications, such as (i) tissue characterisation to allow the selection of proper interventional procedures and (ii) monitoring of atherosclerosis to quantify the effect of pharmaceutical treatments aimed at stabilising plaques, e.g., by stiffening (Aikawa et al. 1998; Loree et al. 1994b) or reducing the lipids (Schartl et al. 2001). Furthermore, this method allows investigation and explanation of strain interpretation artifacts in vascular strain elastograms and it may be used to quantify the amount of stiffening of arterial plaque components within the physiological intraluminal pressure range. Finally, this method only needs a strain elastogram as input. Therefore, any imaging modality capable of measuring strain elastograms can be used. Our reconstruction method may potentially also be applied

in other clinically relevant situations where circular-like objects (e.g., plaques or tumours) are present in an approximately homogeneous medium that is strained, e.g., superficial atherosclerotic arteries, such as the carotid or femoral (Kim et al. 2004) or even breast tumours (Liu et al. 2003; Wellman and Howe 1999), both after appropriately modifying the PFEM inner and/or outer boundary.

CONCLUSION

For the purpose of quantitatively monitoring atherosclerosis and quantifying the effect of pharmaceutical plaque-stabilising treatments, a geometrically-constrained iterative Young's modulus reconstruction method for arterial plaques has been described and applied in vivo. By means of simulations, it was shown that this method seems to be robust in reconstructing a plaque's modulus elastogram from its radial strain elastogram, which is measured using intravascular ultrasound strain elastography, a techniques that is clinically available. The simulations revealed that thin-cap fibroatheromas can be adequately reconstructed; the thinner and stiffer the cap or the softer and larger the lipid pool, the better is the reconstruction of both plaque components and the minimal cap-thickness. Furthermore, reconstructions were (i) independent of the catheter position within the artery and (ii) independent of the strain-noise.

ACKNOWLEDGEMENTS

This research was financially supported by the Dutch Technology Foundation (STW) project number RPG-5442 and the Netherlands Organisation for Scientific Research (NWO). We also acknowledge Volcano Corporation, Inc., Rancho Cordova, CA, USA for their feedback.

REFERENCES

- Aikawa M, Rabkin E, Okada Y, et al. *Lipid lowering by diet reduces matrix metalloproteinase activity and increases collagen content of rabbit atheroma: a potential mechanism of lesion stabilization*. Circulation 1998; 97(24): 2433-44.
- Baldewsing RA, De Korte CL, Schaar JA, Mastik F and Van Der Steen AFW. *Finite element modeling and intravascular ultrasound elastography of vulnerable plaques: parameter variation*. Ultrasonics 2004a; 42(1-9): 723-729.
- Baldewsing RA, de Korte CL, Schaar JA, Mastik F and van der Steen AFW. *A finite element model for performing intravascular ultrasound elastography of human atherosclerotic coronary arteries*. Ultrasound Med Biol 2004b; 30(6): 803-813.
- Baldewsing RA, Schaar JA, Mastik F, Oomens CWJ, van der Steen AFW. *Young's modulus reconstruction for assessing vulnerable atherosclerotic plaque composition in vivo*. Proceedings of the 2004 IEEE International Ultrasonics Ferroelectrics and Frequency Control 50th Anniversary Conference, 2004c, Montreal, Canada, pages 368-371.
- Baldewsing RA, Schaar JA, Mastik F, Oomens CWJ and van der Steen AFW. *Assessment of vulnerable plaque composition by matching the deformation of a parametric plaque model to measured plaque deformation*. IEEE Trans Med Imaging 2005; 24(4): 514-528.
- Barbone PE and Gokhale NH. *Elastic modulus imaging: on the uniqueness and nonuniqueness of the elastography inverse problem in two dimensions*. Inverse Problems 2004; 20(283-296).
- Bergel DH. *The static elastic properties of the arterial wall*. Journal of Physiology 1961; 156(445-457).
- Davies MJ. *The pathophysiology of acute coronary syndromes*. Heart 2000; 83(3): 361-366.
- Davies MJ. *Going from immutable to mutable atherosclerotic plaques*. Am J Cardiol 2001; 88(4A): 2F-9F.
- de Korte CL, van der Steen AFW, Céspedes EI and Pasterkamp G. *Intravascular ultrasound elastography of human arteries: initial experience in vitro*. Ultrasound Med Biol 1998; 24(3): 401-408.
- de Korte CL, Céspedes EI and van der Steen AFW. *Influence of catheter position on estimated strain in intravascular elastography*. IEEE Trans Ultrason Ferroelectr Freq Control 1999; 46(3): 616-625.
- de Korte CL, Pasterkamp G, van der Steen AF, Woutman HA and Bom N. *Characterization of plaque components with intravascular ultrasound elastography in human femoral and coronary arteries in vitro*. Circulation 2000; 102(6): 617-23.
- de Korte CL, Carlier SG, Mastik F, et al. *Morphological and mechanical information of coronary arteries obtained with intravascular elastography; feasibility study in vivo*. Eur Heart J 2002; 23(5): 405-413.
- de Korte CL, Schaar JA, Mastik F, Serruys PW and van der Steen AFW. *Intravascular elastography: from bench to bedside*. J Interv Cardiol 2003; 16(3): 253-259.
- Dobrin PB. *Mechanical properties of arteries*. Physiol Rev 1978; 58(2): 397-460.
- Doyle M, Mastik F, de Korte CL, et al. *Advancing intravascular ultrasonic palpation towards clinical applications*. Ultrasound Med Biol 2001; 27(11): 1471-1480.
- Falk E, Shah PK and Fuster V. *Coronary plaque disruption*. Circulation 1995; 92(3): 657-671.
- Fung YC, *A first course in continuum mechanics*. Londen: Prentice-Hall International, 1969.
- Fung YC, *Biomechanics: Mechanical properties of living tissue*. New York: Springer, 1981.
- Glagov S, Weisenberg E, Zarins CK, Stankunavicius R and Kolettis GJ. *Compensatory enlargement of human atherosclerotic coronary arteries*. N Engl J Med 1987; 316(22): 1371-5.
- Gow BS and Hadfield CD. *The elasticity of canine and human coronary arteries with reference to postmortem changes*. Circ Res 1979; 45(5): 588-594.
- Kim K, Weitzel WF, Rubin JM, et al. *Vascular intramural strain imaging using arterial pressure equalization*. Ultrasound Med Biol 2004; 30(6): 761-71.
- Lee RT, Gordzinsky AJ, Frank EH, Kamm RD and Schoen FJ. *Structure-dependent dynamic mechanical behavior of fibrous caps from human atherosclerotic plaques*. Circulation 1991; 83(1764-1770).
- Lendon CL, Davies MJ, Born GVR and Richardson PD. *Atherosclerotic plaque caps are locally weakened when macrophage density is increased*. Atherosclerosis 1991; 87(87-90).
- Liu HT, Sun LZ, Wang G and Vannier MW. *Analytic modeling of breast elastography*. Med Phys 2003; 30(9): 2340-9.
- Loree HM, Kamm RD, Stringfellow RG and Lee RT. *Effects of fibrous cap thickness on peak circumferential stress in model atherosclerotic vessels*. Circ Res 1992; 71(4): 850-858.

- Loree HM, Grodzinsky AJ, Park SY, Gibson LJ and Lee RT. *Static circumferential tangential modulus of human atherosclerotic tissue*. J Biomech 1994a; 27(2): 195-204.
- Loree HM, Tobias BJ, Gibson LJ, et al. *Mechanical properties of model atherosclerotic lesion lipid pools*. Arterioscler Thromb 1994b; 14(2): 230-4.
- MacNeill BD, Lowe HC, Takano M, Fuster V and Jang IK. *Intravascular modalities for detection of vulnerable plaque: current status*. Arterioscler Thromb Vasc Biol 2003; 23(8): 1333-42.
- Ophir J, Céspedes EI, Garra B, et al. *Elastography: ultrasonic imaging of tissue strain and elastic modulus in vivo*. Eur J Ultrasound 1996; 3(49-70).
- Ponnekanti H, Ophir J, Huang Y and Céspedes I. *Fundamental mechanical limitations on the visualization of elasticity contrast in elastography*. Ultrasound Med Biol 1995; 21(4): 533-43.
- Richardson PD, Davies MJ and Born GVR. *Influence of plaque configuration and stress distribution on fissuring of coronary atherosclerotic plaques*. The Lancet 1989; 2(941-944).
- Richardson PD. *Biomechanics of plaque rupture: progress, problems, and new frontiers*. Ann Biomed Eng 2002; 30(4): 524-36.
- Schaar JA, De Korte CL, Mastik F, et al. *Characterizing vulnerable plaque features with intravascular elastography*. Circulation 2003; 108(21): 2636-41.
- Schaar JA, Muller JE, Falk E, et al. *Terminology for high-risk and vulnerable coronary artery plaques. Report of a meeting on the vulnerable plaque, June 17 and 18, 2003, Santorini, Greece*. Eur Heart J 2004; 25(12): 1077-82.
- Schartl M, Bocksch W, Koschyk DH, et al. *Use of intravascular ultrasound to compare effects of different strategies of lipid-lowering therapy on plaque volume and composition in patients with coronary artery disease*. Circulation 2001; 104(4): 387-92.
- Srinivasan S, Krouskop T and Ophir J. *A quantitative comparison of modulus images obtained using nanoindentation with strain elastograms*. Ultrasound Med Biol 2004; 30(7): 899-918.
- Varghese T, Ophir J, Konofagou E, Kallel F and Righetti R. *Tradeoffs in elastographic imaging*. Ultrasonic Imaging 2001; 23(216-248).
- Virmani R, Kolodgie FD, Burke AP, Farb A and Schwartz SM. *Lessons from sudden coronary death: a comprehensive morphological classification scheme for atherosclerotic lesions*. Arterioscler Thromb Vasc Biol 2000; 20(5): 1262-75.
- Virmani R, Burke AP, Farb A and Kolodgie FD. *Pathology of the unstable plaque*. Prog Cardiovasc Dis 2002; 44(5): 349-56.
- Virmani R, Burke AP, Kolodgie FD and Farb A. *Pathology of the thin-cap fibroatheroma: a type of vulnerable plaque*. J Interv Cardiol 2003; 16(3): 267-72.
- Wellman PS and Howe RD. *Extracting features from tactile maps*. MICCAI 1999; 1133-42.

PART IV

GENERALIZATION

YOUNG'S MODULUS RECONSTRUCTION OF VULNERABLE ATHEROSCLEROTIC PLAQUE COMPONENTS USING DEFORMABLE CURVES

ABSTRACT

BACKGROUND

Rupture, with subsequent thrombosis, of thin-cap fibroatheromas (TCFAs) is a major cause of myocardial infarction. A TCFA has two main components: these are a large, soft lipid pool and a thin, stiff, fibrous cap covering it. Quantification of their morphology and stiffness is essential for monitoring atherosclerosis and quantifying the effect of plaque-stabilizing pharmaceutical treatment. To accomplish this, we have developed a model-based Young's modulus reconstruction method.

METHODS

From a plaque's strain elastogram, measured with an intravascular ultrasound catheter, it reconstructs a plaque's Young's modulus image. To this end, a minimization algorithm automatically varies the morphology and stiffness parameters of a TCFA computer-model, until the corresponding computer-simulated strain elastogram resembles the measured strain elastogram. The model's morphology parameters are the control-points of two deformable Bézier curves; one curve delineates the distal border of the lipid pool region, the other the distal border of the cap region. These component regions are assumed to be homogenous and their stiffness is characterized by a Young's modulus.

RESULTS

Reconstructions from strain elastograms that were (i) simulated using a histology-derived computer-TCFA, (ii) measured from a physical phantom with a soft lipid pool and (iii) simulated with a computer-TCFA whose complexity of its plaque component borders was increased, demonstrated the superior reconstruction/delineation behavior of this method, compared with a previously developed circular reconstruction method, which used only circles for border delineation.

CONCLUSION

This method may become a valuable tool for the quantification of both the morphology and stiffness of vulnerable atherosclerotic plaque components.

THIS CHAPTER IS BASED ON THE PUBLICATION

*"Young's Modulus Reconstruction of Vulnerable Atherosclerotic Plaque Components
using Deformable Curves",*

BY BALDEWSING RA, MASTIK F, SCHAAR JA, SERRUYS PW AND VAN DER STEEN AFW,
IN *ULTRASOUND IN MEDICINE AND BIOLOGY*, 32(2):201-210;2006,

Copyright © 2006 World Federation of Ultrasound in Medicine and Biology.

Parts from this publication were reprinted with their permission.

INTRODUCTION

Rupture, with subsequent thrombosis, of thin-cap fibroatheromas (TCFAs) is a major cause of myocardial infarction (Davies 2000, Falk et al. 1995, Virmani et al. 2000). A TCFA has two main arterial plaque components: these are a large, soft lipid core and an inflamed, thin, fibrous cap covering it (Schaar et al. 2004, Virmani et al. 2000). The plaque-components' material properties and geometry as well as cap-weakening caused by macrophage-inflammation are considered as major mechanical and morphological determinants for plaque-rupture (Davies 2001). Diagnostic techniques need to be developed that provide these determinants (MacNeill et al. 2003), not only to give a measure of plaque-rupture proneness, but also to aid clinicians in choosing appropriate interventional procedures and to be able to quantify the efficiency of pharmaceutical drugs aimed at stabilizing plaques, e.g., by stiffening (Aikawa et al. 1998, Loree et al. 1994) or reducing the lipid (Ambrose et al. 1988).

Intravascular ultrasound (IVUS) is a real-time, clinically available technique that images vessel wall cross-sections, thus providing the location of the inner (i.e., lumen-intima) and outer (i.e., media-adventitia) wall boundaries (Schoenhagen et al. 2002). An add-on to IVUS is IVUS-elastography, which can use cross-correlation processing on pairs of IVUS radio-frequency signals to display mechanical information, namely radial strain, of the vessel cross-section in a so-called IVUS strain elastogram (Brusseau et al. 2001, de Korte et al. 2003, de Korte et al. 2002, Maurice et al. 2004, Perrey et al. 2004, Saijo et al. 2004). However, this cannot be directly interpreted as a plaque material composition image, due to the unknown heterogeneous arterial stress distribution and resulting strain-artifacts (Baldewsing et al. 2004b, de Korte et al. 1996, 1999, Ophir et al. 1996, Shi et al. 2003).

To overcome this limitation, we have developed a new model-based Young's modulus reconstruction method that obtains a material composition image of a plaque by reconstructing a modulus elastogram (i.e., Young's modulus image) from a measured IVUS strain elastogram. Reconstruction is done by a minimization algorithm that matches the strain image output, calculated with a parametric finite element model (PFEM) representation of a TCFA, to the measured strain elastogram by iteratively updating the PFEM morphology and material parameters. The distal borders of the PFEM lipid-pool and cap region are deformable curves, namely Bézier curves, whose control points are the PFEM morphology parameters. The lumen and media borders are extracted from the IVUS echogram. The PFEM material parameters are the Young's modulus of the media (E_{MEDIA}), lipid (E_{LIPID}) and cap (E_{CAP}) regions.

A previously developed circular-PFEM (Baldewsing et al. 2005b) used circles to delineate the border of the lumen and media as well as the borders of the lipid pool and cap region. Consequently, it is hypothesized that the new Bézier-PFEM will give a more accurate and reliable modulus elastogram, for a much larger collection of complicated TFCA plaque-component morphologies, despite the increase in PFEM parameters and a possibly increased instability or nonuniqueness of reconstructions.

To evaluate this hypothesis, we first describe the new Young's modulus reconstruction method. Then, we use both the circular and Bézier-PFEM to reconstruct a modulus elastogram from a strain elastogram that was (i) computer-simulated with a

Acute coronary syndromes and plaque rupture determinants

IVUS elastograms cannot be directly interpreted as plaque component images

Young's modulus reconstruction using deformable curves

Circular versus new Bézier PFEM model

Aims of this study

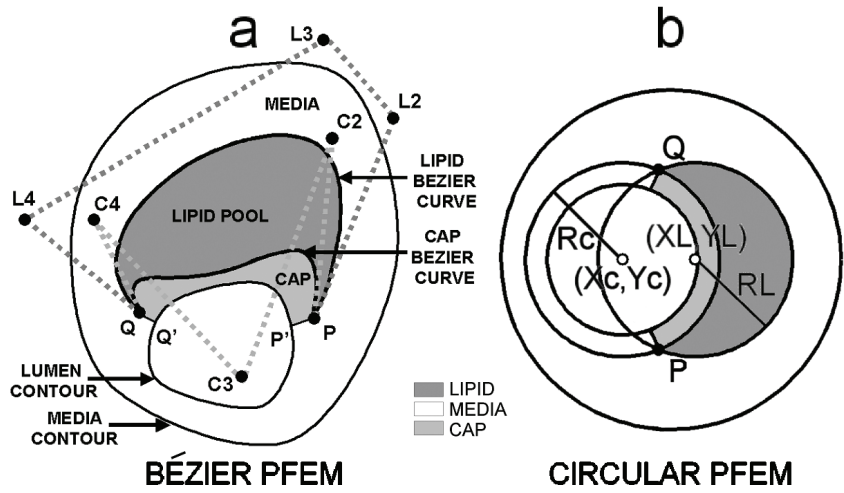


Fig. 1. Bézier parametric finite element model (PFEM) for a vulnerable plaque. The shape of the lipid and cap Bézier curves are determined by the spatial locations of their control points. In this example, there are five control points used for the lipid, namely P, L2, L3, L4 and Q and also five for the cap, namely P, C2, C3, C4 and Q. (b) Circular PFEM for a vulnerable plaque. The lipid and cap region borders are delineated by circles, which are parameterized by their center (X,Y) and a radius R . Letters L and c denote lipid and cap, respectively.

realistic, histology-traced computer-plaque and (ii) measured from a physical vessel-mimicking phantom. Finally, we investigate the reconstruction performance as function of (a) the number of Bézier control-points and (b) cap and lipid pool border-complexity, by performing reconstructions for a computer-simulated plaque whose plaque components' border-complexity can be varied.

MATERIALS AND METHODS

MODEL-BASED YOUNG'S MODULUS RECONSTRUCTION

Our reconstruction method uses a model-based, iterative, inverse solution approach to obtain a modulus image from a plaque's strain image. A description of its main components follows.

Plaque geometry model

An idealized "thin-cap fibroatheroma" (Virmani et al. 2003) was used as a PFEM for a vulnerable plaque (Fig. 1a). The lumen and media border are to be extracted a priori from the echogram, either by a manual tracing or by a contour detection algorithm, e.g., Dijkstra et al. (1999), Klingensmith et al. (2000), Li et al. (1994), von Birgelen et al. (1996). The border of the cap region (PQ) and of the lipid pool region were both defined as deformable curves, namely Bézier curves (Farin 1993). The shape of a Bézier Curve, $BC(t)$, is determined by specifying the spatial locations of an ordered list of N control points cp_i , $i=1\dots N$, $N \geq 2$, as follows:

$$BC(t) = \sum_{i=1}^N cp_i \times B_{i-1}^{N-1}(t) = \sum_{i=1}^N cp_i \times \frac{(N-1)!}{(i-1)!(N-i)!} t^{i-1} (1-t)^{N-i}$$

where $t \in [0,1]$ and the $B_{i-1}^{N-1}(t)$ are Bernstein polynomials that act as blending functions. Note that $t=0$ corresponds with cp_1 and $t=1$ with cp_N . The number of control points for the cap and lipid Bézier curve are denoted as N_{CAP} and N_{LIPID} , respectively. There are $2^*(N_{CAP}+N_{LIPID}-2)$ PFEM geometry parameters, since control-points P and Q are used by both the cap and lipid Bézier curve and each control point has an x and y coordinate. Point P' is the point on the lumen contour that is closest to point P (Q' is defined analogously).

Plaque material deformation model

The PFEM was modelled as a linearly elastic, isotropic, incompressible (Poisson's ratio 0.4999), plane strain material (Baldewsing et al. 2004a). The cap, lipid and

media regions were each assumed homogeneous and their Young's modulus values were denoted as E_{CAP} , E_{LIPID} , and E_{MEDIA} , respectively.

The forward problem consisted of calculating the radial strain of the PFEM when it is subjected to an intraluminal pressure difference. First, the pressure difference upon the lumen border was specified as well as the values of parameter vector V , which contained all parameters of the PFEM, namely the $2 \cdot (N_{CAP} + N_{LIPID} - 2)$ control-points coordinates and the three Young's moduli E_{CAP} , E_{LIPID} , and E_{MEDIA} . Then, the finite element package SEPRAN (Septra Analysis, Technical University Delft, The Netherlands) calculated the Cartesian linear strain tensor components. Next, MATLAB (release 12.1, the MathWorks, Inc., Natick, MA, USA) converted them to polar components using the catheter position as origin. Finally, the radial strain field was interpolated onto a square equidistant reference grid of 100 by 100 points. This radial strain field was called a PFEM strain elastogram. The measured strain elastogram was also interpolated onto the reference grid. The whole process from defining the PFEM parameters up to the calculation of the PFEM strain elastogram was fully automatic.

Forward problem calculation

The modulus elastogram of a plaque was determined by a constrained sequential-quadratic-programming minimization algorithm (Optimization Toolbox, MATLAB). This algorithm finds a value for parameter vector V , such that the corresponding PFEM strain elastogram displays high similarity with the measured strain elastogram of the plaque. The similarity between these strain elastograms was quantified as the root-mean-squared (RMS) error of the strain values at the reference-grid points. The minimization algorithm fully automatically searches a local minimum of the RMS error by iteratively updating the parameter vector V ; every update results in a lower RMS error. The algorithm was stopped after 50 iterations. The resulting value of V defined the modulus elastogram. A detailed mathematical description of the minimization algorithm can be found in the Optimization Toolbox of MATLAB.

Minimization algorithm

To maintain the configuration of a TCFA (Fig. 1a) and automatically to calculate a proper finite element mesh during the minimization process, the following nonlinear constraints were enforced upon the lipid (PQ) and cap (P'PQQ') curves: c_1) The cap curve is not self-intersecting; c_2) the lipid curve is not self-intersecting; c_3) the cap curve and the lipid curve are not intersecting each other; c_4) the cap curve is outside the lumen border; c_5) the lipid curve is outside the lumen border; c_6) the cap curve is inside the media border; and c_7) the lipid curve is inside the media border. Note that all curves and contours of the Bézier plaque model are implemented as equidistant polygons, i.e., each polygon consists of an ordered list of points and each point is at a fixed distance, say h , from its adjacent points.

Constraints and constraint-functions

The minimization algorithm requires differentiability of the scalar-valued constraint-functions $C_1(V)$, $C_2(V)$, ..., $C_7(V)$ that correspond to constraints c_1, c_2, \dots, c_7 . In addition to minimizing the RMS error, the minimization algorithm causes parameter vector V to satisfy $C_i(V) \leq 0$, $i=1,2,\dots,7$. To accomplish differentiability of $C_i(V)$, we incorporated a distance-measure in them, as follows:

Differentiability requirement

- $C_1(V) = \Delta - D$ if the cap is not self-intersecting, else D ; D is the minimum distance between any two nonadjacent cap curve points. Note that D is only defined when V is such that the cap is not self-intersecting. The small quantity Δ indicates a minimum required distance that allows a proper finite element meshing of the plaque regions. $C_2(V)$ is defined analogously to $C_1(V)$.

- $C_3(V) = \Delta - D$ if the cap curve and lipid curve are not intersecting each other, else D ; D is the minimum distance between any point of the cap curve to any point on the lipid curve.

- $C_4(V) = \Delta - D$ if the cap curve is outside the lumen border, else D ; D is the minimum distance between any point on the cap-curve to any point on the lumen border. $C_5(V)$, $C_6(V)$ and $C_7(V)$ are defined analogously to $C_4(V)$.

For each initial state of the Bézier PFEM, the control points of the cap Bézier curve (and analogously the lipid Bézier curve) were automatically placed, as follows. First, a target curve for the cap was manually drawn or automatically defined as a function of the lumen/media border shape. Then, the cap Bézier curve was automatically placed close to the target curve. This placement was done by a nonlinear, least-squares optimization algorithm (program lsqnonlin, Optimization Toolbox, MAT-

Positioning the control points

LAB), which varied the control points until the least-square distance error between the target curve and the cap Bézier curve was minimized.

RECONSTRUCTION OF A THIN-CAP FIBROATHEROMA AND A VESSEL-MIMICKING PHANTOM

To investigate whether the Bézier PFEM allows a more accurate delineation of plaque component borders than the circular PFEM (Fig. 1b), which was previously developed (Baldewsing et al. 2005b), we used both models for reconstructing a modulus elastogram from a strain elastogram that was (i) simulated using a computer-simulated plaque with a realistic thin-cap fibroatheroma geometry and (ii) measured from a vessel-mimicking phantom.

Thin-cap fibroatheroma

The geometry and Young's moduli of this plaque (Fig. 2a) were determined by tracing the histology of an excised human coronary artery (Baldewsing et al. 2004a). The strain elastogram (fig. 2B) of this plaque was simulated using the finite element package Sepran and a linearly elastic, isotropic, incompressible (Poisson's ratio 0.4999), plane strain material model. The pressure differential upon the lumen border was 20 mmHg. For the reconstruction with the Bézier PFEM, N_{CAP} was 5 and N_{LIPID} was 4.

Vessel-mimicking phantom

The phantom had an eccentric soft plaque embedded in a relatively stiff wall (Fig. 3b). The creation of this phantom, the mechanical measurement of its moduli and the processing of its strain elastogram (Fig. 3c) from measured IVUS (Fig. 3a) radio-frequency data are detailed in Baldewsing et al. (2004a). The mechanically-measured moduli of the plaque and wall were, respectively, 4.2 kPa and 16.8 kPa. The strain elastogram was measured using an intraluminal pressure differential of 1 mmHg. For the reconstruction with the Bézier PFEM, N_{LIPID} was 5. The phantom does not have a cap; thus, to model this situation appropriately, the following constraints were enforced upon the circular and Bézier PFEM during the minimization: (i) the cap curve was fixed near the lumen border and (ii) $E_{CAP}=E_{LIPID}$.

VARYING THE PLAQUE BORDER COMPLEXITY AND THE NUMBER OF CONTROL POINTS

Compared with the circular PFEM, the Bézier PFEM theoretically allows a more accurate approximation of plaque component borders, but only if N_{CAP} and N_{LIPID} are high enough. For increasing complexity of the plaque component borders, higher N_{CAP} and N_{LIPID} may be required. However, this gives more parameters to be minimized and, thus, may introduce more local minima and may compromise reconstruction stability.

Sine-modulated plaques

We investigated the effect of the plaque-components' border complexity and the number of control points upon the reconstruction quality. To this end, three sets of reconstructions were performed for a sine-modulated computer plaque, whose plaque-components' border complexity could be varied. Each set used a different number of control points, namely $N_{CAP}=N_{LIPID} = 4, 5, 7$ or 9. The geometry of the cap and lipid curve of the sine-modulated computer plaque was defined by adding a sine-function to a circle segment (Fig. 4a). This addition was done normal to the circle segment curve. The sine function equals $A*\sin(2\pi Kt)$, where $t \in [0,1]$ and $t=0$ corresponds to point P and $t=1$ to point Q. The following values for K, i.e., the plaque-border complexity, were used: $K=1, 1.5$ and 2. The value of A was set to 300 μm , since this was the highest value that still resulted in a feasible plaque geometry. Figures 4b, 4d and 4f show the three corresponding plaque geometries and Figs. 4c, 4e and 4g the corresponding strain elastograms. The lumen and media dimensions of these plaques were chosen to be representative for atherosclerotic human coronary arteries (Glagov et al. 1987). Furthermore, the material properties were set to $E_{LIPID}=2$, $E_{MEDIA}=100$ and $E_{CAP}=120$ kPa and the pressure differential upon the lumen border was set to 1 mmHg; these material properties and pressure differential are similar to the values reported in (Baldewsing et al. 2005b) for an in vivo reconstructed human coronary plaque.

For comparison purposes, the circular PFEM (Fig. 1b) was also used to reconstruct the sine-modulated plaques.

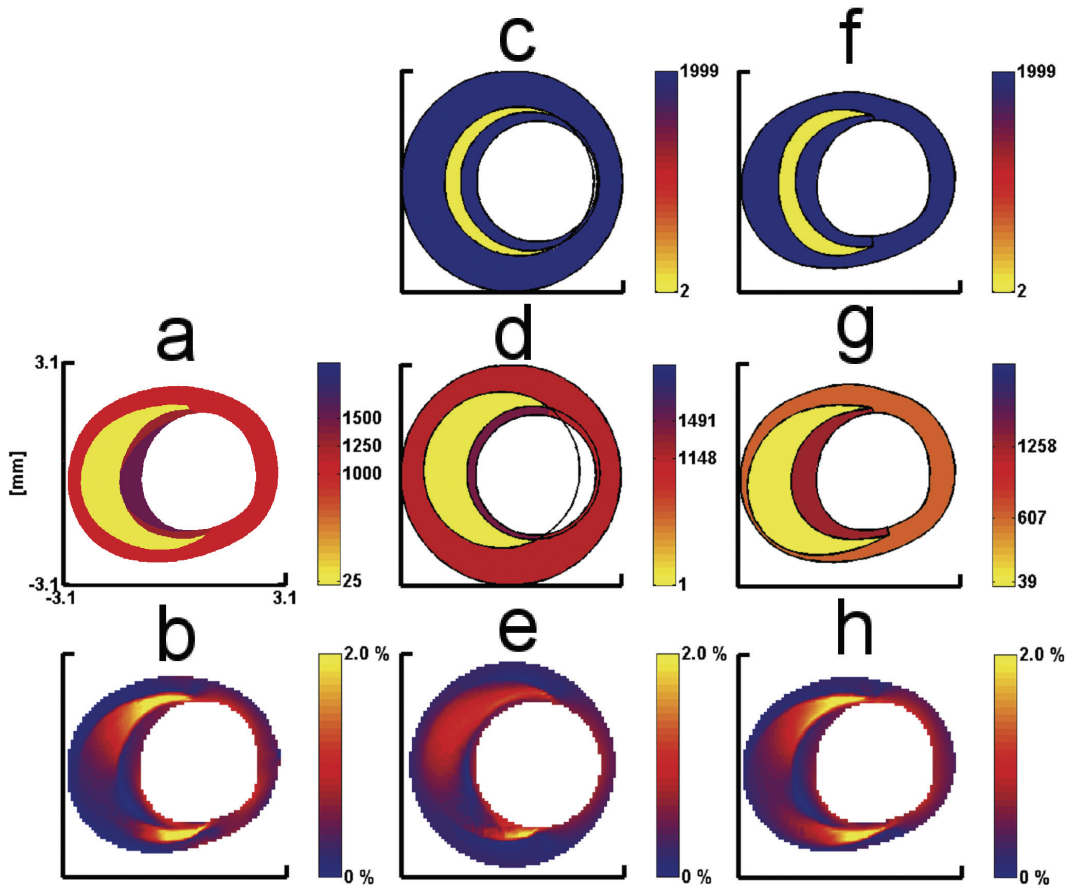


Fig. 2. Circular and Bézier parametric finite element model (PFEM) reconstruction using a simulated strain elastogram of a thin-cap fibroatheroma plaque that was traced from arterial histology. (a) Modulus elastogram of the traced plaque; the Young's moduli of its plaque components are $E_{LIPID}=25$, $E_{MEDIA}=1000$ and $E_{CAP}=1250$ at center and 1500 at side regions. (b) Simulated elastogram computed using (a). Circular PFEM reconstruction: (c) Initial state with $E_{LIPID}=2$, $E_{MEDIA}=1999$ and $E_{CAP}=1999$ kPa. (d) Modulus elastogram reconstructed from (b). (e) PFEM strain elastogram computed using (d). Bézier model reconstruction: (f) Initial state. (g) Modulus elastogram reconstructed from (b). (h) PFEM strain elastogram computed using (g). Young's moduli are in kPa and intraluminal pressure difference is 20 mmHg. The range of each Young's modulus color-bar is [0-2000] kPa.

At the start of the minimization process, the algorithm required an initial state for parameter vector V . For each strain elastogram, a fixed set of three different initial states (Fig. 5) was used to compute three candidate modulus elastograms. The candidate modulus elastogram that gave the smallest RMS error between the PFEM strain elastogram and the input strain elastogram was taken as the final modulus elastogram. The initial states in Fig. 5 were only used for the sine-modulated plaques. The main reasons for choosing this set of initial states was to incorporate a priori plaque information that is practically available, for example: (i) an echogram shows the location of the plaque, which is characterized by intimal thickening and (ii) a strain elastogram may indicate the presence of a soft region by means of a typical strain pattern at the shoulder of the plaque consisting of high strain with adjacent low strain (Schaar et al. 2003). Therefore, all initial states were given a soft lipid pool region that was positioned towards the location of the plaque. The same initial Young's moduli as in Baldewsing et al. (2005a) were used.

RECONSTRUCTION ERROR MEASURES

For the various sine-modulated plaques, the quality of their reconstructions was determined by quantitatively comparing the modulus elastogram of a sine-modulated plaque with its corresponding reconstructed modulus elastogram. The comparison was performed upon specific features of the sine-modulated plaque component

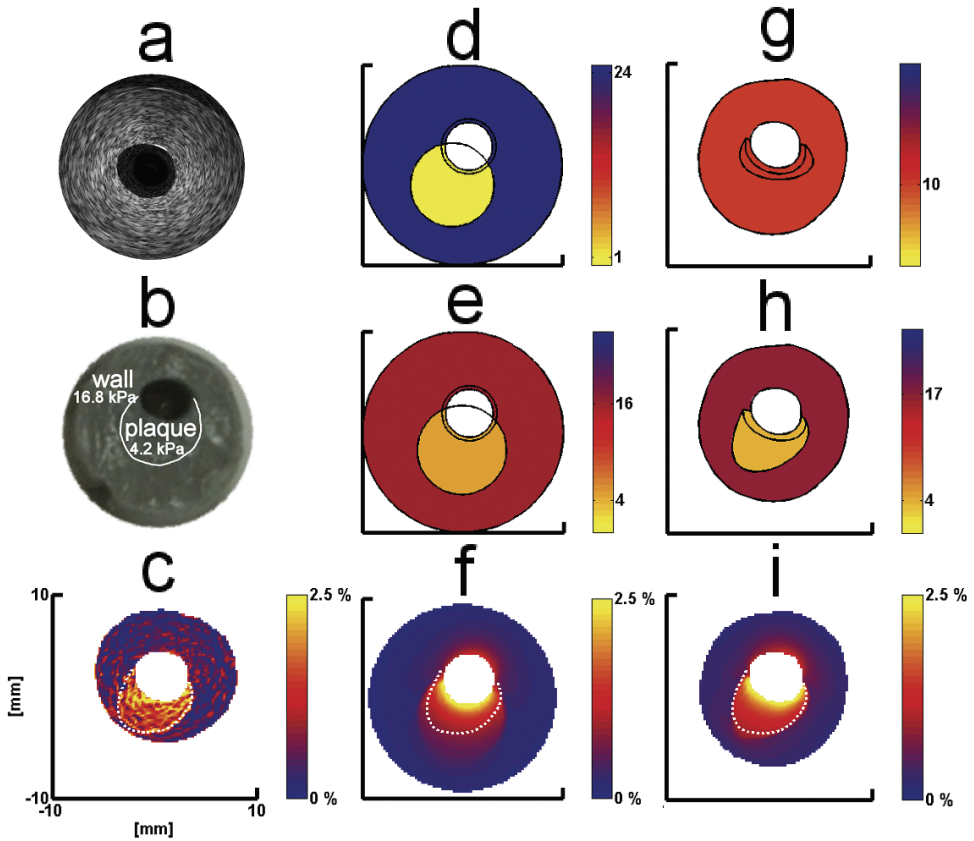


Fig. 3. Circular and Bézier parametric finite element model (PFEM) reconstruction using a measured strain elastogram of a vessel-mimicking phantom; it has a soft region embedded in a stiff wall. (a) Echogram. (b) Optical image of a cross-section of the phantom. (c) Measured strain elastogram. Circular PFEM reconstruction: (d) Initial state with $E_{LIPID}=10$, $E_{MEDIA}=10$ and $E_{CAP}=E_{LIPID}$ kPa. (e) Modulus elastogram reconstructed from (c). (f) PFEM strain elastogram computed using (e). Bézier model reconstruction: (g) Initial state. (h) Modulus elastogram reconstructed from (c). (i) PFEM strain elastogram computed using (h). Young's moduli are in kPa and intraluminal pressure difference is 1 mmHg. The range of each Young's modulus color-bar is [0-25] kPa.

region and corresponding reconstructed plaque component region. These features were the region overlap (RO), surface area (SA) and Young's modulus (YM) of the lipid and cap components and the minimal cap-thickness. The RO error between two regions A and B was defined as $100\% \cdot (1 - 2 \cdot [\text{area of their intersection}] / [\text{area of A} + \text{area of B}])$. The error in their YM, SA and minimal cap-thickness was quantified with the relative error (RE) measure. The RE of a quantity Q with reference value QA and reconstructed value QB was defined as $RE = 100\% \cdot \text{abs}([QB - QA] / [QA])$. The minimal cap-thickness was defined as the shortest distance between cap curve segment PQ and lumen border (Fig. 1). Finally, a qualitative judgement was performed by visually comparing both modulus elastograms as well as the similarity of structural strain patterns in corresponding strain elastograms.

RESULTS

RECONSTRUCTION OF A THIN-CAP FIBROATHEROMA

Typical regions of high and low strain

Figure 2a shows a simulated TCFA that was traced from arterial histology. The circumferential geometry and relatively high stiffness of the cap causes the arterial stress to concentrate on the cap, especially at its edges and around the corners of the lipid pool (Richardson et al. 1989); this redistribution mechanism causes the typical

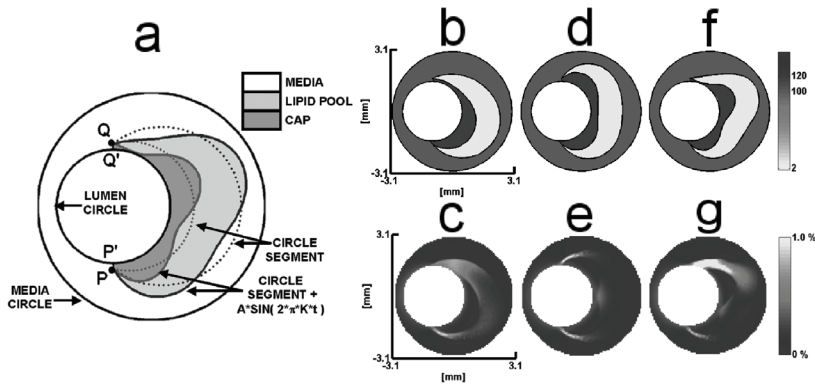


Fig. 4. Sine-modulated plaques. (a) Sine-modulated plaque model. K is the plaque border complexity, A is the sine-amplitude and t is the arclength. (b), (d) and (f) Modulus elastograms corresponding to the plaque model for $K=1, 1.5$ and 2 , respectively, and $A = 300 \mu\text{m}$. (c), (e) and (g) Simulated strain elastograms computed using (b), (d) and (f), respectively. Young's moduli are in kPa and intraluminal pressure difference is 1 mmHg . The range of the Young's modulus color-bar is $[0-150] \text{ kPa}$.

regions of high radial strain at the corners of the lipid pool in Fig. 2b and the relatively low strain at the center of the lipid pool (Loree et al. 1992).

The initial states (Figs. 2c, 2f) show that the Bézier PFEM has the same lumen and media border as the traced plaque (Fig. 2a), in contrast to the circular PFEM. The orders of magnitude of the Young's moduli values are successfully approximated with both models (Figs. 2d, 2g), but the Bézier PFEM (Fig. 2g) results in a more accurate delineation of the lipid pool and cap region. Furthermore, the strain elastogram (Fig. 2h) of the Bézier reconstruction has a better match with the input strain elastogram (Fig. 2b), which can be seen by comparing the high-strain pattern in both lipid pool corners.

The Bézier PFEM gives a better delineation and elastogram-match

RECONSTRUCTION OF A VESSEL-MIMICKING PHANTOM

Figure 3b shows the composition of the vessel-mimicking phantom, which has a soft region embedded in a stiff wall. The echogram (Fig. 3a) cannot be used to identify these two mechanically different regions. However, the measured strain elastogram (Fig. 3c) does reveal the presence of the soft region by means of the high-strain region. This region shows a typical radial strain decay that results from a decreasing stress; this natural stress decrease is due to the circumferential vessel geometry. Only a limited range of phantom material is contained in the elastogram, due to the limited imaging depth of the catheter (approximately 7.6 mm). The heterogeneous strain texture throughout the elastogram is caused by measurement noise and the gradient-based calculation of strain.

A typical strain decay and texture

The initial states (Figs. 3d, 3g) show that the Bézier PFEM has the same lumen border as is visible in the echogram (Fig. 3a), while the circular PFEM has a circle as lumen border. Furthermore, the media borders of both models differ in their size.

Same lumen and different media borders

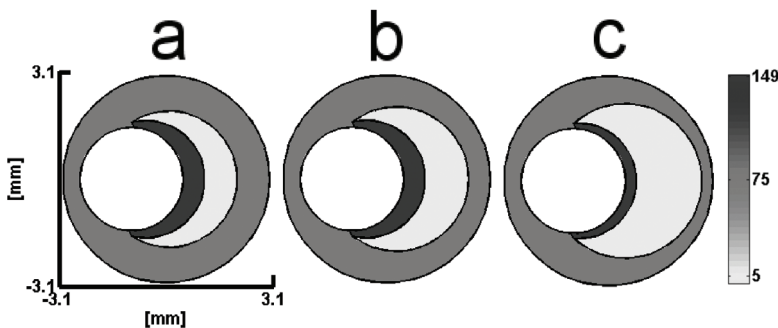


Fig. 5. Initial states used for reconstruction of the sine-modulated plaques with $E_{\text{LIPID}}=5$, $E_{\text{MEDIA}}=75$ and $E_{\text{CAP}}=149 \text{ kPa}$. All initial states have a relatively stiff cap overlaying a soft lipid pool. The range of the Young's modulus color-bar is $[0-150] \text{ kPa}$.

The Bézier PFEM gives a better delineation and elastogram-match

The two Young's moduli are successfully approximated with both models (Figs. 3e, 3h), but the Bézier PFEM (fig. 3H) results in a more accurate delineation of the shape and surface area of the soft plaque region. This is apparent when looking at the border of the high-strain pattern in Fig. 3i and noting that its curvature and its location better matches the input strain elastogram (Fig. 3c) than the border in Fig. 3f does.

VARYING THE PLAQUE BORDER COMPLEXITY AND THE NUMBER OF CONTROL POINTS

Table 1 shows the reconstruction errors as function of plaque border complexity K and the number of control points N ($N_{CAP}=N_{LIPID}=N$) used during reconstruction. The three strain elastograms that were used as reconstruction input are shown in Figs. 4c, 4e and 4g. Quantitative inspection of Table 1 shows the following:

- The use of the Bézier PFEM results in low reconstruction errors, in contrast to the use of the circular PFEM.
- The lowest reconstruction errors are obtained for $N=5$.
- The reconstruction errors are slightly increasing for $N>5$.
- Lower K give lower reconstruction errors, except for the minimal cap thickness and the Young's moduli.
- For all N , the Young's modulus error of the cap is less than 26 kPa and for the lipid pool 3 kPa.

Figure 6a shows a Bézier PFEM reconstruction ($N_{CAP}=N_{LIPID}=5$) of a sine-modulated plaque ($K=2$). Figure 6b shows the corresponding simulated strain elastogram, which has a complex heterogeneous strain pattern from which the shape and surface area of the cap and lipid pool cannot be deduced. Figures 6a and 6c show that the geometry and Young's modulus of the cap and lipid pool are successfully approximated by the reconstruction (Table 1, $N=5$ and $K=2$). Furthermore, there is a

Fig. 6. Bézier PFEM reconstruction from simulated strain elastogram of a sine-modulated plaque having plaque border complexity $K=2$. The reconstruction uses five control points for both the lipid and cap Bézier curve.

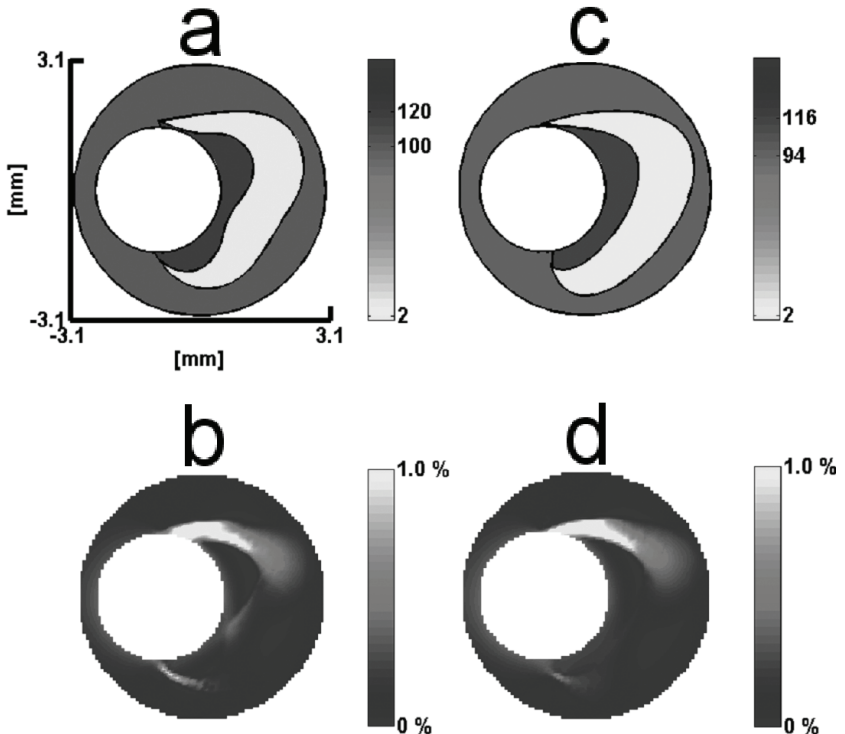
(a) Modulus elastogram of the plaque.

(b) Strain elastogram computed using (a).

(c) Modulus elastogram reconstructed from (b).

(d) PFEM strain elastogram computed using (c).

Young's moduli are in kPa and intraluminal pressure difference is 1 mmHg. The range of each Young's modulus color-bar is [0-150] kPa.



high resemblance between the PFEM strain elastogram that corresponds to this reconstruction (Fig. 6d) and the simulated strain elastogram (Fig. 6b).

TABLE 1: RECONSTRUCTION ERRORS AS FUNCTION OF PLAQUE-BORDER COMPLEXITY (K) AND THE NUMBER OF CONTROL POINTS (N)^A

	REGION OVERLAP ERROR(%)						SURFACE AREA ERROR(%)						THICKNESS ERROR (%)			YOUNG'S MODULUS ERROR (KPA) ^B					
	Cap			Lipid			Cap			Lipid			Cap			Cap		Lipid			
	K =	1	1.5	2	1	1.5	2	1	1.5	2	1	1.5	2	1	1.5	2	1	1.5	2		
Circ. model ^C	39	31	43	21	25	30	51	44	58	8	56	16	56	11	34	26	23	29	0	11	1
N=4	4	7	21	6	21	28	2	4	41	5	46	11	23	44	20	24	12	5	1	0	0
N=5	2	4	10	3	10	11	0	6	6	5	8	11	15	27	8	5	0	4	1	3	0
N=7	1	5	11	3	10	16	1	2	10	6	8	11	17	7	17	22	5	26	1	1	0
N=9	1	5	12	4	20	14	1	3	23	7	38	15	11	46	29	18	13	25	0	3	2

Errors are calculated from the Young's modulus elastograms.

^AN is the same for the lipid pool Bézier curve and the cap Bézier curve.

^BFor all plaques, the Young's modulus of the lipid pool was 2 kPa and that of the cap was 120 kPa.

^CThe circular PFEM was used instead of the Bézier PFEM.

DISCUSSION

This paper describes a new method, which uses deformable curves, for Young's modulus reconstruction of vulnerable atherosclerotic plaque components. The use of this Bézier parametric finite element model (PFEM) reconstruction method, in contrast to the circular PFEM reconstruction method, resulted in much better plaque components delineation, with very low reconstruction errors, even for complex plaque component borders.

The new method uses deformable curves

GENERAL OBSERVATIONS

For the results presented in this paper, it appeared that the lowest reconstruction errors were obtained when using N=5 control points for both the cap and lipid pool curve (i.e., $N_{CAP}=N_{LIPID}=N$); for other plaque geometries, higher N might give better reconstructions. Thus, in practice, one might start with a reconstruction that uses N=5. If, after reconstruction, the resulting strain elastogram does not sufficiently match the measured strain elastogram (e.g., in terms of the RMS error), N should be increased and the reconstruction repeated. However, it should be noted that $N>5$ does not necessarily give lower reconstruction errors than N=5, as Table 1 showed. This may indicate that an increase in N coincides with an increase in the number of nonoptimal local minima of the RMS-error function, to which a reconstruction might converge.

The lowest reconstruction errors were obtained when using 5 control points

In general, the Bézier reconstruction method appeared to be stable, although more parameters were used (e.g., 19 when $N_{CAP}=N_{LIPID}=5$) than with the circular PFEM (only nine), also when a real measured strain elastogram of a vessel-mimicking phantom was used (Fig. 3).

Stability

In any measured strain elastogram, the high/low radial strain regions that result from local border-eccentricities are directly accounted for by the Bézier PFEM, because it uses the actual lumen and media borders as extracted from ultrasound data, which is not the case for the circular PFEM.

Actual vessel-borders are used

The phantom reconstructions (Figs. 3e and 3h) demonstrate that the actual shape of the media border was not needed for obtaining a good reconstruction. This might be because the strain near the media border is very low, due to the natural stress decay caused by the circumferential vessel-wall geometry.

The actual shape of the media border was not needed

MODELLING ASPECTS

As a limitation, only relatively large homogeneous plaque regions have been studied. Furthermore, the thin-cap fibroatheroma (TCFA) was used as PFEM for a plaque, although other types of vulnerable plaques exist, such as eroded plaques or plaques containing calcified nodules. This was done because: (i) TCFA's are consid-

ered to be the precursor lesion of rupture and they account for the majority of plaque rupture (Virmani et al. 2002) and (ii) its use allows a more stable and unique reconstruction of TCFAs, as opposed to the situation where a geometrically nonconstrained FEM is used (Soualmi et al. 1997) to allow the reconstruction of a larger collection of plaques (heterogeneous plaques and plaques containing calcified nodules).

Although it is not known whether the sine-modulated plaque model produces realistic plaque geometries, for the purpose of this study, it is, nevertheless, a practical and systematic way to create noncircular plaque component borders.

Both reconstruction methods use a linearly elastic, isotropic, incompressible (Poisson's ratio=0.4999), plain-strain material deformation model for simulating arterial strain. Baldewsing et al. (2005b) have argued its appropriateness as well its importance for increasing the stability of the reconstruction process and the uniqueness of a reconstruction.

UNIQUENESS

This paper showed a superior behavior of the Bézier reconstruction method compared with the circular one. However, the Bézier reconstruction method does not always perfectly reconstruct the cap and lipid pool component, as illustrated in Fig. 2g by the fact that the lipid pool border between 7 and 9 o'clock is slightly too distal and the middle part of the cap region is slightly too big. This is not only because initial states are sometimes too far away from the real unknown plaque composition, but also because the inverse problem (Barbone et al. 2004) for TCFAs in itself is slightly nonunique, as was shown in Baldewsing et al. (2005a). Practically, the latter means that: (i) caps might be reconstructed as either slightly thinner and stiffer or slightly thicker and softer, while still having similar PFEM strain elastograms; and (ii) local regions where the principal strain is low (e.g., Fig. 2b between 7 and 9 o'clock) may give an incorrect reconstruction of a plaque component border (e.g., the lipid pool border in Fig. 2g between 7 and 9 o'clock).

INITIAL STATES

Number of initial states used

The use of more initial states increases the chance (i) for obtaining a Young's modulus reconstruction with a lower RMS error or (ii) for obtaining a successful Young's modulus reconstruction (a successful Young's modulus reconstruction has a strain elastogram with similar high and low strain regions as the measured strain elastogram), but it increases the total reconstruction time. For the sine-modulated plaques, only three initial states with a priori available plaque information (Fig. 5) were used, to reduce reconstruction time and still obtain successful reconstructions, as Table 1 shows.

Low inter-variability for successful reconstructions

The three reconstructions corresponding to the three initial states (Fig. 5) can sometimes differ, similarly as shown in Baldewsing et al. (2005b), but this not a restriction of the method. This is because the method itself takes from the three individual reconstructions the one that has a strain elastogram with the lowest RMS error. The fact that there is reconstruction variability is the main argument to use not just one initial state, but more. Finally, in Baldewsing et al. (2005b), it was shown that the variability between successful Young's modulus reconstructions is small; for the Bézier reconstruction method, this is also the case.

CLINICAL APPLICATIONS

A new way of intravascular tissue characterization

The Bézier PFEM reconstruction method is a new way of intravascular tissue characterization that may be used for clinical applications, such as (i) aiding clinicians in choosing appropriate interventional procedures and (ii) quantify the efficiency of pharmaceutical drugs aimed at stabilizing plaques, e.g., by stiffening (Aikawa et al. 1998, Loree et al. 1994) or reducing the lipid (Ambrose et al. 1988). Furthermore, this method only needs a strain elastogram of an object as input. Consequently, any imaging modality that allows the processing of strain elastograms can be used (Plewes et al. 2000, Rogowska et al. 2004). Finally, our reconstruction method may potentially also be applied in other clinically relevant situations where relatively softer/stiffer objects, such as plaques or tumors, are present in an approximately homogeneous medium that is deformed, e.g., superficial arteries, such as the carotid or femoral (Kim et al. 2004), or breast tumors (Liu et al. 2003, Wellman et al. 1999).

CONCLUSION

A new model-based Young's modulus reconstruction method is developed that uses deformable curves to delineate vulnerable atherosclerotic plaque components. As such, this method (i) may aid clinicians in monitoring atherosclerosis and choosing appropriate interventional procedures and (ii) may be used to quantify the efficiency of pharmaceutical drugs that aim at stabilizing plaques by stiffening or reducing the lipid.

ACKNOWLEDGEMENTS

This research was financially supported by the Dutch Technology Foundation (STW) project number RPG-5442 and the Netherlands Organization for Scientific Research (NWO). We also acknowledge Volcano Corporation, Inc., Rancho Cordova, CA, USA for their feedback.

REFERENCES

- Aikawa M, Rabkin E, Okada Y et al. *Lipid lowering by diet reduces matrix metalloproteinase activity and increases collagen content of rabbit atheroma: a potential mechanism of lesion stabilization*. Circulation 1998;97:2433-44.
- Ambrose JA, Tannenbaum MA, Alexopoulos D et al. *Angiographic progression of coronary artery disease and the development of myocardial infarction*. Journal of the American College of Cardiology 1988;12:56-62.
- Baldewsing RA, de Korte CL, Schaar JA, Mastik F, van der Steen AFW. *A finite element model for performing intravascular ultrasound elastography of human atherosclerotic coronary arteries*. Ultrasound Med Biol 2004a;30:803-13.
- Baldewsing RA, De Korte CL, Schaar JA, Mastik F, van der Steen AFW. *Finite element modeling and intravascular ultrasound elastography of vulnerable plaques: parameter variation*. Ultrasonics 2004b;42:723-9.
- Baldewsing RA, Mastik F, Schaar JA, Serruys PW, van der Steen AFW. *Robustness of reconstructing the Young's modulus distribution of vulnerable atherosclerotic plaques using a parametric plaque model*. Ultrasound Med Biol 2005a;31:1631-45.
- Baldewsing RA, Schaar JA, Mastik F, Oomens CWJ, van der Steen AFW. *Assessment of vulnerable plaque composition by matching the deformation of a parametric plaque model to measured plaque deformation*. IEEE Trans Med Imaging 2005b;24:514-28.
- Barbone PE, Gokhale NH. *Elastic modulus imaging: on the uniqueness and nonuniqueness of the elastography inverse problem in two dimensions*. Inverse Problems 2004;20:283-96.
- Brusseau E, Fromageau J, Finet G, Delachartre P, Vray D. *Axial strain imaging of intravascular data: results on polyvinyl alcohol cryogel phantoms and carotid artery*. Ultrasound Med Biol 2001;27:1631-42.
- Davies MJ. *The pathophysiology of acute coronary syndromes*. Heart 2000;83:361-6.
- Davies MJ. *Going from immutable to mutable atherosclerotic plaques*. Am J Cardiol 2001;88:2F-9F.
- de Korte CL, Céspedes EI, van der Steen AFW. *Influence of catheter position on estimated strain in intravascular elastography*. IEEE Trans Ultrason Ferroelectr Freq Control 1999;46:616-25.
- de Korte CL, Schaar JA, Mastik F, Serruys PW, van der Steen AFW. *Intravascular elastography: from bench to bedside*. J Interv Cardiol 2003;16:253-9.
- de Korte CL, Siervogel MJ, Mastik F et al. *Identification of atherosclerotic plaque components with intravascular ultrasound elastography in vivo: a Yucatan pig study*. Circulation 2002;105:1627-30.
- Dijkstra J, Koning G, Reiber JH. *Quantitative measurements in IVUS images*. Int J Card Imaging 1999;15:513-22.
- Falk E, Shah PK, Fuster V. *Coronary plaque disruption*. Circulation 1995;92:657-71.
- Farin G, *Curves and surfaces for computer aided geometric design. A practical guide.*, 3 ed. San Diego, CA: Academic Press, Inc., 1993.
- Glagov S, Weisenberg E, Zarins CK, Stankunavicius R, Kolettis GJ. *Compensatory enlargement of human atherosclerotic coronary arteries*. N Engl J Med 1987;316:1371-5.
- Kim K, Weitzel WF, Rubin JM et al. *Vascular intramural strain imaging using arterial pressure equalization*. Ultrasound Med Biol 2004;30:761-71.
- Klingensmith JD, Shekhar R, Vince DG. *Evaluation of three-dimensional segmentation algorithms for the identification of luminal and medial-adventitial borders in intravascular ultrasound images*. IEEE Trans Med Imaging 2000;19:996-1011.
- Liu HT, Sun LZ, Wang G, Vannier MW. *Analytic modeling of breast elastography*. Med Phys 2003;30:2340-9.
- Loree HM, Kamm RD, Stringfellow RG, Lee RT. *Effects of fibrous cap thickness on peak circumferential stress in model atherosclerotic vessels*. Circ Res 1992;71:850-8.
- Loree HM, Tobias BJ, Gibson LJ et al. *Mechanical properties of model atherosclerotic lesion lipid pools*. Arterioscler Thromb 1994;14:230-4.
- MacNeill BD, Lowe HC, Takano M, Fuster V, Jang IK. *Intravascular modalities for detection of vulnerable plaque: current status*. Arterioscler Thromb Vasc Biol 2003;23:1333-42.
- Maurice RL, Ohayon J, Finet G, Cloutier G. *Adapting the Lagrangian speckle model estimator for endovascular elastography: theory and validation with simulated radio-frequency data*. J Acoust Soc Am 2004;116:1276-86.

- Ophir J, Céspedes EI, Garra B et al. *Elastography: ultrasonic imaging of tissue strain and elastic modulus in vivo*. Eur J Ultrasound 1996;3:49-70.
- Perrey C, Bojara W, Holt S, Lindstaedt M, Ermert H. *Intravascular ultrasound strain imaging with rotating single element transducer: initial in vivo experiments*. Proceedings of the Second International Conference on the Ultrasonic Measurement and Imaging of Tissue Elasticity 2004;49-.
- Plewes DB, Bishop J, Samani A, Sciarretta J. *Visualization and quantification of breast cancer biomechanical properties with magnetic resonance elastography*. Phys Med Biol 2000;45:1591-610.
- Richardson PD, Davies MJ, Born GVR. *Influence of plaque configuration and stress distribution on fissuring of coronary atherosclerotic plaques*. The Lancet 1989;2:941-4.
- Rogowska J, Patel NA, Fujimoto JG, Brezinski ME. *Optical coherence tomographic elastography technique for measuring deformation and strain of atherosclerotic tissues*. Heart 2004;90:556-62.
- Saijo Y, Tanaka A, Owada N, Akino Y, Nitta S. *Tissue velocity imaging of coronary artery by rotating-type intravascular ultrasound*. Ultrasonics 2004;42:753-7.
- Schaar JA, De Korte CL, Mastik F et al. *Characterizing vulnerable plaque features with intravascular elastography*. Circulation 2003;108:2636-41.
- Schaar JA, Muller JE, Falk E et al. *Terminology for high-risk and vulnerable coronary artery plaques. Report of a meeting on the vulnerable plaque, June 17 and 18, 2003, Santorini, Greece*. Eur Heart J 2004;25:1077-82.
- Schoenhagen P, Nissen S. *Understanding coronary artery disease: tomographic imaging with intravascular ultrasound*. Heart 2002;88:91-6.
- Shi H, Varghese T, Chen Q, Gimelli G. *Correction for simultaneous catheter eccentricity and tilt in intravascular elastography*. Ultrason Imaging 2003;25:262-83.
- Virmani R, Burke AP, Farb A, Kolodgie FD. *Pathology of the unstable plaque*. Prog Cardiovasc Dis 2002;44:349-56.
- Virmani R, Burke AP, Kolodgie FD, Farb A. *Pathology of the thin-cap fibroatheroma: a type of vulnerable plaque*. J Interv Cardiol 2003;16:267-72.
- Virmani R, Kolodgie FD, Burke AP, Farb A, Schwartz SM. *Lessons from sudden coronary death: a comprehensive morphological classification scheme for atherosclerotic lesions*. Arterioscler Thromb Vasc Biol 2000;20:1262-75.
- von Birgelen C, Di Mario C, Li W et al. *Morphometric analysis in three-dimensional intracoronary ultrasound: an in vitro and in vivo study performed with a novel system for the contour detection of lumen and plaque*. Am Heart J 1996;132:516-27.
- Wellman PS, Howe RD. *Extracting features from tactile maps*. MICCAI 1999;1133-42.

AN INVERSE METHOD FOR IMAGING THE LOCAL ELASTICITY OF ATHEROSCLEROTIC CORONARY PLAQUES

ABSTRACT

BACKGROUND

Intravascular ultrasound (IVUS) strain elastography is a clinically validated medical imaging modality that detects rupture-prone coronary plaques and provides mechanical information related to their rupture-proneness. It accomplishes this by measuring their cross-sectional radial strain distribution (i.e., elastogram) using an intravascular ultrasound catheter. Due to the unknown heterogeneous stress distribution, an elastogram cannot be interpreted as a material composition image. To overcome this limitation, we developed a fully automatic, inverse method that reconstructs the heterogeneous elasticity (i.e., Young's modulus) distribution of an arbitrary heterogeneous plaque from its measured elastogram.

METHODS

The method was evaluated and its optimal settings were determined by applying it to finite element simulated elastograms of four realistic histology-traced human coronary plaques, two resembled a thin-cap fibroatheroma, i.e., a plaque with a soft lipid pool covered by a thin fibrous cap, the other plaques had multiple regions of soft and stiff tissue. The relative error in reconstructed soft tissue area (STA) and soft tissue overlap (STO) were used as performance metrics. Finally, it was applied to two elastograms, one measured in vitro and the other in vivo, from two human atherosclerotic coronary arteries.

RESULTS

The method approximated the true Young's modulus distribution of all simulated plaques; the mean[%(std[%])] error in STA=27(21) and in STO=41(16), irrespective of the catheter position in the artery; a centred catheter gave the best results with STA=18(11) and STO=35(12). The in vitro reconstruction was in agreement with histology.

CONCLUSION

IVUS strain elastography in combination with our inverse method has potential to become an all-in-one modality for detecting plaques, for assessing information related to their rupture-proneness and for imaging their elastic material composition.

THIS CHAPTER IS BASED ON THE MANUSCRIPT

"An Inverse Method for Imaging the Local Elasticity of Atherosclerotic Coronary Plaques",

BY BALDEWSING RA, MASTIK F, SCHAAR JA, SERRUYS PW AND VAN DER STEEN AFW,

MANUSCRIPT HAS BEEN SUBMITTED,

Copyright © 2006 Radjkumarsing Anand Baldewsing.

INTRODUCTION

Rupture, with subsequent thrombosis, of thin-cap fibroatheromas (TCFAs) is a major cause of acute coronary syndromes (Davies 2000, Falk et al. 1995). A TCFA has two main arterial plaque components, namely a large, soft lipid core and an inflamed, thin, fibrous cap that shields the thrombogenic core from the blood (Schaar et al. 2004a). The major mechanical and morphological determinants for plaque-rupture are considered to be the plaque-components' material properties and geometry, as well as, cap-weakening caused by macrophage-inflammation (Davies 2001). The majority of vulnerable plaques resemble a TCFA and the remainder has a more complex heterogeneous material composition (Virmani et al. 2000).

Clinical techniques are needed to detect these plaques and to assess their rupture determinants (MacNeill et al. 2003). This is not only necessary to elucidate the mechanisms involved in plaque development (Zohdi et al. 2004) or to give a better measure of rupture-proneness (Yang et al. 2005), but also to aid clinicians in choosing optimal interventional strategies and to be able to quantify the efficiency of pharmaceutical treatments that aim at stabilizing plaques, e.g., by stiffening or reducing the lipid (Aikawa et al. 1998, Brown et al. 1993, Loree et al. 1994, Van Mieghem et al. 2005).

Intravascular ultrasound (IVUS) strain elastography is a clinically available, validated technique that reveals mechanical plaque information by measuring local arterial radial strain and visualizing it in a so-called IVUS strain elastogram (de Korte et al. 2003). This strain is related to aforementioned rupture-determinants (Schaar et al. 2003). It is determined from time-shifts obtained by cross-correlation processing on pairs of IVUS radiofrequency gated signals, each measured using an IVUS catheter at a different level of intracoronary pressure (de Korte et al. 1998). Strain, in itself, is a clinically and diagnostically relevant quantity (de Korte et al. 2002c, Schaar et al. 2004b). However, an IVUS strain elastogram cannot be directly interpreted as a plaque material composition image due to the unknown heterogeneous arterial stress distribution and inherent strain interpretation artefacts (Baldeuswing et al. 2004b, de Korte et al. 1996, 1999, Ophir et al. 1996, Shi et al. 2005).

To overcome this limitation, we have previously developed an automatic model-based Young's modulus reconstruction framework that obtains a material composition image of a plaque by reconstructing a modulogram (i.e., Young's modulus image) from a measured IVUS strain elastogram (Baldeuswing et al. 2005b; 2006). Reconstruction was done by an optimization algorithm that matches the strain image output of Parametric Finite Element Model (PFEM) representation of a TCFA, to the measured strain elastogram by iteratively updating the PFEM morphology and Young's moduli parameters. The reconstructed modulogram shows the Young's modulus value and morphology of a cap, lipid pool and surrounding media region. However, since this framework uses a TCFA-PFEM it has as practical limitation that is only works well for plaques that resemble a TCFA.

To eliminate this restriction, we describe in this chapter an inverse method that can automatically reconstruct the heterogeneous Young's modulus (YM) distribution of an arbitrary heterogeneous plaque from its radial strain. This radial strain may be measured with an IVUS catheter at any position within the vessel. This method is an extension of the previous framework to which the following adaptations were

Acute coronary syndromes and plaque-rupture determinants

Why clinical techniques are needed

IVUS elastograms cannot be directly interpreted as plaque component images

Limitation of previous Young's modulus reconstruction method

An inverse method suited for arbitrary plaques

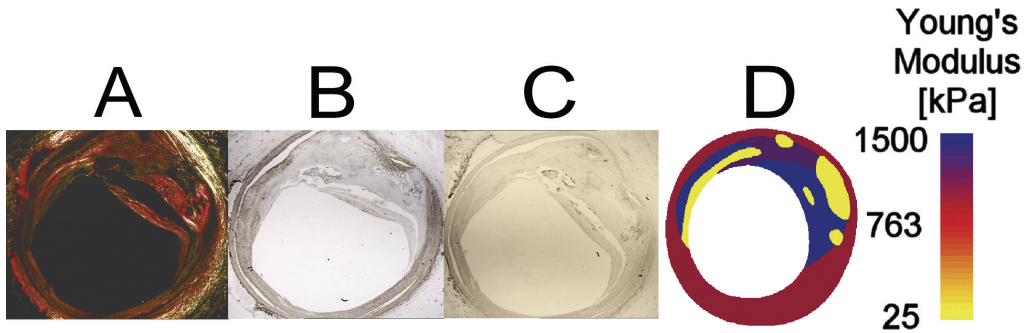


Fig. 1. Histology and corresponding traced Young's modulus distribution of a human atherosclerotic coronary artery with an eccentric, heterogeneous plaque between 9 and 4 o'clock. Histology: (a) Collagen, (b) Smooth muscle cells and (c) Macrophages. (d) Young's modulus distribution traced from the histology.

made: (i) Use of a "corrected" radial strain elastogram in order to make our method less sensitive upon the position of the catheter, (ii) use of the measured "corrected" radial strain elastogram to automatically define initial YM distributions and (iii) use of a compounding approach to obtain a heterogeneous YM distribution from individual YM reconstructions.

Aims of this study

First, we describe the new inverse method. Then, we apply it to finite element simulated strain elastograms of four realistic, histology-traced plaques (2 TCFAs and 2 heterogeneous ones), imaged at various catheter positions. Next, these plaques were used to determine the optimal method-settings. Finally, the method was applied to two measured strain elastograms, one measured in vitro and the other in vivo, from two human atherosclerotic coronary arteries.

MATERIALS AND METHODS

HISTOLOGY-TRACED MODULOGRAMS OF ATHEROSCLEROTIC ARTERIES

Four modulograms (e.g., Fig. 1D) were defined from the histology (e.g., Fig 1a-c) of four excised atherosclerotic human coronary arteries, as follows. Collagen (COLL), smooth muscle cells (SMC) and macrophages ($M\Phi$) were delineated from their histology picture; lipid (LIP) was defined as a region without COLL and SMC. Next, the delineations were combined into a geometry picture. Finally, each region in this picture was assigned a Young's modulus value according to its constituents: COLL=1500, SMC=1000, LIP=50, COLL+SMC=1250, COLL+(LIP or $M\Phi$) =750, SMC+(LIP or $M\Phi$)=500, LIP+ $M\Phi$ =25 kPa (Baldewsing et al. 2004a).

SIMULATING AND CORRECTING RADIAL STRAIN ELASTOGRAMS

Radial strain

The infinitesimal strain tensor was calculated with the commercially available finite element package SEPRAN (Septra Analysis, Technical University Delft, The Netherlands); the infinitesimal radial strain component (ϵ_{radial}) was, subsequently, computed using the centre of the catheter as origin. Arterial tissue was modelled as a linearly elastic, isotropic, incompressible (Poisson's ratio=0.4999) material in a 2D plane strain state. This is an appropriate model for small, quasi-static, arterial deformation (Baldewsing et al. 2004a). A pressure differential of 20 mmHg was applied to the lumen (i.e., inner boundary of the artery).

Corrected strain

Different positions of catheter in the lumen will give different radial strain elastograms, according to the formula $\epsilon_{\text{radial}} = \epsilon_{\text{prin}} \cdot \cos(2\alpha)$, derived in (Baldewsing et al. 2005a), where ϵ_{prin} is the principal compressive strain and α is the angle between (i) the direction of the principal axis of ϵ_{prin} and (ii) the line between catheter centre and tissue point (i.e., the line that defines the radial direction). The dependence of ϵ_{radial} upon catheter position can be reduced by considering

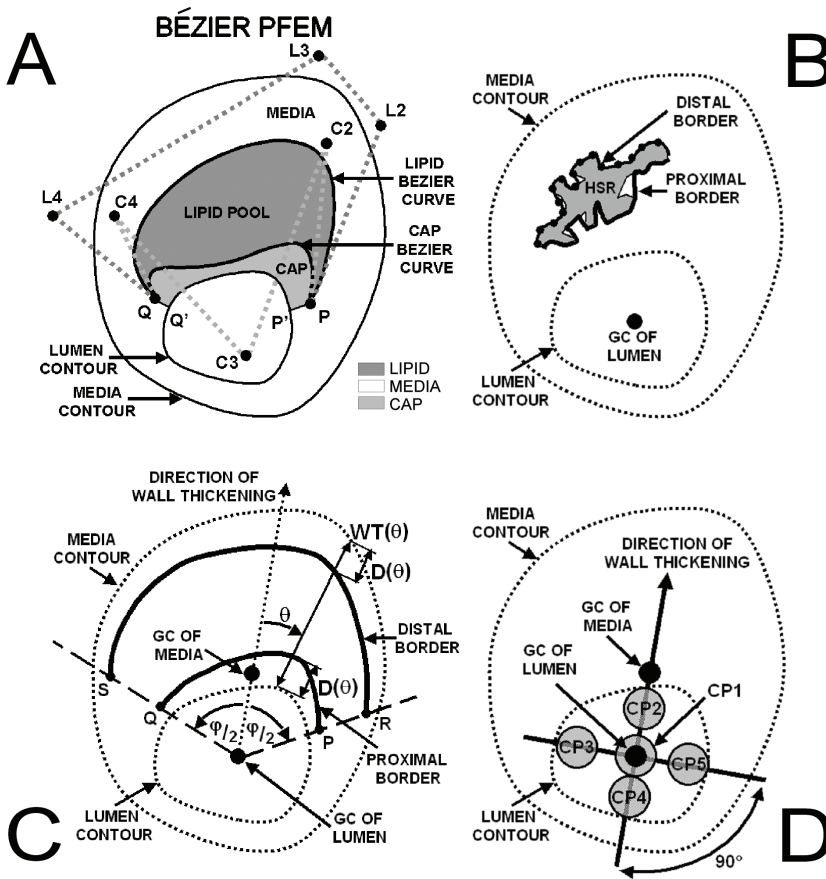


Fig. 2.

(a) Bezier Parametric Finite Element Model (PFEM) for a Vulnerable Plaque. The shape of the lipid and cap Bezier curves are determined by the spatial locations of their control points. In this example there are 5 control points used for the lipid, namely P, L2, L3, L4 and Q, and also 5 for the cap, namely P, C2, C3, C4 and Q.

(b) Definition of the proximal and distal border, from a high-strain region (HSR), for the creation of a local initial state.

(c) Definition of the proximal and distal border for the creation of a global initial state.

(d) Definition of simulated catheter positions; the bright circles indicate the tip of the catheter with diameter=1.1 mm.

$\varepsilon_{\text{prin}}$ instead of $\varepsilon_{\text{radial}}$. In theory, $\varepsilon_{\text{prin}}$ can be approximated from $\varepsilon_{\text{radial}}$ using aforementioned formula. However, in practice, α is unknown since the principal axis direction is unknown. As a practical estimate for this unknown direction, we take the line between the geometric centre (GC) of the lumen and tissue point. This is because, a principle axis is mainly directed perpendicular to the lumen boundary, especially where the arterial tissue is homogeneous (Baldewsing et al. 2005a, de Korte et al. 1999). Thus, the correction becomes $\varepsilon_{\text{COR}} = |\varepsilon_{\text{radial}} / \cos(2\beta)|$, where β is the angle between (i) the line from the GC of the lumen towards tissue point and (ii) the line between catheter centre and tissue point. Wherever $\beta \neq 45^\circ$ this correction is applied and makes ε_{COR} the best available approximation for $\varepsilon_{\text{prin}}$; moreover, when β equals α , $\varepsilon_{\text{COR}} = \varepsilon_{\text{prin}}$. Since $\varepsilon_{\text{prin}}$ is positive, the absolute operator, $|\cdot|$, is used to ensure that ε_{COR} is also positive.

THE INVERSE METHOD

Our inverse method is an extension of a previous Young's modulus reconstruction framework (Baldewsing et al. 2005b; 2006) that was mainly suited for reconstruction of thin-cap fibroatheromas. First, we briefly describe this framework, then, each extension is detailed.

An individual Young's modulus reconstruction was fully automatic obtained from a measured strain elastogram, as follows: A nonlinear, constrained optimization algorithm (procedure `fmincon`, Optimization Toolbox, MATLAB, release 12.1, the MathWorks, Inc., Natick, MA, USA) iteratively adjusted the initial morphology and Young's modulus parameters of a PFEM (Fig. 2a), to minimize the difference, i.e., the root mean squared (RMS) error, between the PFEM simulated strain elastogram

Existing Young's modulus reconstruction framework

Fig. 3. Creation of initial states and corresponding individual Young's modulus reconstructions.

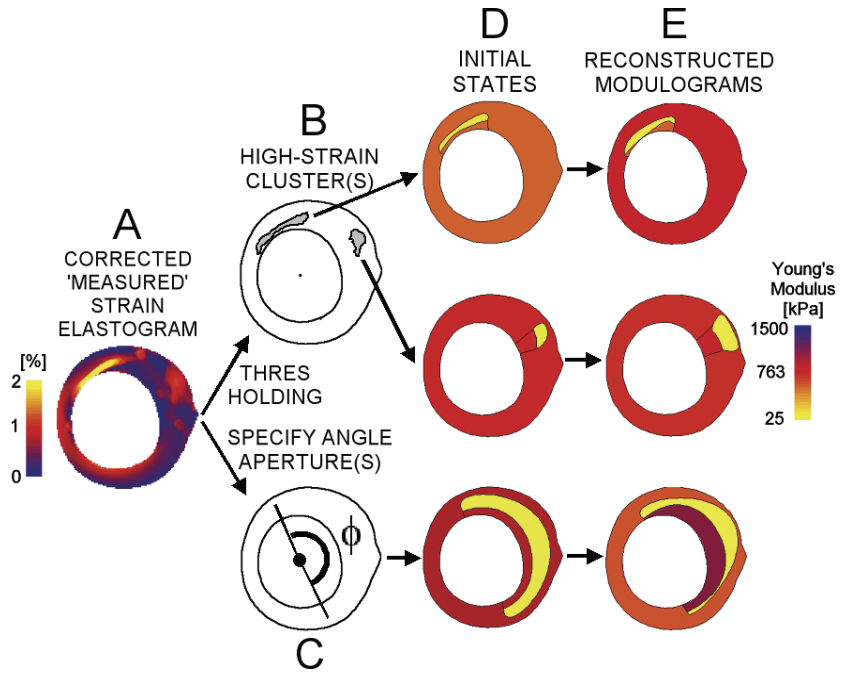
(a) Measured corrected strain elastogram.

(b) Creation of high strain regions (HSR) by thresholding (a); each HSR gives rise to a local initial state, shown in (d).

(c) Specifying angle aperture(s) ϕ ; each ϕ gives rise to a global initial state, as shown in (d).

(d) Local and global initial states created from (b) and (c), respectively.

(e) Individual reconstructed modulograms.



and the measured strain elastogram. The algorithm was stopped after 20 iterations. The resulting PFEM defined the reconstructed modulogram. A detailed mathematical description of the minimization algorithm can be found in the Optimization Toolbox of MATLAB.

Modelling of the PFEM

The PFEM was modelled as an idealized TCFA (Virmani et al. 2003) (Fig. 2a). The distal border of its cap region (PQ) and of its lipid pool region were defined as Bézier curves. The shape of a Bézier curve is determined by specifying the spatial locations of an ordered list of control points. This paper uses five control points for both curves, since it was shown in (Baldewsing et al. 2006) that this is an optimal value for Young's modulus reconstruction and delineation of plaque components. The PFEM was modelled as a linearly elastic, isotropic, incompressible (Poisson's ratio 0.4999), plane strain material. The cap, lipid, and media plaque component were each assumed homogeneous and their Young's modulus value was denoted as E_{CAP} , E_{LIPID} , and E_{MEDIA} , respectively. Straightforward linear and nonlinear constraints were enforced upon the PFEM parameters during reconstruction to ensure that the TCFA topology was preserved and could be properly filled with finite elements.

FULLY AUTOMATIC CREATION OF INITIALS STATES

The closer an IS is chosen to the true Young's modulus distribution, the better the reconstruction

An initial state (IS), i.e., initial values for the PFEM parameters, has to be defined at the start of each individual Young's modulus reconstruction. Since we use a gradient-based optimization algorithm, it follows that, the closer an IS is chosen to the true Young's modulus distribution, the higher the chance for the resulting Young's modulus reconstruction to correctly resemble (a part of) that distribution. A plaque often resembles a TCFA (e.g., Fig. 2a) or has a heterogeneous composition (e.g., Fig. 1d). Consequently, for each corrected measured strain elastogram, we define two types of IS, namely a local IS (LIS) (Fig. 3a,b) and a global IS (GIS) (Fig. 3a,c). A GIS is created so that it resembles a TCFA. A LIS is created so that it resembles a (small) localized region of soft tissue. The reason for defining an LIS in this manner is that, heterogeneous plaques are likely to contain multiple localized regions of soft tissue, which partly appear in a strain elastogram as an identifiable localized region of high strain.

Creation of local initial states

LISs were fully automatic created, as follows (Fig. 3b,d). First, localized regions of high strain (HSRs) were identified from the corrected strain elastogram. To this end,

all strain points with a strain larger than some strain-threshold value (ϵ_{thresh}) were identified and uniquely divided into disjoint regions using a clustering-distance of 300 micrometer. For each HSR an LIS was defined (Fig. 3d) by positioning the PFEM lipid Bézier curve tightly distal from it and the PFEM cap Bézier curve tightly proximal from it. This positioning was done by a nonlinear, least-squares optimization algorithm (procedure lsqnonlin, Optimization Toolbox, MATLAB) that minimized the least-square distance error between the distal/proximal HSR edge and the lipid/cap Bézier curve (Fig. 2b). The distal/proximal HSR edge was defined as those HSR points that lay the farthest/closest from/to the geometric centre of the lumen, as illustrated in Fig. 2b.

Finally, the initial E_{CAP} , E_{LIPID} and E_{MEDIA} of the PFEM components were defined using the following formula, which is valid for an linearly elastic, isotropic, incompressible, homogeneous, axisymmetric tube (Timoshenko et al. 1970). *Assigning initial Young's moduli*

$$E = \frac{3a^2b^2}{2(b^2 - a^2)R^2e} P$$

where E =initial Young's modulus of the considered plaque component region (either the cap or the lipid pool), e = the average corrected strain inside this region, R =the distance from the geometric centre (GC) of the lumen (GC_{LUMEN}) to the GC of the region (GC_{REGION}). a is the distance between GC_{LUMEN} and the point on the lumen that intersects the line between GC_{LUMEN} and GC_{REGION} ; b is defined similarly using the media instead of the lumen. P is the pressure applied to the lumen. When using this formula for defining the initial E_{LIPID} , the following lower value for P was used to partly compensate/correct for the natural stress decay.

$$\left(1 - \frac{b^2}{(b^2 - a^2)} \frac{r^2 - a^2}{r^2}\right) P$$

This stress decay formula is also exactly valid for the aforementioned tube. The initial value of E_{MEDIA} was set to E_{CAP} .

GISs, resembling a TCFA, were fully automatic created, as follows (Fig. 3c,d). First, the direction of wall thickening was determined as the line from GC_{LUMEN} to geometric centre of the media (Fig. 2c). Next, the angular aperture ϕ of the PFEM lipid pool was set symmetrically around the wall thickening direction. Then, a proximal/distal border was defined, away from the lumen/media contour, at an angle-dependent (θ) distance $D(\theta)$; $D(\theta) = 20\%$ of the wall thickness at angle θ , $WT(\theta)$, as shown in Fig. 2c. Line segments SQ and RP were added to the distal border. Finally, the cap/lipid Bézier curve were placed close to the distal/proximal borders, as was described for the LIS. The initial E_{CAP} , E_{LIPID} and E_{MEDIA} were also defined as was done for a local initial states creation. *Creation of global initial states*

COMPOUNDING PROCEDURE

The final compounded modulogram (CM) was defined as a normalized weighted sum of the k individual reconstructed modulograms (Fig. 3e), M_i $i=1..k$, that resulted from a set of k local and global initial states (Fig. 3d), namely as (Fig. 4):

$$CM = \frac{\sum_{i=1}^k (M_i \otimes W_i)}{\sum_{i=1}^k W_i}$$

where ' \otimes ', ' Σ ' and ' $-$ ' are pixelwise multiplication, summation and division, respectively. The weight elastograms (W_i) were defined, as follows. For each M_i , the corresponding corrected strain elastogram (C_i) was computed (Fig. 4b). Then, the strain-error elastogram (SE_i) (Fig. 4c) was computed as $SE_i = \text{abs}(C_i - C_{\text{INPUT}})$, where

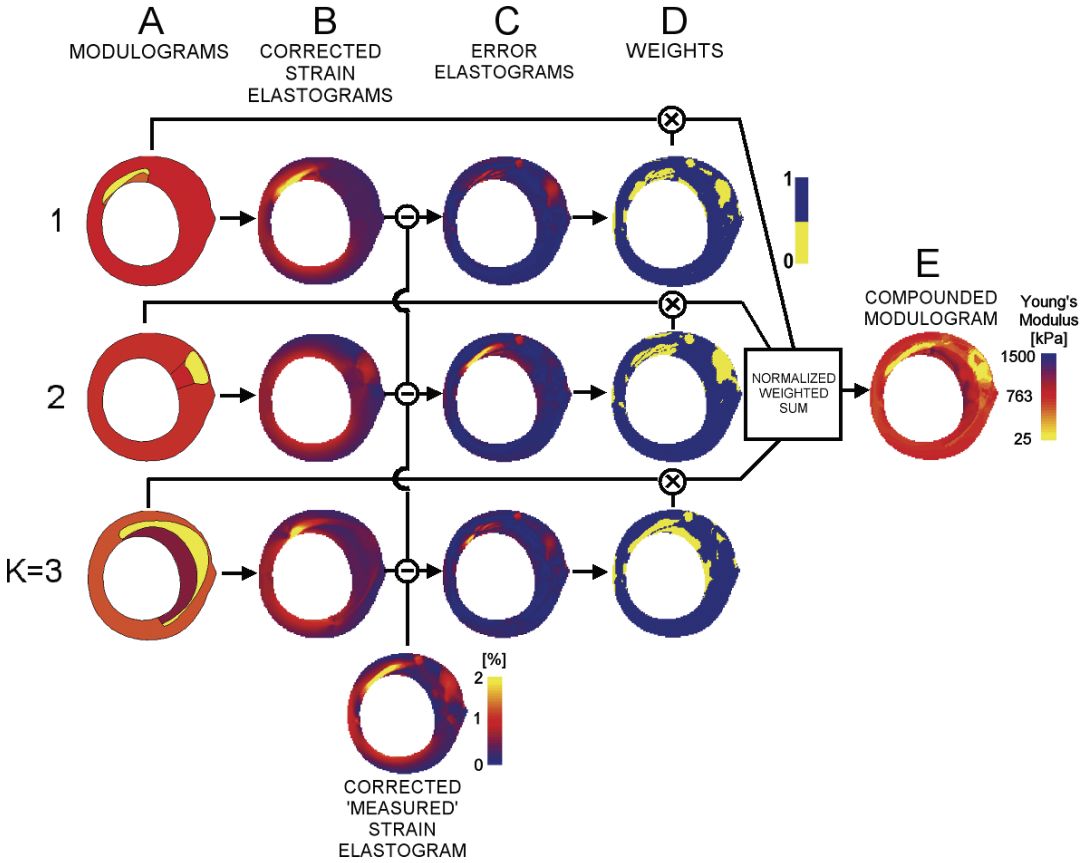


Fig. 4. Creation of the final compounded heterogeneous modulogram from k individual modulograms. (a) Individual reconstructed modulograms. (b) Corrected strain elastograms corresponding to (a). (c) Error elastograms between (b) and the corrected measured strain elastogram shown at the bottom. (d) Weights defined by thresholding (c). (e) The final compounded heterogeneous modulogram.

C_{INPUT} is the corrected "measured" strain elastogram. Finally, W_i was defined by thresholding SE_i , i.e., for each tissue point (x,y) (Fig. 4d):

$$W_i(x, y) = \begin{cases} 1 & \text{if } SE_i(x, y) \leq \epsilon_{\text{error}} \\ 0 & \text{else} \end{cases}$$

By defining W_i in this manner, the parts in M_i that are likely to resemble the true modulus distribution are compounded. According to the formula, the value of CM becomes undefined, when $W_i(x,y)=0 \forall i \in [1,k]$ at some tissue point location (x,y) . To resolve this, $CM(x,y)$ is assigned the Young's modulus value $M_j(x,y)$, where $j \in [1,k]$ is chosen such that C_j has the lowest RMS error with C_{INPUT} .

VARIATION OF METHOD INPUT AND METHOD SETTINGS

To investigate the performance of our inverse method and to find its optimal settings, we performed reconstructions for different inputs, namely 4 plaques (2 TCFA and 2 heterogeneous ones) that were imaged at 5 different catheter positions, CP_i $i=1..5$, (Fig. 2d). Furthermore, the following method settings were varied: the strain-threshold value (ϵ_{thres}), the strain-error threshold value (ϵ_{error}), the angle aperture ϕ of the PFEM lipid pool and the number of global initial states (N_{GI}). Tables 1-4 show the investigated combinations of inputs and settings, as well as, the resulting mean(std) values for the reconstruction performance measures (these measures are described in the next paragraph).

RECONSTRUCTION PERFORMANCE METRICS

For each considered variation of method input and settings, the reconstructed compounded modulogram was quantitatively compared with the corresponding true modulus elastogram. As performance measures, the relative error in the reconstructed soft tissue area (STA) and soft tissue overlap (STO) were used. Soft tissue was defined as all points in a modulogram with a Young's modulus ≤ 400 kPa. The relative error in STA and STO between the reconstructed soft tissue distribution A and true soft tissue distribution B was, respectively, defined as

$$\text{STA} = \left| \frac{\text{area}(A) - \text{area}(B)}{\text{area}(B)} \right| \times 100\% , \text{STO} = \left(1 - \frac{2 \times \text{area}(A \cap B)}{\text{area}(A) + \text{area}(B)} \right) \times 100\%$$

Finally, a qualitative judgment was performed by visually comparing both modulus elastograms.

IN VITRO AND IN VIVO APPLICATION

The method was applied to two strain elastograms, one measured *in vitro* and the other *in vivo*, from two human atherosclerotic coronary arteries. Their strain elastograms were processed from the measured IVUS radio-frequency data, as detailed in (Baldewsing et al. 2005b).

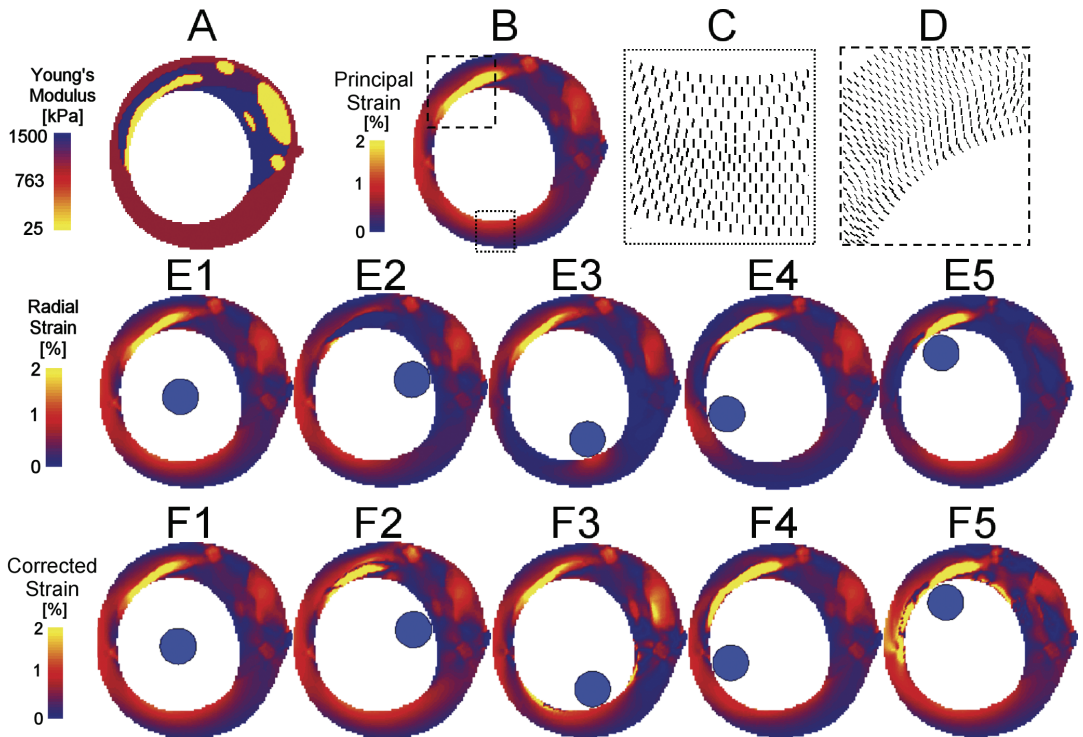


Fig. 5. FEM simulated radial, corrected and principal strain (value and direction) elastograms for different catheter positions within a human atherosclerotic coronary artery with an eccentric, heterogeneous plaque between 9 and 4 o'clock. (a) Young's modulus distribution of the artery. (b) Principal compressive strain value elastogram computed from (a). (c) and (d) Enlargement of the principal compressive strain directions for the regions indicated in (b). (e1-e5) Radial strain elastograms computed from (a). (f1-f5) Corrected strain elastograms corresponding to (e1-e5), respectively. The applied pressure differential was 20 mmHg. The blue circles indicate the tip of the catheter with diameter=1.1 mm.

RESULTS

SIMULATING AND CORRECTING RADIAL STRAIN ELASTOGRAMS

Figure 5 illustrates (i) the dependence of the radial strain (ϵ_{radial}) upon the position of the catheter within the lumen, (ii) the relation between ϵ_{radial} and the principal strain (ϵ_{prin}) and (iii) the difference and similarities between various corrected strain (ϵ_{cor}) elastograms.

Figures 5e1-e5 shows that the radial strain elastograms differ from each other and from the principal strain elastogram (Fig. 5b). These differences are in agreement with the relationship $\epsilon_{\text{radial}} = \epsilon_{\text{prin}} \cdot \cos(2\alpha)$. For example, in Fig. 5e1 the radial strain between 4-8 o'clock is the same near the lumen border, since $\alpha \approx 0^\circ$. In contrast, in Fig. 5e3 the strain profile is low-high-low, since $\alpha \approx 45^\circ, 0^\circ, 45^\circ$, respectively.

Figures 5e2 and 5e5 show a zero (in fact it is negative, but only positive strain is shown) strain region between 10-11 o'clock near the lumen border, while in Figs. 5e1, 5e3 and 5e4 they are high; this is explained by the fact that the principle strain directions, at that region, are mostly directed to the left of the geometric centre of the lumen, as shown in Fig. 5d.

Figures 5f1-f5 show that the corrected strain elastograms are similar to each other and also to the principal strain elastogram. For example, the cross-shaped strain pattern at 3-4 o'clock is always apparent, as well as the high strain region between 10-12 o'clock. Within the latter region, there are also clear differences. For example, in Figs. 5f4 and 5f5 the high strain region between 10-12 o'clock is more elongated than in Figs. 5f1-f3. This difference agrees with the relationship $\epsilon_{\text{cor}} = |\epsilon_{\text{radial}} / \cos(2\beta)|$, since $\beta \approx 45^\circ$ between 10-11 o'clock, in Figs. 5f4 and 5f5.

SIMULATED-PLAQUE RECONSTRUCTIONS

Figure 6 shows that all four simulated plaques are well reconstructed; most soft tissue is correctly reconstructed. There are some local deviations. For example, some very stiff regions are reconstructed as moderately stiff, e.g., the cap region in Fig. 6a, the stiff region in Fig. 6c between 9-12 o'clock laying behind the soft region and the two stiff regions in Fig. 6d between 4-5 o'clock and 6-8 o'clock.

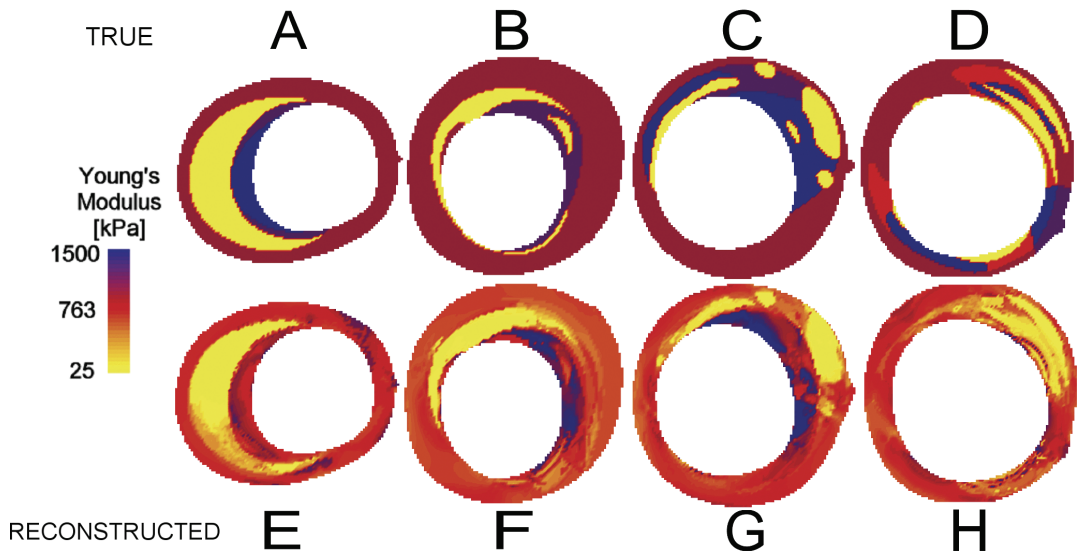


Fig. 6. Compounding results for four simulated plaques. (a-d) True modulograms. (e-h) Reconstructed final compounded modulograms corresponding to (a-d), respectively.

VARIATION OF METHOD INPUT AND SETTINGS

Quantitative inspection of the mean reconstructed STA and STO errors for the four simulated plaques, as function of catheter position (CP_i) (Table 1) and the strain threshold level ($\varepsilon_{\text{thres}}$) (Table 2), resulted in the following observations:

-Both the TCFAs and heterogeneous plaques are well reconstructed: the mean[%](std[%]) error in STA=27(21) and in STO=41(16), irrespective of the catheter position in the artery. A centred catheter, CP_1 , gave the best results, with STA=18(11) and STO=35(12). A catheter positioned towards the plaque, CP_2 , gave the worst results, with STA=42(24) and STO=53(9).

-A strain threshold $\varepsilon_{\text{thres}}=0.9\%$ seems optimal.

Quantitative inspection of the mean reconstructed STA and STO errors for the four simulated plaques, as function of the # of global initializations (N_{GI}) and angle apertures (φ) (Table 3) and strain-error threshold ($\varepsilon_{\text{error}}$) (Table 4), resulted in the following observations:

-An angle aperture $\varphi=180^\circ$, used for creating a GIS, seems optimal; if more GIS are created using other φ ($=135^\circ$ or 225°), better results are obtained. However, the difference between using two or three GIS is small, thus, an $N_{\text{GI}}=2$ seems optimal (less N_{GI} means less reconstructions).

-A strain-error threshold $\varepsilon_{\text{error}}=0.2\%$ seems optimal.

TABLE 1:
MEAN(STD) SOFT TISSUE AREA (STA) ERROR[%] AND SOFT TISSUE OVERLAP (STO) ERROR[%] AS FUNCTION OF CATHETER POSITION (CP_i)

	STA	STO
CP_1	18 (11)	35 (12)
CP_2	42 (24)	53 (9)
CP_3	17 (21)	31 (16)
CP_4	22 (10)	34 (12)
CP_5	35 (26)	54 (14)
Overall mean(std)	27 (21)	41 (16)

Mean(std) was calculated from the reconstruction results obtained with all four simulated plaques and using the strain-threshold levels $\varepsilon_{\text{thres}}=0.7, 0.9$ and 1.2% . Three global initial states were used (with angle apertures $\varphi=225^\circ, 180^\circ$ and 135°) and $\varepsilon_{\text{error}}=0.2\%$.

TABLE 2:
MEAN(STD) SOFT TISSUE AREA (STA) ERROR[%] AND SOFT TISSUE OVERLAP (STO) ERROR[%] AS FUNCTION OF STRAIN-THRESHOLD LEVEL ($\varepsilon_{\text{thres}}$)

$\varepsilon_{\text{thres}}(\%)$	STA	STO
0.7	25 (23)	41 (16)
0.9	25 (20)	41 (16)
1.2	32 (22)	43 (16)

Mean(std) was calculated from the reconstruction results obtained using all four simulated plaques and all five simulated catheter positions. Three global initial states were used (with angle apertures $\varphi=225^\circ, 180^\circ$ and 135°) and $\varepsilon_{\text{error}}=0.2\%$.

TABLE 3:
MEAN(STD) SOFT TISSUE AREA (STA) ERROR[%] AND SOFT TISSUE OVERLAP (STO) ERROR[%] AS FUNCTION OF THE # OF GLOBAL INITIALIZATIONS (N_{GI}) AND THE USED ANGLE APERTURES (φ)

N_{GI}	φ	STA	STO
1	135	28 (18)	41 (10)
1	180	26 (17)	42 (10)
1	225	34 (14)	43 (9)
2	135, 180	18 (13)	36 (14)
2	135, 225	30 (17)	39 (14)
2	180, 225	22 (9)	37 (13)
3	135, 180, 225	19 (10)	37 (13)

Mean(std) was calculated from the reconstruction results obtained with all four simulated plaques and using the strain-error values $\varepsilon_{\text{error}}=0.1, 0.2$ and 0.3% . The catheter position is at the geometric center of the lumen and $\varepsilon_{\text{thres}}=0.9\%$.

TABLE 4:
MEAN(STD) SOFT TISSUE AREA (STA) ERROR[%] AND SOFT TISSUE OVERLAP (STO) ERROR[%] AS
FUNCTION OF THE STRAIN-ERROR THRESHOLD (ϵ_{error})

$\epsilon_{\text{error}}(\%)$	STA	STO
0.1	28 (13)	42 (15)
0.2	24 (17)	37 (10)
0.3	25 (15)	39 (10)

Mean(std) was calculated from the reconstruction results obtained with all four simulated plaques and using all combinations of # of global initializations ($N_{\text{GI}}=1, 2$ or 3) and angle apertures ($\varphi=225^\circ, 180^\circ$ or 135°). The catheter position is at the geometric center of the lumen and $\epsilon_{\text{thres}}=0.9\%$.

IN VITRO AND IN VIVO RECONSTRUCTION

In vitro result

Figure 7 shows the reconstruction of a plaque from its in vitro measured strain elastogram. The modulogram shows soft and stiff regions, which colocalize with those in histology. For example, the plaque (from 9 to 6 o'clock) consists of a proximal layer of stiff collagenous cap (Fig. 7d), which covers a region that (i) lacks smooth muscle cells (Fig. 7e) and (ii) is heavily infiltrated by macrophages (Fig. 7f). The modulogram shows in this region as a stiff cap with a large, softer region behind it.

In vivo result

Figure 8 shows the reconstruction of a plaque from its in vivo measured strain elastogram. The echogram (Fig. 8a) shows that the plaque is eccentric and located between 10 and 5 o'clock. The corresponding strain elastogram (Fig. 8b) indicates that this plaque is vulnerable/rupture-prone, since the shoulders of the plaque are highly strained (Schaar et al. 2003). Finally, the modulogram suggests that this plaque is a typical thin-cap-fibratheroma, since the reconstructed elastic material composition consists of a stiff region (i.e., the cap), which covers a large, soft region (i.e., the lipid pool).

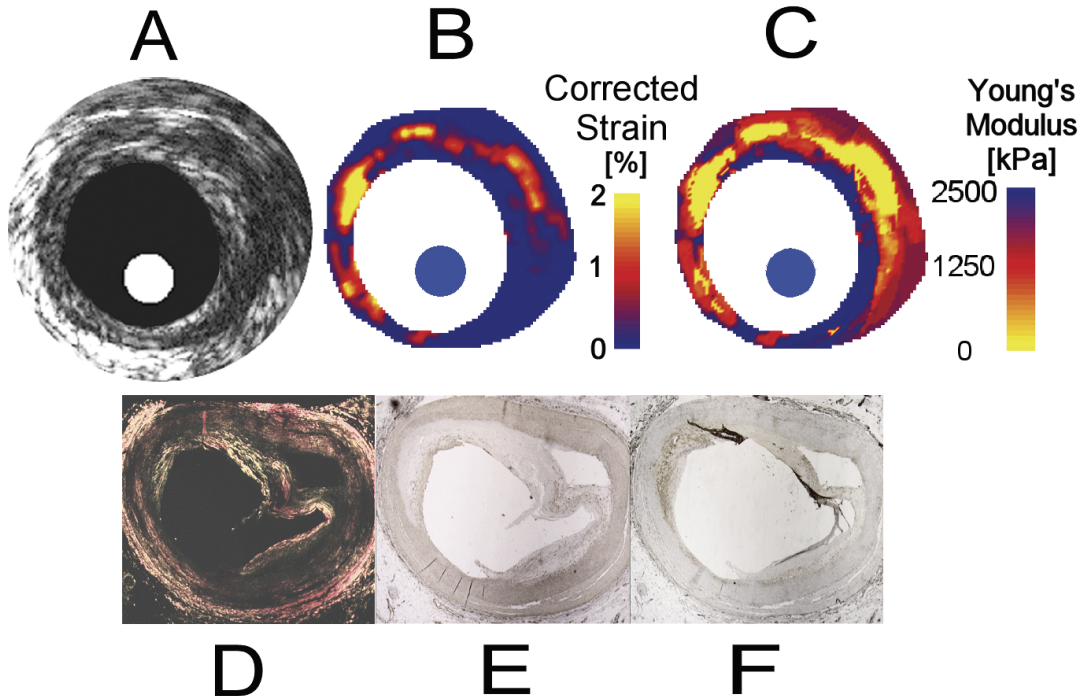


Fig. 7. In vitro elasticity (strain and modulus) imaging of a human coronary artery with a circular, heterogeneous plaque. (a) Echogram. (b) Measured corrected strain elastogram. (c) Compounded modulogram reconstructed from (b). Histology: (d) Collagen, (e) Smooth muscle cells and (f) Macrophages. The bright and blue circles indicate the tip of the catheter with $\text{Ø}=1.1$ mm.

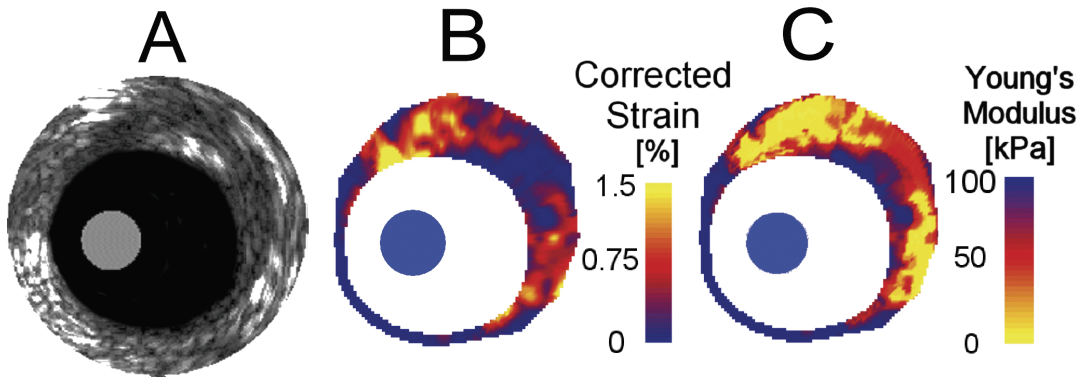


Fig. 8. In vivo elasticity (strain and modulus) imaging of a human coronary artery with an eccentric, vulnerable plaque. (a) Echogram. (b) Measured corrected strain elastogram. (c) Compounded modulogram reconstructed from (b). The bright and blue circles indicate the tip of the catheter with $\text{Ø}=1.1$ mm.

DISCUSSION

For the purpose of quantifying the efficiency of pharmaceutical plaque-stabilizing treatments, we developed a fully automatic, inverse method that reconstructs the local elasticity (i.e., Young's modulus) distribution of arbitrary heterogeneous plaques from their measured radial strain elastogram; this method is an extension of our previous reconstruction framework, which was mainly suited for TCFA plaques. The new method was evaluated and its optimal settings were determined using histology-traced human coronary plaques. Finally, it was applied to two elastograms, one measured in vitro and the other in vivo, from two human atherosclerotic coronary arteries. The method gave good results for all plaques, especially when the catheter was centred. The in vitro reconstruction was in agreement with histology.

An inverse method suited for arbitrary plaques

INVERSE ELASTICITY PROBLEM FOR CORONARY PLAQUES

The following factors make the inverse elasticity problem for coronary plaques using IVUS-derived deformation a different and difficult task, when compared with the inverse elasticity problem for other organs, such as the breast (Céspedes et al. 1993), where user-controlled, non-invasive, ultrasound-derived deformation is used:

Difficulties

- Plaques have a complex, heterogeneous material composition.
- There is an inherent decay of deformation (strain and displacement) from the lumen towards the media border, due to the inherent stress decay that is caused by the circumferential geometry of the vessel wall; along the decay direction, the signal-to-noise ratio of the measured strain decreases.
- There is no control of the main deformation source (namely, the pulsating intracoronary blood) and measurement device (namely, the catheter). This limits the applicability of available deformation-processing methods that utilize control of the source and device.
- The spatial resolution of the measured radial strain is merely $200\ \mu\text{m}$ with the currently used deformation processing algorithm (de Korte et al. 1998).

Heterogeneity

Decay of deformation

No control of source and device

Spatial resolution

Currently, only a few groups have reported methods for solving the arterial inverse elasticity problem using (simulated) ultrasound-derived deformation, e.g., (Aglyamov et al. 2004, Beattie et al. 1998, Chandran et al. 2003, Gokhale 2003, Kanai et al. 2003, Kim et al. 2004, Lupotti et al. 2003, Soualmi et al. 1997, Vorp et al. 1995, Wan et al. 2001). However, it was not shown whether those methods could work when using the cross-sectional radial strain distribution of an arbitrary heterogeneous atherosclerotic coronary plaque. IVUS elastography/palpography is a clinically available technique that provides coronary strain elastograms in vivo (de Korte et al. 2002b, 2003; Schaar et al. 2004b). When our method is used as an addition to IVUS

Efforts from other research groups

elastography/palpography, investigators will finally have an all-in-one modality that can (i) detect vulnerable plaques (Schaar et al. 2004b), (ii) assess information related to their rupture-proneness (Schaar et al. 2003) and (iii) image their elastic material composition.

CORRECTED RADIAL STRAIN ELASTOGRAMS

Corrected strain elastograms look alike

During in vivo acquisitions, the catheter is moving continuously. This means that for different positions, different radial strain elastograms will be obtained, which might give different reconstructions when used as input for our method. Instead, by using the corrected strain elastogram ($\varepsilon_{\text{COR}} = |\varepsilon_{\text{radial}} / \cos(2\beta)|$), the dependence upon catheter position is reduced, since corrected strain elastograms will often look alike; Furthermore, an overall increase in strain is obtained. These properties are beneficial for increasing the robustness and uniqueness of our method.

FULLY AUTOMATIC CREATION OF INITIALS STATES

Initial states creation doesn't have to be done precise

Once the distal and the proximal high-strain region edges are created, the cap and the lipid curves of the Bézier PFEM are automatically positioned near them, respectively. This positioning does not have to be exact, since the optimization process will steer the Bézier PFEM. Similarly, the formula used for specifying initial Young's modulus values of the Bézier PFEM only has to give approximate Young's modulus values.

COMPOUNDING PROCEDURE

Now we use information from all individual modulograms, by compounding them

The described method is more efficient and better suited for arbitrary plaques, as opposed to our previous method. This is because our previous method takes only one final modulogram, from a set of individual reconstructed modulograms, namely the one with the lowest RMS error for its strain elastogram. In contrast, now we use information from all individual modulograms, by compounding them. This compounded modulogram, showing local elasticity fluctuations, is likely to be a better estimate (in term of the RMS error) than any individual modulogram, when applied to an arbitrary heterogeneous plaque.

Compounding comes with a price

The cost to be paid is that incorrect Young's modulus (YM) values can be compounded; this is because the measured strain elastogram and the strain elastogram of an individual modulogram can both have a local region of similar (high or low) strain, but a different underlying YM, due to the following physical situations.

- A region of high strain may occur when, e.g., (i) there is, simply, soft tissue present or (ii) there is stiff tissue present, which is subjected to high (circumferential) stress.
- A region of low strain may occur when, e.g., (i) there is, simply, stiff tissue present or (ii) there is soft tissue present but the deforming stress is either low due to natural stress decay or it is carried by surrounding stiff tissue.

When are compounding errors expected

Most of these situations are correctly accounted for by our method because the Bézier PFEM uses the local, strain (directly), stress (indirectly) and YM (directly) during the optimization process. Only, when the local stress itself is almost zero or when the Bézier PFEM shape is too different from the real local plaque structure, compounding errors can be expected.

Simple weight function

For illustrational purposes we have used a simple weight function for the compounding, however, more complex functions may be used, which, for example, account for the intraluminal blood pressure, local strain (relative error) value, or the overall r^{-2} strain decay.

VARIATION OF METHOD INPUT AND SETTINGS

A centred catheter, gives the best reconstruction

A centred catheter, CP₁ (Fig. 2d), gave, on average, the best reconstructions, while a catheter positioned towards the plaque, CP₂, gave the worst. This can be explained, as follows. The corrected strain elastograms for various catheter positions will in

general, look similar, but not always. Deviations will be present, especially when the plaque resembles TCFA and the catheter is at CP_2 ; since then, angle β deviates significantly from unknown angle α at the high principal strain regions near the lipid pool shoulders. When the catheter is at CP_1 , this is much less the case (Baldeensing et al. 2005a). The same reasoning is often valid for heterogeneous plaques.

A strain threshold $\varepsilon_{\text{thres}}=0.9\%$ used to create local initial states (LISs), seems optimal to use. An optimum value is to be expected. This is because, on the one hand, a low $\varepsilon_{\text{thres}}$ gives less (possibly just one) LISs and each has a large potential heterogeneous plaque area that is represented by a single (piecewise homogenous) Bézier PFEM. On the other hand, a high $\varepsilon_{\text{thres}}$ gives more and smaller LISs, whose representation by a very localized Bézier PFEM, will not be correct.

A strain threshold of 0.9% is optimal

Similarly, a strain-error threshold $\varepsilon_{\text{error}}=0.2\%$ used to identify parts of modulograms to be compounded, seems optimal to use; when $\varepsilon_{\text{error}}$ is low, only small parts of the individual modulograms are compounded, when $\varepsilon_{\text{error}}$ approaches 0, nothing is compounded and only the individual modulogram with the lowest RMS error for its strain elastogram remains as the final compounded modulogram, which will generally not be representative for heterogeneous plaques. On the other hand, when $\varepsilon_{\text{error}}$ is high, large parts of each modulogram are compounded, which will include erroneous parts.

A strain-error threshold of 0.2% is optimal

UNIQUENESS

Our method solves the inverse elasticity problem by taking the measured strain elastogram and uses it to reconstruct a modulogram, which gives a strain elastogram that resembles the measurement, as much as possible. The question remains whether or not there exists a unique modulogram that underlies a measured strain elastogram. Mathematically (Barbone et al. 2002, Barbone et al. 2004) and practically, the answer is no, because, e.g., (i) measurements suffer from noise, (ii) the computer model only models a part of the true tissue structure and behaviour and (iii) there is information loss (in coronaries we, currently, only look at the radial component of the strain).

There doesn't exist a unique modulogram

However, from a clinical point of view, the 'level' of uniqueness is of more importance; modulograms are allowed to display the absolute Young's modulus (YM) value with an error margin, as long as the margin is low enough to still give an YM distribution that clearly indicates a large YM contrast between stiff and soft plaque structures. This is what was already observed by Baldeensing et al. (2005a): (i) a cap region can be reconstructed as either slightly thinner and stiffer or slightly thicker and softer, while still having similar strain elastograms; and (ii) local regions where the principal strain is low may give an incorrect reconstruction of a plaque component border, but (iii) in all cases, still, a large YM contrast between soft and stiff plaque components was found in the reconstructed modulogram.

From a clinical point of view, the 'level' of uniqueness is of more importance

The simulations and in vitro results, presented in the current paper, show good agreement between true and reconstructed modulograms, with the expected slight deviations in absolute YM values.

A pressure difference of 20 mmHg for the in vitro artery and only 1 mmHg for the in vivo artery resulted in both cases in elastograms with radial strains up to 2% (Figs. 7b, 8b). This result is in agreement with previous studies (de Korte et al. 2000a, de Korte et al. 2002a). The difference suggests that excising an artery may induce mechanical stiffening (Gow et al. 1979, Schaar et al. 2002). This is possibly caused by differences in factors between situations in vitro and in vivo (e.g., cell inactivity or too much longitudinal pre-stretch). As expected from linear elasticity this pressure difference of a factor of 20 with similar strain is reflected in the reconstructed Young's moduli values.

Excising an artery may induce mechanical stiffening

The uniqueness of our method is expected to improve, when more strain tensor components (e.g., lateral or shear) are measured (Techavipoo et al. 2005). This is because, then, more features can be incorporated in the minimization of an appropriately modified RMS error function. Furthermore, a more reliable (in terms of a lower RMS error) modulogram might be obtained by post-processing the compounded modulogram using a local reconstruction method that fine-tunes the YM locally, of course at the expense of more processing time.

Improving the uniqueness and reliability of a reconstruction

CLINICAL APPLICATIONS

<i>A new way of tissue characterization</i>	The described method is a new way of tissue characterization, suitable for clinical applications, such as monitoring atherosclerosis and pharmaceutical-induced plaque stabilization (Aikawa et al. 1998, Brown et al. 1993, Loree et al. 1994).
<i>Use deformation input from other imaging modalities</i>	The method can also be used in combination with any other imaging modality that is capable of measuring deformation (strain or displacement), for example, (Intra)vascular OCT elastography (Rogowska et al. 2004), MRI elastography (Plewes et al. 2000).
<i>Application to other organs</i>	Since our method only needs a deformation elastogram as input, it may also be applied to other organs from which one or more deformation components are measurable, such as the breast (Liu et al. 2003, Plewes et al. 2000) and the prostate (Konig et al. 2005, Souchon et al. 2003) or superficial arteries, such as the femoral (de Korte et al. 2000b) or the carotid (Maurice et al. 2005, Ribbers et al. 2005).
<i>Perform in vivo stress analysis</i>	Our method, in combination with IVUS elastography, provides in vivo plaque morphology, strain and Young's modulus, consequently, one can perform in vivo finite element based stress analysis. This may be a more reliable analysis than when a priori Young's modulus values, plaque model or plaque structure obtained from tracing histology is used (Chau et al. 2004, Cheng et al. 1993, Finet et al. 2004, Li et al. 2005, Loree et al. 1992, Tang et al. 2004, Veress et al. 1998).
<i>Plaque-vulnerability indices</i>	Furthermore, it may aid the development and validation of plaque-vulnerability indices, which are defined from local strain, stress and Young's modulus information (Bank et al. 2000, Yang et al. 2005, Zohdi et al. 2004).
<i>Requirements</i>	Although the reconstruction results, presented in this paper, are promising, sensitivity and specificity studies in vitro and in vivo using a large population will be needed to establish our method as a fully automatic, clinical/research tool for in vivo plaque characterization.

CONCLUSION

Intravascular ultrasound (IVUS) elastography is a clinically validated medical imaging modality that detects rupture-prone coronary artery plaques and provides information related to their rupture-proneness by measuring their cross-sectional radial strain distribution (i.e., elastogram) using an intravascular ultrasound catheter. We developed a fully automatic, inverse method, to reconstruct the local elasticity (i.e., Young's modulus) distribution of an arbitrary atherosclerotic plaque from its measured elastogram. Results from simulated elastograms of plaques showed that the method works successfully, for both thin-cap fibroatheromas as well as heterogeneous plaques; the best results are obtained with a catheter centred in the artery. Furthermore, it was applied to two measured elastograms, one measured in vitro and the other in vivo, from two human atherosclerotic coronary arteries. In conclusion, IVUS elastography in combination with our inverse method has potential to become an all-in-one modality for detecting plaques, for assessing information related to their rupture-proneness and for imaging their elastic material composition.

ACKNOWLEDGEMENTS

This research was financially supported by the Dutch Technology Foundation (STW) project number RPG-5442 and the Netherlands Organization for Scientific Research (NWO). This research line is supported by an R&D agreement with Volcano Corporation, Inc., Rancho Cordova, CA, USA.

REFERENCES

- Aglyamov S, Skovoroda AR, Rubin JM, O'Donnell M, Emelianov SY. *Model-based reconstructive elasticity imaging of deep venous thrombosis*. IEEE Trans Ultrason Ferroelectr Freq Control 2004;51:521-31.
- Aikawa M, Rabkin E, Okada Y, Voglic SJ, Clinton SK, Brinckerhoff CE, Sukhova GK, Libby P. *Lipid lowering by diet reduces matrix metalloproteinase activity and increases collagen content of rabbit atheroma: a potential mechanism of lesion stabilization*. Circulation 1998;97:2433-44.
- Baldewsing RA, de Korte CL, Schaar JA, Mastik F, van der Steen AFW. *A finite element model for performing intravascular ultrasound elastography of human atherosclerotic coronary arteries*. Ultrasound Med Biol 2004a;30:803-13.
- Baldewsing RA, De Korte CL, Schaar JA, Mastik F, van der Steen AFW. *Finite element modeling and intravascular ultrasound elastography of vulnerable plaques: parameter variation*. Ultrasonics 2004b;42:723-9.
- Baldewsing RA, Mastik F, Schaar JA, Serruys PW, van der Steen AFW. *Robustness of reconstructing the Young's modulus distribution of vulnerable atherosclerotic plaques using a parametric plaque model*. Ultrasound Med Biol 2005a;31:1631-45.
- Baldewsing RA, Schaar JA, Mastik F, Oomens CWJ, van der Steen AFW. *Assessment of vulnerable plaque composition by matching the deformation of a parametric plaque model to measured plaque deformation*. IEEE Trans Med Imaging 2005b;24:514-28.
- Baldewsing RA, Mastik F, Schaar JA, Serruys PW, van der Steen AFW. *Young's modulus reconstruction of vulnerable atherosclerotic plaque components using deformable curves*. Ultrasound in Med Biol 2006;32:201-10;
- Bank AJ, Versluis A, Dodge SM, Douglas WH. *Atherosclerotic plaque rupture: a fatigue process?* Med Hypotheses 2000;55:480-4.
- Barbone PE, Bamber JC. *Quantitative elasticity imaging: what can and cannot be inferred from strain images*. Phys Med Biol 2002;47:2147-64.
- Barbone PE, Gokhale NH. *Elastic modulus imaging: on the uniqueness and nonuniqueness of the elastography inverse problem in two dimensions*. Inverse Problems 2004;20:283-96.
- Beattie D, Xu C, Vito R, Glagov S, Whang MC. *Mechanical analysis of heterogeneous, atherosclerotic human aorta*. J Biomech Eng 1998;120:602-7.
- Brown BG, Zhao XQ, Sacco DE, Albers JJ. *Lipid lowering and plaque regression. New insights into prevention of plaque disruption and clinical events in coronary disease*. Circulation 1993;87:1781-91.
- Céspedes EI, Ophir J, Ponnekanti H, Maklad N. *Elastography: elasticity imaging using ultrasound with application to muscle and breast in vivo*. Ultras Imag 1993;17:73-88.
- Chandran KB, Mun JH, Choi KK, Chen JS, Hamilton A, Nagaraj A, McPherson DD. *A method for in-vivo analysis for regional arterial wall material property alterations with atherosclerosis: preliminary results*. Med Eng Phys 2003;25:289-98.
- Chau AH, Chan RC, Shishkov M, MacNeill B, Iftimia N, Tearney GJ, Kamm RD, Bouma BE, Kaazempur-Mofrad MR. *Mechanical analysis of atherosclerotic plaques based on optical coherence tomography*. Ann Biomed Eng 2004;32:1494-503.
- Cheng GC, Loree HM, Kamm RD, Fishbein MC, Lee RT. *Distribution of circumferential stress in ruptured and stable atherosclerotic lesions. A structural analysis with histopathological correlation*. Circulation 1993;87:1179-87.
- Davies MJ. *The pathophysiology of acute coronary syndromes*. Heart 2000;83:361-6.
- Davies MJ. *Going from immutable to mutable atherosclerotic plaques*. Am J Cardiol 2001;88:2F-9F.
- de Korte CL, Carlier SG, Mastik F, Doyley MM, van der Steen AF, Serruys PW, Bom N. *Morphological and mechanical information of coronary arteries obtained with intravascular elastography; feasibility study in vivo*. Eur Heart J 2002a;23:405-13.
- de Korte CL, Carlier SG, Mastik F, Doyley MM, van der Steen AFW, Serruys PW, Bom N. *Morphological and mechanical information of coronary arteries obtained with Intravascular elastography: a feasibility study in vivo*. European Heart Journal 2002b;23:405-13.
- de Korte CL, Céspedes EI, van der Steen AFW. *Influence of catheter position on estimated strain in intravascular elastography*. IEEE Trans Ultrason Ferroelectr Freq Control 1999;46:616-25.
- de Korte CL, Pasterkamp G, van der Steen AF, Woutman HA, Bom N. *Characterization of plaque components with intravascular ultrasound elastography in human femoral and coronary arteries in vitro*. Circulation 2000a;102:617-23.

- de Korte CL, Pasterkamp G, van der Steen AFW, Woutman HA, Bom N. *Characterization of plaque components using intravascular ultrasound elastography in human femoral and coronary arteries in vitro*. Circulation 2000b;102:617-23.
- de Korte CL, Schaar JA, Mastik F, Serruys PW, van der Steen AFW. *Intravascular elastography: from bench to bedside*. J Interv Cardiol 2003;16:253-9.
- de Korte CL, Siervogel M, Mastik F, Strijder C, Velema E, Pasterkamp G, van der Steen AFW. *Intravascular Elastography in Yucatan pigs: validation in vivo*. European Heart Journal 2001;22:251.
- de Korte CL, Siervogel MJ, Mastik F, Strijder C, Schaar JA, Velema E, Pasterkamp G, Serruys PW, van der Steen AFW. *Identification of atherosclerotic plaque components with intravascular ultrasound elastography in vivo: a Yucatan pig study*. Circulation 2002c;105:1627-30.
- de Korte CL, van der Steen AFW, Céspedes EI, Pasterkamp G. *Intravascular ultrasound elastography of human arteries: initial experience in vitro*. Ultrasound Med Biol 1998;24:401-8.
- Falk E, Shah PK, Fuster V. *Coronary plaque disruption*. Circulation 1995;92:657-71.
- Finet G, Ohayon J, Rioufol G. *Biomechanical interaction between cap thickness, lipid core composition and blood pressure in vulnerable coronary plaque: impact on stability or instability*. Coron Artery Dis 2004;15:13-20.
- Gokhale NH. *A fast iterative method for elastic modulus imaging*. Thesis 2003;
- Gow BS, Hadfield CD. *The elasticity of canine and human coronary arteries with reference to postmortem changes*. Circ Res 1979;45:588-94.
- Kanai H, Hasegawa H, Ichiki M, Tezuka F, Koiwa Y. *Elasticity imaging of atheroma with transcutaneous ultrasound: preliminary study*. Circulation 2003;107:3018-21.
- Kim K, Weitzel WF, Rubin JM, Xie H, Chen X, O'Donnell M. *Vascular intramural strain imaging using arterial pressure equalization*. Ultrasound Med Biol 2004;30:761-71.
- Konig K, Scheipers U, Pesavento A, Lorenz A, Ermert H, Senge T. *Initial experiences with real-time elastography guided biopsies of the prostate*. J Urol 2005;174:115-7.
- Li ZY, Howarth S, Trivedi RA, JM UK-I, Graves MJ, Brown A, Wang L, Gillard JH. *Stress analysis of carotid plaque rupture based on in vivo high resolution MRI*. J Biomech 2005;
- Liu HT, Sun LZ, Wang G, Vannier MW. *Analytic modeling of breast elastography*. Med Phys 2003;30:2340-9.
- Loree HM, Kamm RD, Stringfellow RG, Lee RT. *Effects of fibrous cap thickness on peak circumferential stress in model atherosclerotic vessels*. Circ Res 1992;71:850-8.
- Loree HM, Tobias BJ, Gibson LJ, Kamm RD, Small DM, Lee RT. *Mechanical properties of model atherosclerotic lesion lipid pools*. Arterioscler Thromb 1994;14:230-4.
- Lupotti FA, Mai JJ, Pellot-Barakat C, Insana MF. *Vascular elasticity from regional displacement estimates*. Proceedings of the 2003 IEEE International Ultrasonics Symposium 2003;1895-8.
- MacNeill BD, Lowe HC, Takano M, Fuster V, Jang IK. *Intravascular modalities for detection of vulnerable plaque: current status*. Arterioscler Thromb Vasc Biol 2003;23:1333-42.
- Maurice RL, Brusseau E, Finet G, Cloutier G. *On the potential of the Lagrangian speckle model estimator to characterize atherosclerotic plaques in endovascular elastography: in vitro experiments using an excised human carotid artery*. Ultrasound Med Biol 2005;31:85-91.
- Ophir J, Céspedes EI, Garra B, Ponnekanti H, Huang Y, Maklad N. *Elastography: ultrasonic imaging of tissue strain and elastic modulus in vivo*. Eur J Ultrasound 1996;3:49-70.
- Plewes DB, Bishop J, Samani A, Sciarretta J. *Visualization and quantification of breast cancer biomechanical properties with magnetic resonance elastography*. Phys Med Biol 2000;45:1591-610.
- Ribbers H, Holewijn S, Blankensteijn JD, de Korte CL. *Non-invasive two dimensional elastography of the carotid artery*. Proceedings of the 2005 IEEE International Ultrasonics Symposium 2005;611-2.
- Rogowska J, Patel NA, Fujimoto JG, Brezinski ME. *Optical coherence tomographic elastography technique for measuring deformation and strain of atherosclerotic tissues*. Heart 2004;90:556-62.
- Schaar JA, De Korte CL, Mastik F, Strijder C, Pasterkamp G, Boersma E, Serruys PW, Van Der Steen AFW. *Characterizing vulnerable plaque features with intravascular elastography*. Circulation 2003;108:2636-41.
- Schaar JA, de Korte CL, Mastik F, van der Steen AFW. *Effect of temperature increase and freezing on intravascular elastography*. Ultrasonics 2002;40:879-81.

- Schaar JA, Muller JE, Falk E et al. *Terminology for high-risk and vulnerable coronary artery plaques. Report of a meeting on the vulnerable plaque, June 17 and 18, 2003, Santorini, Greece.* Eur Heart J 2004a;25:1077-82.
- Schaar JA, Regar E, Mastik F et al. *Incidence of vulnerable plaque patterns in humans: assessment with three-dimensional intravascular palpography and correlation with clinical presentation.* Circulation 2004b;109:2716-9.
- Shi H, Chen Q, Varghese T. *A general solution for catheter position effects for strain estimation in intravascular elastography.* Ultrasound Med Biol 2005;31:1509-26.
- Souchon R, Rouviere O, Gelet A, Detti V, Srinivasan S, Ophir J, Chapelon JY. *Visualisation of HIFU lesions using elastography of the human prostate in vivo: preliminary results.* Ultrasound Med Biol 2003;29:1007-15.
- Tang D, Yang C, Zheng J, Woodard PK, Sicard GA, Saffitz JE, Yuan C. *3D MRI-based multicomponent FSI models for atherosclerotic plaques.* Ann Biomed Eng 2004;32:947-60.
- Techavipoo U, Varghese T. *Improvements in elastographic contrast-to-noise ratio using spatial-angular compounding.* Ultrasound Med Biol 2005;31:529-36.
- Timoshenko SP, Goodier JN, *Theory of elasticity.* Singapore: McGraw-Hill, 1970.
- Van Mieghem CA, Bruining N, Schaar JA et al. *Rationale and methods of the integrated biomarker and imaging study (IBIS): combining invasive and non-invasive imaging with biomarkers to detect subclinical atherosclerosis and assess coronary lesion biology.* Int J Cardiovasc Imaging 2005;21:425-41.
- Veress AI, Cornhill JF, Herderick EE, Thomas JD. *Age-related development of atherosclerotic plaque stress: a population-based finite-element analysis.* Coron Artery Dis 1998;9:13-9.
- Virmani R, Burke AP, Kolodgie FD, Farb A. *Pathology of the thin-cap fibroatheroma: a type of vulnerable plaque.* J Interv Cardiol 2003;16:267-72.
- Virmani R, Kolodgie FD, Burke AP, Farb A, Schwartz SM. *Lessons from sudden coronary death: a comprehensive morphological classification scheme for atherosclerotic lesions.* Arterioscler Thromb Vasc Biol 2000;20:1262-75.
- Vorp DA, Rajagopal KR, Smolinski PJ, Borovetz HS. *Identification of elastic properties of homogeneous, orthotropic vascular segments in distension.* J Biomech 1995;28:501-12.
- Wan M, Li Y, Li J, Cui Y, Zhou X. *Strain imaging and elasticity reconstruction of arteries based on intravascular ultrasound video images.* IEEE Trans Biomed Eng 2001;48:116-20.
- Yang C, Tang D, Zheng J, Woodard PK, Saffitz JE, Sanchez LA, Sicard GA. *A computational plaque vulnerability index based on stress/strain local maximal values for human atherosclerotic plaque vulnerability assessment.* Proceedings of the 2005 Summer Bioengineering Conference 2005;
- Zohdi TI, Holzapfel GA, Berger SA. *A phenomenological model for atherosclerotic plaque growth and rupture.* J Theor Biol 2004;227:437-43.

PART V
SUMMARY

DISCUSSION AND CONCLUSION

MOTIVATION

Atherosclerosis, a disease of the large arteries, is the primary cause of heart disease and stroke. In westernized societies, it is the underlying cause of about 50% of all deaths (Lusis 2000). Acute coronary syndromes such as, angina pectoris, sudden cardiac death and myocardial infarction are primarily caused by thrombus formation due to instantaneous rupture of vulnerable coronary plaques; a plaque is an accumulation of (mainly fatty) material in the arterial wall (Davies 2000, Falk et al. 1995). Thus, detection, characterization, treatment and monitoring of these plaques are of vital importance. This thesis describes a new imaging method, called Modulography, for identifying and characterizing these plaques based on their elastic material property (i.e., Young's modulus) distribution.

Many invasive and non-invasive methods are (being) developed for identifying vulnerable plaques or plaque-features that are suspected to indicate vulnerability (**CHAPTER 1**). Still, none of those methods can solely identify all vulnerability features. Among them are intravascular ultrasound (IVUS) Elastography/Palpography and Modulography, which are currently the only methods capable of providing in vivo mechanical plaque information.

Assessment of mechanical information is vital, since plaque rupture is ultimately a mechanical phenomenon; plaque-cap rupture occurs when it cannot withstand the stresses imposed by the pulsating blood. Furthermore, mechanical information may aid in optimally choosing proper interventional strategies (Baptista et al. 1996) since these are mechanical by nature. Besides that, pharmaceutical treatments induce mechanical stabilization of plaques, e.g., by stiffening or reducing plaque atheroma (Aikawa et al. 1998, Lee 2000, Loree et al. 1994), thus the efficiency of these treatments can be quantified by measuring mechanical information.

Modulography, produces a plaque's modulogram (i.e., Young's modulus image) by solving the inverse elasticity problem. This problem consists of finding 'the' modulogram that underlies a given strain elastogram; for modulography, the strain elastogram is measured using IVUS elastography, which is currently the only clinically available technique that provides coronary strain elastograms in vivo (de Korte et al. 2001, 2002, 2003). Solving the inverse elasticity problem for coronary plaques using IVUS-derived local deformation (strain or displacement) is a different and difficult task, when compared with the inverse elasticity problem for other organs, such as the breast (Céspedes et al. 1993), where user-controlled, non-invasive, ultrasound-derived deformation can be used. This is because (i) plaques have a complex, heterogeneous material composition, (ii) there is an inherent decay of deformation from the lumen towards the media border, due to the inherent stress decay that is caused by the circumferential geometry of the vessel wall; along the decay direction, the signal-to-noise ratio of the measured deformation decreases, (iii) there is no control of the primary deformation source (pulsating intracoronary blood) and measurement device (catheter), which limits the applicability of available deformation-processing methods that utilize control of the source and device, (iv) with the currently used deformation processing algorithm (de Korte et al. 1998) only the radial component of the strain is measured, with a spatial resolution of merely 200 μm .

Finally, the general, unconstrained, inverse elasticity problem in 2D is ill-posed (Barbone et al. 2002, 2004). This means, that either (i) there doesn't exist a unique modulogram that underlies a measured strain elastogram, or (ii) there does exist a unique modulogram, but this cannot be stably obtained due to noise in the deformation measurements.

Currently, only a few methods have been proposed for solving the arterial inverse elasticity problem using (simulated) ultrasound-derived deformation, e.g., (Aglyamov et al. 2004, Beattie et al. 1998, Chandran et al. 2003, Gokhale 2003, Kanai et al. 2003, Kim et al. 2004, Lupotti et al. 2003, Soualmi et al. 1997, Vorp et al. 1995, Wan et al. 2001). However, it was not shown that they could work when using the cross-sectional radial strain distribution of an arbitrary heterogeneous atherosclerotic coronary plaque. To have a method that works on in vivo strain data measured with IVUS elastography/palpography would mean that investiga-

tors will, finally, have an all-in-one modality that can (i) detect vulnerable plaques (Schaar et al. 2004), (ii) assess information related to their rupture-proneness (Schaar et al. 2003) and (iii) image their elastic material composition, all in vivo.

Stimulated by this prospect and by the results of previous methods, we developed a new approach, called Modulography (a concatenation of 'modulus' and 'graphy'), especially suited for solving the inverse elasticity problem using in vivo measured strain of coronary plaques. Compared with other approaches, our approach has two key differences (i) it uses as much as possible a priori plaque information that can be automatically derived from the echogram and strain elastogram and (ii) it, initially, focussed on the largest class of vulnerable plaques, namely the thin-cap fibroatheromas (TCFAs), which can be modelled as a geometrically simple structure. By using this a priori information, the inverse elasticity problem was constrained in such a way that a practically useful and more or less unique modulogram could be obtained in vivo in a stable manner.

The development of Modulography began by first solving the forward elasticity problem, then the inverse elasticity problem for TCFAs, and, finally, making generalizations to our solution-approach for TCFAs, in order to allow imaging of arbitrary plaques.

FORWARD PROBLEM

The first step in solving the inverse elasticity problem is to solve the forward elasticity problem. The forward elasticity problem consists of finding an appropriate constitutive material model for atherosclerotic arteries, which can be used to properly compute their deformation. For this purpose, a computer finite element model (FEM) was proposed, in which the plaque-tissue was modelled as a linearly elastic, isotropic, incompressible, material in a plane strain state (**CHAPTER 2**). It was shown that this FEM could sufficiently model the quasi-static arterial small-strain behaviour of coronary plaques. To this end, computer-simulated elastograms were compared with measured elastograms. Measured elastograms were processed from ultrasound radio-frequency data obtained in vitro from six objects: a vessel mimicking phantom and five excised human atherosclerotic coronary arteries. A FEM was created for each object and used to computer-simulate an elastogram; the FEM's material properties and geometry were obtained from the object's histology. Comparison was performed upon high strain regions (HSR), because these regions have proven to contain plaques that show the hallmarks of vulnerable plaques. Eight HSR were automatically identified from the five arteries. Statistical tests showed that there was no significant difference between simulated and corresponding measured elastograms in location, surface area and mean strain value of a HSR.

Next, the FEM was used to understand and quantify how measured strain elastograms depended upon (i) the elastic material properties and (ii) morphology of vulnerable plaque components, as well as (iii) the used catheter position (**CHAPTER 3**). To this end, IVUS strain elastography measurements were performed with a vessel mimicking phantom, having a soft plaque embedded in a stiff wall, and an human coronary artery containing a vulnerable plaque. Next, FEMs were created to simulate strain elastograms of the same objects. In these FEMs the following parameters were varied: Young's modulus (E), Poisson's ratio (ν) in range 0.49-0.4999, catheter position (translation of 0.8 mm), and cap-thickness (t) in range 50-350 μm . During all variations, the resulting Peak Radial Strain (PRS) was determined and visualized. This study showed that strain elastograms of vulnerable plaques (i) depend highly upon the Young's modulus of lipid and cap, but hardly upon the Poisson's ratio, (ii) different catheter positions result in different strain elastograms, nevertheless, the diagnostically important high strain regions in the lipid shoulders are often still detectable and (iii) peak radial strain increases when cap weakens or cap thickness decreases. These properties (except (ii)) are beneficial for solving the inverse elasticity problem.

INVERSE PROBLEM

Having established a FEM for simulating strain elastograms and noticing that the FEM primarily depended upon the Young's modulus distribution, the next step was to solve the inverse elasticity problem. The initial objective was to develop a solution approach that made the inverse problem as stable as possible and its solution highly unique. Therefore, we developed a Modulography approach that was especially suited for thin-cap fibroatheromas (TCFAs), i.e., plaques with a media region containing a lipid pool covered by a cap (**CHAPTER 4**). A plaque's modulogram is obtained from a measured strain elastogram, as follows. A optimization algorithm matches the strain image output, calculated with a circular Parametric Finite Element Model (PFEM) representation of a TCFA, to the measured strain elastogram, by iteratively updating the PFEM geometry and material parameters. These geometry parameters are the centre coordinates and radii of

circles, which delineate the TCFA media, lipid pool and cap regions. The material parameter for each region is a Young's modulus, E_{MEDIA} , E_{LIPID} and E_{CAP} , respectively. The method was successfully tested on computer-simulated TCFA's ($n=2$), one defined by circles, the other by tracing TCFA histology, and additionally on a physical phantom ($n=1$) having a stiff wall with an eccentric soft region. Finally, it was applied on human coronary plaques in vitro ($n=1$) and in vivo ($n=1$). This study showed for the first time the feasibility of applying Modulography, with the circular PFEM, to various vulnerable plaques, including an in vivo plaque.

As established earlier, a plaque's strain elastogram primarily depends upon the following factors: (i) the plaque components' material composition and (ii) morphology, (iii) catheter position within the vessel and (iv) measurement noise. Therefore, we investigated which plaques can be correctly and robustly reconstructed using Modulography when these factors are varied (**CHAPTER 5**). To this end, a standard plaque was defined as the modulogram that was reconstructed, with the circular PFEM, from an in vivo measured strain elastogram of a human coronary plaque. This standard plaque was used to computer-simulate different strain elastograms, by varying the (i) geometry and material properties of its plaque components, (ii) catheter position and (iii) level of added strain noise. Next, for each elastogram a reconstruction was done. Finally, robustness was evaluated by quantifying the correctly reconstructed size, shape and Young's modulus of each plaque component region and minimal cap-thickness. The results of this study showed that TCFA's can be adequately reconstructed; the thinner and stiffer the cap or the softer and larger the lipid pool, the better is the reconstruction of these components and minimal cap-thickness. Furthermore, reconstructions were (i) independent of catheter position and (ii) independent of strain noise. As such, Modulography, with the circular PFEM, has potential to monitor robustly and quantitatively atherosclerosis in vivo.

GENERALIZATION

Beside a TCFA's composition, atherosclerotic plaques can also have a more complex, heterogeneous material composition consisting of mixture of plaque components, like lipids, fibrotic tissue, calcified nodules or tissues weakened by extra-cellular-matrix breakdown caused by macrophages. Solving the inverse elasticity problem of such complexes requires a different, more local approach, e.g., Soualmi et al. (1997), which doesn't enforce a restriction on the structure of plaque components. Although Soualmi's approach does not require a priori information, the large number of Young's moduli to be computed might prevent a successful convergence of the minimization algorithm.

To, successfully, allow Modulography of arbitrary atherosclerotic plaques, we used a two-step approach. In the first step we generalized the circular PFEM and called it the Bézier PFEM (**CHAPTER 6**). This Bézier PFEM (i) has deformable Bézier curves as distal borders of the PFEM lipid-pool and cap region, instead of circle borders, and (ii) uses as boundaries the true lumen and media contours, as extracted from the IVUS echogram. The geometry parameters are now the control-points of each Bézier curve. The component regions are still assumed to be homogenous and their stiffness is characterized by a Young's modulus. Modulography on strain elastograms that were (i) simulated using a histology-derived computer-TCFA, (ii) measured from a physical phantom with a soft lipid pool and (iii) simulated with a computer-TCFA whose complexity of its plaque component borders was increased, showed that the Bézier PFEM led to a more accurate and reliable modulogram, for a much larger collection of complicated TCFA plaque-component morphologies, than the circular PFEM did. Furthermore, the optimal number of control-points was five. Finally, the method was to be stable, although more parameters were used (e.g., 19 when there are five control-points used for each curve) than with the circular PFEM (only 9).

In the final step, the Modulography framework, which uses the Bézier PFEM, was generalized for application to arbitrary heterogeneous plaques, as follows. (i) A "corrected" radial strain elastogram was used in order to make Modulography less sensitive upon the position of the catheter, (ii) use of the measured "corrected" radial strain elastogram to automatically define initial YM distributions and (iii) use of a compounding approach to obtain a heterogeneous modulogram from individual created modulograms (**CHAPTER 7**). This generalized method was evaluated and its optimal settings were determined by applying it to finite element simulated elastograms of four realistic histology-traced human coronary plaques, two resembled a TCFA, the other plaques had multiple regions of soft and stiff tissue. The relative errors in reconstructed soft tissue area (STA) and soft tissue overlap (STO) were used as performance metrics. Finally, it was applied to two elastograms, one measured in vitro and the other in vivo, from two human atherosclerotic coronary arteries. The method approximated the true Young's modulus distribution of all simulated plaques; the mean[%](std[%]) error in STA=27(21) and in STO=41(16), irrespective of the catheter position in the artery; a centred catheter gave the best results with STA=18(11) and STO=35(12). The in vitro reconstruction was in agreement with histology.

ADVANCING MODULOGRAPHY INTO THE CLINIC

Modulography, in its current form, has already shown promising results. Still, the following research and development will be needed to establish Modulography as a fully automatic, clinical/research tool for *in vivo* plaque characterization. (i) Incorporation of a robust, fully automatic lumen and media contour detection algorithm; this will allow the fully automatic creation of strain elastograms and modulograms. (ii) Development of a robust strain compounding algorithm for creating a single compounded strain elastogram, per cardiac cycle, from a series of strain elastograms obtained within that cycle; this will increase the number of (valid) strain estimates and the signal to noise ratio. This algorithm will be highly inspired by the compounding algorithms for palpography (Doyley et al. 2001, Leung et al. 2005) (iii) Determination of the optimal Modulography-settings for arbitrary *in vivo* situations; for arbitrary situations, these settings should be made depended upon the measurements (intraluminal pressure and strain) in an automated way. (iv) Sensitivity and specificity studies *in vitro* and/or *in vivo* using a large population.

Modulography may be further improved with respect to the following aspects. (i) Increasing the uniqueness of the method. This may be achieved by using more measured strain components (e.g., lateral or shear) (Maurice et al. 2005b, Ribbers et al. 2005, Techavipoo et al. 2005) since, then, more strain features can be incorporated in the minimization of an appropriately modified root-mean-squared (RMS) error function. (ii) Further increasing the reliability (in terms of a lower RMS error) of a modulogram. This may be accomplished by post-processing the modulogram using a local reconstruction method that fine-tunes the Young's modulus locally. (iii) Decreasing the computation time, e.g., using adjoint algorithms (Oberai et al. 2004). These use just one forward FEM calculation for establishing a parameter-vector update while other algorithms, including the one used in this thesis, use at least as many forward FEM calculations as there are parameters to be updated. However, it remains unanswered whether such methods can be modified for the geometrical-constrained approach used by Modulography.

POTENTIAL APPLICATIONS AND IMPLICATIONS

Modulography is a new method for tissue characterization and potentially suitable for clinical applications, such as monitoring atherosclerosis and quantifying pharmaceutical-induced plaque stabilization (Aikawa et al. 1998, Brown et al. 1993, Loree et al. 1994). Modulography can also be used in combination with any other imaging modality that is capable of measuring deformation (strain or displacement), for example, (Intra)vascular OCT elastography (Rogowska et al. 2004), MRI elastography (Plewes et al. 2000). Since Modulography only needs a deformation elastogram as input, it may also be applied to other organs from which one or more deformation components are measurable, such as the breast (Liu et al. 2003, Plewes et al. 2000) and the prostate (Konig et al. 2005, Souchon et al. 2003) or superficial arteries, such as the femoral (de Korte et al. 2000) or the carotid (Maurice et al. 2005a, Ribbers et al. 2005); of course, after properly modifying the inner/outer boundaries of the PFEM. Since Modulography, as an addition to IVUS elastography, provides *in vivo* plaque morphology, strain and YM, one can perform *in vivo* finite element based stress analysis. This may be a more reliable analysis than when *a priori* YM values, plaque model or plaque structure obtained from tracing histology is used (Chau et al. 2004, Cheng et al. 1993, Finet et al. 2004, Li et al. 2005, Loree et al. 1992, Tang et al. 2004, Veress et al. 1998). Furthermore, it may aid the development and validation of plaque-vulnerability indices, which are defined from local strain, stress and YM information (Bank et al. 2000, Yang et al. 2005, Zohdi et al. 2004). Interestingly, now, the principal strain can be shown, instead of the radial strain. The principal strain is a more informative and reliable quantity, because it shows, by its definition, the maximal strain at each tissue-point and this value does not depend upon the catheter position within the lumen (Baldewsing et al. 2005). Finally, Modulography can be used to quantify *in vivo* the amount of non-linearity of plaque components by computing a series of modulograms from a series of *in vivo* measured strain elastograms, each obtained at another known pressure level.

CONCLUSION

Modulography is a new imaging method, which computes the elasticity distribution (Young's modulus) of coronary plaques from their measured strain.

- Modulography allows direct discrimination between soft and stiff plaque-components
- Modulography can be successfully applied to thin-cap fibroatheromas and heterogeneous plaques; the best results are obtained with a catheter centered in the coronary artery
- Modulography has been applied in vitro and in vivo to human atherosclerotic coronary arteries

Modulography has potential, as addition to IVUS strain elastography/palpography, to become an all-in-one tool for detecting plaques, for assessing information related to their rupture-proneness and for imaging their elastic material composition, all in vivo.

To advance Modulography into the clinic, a thorough validation study is required, as well as a pre-processing method for fully automatic assessment of proper strain elastograms in vivo.

REFERENCES

- Aglyamov S, Skovoroda AR, Rubin JM, O'Donnell M, Emelianov SY. *Model-based reconstructive elasticity imaging of deep venous thrombosis*. IEEE Trans Ultrason Ferroelectr Freq Control 2004;51:521-31.
- Aikawa M, Rabkin E, Okada Y, Voglic SJ, Clinton SK, Brinckerhoff CE, Sukhova GK, Libby P. *Lipid lowering by diet reduces matrix metalloproteinase activity and increases collagen content of rabbit atheroma: a potential mechanism of lesion stabilization*. Circulation 1998;97:2433-44.
- Baldewsing RA, Mastik F, Schaar JA, Serruys PW, van der Steen AFW. *Robustness of reconstructing the Young's modulus distribution of vulnerable atherosclerotic plaques using a parametric plaque model*. Ultrasound Med Biol 2005;31:1631-45.
- Bank AJ, Versluis A, Dodge SM, Douglas WH. *Atherosclerotic plaque rupture: a fatigue process?* Med Hypotheses 2000;55:480-4.
- Baptista J, Di Mario C, Ozaki Y, Escaned J, Gil R, de Feyter PJ, Roelandt JRTC, Serruys PW. *Impact of plaque morphology and composition on the mechanisms of lumen enlargement using intracoronary ultrasound and quantitative angiography after balloon angioplasty*. American Journal of Cardiology 1996;77:115-21.
- Barbone PE, Bamber JC. *Quantitative elasticity imaging: what can and cannot be inferred from strain images*. Phys Med Biol 2002;47:2147-64.
- Barbone PE, Gokhale NH. *Elastic modulus imaging: on the uniqueness and nonuniqueness of the elastography inverse problem in two dimensions*. Inverse Problems 2004;20:283-96.
- Beattie D, Xu C, Vito R, Glagov S, Whang MC. *Mechanical analysis of heterogeneous, atherosclerotic human aorta*. J Biomech Eng 1998;120:602-7.
- Brown BG, Zhao XQ, Sacco DE, Albers JJ. *Lipid lowering and plaque regression. New insights into prevention of plaque disruption and clinical events in coronary disease*. Circulation 1993;87:1781-91.
- Céspedes EI, Ophir J, Ponnekanti H, Maklad N. *Elastography: elasticity imaging using ultrasound with application to muscle and breast in vivo*. Ultras Imag 1993;17:73-88.
- Chandran KB, Mun JH, Choi KK, Chen JS, Hamilton A, Nagaraj A, McPherson DD. *A method for in-vivo analysis for regional arterial wall material property alterations with atherosclerosis: preliminary results*. Med Eng Phys 2003;25:289-98.
- Chau AH, Chan RC, Shishkov M, MacNeill B, Iftimia N, Tearney GJ, Kamm RD, Bouma BE, Kaazempur-Mofrad MR. *Mechanical analysis of atherosclerotic plaques based on optical coherence tomography*. Ann Biomed Eng 2004;32:1494-503.
- Cheng GC, Loree HM, Kamm RD, Fishbein MC, Lee RT. *Distribution of circumferential stress in ruptured and stable atherosclerotic lesions. A structural analysis with histopathological correlation*. Circulation 1993;87:1179-87.
- Davies MJ. *The pathophysiology of acute coronary syndromes*. Heart 2000;83:361-6.
- de Korte CL, Carlier SG, Mastik F, Doyley MM, van der Steen AFW, Serruys PW, Bom N. *Morphological and mechanical information of coronary arteries obtained with Intravascular elastography: a feasibility study in vivo*. European Heart Journal 2002;23:405-13.
- de Korte CL, Pasterkamp G, van der Steen AFW, Woutman HA, Bom N. *Characterization of plaque components using intravascular ultrasound elastography in human femoral and coronary arteries in vitro*. Circulation 2000;102:617-23.
- de Korte CL, Schaar JA, Mastik F, Serruys PW, van der Steen AFW. *Intravascular elastography: from bench to bedside*. J Interv Cardiol 2003;16:253-9.
- de Korte CL, Siervogel M, Mastik F, Strijder C, Velema E, Pasterkamp G, van der Steen AFW. *Intravascular Elastography in Yucatan pigs: validation in vivo*. European Heart Journal 2001;22:251.
- de Korte CL, van der Steen AFW, Céspedes EI, Pasterkamp G. *Intravascular ultrasound elastography of human arteries: initial experience in vitro*. Ultrasound Med Biol 1998;24:401-8.
- Doyley M, Mastik F, de Korte CL, Carlier S, Céspedes E, Serruys P, Bom N, van der Steen AFW. *Advancing intravascular ultrasonic palpation towards clinical applications*. Ultrasound Med Biol 2001;27:1471-80.
- Falk E, Shah PK, Fuster V. *Coronary plaque disruption*. Circulation 1995;92:657-71.
- Finet G, Ohayon J, Rioufol G. *Biomechanical interaction between cap thickness, lipid core composition and blood pressure in vulnerable coronary plaque: impact on stability or instability*. Coron Artery Dis 2004;15:13-20.
- Gokhale NH. *A fast iterative method for elastic modulus imaging*. Thesis 2003;

- Kanai H, Hasegawa H, Ichiki M, Tezuka F, Koiwa Y. *Elasticity imaging of atheroma with transcutaneous ultrasound: preliminary study*. *Circulation* 2003;107:3018-21.
- Kim K, Weitzel WF, Rubin JM, Xie H, Chen X, O'Donnell M. *Vascular intramural strain imaging using arterial pressure equalization*. *Ultrasound Med Biol* 2004;30:761-71.
- Konig K, Scheipers U, Pesavento A, Lorenz A, Ermerth H, Senge T. *Initial experiences with real-time elastography guided biopsies of the prostate*. *J Urol* 2005;174:115-7.
- Lee RT. *Plaque stabilization: the role of lipid lowering*. *Int J Cardiol* 2000;74 Suppl 1:S11-5.
- Leung KYE, Baldewsing RA, Mastik F, Schaar JA, Gisolf A, van der Steen AFW. *Motion Compensation for Intravascular Ultrasound Palpography*. *IEEE Trans Ultrason Ferroelectr Freq Control* 2005;(in press).
- Li ZY, Howarth S, Trivedi RA, JM UK-I, Graves MJ, Brown A, Wang L, Gillard JH. *Stress analysis of carotid plaque rupture based on in vivo high resolution MRI*. *J Biomech* 2005;
- Liu HT, Sun LZ, Wang G, Vannier MW. *Analytic modeling of breast elastography*. *Med Phys* 2003;2340-9.
- Loree HM, Kamm RD, Stringfellow RG, Lee RT. *Effects of fibrous cap thickness on peak circumferential stress in model atherosclerotic vessels*. *Circ Res* 1992;71:850-8.
- Loree HM, Tobias BJ, Gibson LJ, Kamm RD, Small DM, Lee RT. *Mechanical properties of model atherosclerotic lesion lipid pools*. *Arterioscler Thromb* 1994;14:230-4.
- Lupotti FA, Mai JJ, Pellot-Barakat C, Insana MF. *Vascular elasticity from regional displacement estimates*. *Proceedings of the 2003 IEEE International Ultrasonics Symposium* 2003;1895-8.
- Lusis AJ. *Atherosclerosis*. *Nature* 2000;407:233-41.
- Maurice RL, Brusseu E, Finet G, Cloutier G. *On the potential of the Lagrangian speckle model estimator to characterize atherosclerotic plaques in endovascular elastography: in vitro experiments using an excised human carotid artery*. *Ultrasound Med Biol* 2005a;31:85-91.
- Maurice RL, Daronat M, Ohayon J, Stoyanova E, Foster FS, Cloutier G. *Non-invasive high-frequency vascular ultrasound elastography*. *Phys Med Biol* 2005b;50:1611-28.
- Oberai AA, Gokhale NH, Doyley MM, Bamber JC. *Evaluation of the adjoint equation based algorithm for elasticity imaging*. *Phys Med Biol* 2004;49:2955-74.
- Plewes DB, Bishop J, Samani A, Sciarretta J. *Visualization and quantification of breast cancer biomechanical properties with magnetic resonance elastography*. *Phys Med Biol* 2000;45:1591-610.
- Ribbers H, Holewijn S, Blankensteijn JD, de Korte CL. *Non-invasive two dimensional elastography of the carotid artery*. *Proceedings of the 2005 IEEE International Ultrasonics Symposium* 2005;611-2.
- Rogowska J, Patel NA, Fujimoto JG, Brezinski ME. *Optical coherence tomographic elastography technique for measuring deformation and strain of atherosclerotic tissues*. *Heart* 2004;90:556-62.
- Schaar JA, De Korte CL, Mastik F, Strijder C, Pasterkamp G, Boersma E, Serruys PW, Van Der Steen AFW. *Characterizing vulnerable plaque features with intravascular elastography*. *Circulation* 2003;108:2636-41.
- Schaar JA, Regar E, Mastik F et al. *Incidence of vulnerable plaque patterns in humans: assessment with three-dimensional intravascular palpography and correlation with clinical presentation*. *Circulation* 2004;109:2716-9.
- Souchon R, Rouviere O, Gelet A, Detti V, Srinivasan S, Ophir J, Chapelon JY. *Visualisation of HIFU lesions using elastography of the human prostate in vivo: preliminary results*. *Ultrasound Med Biol* 2003;29:1007-15.
- Tang D, Yang C, Zheng J, Woodard PK, Sicard GA, Saffitz JE, Yuan C. *3D MRI-based multicomponent FSI models for atherosclerotic plaques*. *Ann Biomed Eng* 2004;32:947-60.
- Techavipoo U, Varghese T. *Improvements in elastographic contrast-to-noise ratio using spatial-angular compounding*. *Ultrasound Med Biol* 2005;31:529-36.
- Veress AI, Cornhill JF, Herderick EE, Thomas JD. *Age-related development of atherosclerotic plaque stress: a population-based finite-element analysis*. *Coron Artery Dis* 1998;9:13-9.
- Vorp DA, Rajagopal KR, Smolinski PJ, Borovetz HS. *Identification of elastic properties of homogeneous, orthotropic vascular segments in distension*. *J Biomech* 1995;28:501-12.
- Wan M, Li Y, Li J, Cui Y, Zhou X. *Strain imaging and elasticity reconstruction of arteries based on intravascular ultrasound video images*. *IEEE Trans Biomed Eng* 2001;48:116-20.
- Yang C, Tang D, Zheng J, Woodard PK, Saffitz JE, Sanchez LA, Sicard GA. *A computational plaque vulnerability index based on stress/strain local maximal values for human atherosclerotic plaque vulnerability assessment*. *Proceedings of the 2005 Summer Bioengineering Conference* 2005;
- Zohdi TI, Holzapfel GA, Berger SA. *A phenomenological model for atherosclerotic plaque growth and rupture*. *J Theor Biol* 2004;227:437-43.

DISCUSSIE EN CONCLUSIE

MOTIVATIE

Atherosclerose, een ziekte van de grotere bloedvaten, is de primaire oorzaak van hartziekten en herseninfarcten. In verweesterde samenlevingen is het de onderliggende oorzaak van ongeveer 50% van alle sterftegevallen (Luisi 2000). Acute coronaire syndromen, zoals angina pectoris (pijn op de borst), hartinfarct (beschadiging/afsterving van hartspierweefsel) of plotselinge dood door hartfalen, worden hoofdzakelijk veroorzaakt door trombus formatie als gevolg van het plotseling scheuren van vulnerabele coronaire plaques; een plaque is een (voornamelijk vette) materiaalophoping in de bloedvaatwand (Davies 2000, Falk et al. 1995). Derhalve is de detectie, karakterisering, behandeling en monitoring van deze plaques van levensbelang. Dit proefschrift beschrijft een nieuwe afbeeldingsmethode, genaamd Modulografie, voor het identificeren en karakteriseren van deze plaques op basis van hun elastische (Young's modulus) materiaal eigenschap verdeling.

Veel invasieve en niet-invasieve methoden zijn (of worden) ontwikkeld om identificatie mogelijk te maken van vulnerabele plaques of plaque-eigenschappen die ervan verdacht worden aan de vulnerabiliteit bij te dragen (**HOOFDSTUK 1**). Tot op heden is geen van deze methoden in staat om, op zichzelf, alle vulnerabiliteit eigenschappen te identificeren. Hieronder vallen intravasculair ultrageluid (IVUS)-Elastografie/Palpografie en Modulografie, die tegenwoordig de enige methoden zijn die in vivo mechanische plaque informatie kunnen verschaffen.

Het vergaren van mechanische informatie is van levensbelang, aangezien het scheuren van een plaque uiteindelijk een mechanisch verschijnsel is; het scheuren van de kap van de plaque gebeurt wanneer de kap de spanning niet kan weerstaan, die veroorzaakt wordt door de pulserende bloeddruk. Daarnaast kan mechanische informatie helpen bij het optimaal bepalen van een goede interventiestrategie (Baptista et al. 1996) aangezien ook deze van mechanische aard is. Bovendien is het zo dat farmaceutische behandelingen mechanische stabilisatie van de plaque bewerkstelligen, bijv. door het verstijven of reduceren van de vetophoping in de plaque (Aikawa et al. 1998, Lee 2000, Loree et al. 1994), hetgeen inhoudt dat de efficiëntie van deze behandelingen kan worden gekwantificeerd door het meten van mechanische informatie.

Modulografie produceert een modulogram van een plaque (dwz. een Young's modulus plaatje) door het oplossen van het inverse elasticiteitsprobleem. Dit probleem bestaat uit het vinden van 'het' modulogram dat een gegeven vervormingselastogram (dwz. een vervormingsplaatje) genereert. Bij Modulografie wordt het vervormingsplaatje bepaald met behulp van IVUS Elastografie, wat op dit moment de enige klinisch-beschikbare techniek is dat vervormingsplaatjes van coronaire bloedvaten in vivo kan verschaffen (de Korte et al. 2001, 2002, 2003). Het oplossen van het inverse elasticiteitsprobleem voor coronaire plaques met behulp van IVUS-bepaalde lokale vervorming (rek of verplaatsing) is een andere en moeilijke taak, in vergelijking met het inverse elasticiteitsprobleem voor andere organen zoals de borsten (Céspedes et al. 1993), waarbij, niet-invasieve, ultrageluid-afgeleide informatie op een gecontroleerde wijze vergaard en gebruikt kan worden. Dit komt door de volgende factoren: (i) plaques hebben een complexe, heterogene materiaal samenstelling, (ii) er is een inherente afname van vervorming vanaf het lumen richting de media rand, hetgeen het gevolg is van de inherente spanningsafname, veroorzaakt door de ronde vorm van de vaatwand, (iii) er is geen controle van de primaire vervormingsbron (de pulserende bloeddruk) en het meetapparaat (de katheter), hetgeen de toepassing beperkt van aanwezige vervormingsprocessing methoden die gebruik maken van controle van bron en apparaat, (iv) de gebruikte processing algoritme (de Korte et al. 1998) meet alleen de radiale component van de vervorming met een spatiële resolutie van slechts 200 μm .

Tot slot, in het algemeen is het niet-gelimiteerde inverse elasticiteitsprobleem in 2D slecht-gesteld (Barbone et al. 2002, 2004). Dit betekent dat er ofwel (i) geen unieke modulogram bestaat voor een gemeten vervormingsplaatje ofwel dat er (ii) wel een unieke modulogram bestaat, maar deze niet stabiel verkregen kan worden vanwege de ruis in de vervormingsmeting.

Tot op heden zijn er slechts een paar methoden voorgesteld om het inverse elasticiteitsprobleem voor bloedvatwanden op te lossen vanuit (gesimuleerde) ultrageluid-afgeleide vervorming, bijv., (Aglyamov et al. 2004, Beattie et al. 1998, Chandran et al. 2003, Gokhale 2003, Kanai et al. 2003, Kim et al. 2004, Lupotti et al. 2003, Soualmi et al. 1997, Vorp et al. 1995, Wan et al. 2001). Voor geen van deze methoden werd aangehouden dat ze zouden werken als de cross-sectionele vervormingsverdeling van een willekeurige, heterogene, atherosclerotische, coronaire plaque wordt gebruikt als input. Het ter beschikking hebben van een methode die werkt voor in vivo vervormingsdata, gemeten met IVUS Elastography/Palpography, zou betekenen dat onderzoekers eindelijk een alles-in-één modaliteit hebben dat in staat is om in vivo (i) vulnerabele plaques te detecteren (Schaar et al. 2004), (ii) informatie te vergaren die gerelateerd is aan hun scheur-gevoeligheid (Schaar et al. 2003) en (iii) hun elastische materiaal samenstelling af te beelden.

Gestimuleerd door dit vooruitzicht en door de resultaten van eerdere methoden hebben wij een nieuwe aanpak ontwikkeld, genaamd Modulografie (een samentrekking van 'modulus' en 'grafie'), die uitermate geschikt is om het inverse elasticiteitsprobleem op te lossen vanuit in vivo gemeten vervorming van coronaire plaques. Vergeleken met andere benaderingen heeft onze aanpak twee belangrijke verschillen (i) er wordt gebruik gemaakt van zoveel mogelijk a priori informatie die automatisch afgeleid kan worden van het echogram en vervormingsplaatje en (ii) in eerste instantie wordt de aandacht gelegd op de grootste klasse van vulnerabele plaques, namelijk de dunne-kap fibroatheromas (TCFAs), welke gemodelleerd kunnen worden als een geometrisch simpel structuur. Door deze geometrische a priori informatie te gebruiken werd het inverse elasticiteitsprobleem zodanig gelimiteerd, waardoor er in vivo een praktisch-buikbaar en min of meer uniek modulogram verkregen kon worden op een stabiele manier.

De ontwikkeling van Modulografie begon met het eerst oplossen van het voorwaartse elasticiteitsprobleem, vervolgens het oplossen van het inverse elasticiteitsprobleem voor TCFAs en, tenslotte, het maken van generalisaties voor onze oplossingsaanpak voor TCFAs, om ervoor te zorgen dat Modulografie van willekeurige plaques mogelijk wordt.

VOORWAARTSE PROBLEEM

De eerste stap bij het oplossen van het inverse elasticiteitsprobleem is het oplossen van het voorwaartse elasticiteitsprobleem. Het voorwaartse elasticiteitsprobleem bestaat uit het vinden van een geschikt constitutief materiaal model voor atherosclerotische vaatwanden, dat gebruikt kan worden om hun vervorming te berekenen. Voor dit doel hebben wij een eindige elementen computer-model (FEM) voorgesteld, waarin het plaque-weefsel gemodelleerd werd als een lineair elastisch, isotroop, volumetrisch onsamendrukbaar, materiaal in een vlakke-tek toestand (**HOOFDSTUK 2**). Er is aangetoond dat deze FEM de quasi-statische, kleine-vervorming, van coronaire plaques voldoende kan modelleren. Hiertoe werden computer-gesimuleerde elastogrammen vergeleken met gemeten elastogrammen. Gemeten elastogrammen werden berekend op basis van IVUS radio-frequente data gemeten in vitro van zes objecten: een vaatwand-nabootsend fantoom en vijf humane atherosclerotische coronaire plaques. Een FEM was gemaakt voor elk object en gebruikt om een elastogram te simuleren; materiaal eigenschappen en geometrie van de FEM werden verkregen van de coupes van de objecten. De vergelijking werd gedaan op basis van hoge-vervorming gebieden (HSRs) aangezien van zulke gebieden is aangetoond dat ze plaques bevatten die de karakteristieke eigenschappen vertonen van vulnerabele plaques. Acht HSRs werden automatisch geïdentificeerd van de vijf vaatwanden. Statistische tests toonden aan dat er geen significant verschil was tussen een gesimuleerd en corresponderend gemeten elastogram met betrekking tot de lokatie, oppervlakte en gemiddelde vervormingswaarde van een HSR.

Vervolgens werd de FEM gebruikt om te begrijpen en kwantificeren hoe gemeten elastogrammen afhangen van (i) the elastische materiaal eigenschappen en (ii) de morfologie van vulnerabele plaque componenten alsook (iii) de gebruikte katheter positie (**HOOFDSTUK 3**). Hiertoe werden IVUS elastogrammen gemeten van een bloedvat-nabootsend fantoom met een zachte plaque ingebed in een stijve wand, en een humane coronaire bloedvat met een vulnerabele plaque. Daarna werden FEMs gemaakt om vervormingselastogrammen te simuleren van dezelfde objecten. In deze FEMs werden de volgende parameters gevarieerd: Young's modulus (E), Poisson's ratio (ν) in het bereik 0.49-0.4999, katheter positie (translatie van 0.8 mm), en kap dikte (t) in het bereik 50-350 μm . Bij alle variaties werd de resulterende maximale radiale vervorming (PRS) bepaald en gevisualiseerd. Deze studie toonde aan dat vervormingselastogrammen van vulnerabele plaques (i) sterk afhangen van de Young's modulus van de vetophoping en de kap, maar niet van de Poisson's ratio, (ii) verschillende katheter posities resulteerde in verschillende elastogrammen, desalniettemin bleven de diagnostisch belangrijke hoge-vervormingsgebieden in de schouder van de vetophoping detecteerbaar en (iii) PRS nam toe wanneer de kap verzwakte of in dikte afnam. Deze eigenschappen, behalve (ii), zijn gunstig voor het oplossen van het inverse elasticiteitsprobleem.

INVERSE PROBLEEM

Nu er een FEM tot stand is gebracht die vervormingelastogrammen kan simuleren en er opgemerkt is dat de FEM hoofdzakelijk afhangt van de Young's modulus distributie, is de volgende stap het oplossen van het inverse elasticiteitsprobleem. De initiële doelstelling was het ontwikkelen van een oplossingsaanpak die het inverse elasticiteitsprobleem zo stabiel mogelijk maakt en de oplossing ervan uiterst eenduidig. Hiertoe ontwikkelden wij een Modulografie-aanpak die speciaal geschikt was voor dunne-kap finbroatheromas (TCFAs), d.w.z., plaques bestaande uit een media gebied rondom een vetophoping die afgedekt is door een dunne fibreuse kap (**HOOFDSTUK 4**). Een plaque's modulogram wordt als volgt verkregen van een gemeten vervormingselastogram. Een optimalisatie algoritme probeert een gesimuleerde vervormingsplaatje, berekend met een circulaire parametrische eindige elementen computer-model (PFEM) representatie van een TCFA, te laten lijken op de gemeten vervormingsplaatje, d.m.v. het herhaaldelijk aanpassen van de PFEM geometrie en materiaal parameters. De geometrie parameters zijn de centrum coördinaten en straal van de cirkels, die de randen van TCFA media, vetophoping en kap gebied beschrijven. De materiaal parameter voor elk gebied is een Young's modulus, E_{MEDIA} , E_{LIPID} and E_{CAP} , respectievelijk. De methode is succesvol getest met computer-gesimuleerde TCFAs ($n=2$), één gedefinieerd met cirkels, de ander door het overtrekken van TCFA histologie, en additioneel op een vaatwand-nabootsend fantoom ($n=1$), bestaande uit een stijve wand met daarin een eccentric, zacht gebied. Als laatste werd het toegepast op humane coronaire plaques in vitro ($n=1$) en in vivo ($n=1$). Deze studie toonde voor het eerste uitvoerbaarheid aan van Modulografie, met het circulaire PFEM, op verscheidene vulnerabele plaques, inclusief een in vivo plaque.

Zoals eerder is vastgesteld hangt een plaque's vervormingselastogram hoofdzakelijk af van de volgende factoren: (i) de materiaal eigenschap en (ii) morfologie van de plaque componenten, (iii) de katheter positie in het bloedvat en (iv) de meet ruis. Vandaar dat wij onderzocht hebben welke plaques correct en robuust gereconstrueerd konden worden met Modulografie wanneer deze factoren gevarieerd werden (**HOOFDSTUK 5**). Hiertoe werd een standaard plaque gedefinieerd als zijnde de modulogram die gereconstrueerd was van een gemeten vervormingselastogram van een humane coronaire plaque. Deze standaard plaque werd gebruikt om verschillende vervormingselastogrammen te computer-simuleren en daarbij het volgende te variëren (i) de geometrie en materiaal eigenschappen van zijn plaque componenten, (ii) de katheter positie en (iii) het niveau van toegevoegde vervormingsruis. Vervolgens werd er voor elk elastogram een reconstructie uitgevoerd. De robuustheid werd geëvalueerd door het kwantificeren van de correct gereconstrueerde grootte, vorm en Young's modulus van elk plaque-component gebied alsook de minimale kap dikte. De resultaten van deze studie toonden aan dat TCFAs adequaat gereconstrueerd kunnen worden: des te dunner en stijver de kap of des te zachter en groter de vetophoping, des te beter is de reconstructie van deze componenten en minimale kap dikte. Daarnaast bleken reconstructies (i) onafhankelijk van de katheter positie en (ii) onafhankelijk van de vervormingsruis. Als zodanig heeft Modulografie, met het circulaire PFEM, de potentie om robuust en kwantitatief atherosclerose in vivo te monitoren.

GENERALISATIE

Naast een TCFA samenstelling kan een atherosclerotische plaque ook een meer complexe, heterogene samenstelling hebben, bestaande uit een mix van plaque componenten zoals vet, fibreus weefsel, gecalcificeerde bolletjes of weefsel verzwakt door extra-cellulaire matrix afbraak door macrofagen. Het oplossen van het inverse elasticiteitsprobleem van zulke complexen vereist een andere, meer lokale benadering, bijv. Soualmi et al. (1997), welke geen restrictie legt op de structuur van plaque componenten. Alhoewel Soualmi's aanpak geen a priori informatie vereist, kan het grote aantal Young's moduli dat gereconstrueerd dient worden, een succesvolle convergentie van het minimaliseringsalgoritme verhinderen.

Om succesvol Modulografie te doen met willekeurige atherosclerotische plaques, hebben wij een twee-staps aanpak gebruikt. In de eerste stap generaliseerden wij het circulaire PFEM en noemen het een Bézier PFEM (**HOOFDSTUK 6**). Dit Bézier PFEM (i) heeft flexibele Bézier curves als distale randen van het PFEM vetophopingsgebied en kap gebied, i.p.v. cirkel randen en (ii) gebruikt als vaatwand randen de werkelijke lumen en media contour, zoals te bepalen is uit het echogram. De geometrie parameters zijn nu de controle-punten van elke Bézier curve. The component gebieden worden nog steeds homogeen verondersteld en hun stijfheid wordt gekarakteriseerd door een Young's modulus. Modulografie van vervormingselastogrammen die waren (i) gesimuleerd met een computer-TCFA die afgeleid was van histologie, (ii) gemeten van een vaatwand-nabootsend fantoom met een zachte vetophoping en (iii) gesimuleerd met een computer-TCFA waarbij de complexiteit van de randen van de plaque-componenten werd vergroot, toonden aan dat de Bézier PFEM leidde tot een accurater en betrouwbaarder modulogram, voor een veel grotere collectie van gecompileerde TCFA plaque-component morfologieën, dan bij gebruikmaking van het circulaire PFEM. Het opti-

male aantal controle-punten bleek vijf te zijn. Tenslotte bleek de methode stabiel te zijn ondanks dat er meer parameters werden gebruikt (bijv. 19 wanneer er vijf controle-punten worden gebruikt voor elke curve) dan bij de circulaire PFEM (slechts 9).

Tijdens de laatste stap werd het Modulografie raamwerk, dat gebruik maakte van de Bézier PFEM, gegeneraliseerd om succesvolle toepassing op willekeurige heterogene atherosclerotische plaques mogelijk te maken, en wel als volgt. (i) Een "gecorrigeerd" radiale vervormingselastogram werd gebruikt om Modulografie minder gevoelig te maken voor de positie van de katheter, (ii) de gemeten "gecorrigeerde" vervormingselastogram werd gebruikt om automatisch initiële Young's modulus distributies te definiëren en (iii) een samenvoegingsprocedure werd gebruikt om een heterogene modulogram te verkrijgen vanuit individueel gemaakte modulogrammen (**HOOFDSTUK 7**). Deze gegeneraliseerde methode werd geëvalueerd en zijn optimale instellingen werden bepaald door de methode toe te passen op eindige elementen computer-gesimuleerde elastogrammen van vier realistische, uit histologie-afgeleide, humane coronaire plaques, twee leken op een TCFA, de anderen hadden een aantal zachte en stijve gebieden. De relatieve fout in gereconstrueerde zachte-weefsel oppervlak (STA) en zachte-weefsel overlap (STO) werd gebruikt als performance maat. Tenslotte werd de methode toegepast op twee elastogrammen, één gemeten in vitro en de andere in vivo, van humane atherosclerotische coronaire bloedvaten. De methode benaderde de werkelijke Young's modulus verdeling van alle gesimuleerde plaques; gemiddelde[%](standaard afwijking[%]) fout in STA=27(21) en in STO=41(16), ongeacht de katheter positie in het bloedvat; een gecentreerde katheter gaf het beste resultaat met STA=18(11) en STO=35(12). The in vitro reconstructie was in overeenstemming met de histologie.

MODULOGRAFIE GEREEDMAKEN VOOR KLINISCH GEBRUIK

Modulografie heeft in zijn huidige vorm al veelbelovende resultaten getoond. Desalniettemin is het volgende vervolgonderzoek en ontwikkeling nodig om van Modulografie een volledig automatische, klinische onderzoeksgereedschap te maken voor in vivo plaque karakterisatie: (i) Gebruikmaking van een robuuste, volledig-automatische lumen en media contourdetectie algoritme; dit zal een volledig-automatische creatie van vervormingelastogrammen en modulogrammen mogelijk maken. (ii) Ontwikkeling van een robuuste vervorming samenstellingsalgoritme voor het maken van een enkel samengestelde vervormingselastogram per hartcyclus, vanuit een serie vervormingselastogrammen verkregen in deze cyclus; dit zal het aantal geldige vervormingsschattingen en de signaal-ruis verhouding doen toenemen. Deze ontwikkeling zal in grote mate geïnspireerd worden door de samenstellingsalgoritme voor Palpografie (Doyley et al. 2001, Leung et al. 2005). (iii) Bepaling van de optimale instellingen voor Modulografie voor willekeurige in vivo situaties; voor willekeurige situaties, zullen deze instellingen afhankelijk gemaakt moeten worden van de metingen (pulserende bloeddruk en vervorming) op een geautomatiseerde wijze. (iv) Sensitiviteit en specificiteit studies in vitro en/of in vivo met een grote populatie.

Modulografie kan verder verbeterd worden op de volgende aspecten. (i) Het verhogen van de uniciteit van de modulogrammen. Dit kan bewerkstelligd worden door meer gemeten vervormingscomponenten te gebruiken (bijv. laterale of schuif vervormingscomponent) (Maurice et al. 2005b, Ribbers et al. 2005, Techavipoo et al. 2005) aangezien dan meer vervormingskenmerken gebruikt kunnen worden bij de minimalisatie van een aangepaste root-mean-squared (RMS) error functie. (ii) Het verhogen van de betrouwbaarheid (dwz. een lagere RMS-error) van de modulogram. Dit kan worden bewerkstelligd door het nabewerken van de modulogram met een lokale reconstructie methode die de Young's modulus lokaal aanpast. (iii) Reduceren van de berekeningstijd, bijv. door het gebruik van adjoint-algoritmen (Oberai et al. 2004). Deze gebruiken slechts één voorwaartse FEM berekening om een parameter-vector aanpassing te bepalen, terwijl andere algoritmen, inclusief het algoritme dat in dit proefschrift wordt gebruikt, tenminste zoveel voorwaartse FEM berekeningen gebruiken als dat er parameters zijn die aangepast moeten worden. Het is echter de vraag of zulke algoritmen aangepast kunnen worden voor de geometrisch-gelimiteerde aanpak die Modulografie gebruikt.

POTENTIËLE TOEPASSINGEN EN IMPLICATIES

Modulografie is een nieuwe methode om weefsel te karakteriseren en potentieel geschikt voor klinische toepassingen zoals het monitoren van atherosclerose en het kwantificeren van farmaceutisch-geïnduceerde plaque stabilisatie (Aikawa et al. 1998, Brown et al. 1993, Loree et al. 1994). Modulografie kan ook in combi-

natie gebruikt worden met elke andere beeldvormingstechniek dat in staat is om vervorming te meten, bijv. (Intra)vascular OCT elastography (Rogowska et al. 2004), MRI elastography (Plewes et al. 2000). Aangezien Modulografie alleen een deformatie elastogram als input nodig heeft, kan het ook toegepast worden op andere organen waarvan één of meerdere deformatie componenten gemeten kunnen worden, zoals de borsten (Liu et al. 2003, Plewes et al. 2000) en het prostaat (Konig et al. 2005, Souchon et al. 2003) of oppervlakkige bloedvaten, zoals de femoraal (de Korte et al. 2000) of de carotis (Maurice et al. 2005a, Ribbers et al. 2005); uiteraard, na het aanpassen van de binnen/buiten rand van de PFEM. Aangezien Modulografie, als toevoeging aan IVUS Elastografie, de in vivo plaque morfologie, vervorming en Young's modulus geeft, kan er een in vivo eindige elementen computer-analyse worden gemaakt. Dit kan een meer betrouwbare analyse zijn dan wanneer er a priori Young's modulus waarden, plaque model of structuur afgeleid uit histologie, worden gebruikt (Chau et al. 2004, Cheng et al. 1993, Finet et al. 2004, Li et al. 2005, Loree et al. 1992, Tang et al. 2004, Veress et al. 1998). Bovendien kan Modulografie de ontwikkeling en validatie stimuleren van plaque-vulnerabiliteit indices, die gebaseerd zijn op lokale vervorming, spanning en Young's modulus informatie (Bank et al. 2000, Yang et al. 2005, Zohdi et al. 2004). Een interessant gegeven is dat er nu de principale vervorming getoond kan worden i.p.v. de radiale vervorming. De principale vervorming is een meer informatiever en betrouwbaarder grootheid, omdat deze, per definitie, de maximale vervorming aangeeft in elk weefsel-punt en deze niet afhangt van de katheter positie in het bloedvat (Baldewising et al. 2005). Tenslotte kan Modulografie gebruikt worden om in vivo de niet-lineariteit te bepalen van plaque-componenten door een serie modulogrammen te bepalen vanuit een serie in vivo gemeten vervormingselastogrammen, elk verkregen bij een ander bloeddruk-niveau.

CONCLUSIE

Modulografie is een nieuwe beeldvormende methode, die de elasticiteitsverdeling (Young's modulus) van coronaire plaques bepaalt op basis van hun gemeten vervorming.

- Modulografie geeft directe onderscheiding van zachte en stijve plaque-componenten
- Modulografie kan succesvol toegepast worden op dunne-kap fibroatheromas en heterogene plaques; het beste resultaat wordt verkregen wanneer de katheter gecentreerd is in het coronaire bloedvat
- Modulografie is toegepast in vitro en in vivo op humane atherosclerotische coronaire bloedvaten

Modulografie heeft potentie, als toevoeging aan IVUS Elastografie/Palpografie, om een alles-in-één gereedschap te worden om plaques te detecteren, om informatie te vergaren die gerelateerd is aan hun scheur-gevoeligheid en om hun elastische materiaalsamenstelling te visualiseren, dit alles in vivo.

Om Modulografie in de kliniek toegepast te krijgen is er een uitvoerige validatie studie nodig, alsook een pre-processing methode om, in vivo en volledig automatisch, correcte vervormingselastogrammen te vergaren.

REFERENTIES

- Aglyamov S, Skovoroda AR, Rubin JM, O'Donnell M, Emelianov SY. *Model-based reconstructive elasticity imaging of deep venous thrombosis*. IEEE Trans Ultrason Ferroelectr Freq Control 2004;51:521-31.
- Aikawa M, Rabkin E, Okada Y, Voglic SJ, Clinton SK, Brinckerhoff CE, Sukhova GK, Libby P. *Lipid lowering by diet reduces matrix metalloproteinase activity and increases collagen content of rabbit atheroma: a potential mechanism of lesion stabilization*. Circulation 1998;97:2433-44.
- Baldewsing RA, Mastik F, Schaar JA, Serruys PW, van der Steen AFW. *Robustness of reconstructing the Young's modulus distribution of vulnerable atherosclerotic plaques using a parametric plaque model*. Ultrasound Med Biol 2005;31:1631-45.
- Bank AJ, Versluis A, Dodge SM, Douglas WH. *Atherosclerotic plaque rupture: a fatigue process?* Med Hypotheses 2000;55:480-4.
- Baptista J, Di Mario C, Ozaki Y, Escaned J, Gil R, de Feyter PJ, Roelandt JRTC, Serruys PW. *Impact of plaque morphology and composition on the mechanisms of lumen enlargement using intracoronary ultrasound and quantitative angiography after balloon angioplasty*. American Journal of Cardiology 1996;77:115-21.
- Barbone PE, Bamber JC. *Quantitative elasticity imaging: what can and cannot be inferred from strain images*. Phys Med Biol 2002;47:2147-64.
- Barbone PE, Gokhale NH. *Elastic modulus imaging: on the uniqueness and nonuniqueness of the elastography inverse problem in two dimensions*. Inverse Problems 2004;20:283-96.
- Beattie D, Xu C, Vito R, Glagov S, Whang MC. *Mechanical analysis of heterogeneous, atherosclerotic human aorta*. J Biomech Eng 1998;120:602-7.
- Brown BG, Zhao XQ, Sacco DE, Albers JJ. *Lipid lowering and plaque regression. New insights into prevention of plaque disruption and clinical events in coronary disease*. Circulation 1993;87:1781-91.
- Céspedes EI, Ophir J, Ponnekanti H, Maklad N. *Elastography: elasticity imaging using ultrasound with application to muscle and breast in vivo*. Ultras Imag 1993;17:73-88.
- Chandran KB, Mun JH, Choi KK, Chen JS, Hamilton A, Nagaraj A, McPherson DD. *A method for in-vivo analysis for regional arterial wall material property alterations with atherosclerosis: preliminary results*. Med Eng Phys 2003;25:289-98.
- Chau AH, Chan RC, Shishkov M, MacNeill B, Iftimia N, Tearney GJ, Kamm RD, Bouma BE, Kaazempur-Mofrad MR. *Mechanical analysis of atherosclerotic plaques based on optical coherence tomography*. Ann Biomed Eng 2004;32:1494-503.
- Cheng GC, Loree HM, Kamm RD, Fishbein MC, Lee RT. *Distribution of circumferential stress in ruptured and stable atherosclerotic lesions. A structural analysis with histopathological correlation*. Circulation 1993;87:1179-87.
- Davies MJ. *The pathophysiology of acute coronary syndromes*. Heart 2000;83:361-6.
- de Korte CL, Carlier SG, Mastik F, Doyley MM, van der Steen AFW, Serruys PW, Bom N. *Morphological and mechanical information of coronary arteries obtained with Intravascular elastography: a feasibility study in vivo*. European Heart Journal 2002;23:405-13.
- de Korte CL, Pasterkamp G, van der Steen AFW, Woutman HA, Bom N. *Characterization of plaque components using intravascular ultrasound elastography in human femoral and coronary arteries in vitro*. Circulation 2000;102:617-23.
- de Korte CL, Schaar JA, Mastik F, Serruys PW, van der Steen AFW. *Intravascular elastography: from bench to bedside*. J Interv Cardiol 2003;16:253-9.
- de Korte CL, Siervogel M, Mastik F, Strijder C, Velema E, Pasterkamp G, van der Steen AFW. *Intravascular Elastography in Yucatan pigs: validation in vivo*. European Heart Journal 2001;22:251.
- de Korte CL, van der Steen AFW, Céspedes EI, Pasterkamp G. *Intravascular ultrasound elastography of human arteries: initial experience in vitro*. Ultrasound Med Biol 1998;24:401-8.
- Doyley M, Mastik F, de Korte CL, Carlier S, Céspedes E, Serruys P, Bom N, van der Steen AFW. *Advancing intravascular ultrasonic palpation towards clinical applications*. Ultrasound Med Biol 2001;27:1471-80.
- Falk E, Shah PK, Fuster V. *Coronary plaque disruption*. Circulation 1995;92:657-71.
- Finet G, Ohayon J, Rioufol G. *Biomechanical interaction between cap thickness, lipid core composition and blood pressure in vulnerable coronary plaque: impact on stability or instability*. Coron Artery Dis 2004;15:13-20.
- Gokhale NH. *A fast iterative method for elastic modulus imaging*. Thesis 2003;

- Kanai H, Hasegawa H, Ichiki M, Tezuka F, Koiwa Y. *Elasticity imaging of atheroma with transcutaneous ultrasound: preliminary study*. Circulation 2003;107:3018-21.
- Kim K, Weitzel WF, Rubin JM, Xie H, Chen X, O'Donnell M. *Vascular intramural strain imaging using arterial pressure equalization*. Ultrasound Med Biol 2004;30:761-71.
- Konig K, Scheipers U, Pesavento A, Lorenz A, Ermerth H, Senge T. *Initial experiences with real-time elastography guided biopsies of the prostate*. J Urol 2005;174:115-7.
- Lee RT. *Plaque stabilization: the role of lipid lowering*. Int J Cardiol 2000;74 Suppl 1:S11-5.
- Leung KYE, Baldewsing RA, Mastik F, Schaar JA, Gisolf A, van der Steen AFW. *Motion Compensation for Intravascular Ultrasound Palpography*. IEEE Trans Ultrason Ferroelectr Freq Control 2005;(in press).
- Li ZY, Howarth S, Trivedi RA, JM UK-I, Graves MJ, Brown A, Wang L, Gillard JH. *Stress analysis of carotid plaque rupture based on in vivo high resolution MRI*. J Biomech 2005;
- Liu HT, Sun LZ, Wang G, Vannier MW. *Analytic modeling of breast elastography*. Med Phys 2003;2340-9.
- Loree HM, Kamm RD, Stringfellow RG, Lee RT. *Effects of fibrous cap thickness on peak circumferential stress in model atherosclerotic vessels*. Circ Res 1992;71:850-8.
- Loree HM, Tobias BJ, Gibson LJ, Kamm RD, Small DM, Lee RT. *Mechanical properties of model atherosclerotic lesion lipid pools*. Arterioscler Thromb 1994;14:230-4.
- Lupotti FA, Mai JJ, Pellot-Barakat C, Insana MF. *Vascular elasticity from regional displacement estimates*. Proceedings of the 2003 IEEE International Ultrasonics Symposium 2003;1895-8.
- Lusis AJ. Atherosclerosis. Nature 2000;407:233-41.
- Maurice RL, Brusseu E, Finet G, Cloutier G. *On the potential of the Lagrangian speckle model estimator to characterize atherosclerotic plaques in endovascular elastography: in vitro experiments using an excised human carotid artery*. Ultrasound Med Biol 2005a;31:85-91.
- Maurice RL, Daronat M, Ohayon J, Stoyanova E, Foster FS, Cloutier G. *Non-invasive high-frequency vascular ultrasound elastography*. Phys Med Biol 2005b;50:1611-28.
- Oberai AA, Gokhale NH, Doyley MM, Bamber JC. *Evaluation of the adjoint equation based algorithm for elasticity imaging*. Phys Med Biol 2004;49:2955-74.
- Plewes DB, Bishop J, Samani A, Sciarretta J. *Visualization and quantification of breast cancer biomechanical properties with magnetic resonance elastography*. Phys Med Biol 2000;45:1591-610.
- Ribbers H, Holewijn S, Blankensteijn JD, de Korte CL. *Non-invasive two dimensional elastography of the carotid artery*. Proceedings of the 2005 IEEE International Ultrasonics Symposium 2005;611-2.
- Rogowska J, Patel NA, Fujimoto JG, Brezinski ME. *Optical coherence tomographic elastography technique for measuring deformation and strain of atherosclerotic tissues*. Heart 2004;90:556-62.
- Schaar JA, De Korte CL, Mastik F, Strijder C, Pasterkamp G, Boersma E, Serruys PW, Van Der Steen AFW. *Characterizing vulnerable plaque features with intravascular elastography*. Circulation 2003;108:2636-41.
- Schaar JA, Regar E, Mastik F et al. *Incidence of vulnerable plaque patterns in humans: assessment with three-dimensional intravascular palpography and correlation with clinical presentation*. Circulation 2004;109:2716-9.
- Souchon R, Rouviere O, Gelet A, Detti V, Srinivasan S, Ophir J, Chapelon JY. *Visualisation of HIFU lesions using elastography of the human prostate in vivo: preliminary results*. Ultrasound Med Biol 2003;29:1007-15.
- Tang D, Yang C, Zheng J, Woodard PK, Sicard GA, Saffitz JE, Yuan C. *3D MRI-based multicomponent FSI models for atherosclerotic plaques*. Ann Biomed Eng 2004;32:947-60.
- Techavipoo U, Varghese T. *Improvements in elastographic contrast-to-noise ratio using spatial-angular compounding*. Ultrasound Med Biol 2005;31:529-36.
- Veress AI, Cornhill JF, Herderick EE, Thomas JD. *Age-related development of atherosclerotic plaque stress: a population-based finite-element analysis*. Coron Artery Dis 1998;9:13-9.
- Vorp DA, Rajagopal KR, Smolinski PJ, Borovetz HS. *Identification of elastic properties of homogeneous, orthotropic vascular segments in distension*. J Biomech 1995;28:501-12.
- Wan M, Li Y, Li J, Cui Y, Zhou X. *Strain imaging and elasticity reconstruction of arteries based on intravascular ultrasound video images*. IEEE Trans Biomed Eng 2001;48:116-20.
- Yang C, Tang D, Zheng J, Woodard PK, Saffitz JE, Sanchez LA, Sicard GA. *A computational plaque vulnerability index based on stress/strain local maximal values for human atherosclerotic plaque vulnerability assessment*. Proceedings of the 2005 Summer Bioengineering Conference 2005;
- Zohdi TI, Holzapfel GA, Berger SA. *A phenomenological model for atherosclerotic plaque growth and rupture*. J Theor Biol 2004;227:437-43.

PART VI
APPENDICES

APPENDIX A: LINEAR ELASTICITY THEORY AND TISSUE DEFORMATION MODEL

Mathematical models, based on physical principles and laws (e.g., Newton's laws) have been developed to approximate the real behaviour of matter (e.g., the artery deformation) under influence of external forces (e.g., pulsating blood pressure). Newton's second law states that any body is in equilibrium with its external forces. For (semi-) static problems (e.g., artery deformation at certain pressure) and negligible external forces (e.g., gravitation on artery), this can be mathematically stated as

$$\sum_{j=1}^3 \frac{\partial \sigma_{ij}}{\partial x_j} = 0 \quad i = 1, 2, 3 \quad (1)$$

where a subscript i or j refers to respectively the i -th or j -th Cartesian coordinate axis. σ_{ij} is the (i,j) -th component of the second order symmetric stress tensor and x_j is the j -th space coordinate. $\frac{\partial f}{\partial t}$ means the partial derivative of function f to variable t . This equation must be satisfied in each point of the body. When external force is applied to the body, displacement and strains will result. For small displacements u_i and strains ε_{ij} , the following linear relation is then valid:

$$\varepsilon_{ij} = \frac{1}{2} \left\{ \frac{\partial u_i}{\partial x_j} + \frac{\partial u_j}{\partial x_i} \right\} \quad i, j = 1, 2, 3 \quad (2)$$

The part in any elasticity model that has to be determined experimentally is the used constitutive relation (Atanackovic TM and Guran A. *Theory of elasticity, for scientists and engineers*. Boston, Birkhauser; 2000).

This relation defines how the tissue locally deforms (causing strains ε_{ij}) when subjected to internal stresses (σ_{ij}). The most general linear relation, valid for small strains, is

$$\sigma_{ij} = \sum_{k,l=1}^3 C_{ijkl} \varepsilon_{kl} \quad i, j = 1, 2, 3 \quad (3)$$

where each of the 81 C_{ijkl} are material parameters of which only 21 are really independent due to stress and strain symmetries and strain-energy considerations. Increasing the number of material symmetries of the tissue decreases the number of material parameters. For example, transversely isotropic material has the same material properties in a certain plane, which differ from the material properties in the perpendicular direction (e.g. cortical bone). Such material can be described by using only five material parameters. Furthermore, when the tissue is isotropic in all directions, there is no preferred material deformation direction and therefore, only two material parameters are needed. This reduces the constitutive relation to

$$\sigma_{ij} = \lambda(\varepsilon_{11} + \varepsilon_{22} + \varepsilon_{33})\delta_{ij} + 2\mu\varepsilon_{ij} \quad i, j = 1, 2, 3 \quad (4)$$

where $\mu = E/\{2(1+\nu)\}$ and $\lambda = E\nu/\{(1+\nu)(1-2\nu)\}$ are the Lamé material parameters in which E is the Young's modulus and ν is the Poisson's ratio. De Kronecker delta symbol δ_{ij} is 1 when $i=j$, otherwise 0. Assuming that the tissue is almost or totally incompressible, $\nu \approx 0.5$, reduces this relation to

$$\sigma_{ij} = -P\delta_{ij} + \frac{2}{3}E\varepsilon_{ij} \quad i, j = 1, 2, 3 \quad (5)$$

where P is the static pressure in the tissue. This is the simplest model available and depends on only one material parameter E . Incompressibility is mathematically stated as

$$\frac{\partial u_1}{\partial x_1} + \frac{\partial u_2}{\partial x_2} + \frac{\partial u_3}{\partial x_3} = 0 \quad (6)$$

which physically models zero-volume change. Combination of equations (1), (2) and (5) results in four equations in four unknowns $u_1 = u_1(x_1, x_2, x_3)$, $u_2 = u_2(x_1, x_2, x_3)$, $u_3 = u_3(x_1, x_2, x_3)$ and $P = P(x_1, x_2, x_3)$:

$$\frac{\partial P}{\partial x_i} + \frac{2}{3} \frac{\partial}{\partial x_i} \left\{ E \frac{\partial u_i}{\partial x_i} \right\} + \frac{2}{3} \sum_{j=1, j \neq i}^3 \frac{\partial}{\partial x_i} \left\{ E \left(\frac{\partial u_i}{\partial x_j} + \frac{\partial u_j}{\partial x_i} \right) \right\} = 0 \quad i, j=1, 2, 3 \quad (7)$$

$$\frac{\partial u_1}{\partial x_1} + \frac{\partial u_2}{\partial x_2} + \frac{\partial u_3}{\partial x_3} = 0 \quad (8)$$

As can be seen, only one material parameter, the Young's modulus $E = E(x_1, x_2, x_3)$, is needed to describe the deformation of the tissue in equilibrium. When the tissue deformation is such that there is negligible strain in one of the three directions, say x_3 , the tissue is in "plane-strain" condition and this reduces the four 3D equations to three 2D equations in three unknowns $u_1 = u_1(x_1, x_2)$, $u_2 = u_2(x_1, x_2)$ and $P = P(x_1, x_2)$:

$$\frac{\partial P}{\partial x_1} + \frac{2}{3} \frac{\partial}{\partial x_1} \left\{ E \frac{\partial u_1}{\partial x_1} \right\} + \frac{2}{3} \frac{\partial}{\partial x_2} \left\{ E \left(\frac{\partial u_1}{\partial x_2} + \frac{\partial u_2}{\partial x_1} \right) \right\} = 0 \quad (9)$$

$$\frac{\partial P}{\partial x_2} + \frac{2}{3} \frac{\partial}{\partial x_2} \left\{ E \frac{\partial u_2}{\partial x_2} \right\} + \frac{2}{3} \frac{\partial}{\partial x_1} \left\{ E \left(\frac{\partial u_2}{\partial x_1} + \frac{\partial u_1}{\partial x_2} \right) \right\} = 0 \quad (10)$$

$$\frac{\partial u_1}{\partial x_1} + \frac{\partial u_2}{\partial x_2} = 0 \quad (11)$$

When calculating tissue displacement for a prescribed Young's modulus distribution $E = E(x_1, x_2)$, the solution of this system of three differential equations is approximated using a finite element package. To have a unique solution for this system of differential equations, boundary conditions, such as displacement and/or stress, have to be prescribed on part of the boundary of the tissue.

APPENDIX B: RELATIONSHIP BETWEEN PRINCIPAL AND RADIAL STRAIN

The theory of elasticity provides the theoretical foundation for the concept of principal strain and its properties (Fung YC, *A first course in continuum mechanics*. London: Prentice-Hall International, 1969). Consider an isotropic, incompressible ($\nu=0.5$) tissue in a 2D plane strain deformation state. Then, at each tissue point, there exists a unique set of two vectors that are perpendicular to each other. One vector indicates the direction of the maximal compressive strain (ϵ_{mc}), the other the direction of maximal tensile strain (ϵ_{mt}). These two vectors and the two values ϵ_{mc} and ϵ_{mt} are, respectively, the eigenvectors and eigenvalues of the symmetric strain tensor E . The eigenvectors are called principal axes and the corresponding eigenvalues ϵ_{mc} and ϵ_{mt} are called principal strains. Because we consider only incompressible tissue in a plane strain state, we have $\epsilon_{mt} = -\epsilon_{mc}$.

The relationship between the radial strain (ϵ_{rr}) and ϵ_{mc} , at each tissue point, equals $\epsilon_{rr} = \epsilon_{mc} \cos(2\alpha)$, where α is the angle between the vector of ϵ_{mc} and the line between catheter centre and tissue point (i.e., the line that defines the radial direction). This relationship is derived on the next page.

DERIVATION:

Consider the symmetric strain tensor E of an arbitrary point in the deformed tissue. Next, position a 2D coordinate system O , at that point, with its axes aligned to the principal axes of E . Then, E has the following matrix components,

$$\Sigma_O = \begin{bmatrix} \varepsilon_{mc} & 0 \\ 0 & \varepsilon_{mt} \end{bmatrix} \quad (1)$$

Now, rotate system O with angle α so that its x -axis coincides with the line between catheter centre and tissue point (i.e., the radial direction). In the rotated system, O^{rotated} , E has the following components

$$\Sigma_{O^{\text{rotated}}} = \begin{bmatrix} \varepsilon_{rr} & \varepsilon_{rt} \\ \varepsilon_{tr} & \varepsilon_{tt} \end{bmatrix} \quad (2)$$

where $\varepsilon_{rt} = \varepsilon_{tr}$ is the shear strain and $\varepsilon_{tt} = -\varepsilon_{rr}$, is the circumferential strain. Since coordinate systems O and O^{rotated} are rotated with respect to each other, Σ_O and $\Sigma_{O^{\text{rotated}}}$ must obey the transformation law for rotated coordinate systems, namely

$$\Sigma_{O^{\text{rotated}}} = R \Sigma_O R^T, \quad (3)$$

$$R = \begin{bmatrix} \cos \alpha & \sin \alpha \\ -\sin \alpha & \cos \alpha \end{bmatrix} \quad (4)$$

where R is the rotation matrix. Expansion yields

$$\begin{aligned} \begin{bmatrix} \varepsilon_{rr} & \varepsilon_{rt} \\ \varepsilon_{tr} & \varepsilon_{tt} \end{bmatrix} &= \varepsilon_{mc} \begin{bmatrix} -(\sin^2 \alpha - \cos^2 \alpha) & -2 \sin \alpha \cos \alpha \\ -2 \sin \alpha \cos \alpha & \sin^2 \alpha - \cos^2 \alpha \end{bmatrix} \\ &= \varepsilon_{mc} \begin{bmatrix} \cos 2\alpha & -\sin 2\alpha \\ -\sin 2\alpha & -\cos 2\alpha \end{bmatrix} \end{aligned} \quad (5)$$

where the last identity results from using double angle formulas. QED.

PART VII
MISCELLANEOUS

LIST OF SYMBOLS AND ABBREVIATIONS

SYMBOLS

\emptyset =diameter

A=amplitude of sine-function in the sine-modulated plaque model [μm]

c_i =i-th constraint

C_i =i-th corrected strain elastogram [%] (in chapter 6 it means the i-th constraint-function)

C_{INPUT} =corrected "measured" strain elastogram, used as input for reconstructions [%]

CP_i =i-th catheter position

E=Young's modulus [kPa]

$E_{\text{CAP}}=E_C$ =Young's modulus of the cap region in the parametric finite element model [kPa]

$E_{\text{LIPID}}=E_L$ =Young's modulus of the lipid pool region in the parametric finite element model [kPa]

$E_{\text{MEDIA}}=E_M$ =Young's modulus of the media region in the parametric finite element model [kPa]

K=integer that indicates plaque-border complexity

M_i =i-th modulogram [kPa]

modulogram=image of the Young's modulus distribution

N_{CAP} =number of control points for the cap Bézier curve

N_{LIPID} =number of control points for the lipid Bézier curve

P1, P2, P3, P4, P5 = specific catheter positions

SE_i =i-th strain-error elastogram [%]

V=parameter vector containing all parameters, i.e. control-points coordinates and three Young's moduli, of the Bézier-PFEM

W_i =i-th weight-error elastogram [-]

GREEK SYMBOLS

α =angle between (i) the direction of the principal axis of the principal compressive strain and (ii) the line between catheter centre and tissue point (i.e., the line that defines the radial direction) [$^\circ$]

β =angle between (i) the line from the geometric centre of the lumen towards tissue point and (ii) the line between catheter centre and tissue point (i.e., the line that defines the radial direction) [$^\circ$]

Δ =minimum required distance for allowing a proper finite element meshing

ε_{COR} =corrected strain [%]

$\varepsilon_{\text{error}}$ =strain-error threshold level [%]

ε_{mc} =maximal compressive strain [%]

ε_{mt} =maximal tensile strain [%]

$\varepsilon_{\text{prin}}$ =principal compressive strain [%]

$\varepsilon_{\text{radial}}=\varepsilon_{\text{rr}}$ =radial strain [%]

$\varepsilon_{\text{thres}}$ =strain-threshold level [%]

$\varepsilon_x, \varepsilon_y, \varepsilon_z$ =strain in the x, y, z direction, respectively

μ =mean radial strain

ν =Poisson's ratio [-]

σ =standard deviation of radial strain

ϕ =angle aperture between lipid pool shoulders, with respect to the geometric centre of the lumen [$^\circ$]

ABBREVIATIONS

CM=compounded modulogram
 COLL=collagen
 FEM=finite element model
 fps=frames per second
 GC=geometric centre
 GC_{LUMEN}=geometric centre of the lumen
 GIS=global initial state
 GUI=graphical user interface
 HSR=high-strain region
 IS=initial state
 IVUS=Intravascular ultrasound
 LIP=lipid
 LIS=local initial state
 MΦ=macrophages
 MHz=mega herz
 MRI=magnetic resonance imaging
 n.a.=not available
 N_{GI}=number of global initial states
 OCT=optical coherence tomography
 PFEM=parametric (or plaque) finite element model
 PRS=peak radial strain
 PVA=polyvinyl alcohol cryogel
 rf=RF=radio frequency
 RE=relative error
 RMS=root mean squared
 RO=region overlap
 SA=surface area
 SMC=smooth muscle cells
 SNR=signal to noise ratio
 std=standard deviation
 STA=soft tissue area
 STO=soft tissue overlap
 TCFA=thin-cap fibroatheroma
 YM=Young's modulus

VESSEL PHANTOM & BÉZIER MODEL

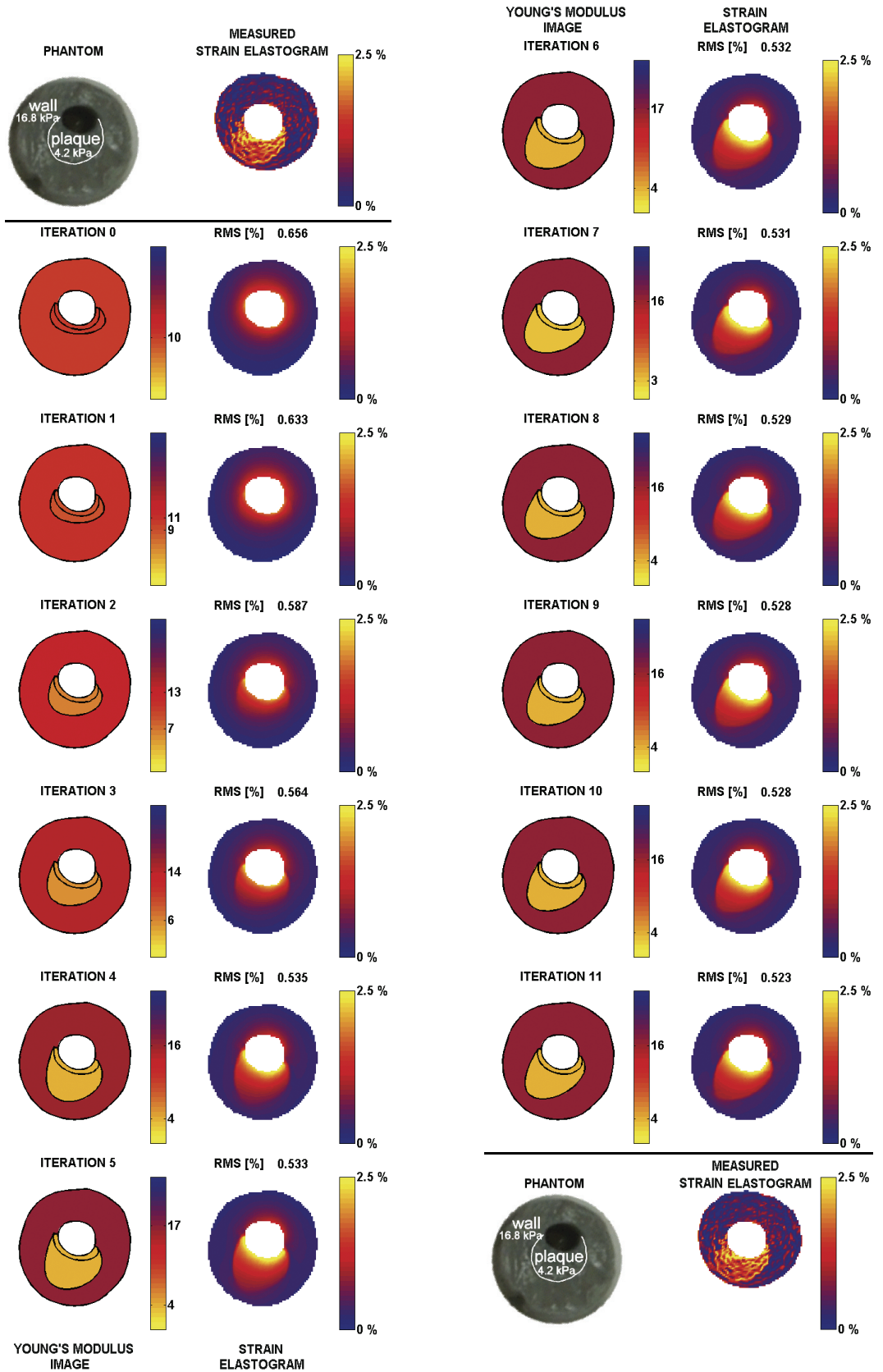
MODULOGRAPHY OF A VESSEL PHANTOM

On the next page a vessel phantom is shown (top, left) and (bottom, right). It has a soft plaque (Young's modulus=4.2 kPa) embedded in a stiff wall (Young's modulus=16.8 kPa). The measured strain elastogram of this phantom shows high strain near the inner border, which gradually decays towards the outer border. This measured strain elastogram is used as input for performing Modulography using the Bézier plaque model.

The first 11 iteration steps of the Modulography reconstruction process are shown. At each iteration step, the Young's modulus image (left) and the corresponding strain elastogram (right) is shown. Furthermore, the iteration step is provided and the root-mean-squared error (RMS) between the current strain elastogram and the measured strain elastogram

The Young's modulus colorbar ranges from 0 to 25 kPa. The intraluminal pressure differential, used to deform the phantom, is 1 mmHg.

Chapter 6 provides a detailed description of the reconstruction method and a discussion of the reconstruction result.



THIN-CAP FIBROATHEROMA & BÉZIER MODEL

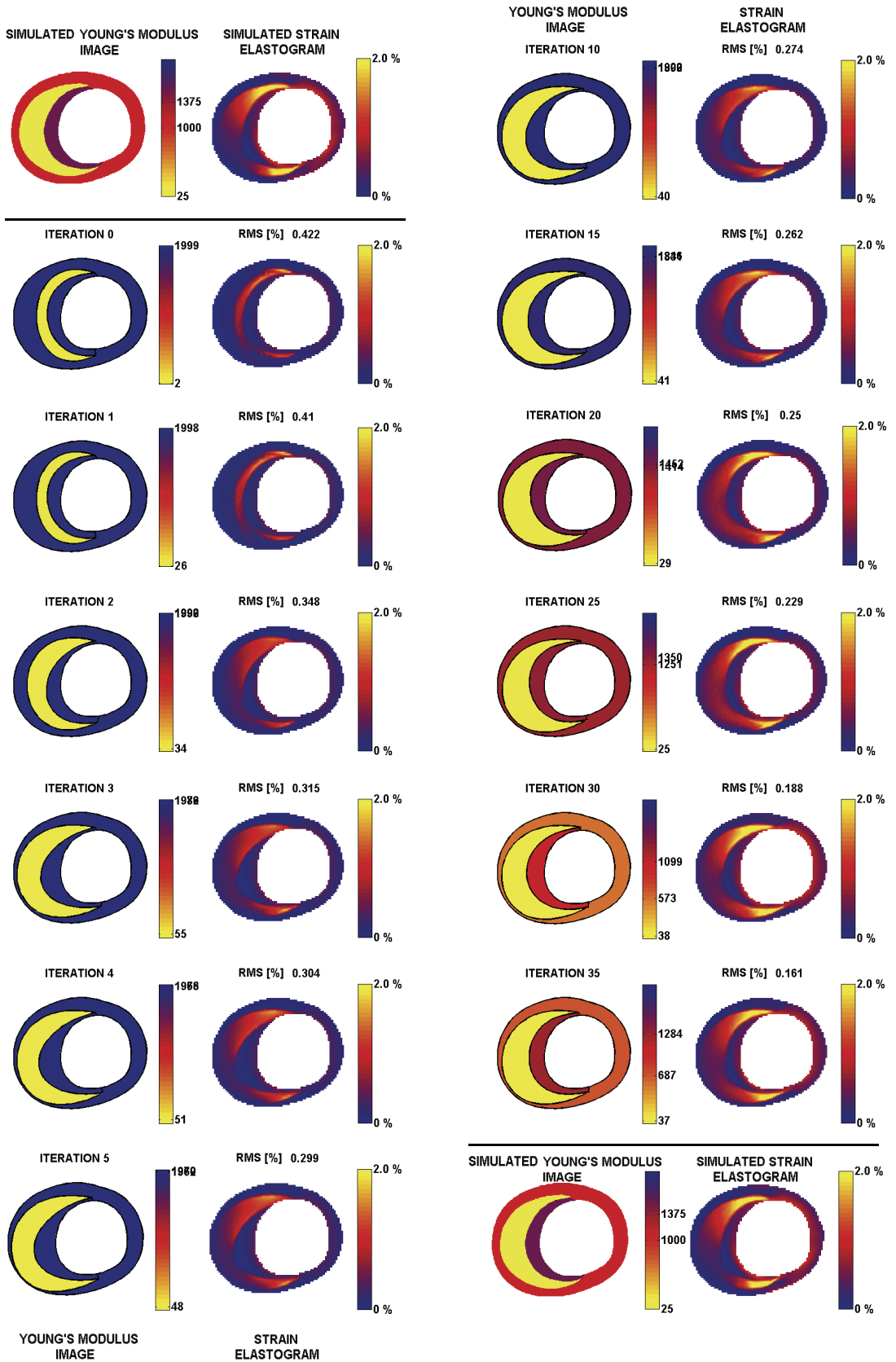
MODULOGRAPHY OF A THIN-CAP FIBROATHEROMA

On the next page a simulated thin-cap fibroatheroma plaque is shown (top, left) and (bottom, right). It has a soft lipid pool (Young's modulus=25 kPa) covered by a stiff thin cap (Young's modulus=1375 kPa). The corresponding simulated strain elastogram of this plaque shows high strain near the shoulders of the lipid pool and low strain at the center of it. This simulated strain elastogram is used as input for performing Modulography using the Bézier plaque model.

Some of the first 35 iteration steps of the Modulography reconstruction process are shown. At each iteration step, the Young's modulus image (left) and the corresponding strain elastogram (right) is shown. Furthermore, the iteration step is provided and the root-mean-squared error (RMS) between the current strain elastogram and the measured strain elastogram

The Young's modulus colorbar ranges from 0 to 2000 kPa. The intraluminal pressure differential, used to deform the plaque, is 20 mmHg.

Chapter 6 provides a detailed description of the reconstruction method and a discussion of the reconstruction result.



THIN-CAP FIBROATHEROMA & CIRCULAR MODEL

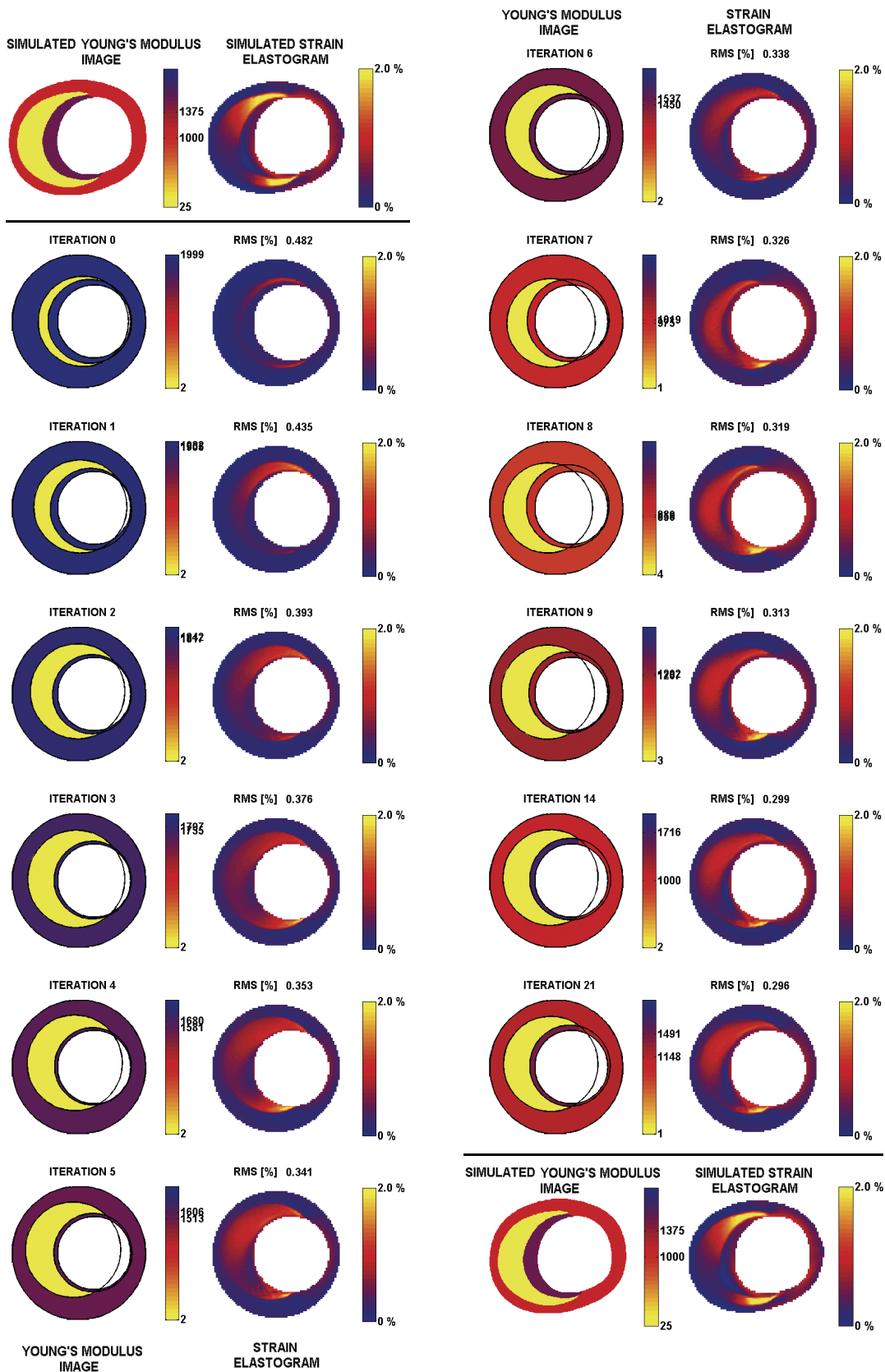
MODULOGRAPHY OF A THIN-CAP FIBROATHEROMA

On the next page a simulated thin-cap fibroatheroma plaque is shown (top, left) and (bottom, right). It has a soft lipid pool (Young's modulus=25 kPa) covered by a stiff thin cap (Young's modulus=1375 kPa). The corresponding simulated strain elastogram of this plaque shows high strain near the shoulders of the lipid pool and low strain at the center of it. This simulated strain elastogram is used as input for performing Modulography using the Circular plaque model.

Some of the first 21 iteration steps of the Modulography reconstruction process are shown. At each iteration step, the Young's modulus image (left) and the corresponding strain elastogram (right) is shown. Furthermore, the iteration step is provided and the root-mean-squared error (RMS) between the current strain elastogram and the measured strain elastogram

The Young's modulus colorbar ranges from 0 to 2000 kPa. The intraluminal pressure differential, used to deform the plaque, is 20 mmHg.

Chapter 4 provides a detailed description of the reconstruction method and a discussion of the reconstruction result.



IN VIVO HUMAN PLAQUE & CIRCULAR MODEL

MODULOGRAPHY OF A HUMAN CORONARY PLAQUE IN VIVO

On the next page an echogram of a human coronary artery is shown (top, left) and (bottom, right). Its inner and outer boundary are delineated in green. The in vivo measured strain elastogram of this artery shows high strain near the shoulders of the arterial plaque. This measured strain elastogram is used as input for performing Modulography using the Circular plaque model.

Some of the first 25 iteration steps of the Modulography reconstruction process are shown. At each iteration step, the Young's modulus image (left) and the corresponding strain elastogram (right) is shown. Furthermore, the iteration step is provided and the root-mean-squared error (RMS) between the current strain elastogram and the measured strain elastogram

The Young's modulus colorbar ranges from 0 to 250 kPa. The intraluminal pressure differential, used to deform the plaque, is 1 mmHg.

Chapter 4 provides a detailed description of the reconstruction method and a discussion of the reconstruction result.



CURRICULUM VITAE

Radjkumarsing (Radj) Anand Baldewsing was born on March 30, 1977 in The Hague, The Netherlands. From 1989 till 1995 he got his secondary education (Gymnasium) at 'Het Maerlant Lyceum' in The Hague.

In 1995, he went to the Delft University of Technology and studied Technical Mathematics. He received his Bachelor of Science degree (Cum Laude) and his Master of Science degree (Cum Laude), in 1996 and 2001, respectively. His master thesis was completed at the department of Systems Theory. It dealt with the modeling and stability analysis of pulse-width modulated switched electrical networks.

Subsequently, in May 2001, he started working towards a Ph.D. degree at the Biomedical Engineering department, Thoraxcenter, Erasmus University Medical Center, Rotterdam. His Ph.D. project focussed on solving the inverse elasticity problem for atherosclerotic coronary arteries. His solution approach automatically derives the arterial elasticity distribution from the arterial deformation. This deformation is processed from intravascular ultrasound (IVUS) data, which is measured using an IVUS catheter. His research endeavours are described in this thesis.

During his Ph.D. project he encountered the following research areas, techniques and subjects: vulnerable plaque imaging and characterization, IVUS, elastography, palpography, finite element modeling and forward/inverse elasticity problems. He also participated in two vulnerable plaque detection projects, one from the Interuniversity Cardiology Institute of the Netherlands ICIN (project number: ICIN-32) and the other from the Netherlands Organization for Scientific Research NWO (project number: RPG-5442).

Currently, he is exploring the world of financial mathematics.



LIST OF PUBLICATIONS

PAPERS (PEER-REVIEWED)

- Baldewising RA, Mastik F, Schaar JA, Serruys PW, Van der Steen AFW. *An inverse method for imaging the local elasticity of atherosclerotic coronary plaques*. 2006; (submitted).
- van der Steen AFW, Baldewising RA, Degertekin FL, Emelianov E, Frijlink ME, Furukawa Y, Goertz D, Karman M, Khuri-Yakub PT, Kim K, Mastik F, Moriya T, Oralkan O, Saijo Y, Schaar JA, Serruys PW, Sethuraman S, Tanaka A, Vos HJ, Witte R, O'Donnell M. *IVUS beyond the horizon*. EuroIntervention, 2006; (in press).
- Leung KYE, Baldewising RA, Mastik F, Schaar JA, Gisolf A, Van der Steen AFW. *Motion compensation for intravascular ultrasound palpography*. IEEE Ultrasonics Ferroelectrics and Frequency Control, 2006; (in press).
- Schaar JA, Van der Steen AFW, Mastik F, Baldewising RA, Serruys PW. *Intravascular palpography for vulnerable plaque assessment*. Journal of the American College of Cardiology, 2006; 47(8)(Suppl. C): 86C-91C.
- Baldewising RA, Mastik F, Schaar JA, Serruys PW, Van der Steen AFW. *Young's modulus reconstruction of vulnerable atherosclerotic plaque components using deformable curves*. Ultrasound in Medicine and Biology, 2006; 32(2): 201-210.
- Baldewising RA, Mastik F, Schaar JA, Serruys PW, Van der Steen AFW. *Robustness of reconstructing the young's modulus distribution of vulnerable atherosclerotic plaques using a parametric plaque model*. Ultrasound in Medicine and Biology, 2005; 31(12): 1631-1645.
- Baldewising RA, Schaar JA, Mastik F, Oomens CWJ, Van der Steen AFW. *Assessment of vulnerable plaque composition by matching the deformation of a parametric plaque model to measured plaque deformation*. IEEE Transactions on Medical Imaging (Special issue on Vascular Imaging), 2005; 24(4): 514-528.
- Idzenga T, Pel JJM, Baldewising RA, van Mastrigt R. *Perineal noise recording as a non-invasive diagnostic method of urinary bladder outlet obstruction: a study in polyvinyl alcohol and silicone model urethras*. Neurourology and Urodynamics, 2005; 24(4): 381-388.
- Pel JJM, Idzenga T, Baldewising RA, Van Mastrigt R. *Measurement of noise in a model urethra of polyvinyl alcohol cryogel at different degrees of urethral obstruction*. Klinische Fysica, 2004: 26-31.
- Baldewising RA, de Korte CL, Schaar JA, Mastik F, van der Steen AFW. *A finite element model for performing intravascular ultrasound elastography of human atherosclerotic coronary arteries*. Ultrasound in Medicine and Biology, 2004; 30(6): 803-813.
- Baldewising RA, De Korte CL, Schaar JA, Mastik F, Van der Steen AFW. *Finite element modeling and intravascular ultrasound elastography of vulnerable plaques: parameter variation*. Ultrasonics, 2004; 42: 723-729.
- Schaar JA, de Korte CL, Mastik F, Baldewising R, Regar E, de Feyter P, Slager CJ, van der Steen AFW, Serruys PW. *Intravascular palpography for high-risk vulnerable plaque assessment*. Herz, 2003; 6: 488-495.

PROCEEDINGS

- Baldewising RA, Mastik F, Schaar JA, van der Steen AFW. *A compounding method for reconstructing the heterogeneous young's modulus distribution of atherosclerotic plaques from their radial strain*. Proceedings of the Fourth International Conference on the Ultrasonic Measurement and Imaging of Tissue Elasticity 2005, Texas, USA, page 68.
- Leung KYE, Baldewising RA, Mastik F, Danilouchkine MG, Schaar JA, Gisolf A, van der Steen AFW. *Motion compensation for intravascular ultrasound palpography for in vivo vulnerable plaque detection*. Proceedings of the Fourth International Conference on the Ultrasonic Measurement and Imaging of Tissue Elasticity 2005, Texas, USA, page 67.
- Baldewising RA, Mastik F, Schaar JA, van der Steen AFW. *Deformable bezier curves for young's modulus reconstruction and delineation of vulnerable atherosclerotic plaque components*. 2005 IEEE International Ultrasonics Symposium, Rotterdam, The Netherlands, pages 249-252.
- Leung KYE, Baldewising RA, Mastik F, Schaar JA, Gisolf A, van der Steen AFW. *Motion compensation for intravascular ultrasound palpography for in vivo vulnerable plaque detection*. 2005 IEEE International Ultrasonics Symposium, Rotterdam, The Netherlands, pages 253-256.
- Baldewising RA, Schaar JA, Mastik F, Oomens CWJ, van der Steen AFW. *Young's modulus reconstruction for assessing vulnerable atherosclerotic plaque composition in vivo*. 2004 IEEE International Ultrasonics Ferroelectrics and Frequency Control 50th Anniversary Conference, 2004, Montreal, Canada, pages 368-371.
- Baldewising RA, Mastik F, Schaar JA, van der Steen AFW. *Robust assessment of arterial plaque composition in vivo using a parametric plaque model based young's modulus reconstruction method*. Proceedings of the Third International Conference on the Ultrasonic Measurement and Imaging of Tissue Elasticity 2004, Cumbria, UK, page 85.
- Van der Steen AFW, de Korte CL, Schaar JA, Mastik F, Baldewising RA, Serruys PW. *3D intravascular ultrasound palpography for vulnerable plaque detection*. Proceedings of the 2004 IEEE International Symposium on Biomedical Imaging. Arlington, USA, pages 49-52.
- Baldewising RA, Schaar JA, Mastik F, Oomens CWJ, Van der Steen AFW. *Ivus modulography of vulnerable plaques using a parametric finite element model; validation on a phantom and human coronary artery*. Proceedings of the Second International Conference on the Ultrasonic measurement and Imaging of Tissue Elasticity 2003, Texas, USA, page 75.
- Baldewising RA, Oomens CWJ, Van der Steen AFW. *Intravascular young's modulus reconstruction using a parametric finite element model*. 2003 IEEE International Ultrasonics Symposium Proceedings, Honolulu, Hawaii, pages 1879-1882.
- Baldewising RA, de Korte CL, Mastik F, Schaar JA, van der Steen AFW. *Comparison of finite element model elastograms and ivus elastograms acquired from phantoms and arteries*. 2002 IEEE Ultrasonics Symposium Proceedings, Munich, Germany, pages 1873-1876.

ABSTRACTS

- Baldewising RA, Mastik F, Schaar JA, van der Steen AFW. *Deformable bezier curves for young's modulus reconstruction and delineation of vulnerable atherosclerotic plaque components*. 2005 IEEE International Ultrasonics Symposium, Rotterdam, The Netherlands, pages 208-209.
- Leung KYE, Baldewising RA, Mastik F, Schaar JA, Gisolf A, van der Steen AFW. *Motion compensation for intravascular ultrasound palpography for in vivo vulnerable plaque detection*. 2005 IEEE International Ultrasonics Symposium, Rotterdam, The Netherlands, pages 209-210.
- Baldewising RA, Schaar JA, Mastik F, Oomens CWJ, van der Steen AFW. *Young's modulus reconstruction for assessing vulnerable atherosclerotic plaque composition in vivo*. 2004 IEEE International Ultrasonics Ferroelectrics and Frequency Control 50th Anniversary Conference, Montreal, Canada, pages 313-314.
- Schaar JA, Mastik F, Baldewising RA, de Korte CL, Regar E, McFadden E, de Feyter P, Krams R, van Deel ED, Slager CJ, Duncker DJ, Serruys PW, van der Steen AFW. *Intravascular palpography: a new method to diagnose vulnerable plaque*. Jubileum Wetenschapsdag Nederlandse Hartstichting 2004, Leiden, The Netherlands. Poster 115.
- Van der Steen AFW, Schaar JA, Mastik F, de Korte CL, Baldewising R, Serruys PW. *Intravascular ultrasound palpography for vulnerable plaque detection*. International Workshop Endocoronary Biomechanics and Restenosis 2003, Paris, France.
- Baldewising RA, Oomens CWJ, Van der Steen AFW. *Intravascular young's modulus reconstruction using a parametric finite element model*. 2003 IEEE International Ultrasonics Symposium, Honolulu, Hawaii, pages 432-433.
- Baldewising RA, De Korte CL, Schaar JA, Mastik F, Van der Steen AFW. *Finite element modelling and intravascular ultrasound elastography of phantoms and coronary arteries: parameter variation*. Ultrasonics International 2003, Granada, Spain.
- Baldewising RA, de Korte CL, Mastik F, van der Steen AFW. *Comparison of finite element model elastograms and ivus elastograms acquired from phantoms and arteries*. 2002 IEEE Ultrasonics Symposium, Munich, Germany, pages 277-278.
- Schaar JA, de Korte CL, Mastik F, Strijder C, Pasterkamp G, Baldewising RA, Serruys PW, van der Steen AFW. *Intravascular elastography detects the weak vulnerable plaque*. XXII congress of the European Society of Cardiology 2002. European Heart Journal, Volume 4 (Abstr. Suppl), page 72.

BOOK CHAPTERS

Baldewsing RA, Schaar JA, Mastik F, van der Steen AFW. *Local elasticity imaging of vulnerable atherosclerotic coronary plaques*. Advances in Cardiology, 2006; (in press) Chapter in "Atherosclerosis, Large Arteries and Cardiovascular Risk", Editors: Safar ME and Frohlich ED., S. Karger AG, Switzerland.

Baldewsing RA, Schaar JA, de Korte CL, Mastik F, Serruys PW, van der Steen AFW. *Intravascular ultrasound elastography: a clinician's tool for assessing vulnerability and material composition of plaques*. Studies in Health Technology and Informatics, 2005; 113: 75-96. Chapter in "Plaque Imaging: Pixel to Molecular Level", Editors: Suri, Yuan, Wilson and Laximarayan, IOS press, The Netherlands, ISBN 1-58603-516-9.

INVITED LECTURE

Baldewsing RA. *Modulography*, 3rd International Vulnerable Plaque Meeting, Capri, Italy, 12-13 June 2005.

ACKNOWLEDGEMENT

Herewith, I express my sincere gratitude to **everyone** that has contributed to the realization of this thesis, particularly:

My **parents** for bringing me into this world.

My **parents' parents** for bringing my parents into this world. (indeed, all my **ancestors** for ...).

My **family** for raising and supporting me in all possible ways.

My **friends** for helping me release work-related stress in the weekends.

My **thesis supervisors** for daring to be my thesis supervisors with all its responsibilities. **Antonius (Ton) F.W. van der Steen**, special thanks for coaching me on how to write, less-redundant, less-inconsistent and less-long articles.

I promise you that this is the last time you will encounter a sentence, as small as this one, in any of my future writings.

Patrick W.J.C. Serruys, if there is someone, who has the means to advance Modulography into the clinic, it is you. I hope that you will perform this task.

My **thesis graduation committee** for asking only questions to me that I can answer either correctly and/or satisfactorily during my thesis defense.

My **co-authors** for helping me polishing our articles.

Chris L. de Korte from the University Medical Centre St. Radboud, Nijmegen for giving my PhD project a good start, by being my mentor during the first year. Additional thanks for making me a stress-balls-throwing practitioner. Thanks to your thesis 'Intravascular ultrasound elastography', you have allowed Modulography to be born. As such, I am confident that you will appreciate proposition #11.

Jeffrey C. Bamber, from the Institute of Cancer Research and the Royal Marsden NHS Trust, U.K. for having me at your department, so I could discover/learn certain aspects of inverse problems from

Paul E. Barbone (Boston University, U.S.A.), who was at your department for a one-year sabbatical (thanks Paul).

Alex Kolen, from Maastricht University, thanks for providing me accommodation during my visit to Bamber's department.

Cees W.J. Oomens from Eindhoven University of Technology, for advising me on which road to take during my Modulography-journey (namely, the road of 'use as much as possible a priori information').

Rael van Loon and **Ralf A. Boerboom**, both from Eindhoven University of Technology, for providing me with essential finite element subroutines.

My **colleagues** at the Biomedical Engineering department of the Erasmus MC, for being friendly, humorous and informal, please keep it this way for ever ;)

Dr.² JA Schaar. I hope that I have succeeded in representing the minorities and if you have any questions about mathematics, just ask me. It was an honour to have someone of your caliber as

workroom-mate, especially because you always talked ‘huis-tuin-en-keuken’ language to me. Thanks to your thesis, ‘Palpography’, and Palpography’s use in the clinic, Modulography has its established big brother it needs to make it into the clinic.

My **secretarial staff** (yes, I know, I should write: our department’s secretarial staff, but it just felt like that): Mieke A.T.M. Pruijsten - ten Hacken, Monique Hanegraaff and Riekje Daane for always being more than friendly and for helping me out with all sorts of non-technical bureaucratic business.

My **computer-network staff** (yes, I know ...): Robert (Rob) H. van Bremen and Roland van Lindt for being my computer’s personal physicians.

The ladies working at the coffee-corner at the 3rd floor of the Erasmus MC, who were always in for a discussion or joke.

Gert-Jan M. Pieters, for keeping each other motivated during college and each other’s Ph.D. years and for the semi-annual ‘Billy Beer’ meetings. I hope to continue this tradition, even after you have become a professor.

The always kind and inspiring **mathematics-teachers** from the Delft University of Technology, who were, and still are, available for answering my questions.

The **companies**, mentioned at the beginning of this thesis, for their sponsorship.

and more than particularly:

Frits Mastik, for being an employee at the Biomedical Engineering department of the Erasmus MC, during my Ph.D. years there. For always being present at work when I arrived in the late mornings and for still being there when I left in the early evenings. For always listening to me and helping me out (even before I realized that I would need help) with computers, soft/hardware, data analyses, mathematics, measurements, IVUS, elastography, palpography, modulography, colleagues, writing articles, addressing sponsors, assisting with creating this thesis, and much more.

Without your experience and knowledge I would not have come this far with my research (I know, you have a different opinion about this, but it’s my acknowledgement ;)). I hope that in the future many (under)graduate students, post-docs, professors, clinicians, technicians and other employees from the Biomedical Engineering department will be able to enjoy your company.

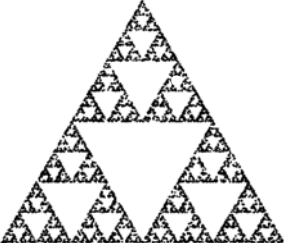
As a final note, I hope for your sakes, that there will always be a ‘**Frits Mastik**’ at my future job(s) if there isn’t one, I know where to find you!

COLOPHON:

This thesis was made by the author using Adobe Framemaker 7.0. The text font is Sylfaen. The thesis was printed on 90 gram/m² G-print paper (17 by 24 cm) from a pdf-file generated with Adobe Acrobat 7.0 (Option: PressQuality). The pages were glued to the cover using a perfect-binding process. The cover is in 'process black' color, matt-laminated, with spot-UV varnish for the text.

MODULOGRAFIE:

VISUALISATIE VAN DE ELASTICITEIT VAN ATHEROSCLEROTISCHE PLAQUES

1. Modulografie identificeert en karakteriseert vetophopingen in kransslagaderen.
[DIT PROEFSCHRIFT]
2. Unicité van het inverse elasticiteitsprobleem is gewenst, maar niet noodzakelijk om een praktisch bruikbare oplossing te genereren.
[DIT PROEFSCHRIFT]
3. Radiële vervorming van bloedvaten is sterk afhankelijk van de stijfheid parameter (=Young's modulus), maar bijna niet van de samendrukbaarheid parameter (=Poisson's ratio); dit is een gewenste eigenschap voor het oplossen van het inverse elasticiteitsprobleem.
[DIT PROEFSCHRIFT]
4. Rek ("strain") en spanning ("stress") zijn als man en vrouw; door hen op de juiste wijze te verenigen, ontstaat automatisch een kind genaamd "Young's modulus".
[DIT PROEFSCHRIFT]
5. Versimpelen van complexe problemen leidt tot oplossingen.
[DIT PROEFSCHRIFT]
6. Gödel's tweede onvolledigheidsstelling (Gödel, 1931) impliceert dat iedereen, die ervan uitgaat dat de wiskunde vrij is van tegenspraken, gelovig is.
[GÖDEL K., "ÜBER FORMAL UNENTSCHEIDBARE SÄTZE DER PRINCIPIA MATHEMATICA UND VERWANDTER SYSTEME", MONATSHEFTE FÜR MATHEMATIK UND PHYSIK, 1931;38:173-98.]
7. Vooruitgang induceert achteruitgang.
8. De zogeheten impactfactor van een blad is geen bruikbare maat voor de wetenschappelijke impact van een artikel in dat blad.
9. Toevoegen van een weg aan een bestaand wegennetwerk leidt in sommige gevallen tot langzamer verkeer, meer filevorming of langere reistijden.
[BRAESS D., "ÜBER EIN PARADOXON AUS DER VERKEHRSPANUNG", UNTERNEHMENSFORSCHUNG, 1968;12:258-68.]
10. Onvoorspelbare beweging resulteert toch vaak in een voorspelbaar resultaat.
Ter illustratie, doe het volgende:
 - a) Teken een stip ergens in een gelijkzijdige driehoek,
 - b) Kies willekeurig (m.b.v. een dobbelsteen) een hoekpunt van deze driehoek,
 - c) Zet een nieuwe stip halverwege de huidige stip en het gekozen hoekpunt,
 - d) Herhaal stap b) en c) vaak (zeg meer dan 100 keer),
 - e) Verwijder de eerste 25% van de getekende stippen.

Het resultaat benadert de afbeelding hiernaast, een zogeheten fractal, die bekend staat als "Sierpinski's driehoek".
11. Echografie, Elastografie, Modulografie.
[VRIJ NAAR C. JULIUS CAESAR, 100-44 v.C.]

MODULOGRAPHY:

ELASTICITY IMAGING OF ATHEROSCLEROTIC PLAQUES

1. Modulography identifies and characterizes fat deposits within coronary artery walls.
[THIS THESIS]
2. Uniqueness of the inverse elasticity problem is desired, but not necessarily required to generate practically useful solutions.
[THIS THESIS]
3. Radial deformation of blood vessels depends upon the stiffness parameter (=Young's modulus), but hardly upon the compressibility parameter (=Poisson's ratio); this is a desired property for solving the inverse elasticity problem.
[THIS THESIS]
4. Strain and stress are like a man and woman; unite them in a proper way and a child will be automatically born, named "Young's modulus".
[THIS THESIS]
5. Simplifying complex problems leads to solutions.
[THIS THESIS]
6. Gödel's second incompleteness theorem (Gödel, 1931) implies that everyone, who assumes that mathematics is free of inconsistencies, is a believer.
[GÖDEL K., "ÜBER FORMAL UNENTSCHEIDBARE SÄTZE DER PRINCIPIA MATHEMATICA UND VERWANDTER SYSTEME", MONATSSHEFTE FÜR MATHEMATIK UND PHYSIK, 1931;38:173-98.]
7. Progress induces regression.
8. The so-called impact factor of a journal is not a useful measure for the scientific impact of an article in that journal.
9. The addition of a road to an existing road-network leads in some cases to slower traffic, more traffic jams or longer traveling times.
[BRAESS D., "ÜBER EIN PARADOXON AUS DER VERKEHRSPLANUNG", UNTERNEHMENSFORSCHUNG, 1968;12:258-68.]
10. Unpredictable movement often still results in a predictable result.
As an example, do the following:
 - a) Draw a dot somewhere in an equilateral triangle,
 - b) Choose at random (e.g., using a dice) a vertex of this triangle,
 - c) Draw a new dot halfway between the current dot and the chosen vertex,
 - d) Repeat step b) and c) a number of times (say, more than 100),
 - e) Remove the first 25% of drawn dots.

The result approximates the image alongside, a so-called fractal, which is also known as "Sierpinski's triangle".
11. Echography, Elastography, Modulography.
[ADAPTED FROM C. JULIUS CAESAR, 100-44 B.C.]

